Modeling and determining of power conditioning strategies for distributed power networks for aeronautical and spaceborne applications

Quentin Hilpert

RÉPUBLIQUE FRANÇAISE
Liberté Égalité Fraternité

Université de Toulouse

Doctorat de l'Université de Toulouse

préparé à Toulouse INP

Modélisation et détermination des stratégies de conditionnement de puissance pour des réseaux de puissance répartis pour des applications embarquées aéronautiques et spatiales

---

Thèse présentée et soutenue, le 2 mai 2024 par

Quentin HILPERT

École doctorale
SYSTEMES

Spécialité
Systèmes embarqués et Automatique

Unité de recherche
LAPLACE - Laboratoire PLAsma et Conversion d'Énergie

Thèse dirigée par
Stéphane CAUX et François BONNET

Composition du jury
M. Pascal MAUSSION, Président, Toulouse INP
Mme Claire VALENTIN, Rapporteuse, Université Lyon 1
Mme Manuela SECHILARIU, Rapporteuse, Université de Technologie de Compiègne
Mme Antoneta-Iuliana BRATCU, Examinatrice, Grenoble INP
M. Stéphane CAUX, Directeur de thèse, Toulouse INP
M. François BONNET, Co-directeur de thèse, CNES

Membres invités
Mme Ada CZESNAKOWSKA, Airbus

Acknowledgements

Tout au long de cette thèse qui a débuté en Octobre 2018 au laboratoire LAPLACE en partenariat avec le CNES et cofinancée par Airbus Defence & Space, j'ai eu la chance de côtoyer un grand nombre de personnes de très grande valeur, auprès desquelles je n'ai cessé d'apprendre et de m'épanouir, tant sur le plan professionnel que personnel. Cette expérience m'a profondément marqué et je ne pouvais commencer ce manuscrit sans les évoquer et m'adresser à eux.

Je souhaite tout d'abord remercier mon directeur de thèse, Stéphane Caux, professeur à l'INP de Toulouse et chercheur au laboratoire LAPLACE au sein du groupe de recherche CODIASE que j'ai intégré durant ma thèse. Je le remercie de m'avoir accompagné tout au long de cette période, malgré les aléas de parcours, et en particulier pour son support et ses conseils dans la recherche d'un équilibre entre les aspects académiques et industriels qui étaient parfois compliqués à allier. Son expérience de directeur de thèse et de recherche m'a souvent aidé à prendre le recul nécessaire pour aborder les différentes problématiques étudiées pour mener à bout ces travaux. Merci.

Je tiens ensuite à remercier mon co-directeur de thèse, François Bonnet, chef du service d'architecture électrique et avionique au CNES pendant la durée de ma thèse, qui a toujours fait en sorte que le projet puisse avancer dans les meilleures conditions, tant sur les aspects techniques qu'humains. Ses connaissances du domaine spatial, son sens du partage m'ont beaucoup apporté et ont fortement contribué à l'aboutissement de cette thèse. Nos échanges et discussions, qui nous ont parfois emmenés dans d'autres galaxies comme lors de l'ESPC 2019 à Juan-les-pins, resteront des souvenirs impérissables. Merci.

Je souhaite également remercier les deux rapporteures, Madame Claire Valentin, professeure à l'Université Lyon 1 et chercheuse au Laboratoire d'Automatique, de Génie des Procédés et de Génie Pharmaceutique (LAGEPP) et Madame Manuela Sechilariu, professeure à l'Université de Technologie de Compiègne (UTC) et directrice du laboratoire Avenues, d'avoir accepté de réviser mon manuscrit de thèse et pour la richesse de leurs retours. Je remercie également les autres membres du jury, Madame Antoneta-Iuliana Bratcu, maitre de conférence au GIPSA Lab de l'INP de Grenoble, Monsieur Pascal Maussion, Professeur à l'INP de Toulouse et chercheur au laboratoire LAPLACE, et Madame Ada Czesnakowska, responsable R&T chez Airbus Defence & Space d'avoir accepté d'évaluer mes travaux de thèse.

Pendant ces années j'ai eu la chance de pouvoir travailler au sein de différentes structures où je me suis toujours senti accueilli et entouré. J'ai tout d'abord une pensée pour tous mes collègues du laboratoire LAPLACE avec qui j'ai passé de très beaux moments autour de sujets de science… mais pas que ! Je voudrais citer mes collègues de bureau : Pawel, Grégoire et Youssef, bien que ce dernier se soit rapidement échappé. Je pense également à ceux de mes bureaux annexes : Andrea et Abdulrahman pour le bureau « café », Davin et Joseph pour le bureau « galettes des rois ». Merci à eux et plus généralement à tous les doctorants du laboratoire pour tous les moments vécus ensemble pendant cette période.

Sur la deuxième partie de ma thèse, j'ai également eu la chance de trouver une équipe incroyable au CNES. Je tiens tout particulièrement à remercier les idiots du bureau pour leur accueil, leur soutien, et pour l'ambiance indescriptible que j'ai trouvée auprès d'eux : Clément, Laurent, Rémi, Pierre, Sylou et Antoine. Le bob de la vérité et les lunettes de la clairvoyance ne suffiraient pas à voir combien je leur

suis reconnaissant… Je remercie d'une manière générale toute l'équipe d'architecture électrique et avionique ainsi que toutes les personnes que j'ai pu côtoyer au quotidien, à la pause-café du matin ou au laboratoire électrique pour leur aide, et leur bonne humeur. Je pense également à « mes » deux stagiaires Steven et Curtis qui m'ont aidé dans mon travail et qui ont, je l'espère pu également profiter de cette ambiance. Ce fut un immense plaisir de travailler dans un tel contexte, ce qui explique la place tout à fait particulière que le CNES a et aura toujours à mes yeux.

J'ai également eu la chance d'être accompagné par le département électrique d'Airbus Defense & Space que j'ai rejoint à la fin de ma thèse. Je remercie Bruno Samaniego et Marc Malagoli pour leur accompagnement et leur implication au début de la thèse notamment lors de la mise en place de ce partenariat. Leur expérience et leur connaissance des aspects industriels m'ont beaucoup appris et leur engagement dans le développement des moyens de démonstration ont grandement joué dans l'aboutissement de cet aspect de la thèse. Je veux également remercier les personnes ayant œuvré à la conception des MOBI, Xavier, Jacquis et Loïc, pour leur investissement dans ce sujet malgré des demandes toujours plus nombreuses et des complications certaines – un confinement par exemple. Merci à eux et à toute l'équipe TESED1 d'une manière générale pour leur accueil à la fin de la thèse. L'ambiance toujours joviale, respectueuse et raffinée que j'ai trouvée à mon arrivée dans l'équipe m'ont offert un second souffle pour finaliser ces travaux.

Enfin je voudrais remercier toute ma famille pour son soutien indéfectible pendant cette période qui fut, par moment, une vraie épreuve à traverser. Ils ont été une source de réconfort et d'encouragements permanente et ils savent la reconnaissance que j'ai pour eux. Au moment d'arriver au terme de cette étape de ma vie, j'ai également une pensée particulière pour mes grands-parents qui ont toujours été une source d'inspiration et à qui j'aurais été fier de pouvoir présenter ce travail. Ils m'ont accompagné d'une certaine manière durant la finalisation de ce manuscrit et j'ai souvent cherché dans leur souvenir la force de continuer. Je leur dédie cette thèse.

Pour conclure, je souhaitais formuler un dernier remerciement tout particulier à celle qui a partagé chaque moment de réussite mais aussi de doute et de découragement avec moi et qui fut un véritable pilier tout au long de cette période. Wendy, je n'aurais jamais pu arriver au bout sans toi, je te le dois :

Merci.

Abstract

The electrical power system (EPS) is one of the most critical systems, if not the most critical, of a spacecraft considering that a spacecraft is nothing but an electrical system and the purpose of the EPS is to generate, condition, store and distribute electrical power to the entire system. In other words, it is the first link in the food chain and if it stops working, the whole system is lost. The resulting need for robustness and reliability, as well as the particularly isolated and hostile environment in which it must operate, have guided the design choices of the EPS and led to a system with very high efficiency, electrically speaking, but at the cost of a lack of flexibility. Nevertheless, the current context and recent developments give the opportunity to deeply rethink the design of the EPS and this is what CNES and Airbus have been doing for several years. The modular and distributed electrical architecture that has emerged from these developments offers many possibilities in terms of control, but also challenges in terms of stability and optimization. The objective of this thesis is to demonstrate that control laws integrated in the conditioning modules allow a regulation of the battery charge and a stability of the onboard network whatever the topology of the power bus and the consumption profiles.

To do this, a parametric modeling of the system was carried out by being inspired by the modeling methods used in the problems of terrestrial microgrids. The models of the various elements of the system were thus integrated under Matlab and Matlab Simulink in order to simulate a typical system inspired by satellites developed by the CNES. A thorough bibliographical study was carried out to identify control laws used in similar problems and which would be of interest to be adapted to space applications. These control laws have been tested in simulation, with particular attention to the stability constraints, which allowed to select the most suitable ones in order to validate them experimentally on a demonstrator set up on the same model. Based on these results, a global strategy is proposed.

List of acronyms

AC	Alternative Current
ADC	Analog to Digital Converter
ADS	Airbus Defence and Space
AIT	Assembly Integration and Test
AOCS	Attitude & Orbit Control System
BCDU	Battery Charge Discharge Unit
BCR	Battery Charge Regulation
BDR	Battery Discharge Regulation
BMS	Battery Management System
BODI	BOitier de DIstribution
BOL	Beginning Of Life
BOMO	BOitier MOdulaire
CAN	Controlled Area Network
CC	Coulombic Counter
CC/CV	Constant Currant / Voltage
CM	Cell Module
CNES	Centre National d'Etudes Spatiales
COTS	Components Off The Shelf
CPL	Constant Power Load
DAC	Digital to Analog Converter
DC	Direct Current
DCMG	DC Microgrid
DCSU	DC Switching Unit
DDCU	DC/DC Converting Unit
DER	Distributed Energy Resources
DET	Direct Energy Transfer
DHS	Data Handling System
DL	Dynamic Load
ECSS	European Cooperation for Space Standardization
EMC	Electro Magnetic Compatibility
EMF	ElectroMotive Force
EOL	End Of Life
EPS	Electrical Power System
ESA	European Space Agency
EVA	Extra Vehicular Activity
FDIR	Fault Detection Isolation, Recovery
FPGA	Field Programmable Gate Array
FRB	Fully Regulated Bus
FSBBC	Four Switch Buck-Boost Converter
GEO	Geostationary Orbit
GMPM	Gain / Phase Margins
HMI	Human Machine Interface
IOA	In Orbit Assembly

ISS	International Space Station
LCL	Latch Current Limiter
LEO	Low Earth Orbit
LPPT	Limited Power Point Tracker
LTI	Linear Time Invariant
MBMS	Master BMS
MBSU	Main Bus Switching Unit
MEA	Main Error Amplifier
MEA	More Electrical Aircraft
MG	Micro Grid
MOBI	MOdule Batterie Intelligent
MOSFET	Metal Oxide Semiconductor Field Effect Transistor
MPP	Maximum Power Point
MPPT	MPP Tracker
NG	Nano Grid
NRB	Non Regulated Bus
OBC	On Board Computer
OBS	On Board Software
OCV	Open Circuit Voltage
PCDU	Power Conditioning and Distribution Unit
PCU	Power Conditioning Unit
PDU	Power Distribution Unit
POL	Point Of Load
PV	PhotoVoltaic
PWM	Pulse Width Modulation
RAMS	Reliability, Availability, Maintainability and Safety
RL	Resistive Load
RPCM	Remote Power Controller Module
RTG	Radioisotope Thermoelectric Generator
RTU	Remote Terminal Unit
S3R	Sequential Switching Shunt Regulator
SAS	Solar Array Simulator
SAW	Solar Array Wing
SEE	Single Event Effects
SOC	State Of Charge
SOH	State Of Health
SOT	State Of Temperature
SRB	Semi Regulated Bus
SSU	Sequential Shunt Unit
SUT	System Under Test
TC	TeleCommand
TCS	Thermal Control System
TM	TeleMeasure
TSP	Time and Space Partitioning
UV	UltraViolet
ZOH	Zero-Order Hold

Table of content

CHAPTER 1.

Introduction & context

Summary

This PhD thesis is integrated in a strong and mutating industrial context. To understand the stakes of the current period of technological ruptures and the motivations which pushed to undertake these works, it is necessary at first to go back a little bit and to study the legacy which the history of the space industry bequeaths to us.

Since it beginnings in the late 50s, the space industry has evolved in successive cycles, each lasting approximately 15 years, as presented in [1] and [2] and shown in Figure 1.1. This highly strategic sector requires to master advanced technologies, needing a significant long-term investment which, for a very long time, has only been made possible by public space programs through national agencies such as the CNES (Centre National d'Etudes Spatiales) in France. The demonstration of technological mastery was thus the first factor of development of the space industry at the beginning of the cold war. This "space race" was the golden age of the space exploration – both with humans and robots – and like all races, the goal was to be the first: it began with Spoutnik 1, the first artificial Earth satellite sent by the USSR in 1957, followed by the first man in space, the first picture of the Earth, the first step of a human on the Moon, etc. Even the first crash on another planet has been registered. It ended with the first flyby of all inner solar system's planets and Jupiter. More than the mere demonstration of a savoir-faire, these premières have also deeply marked the collective imagination and our vision of our planet. In term of number of launches, this period corresponds to a constant increase of the number of objects put in orbit.

The second cycle corresponds to a stagnation of the number of objects sent and to the appearance of bigger and more durable projects. It is the time of the first generation of space stations (Salyut, Skylab) and of the consolidation of the strategical military applications such as the Global Positioning System (GPS), telecommunications and Earth observation which have then been progressively opened to civil uses.

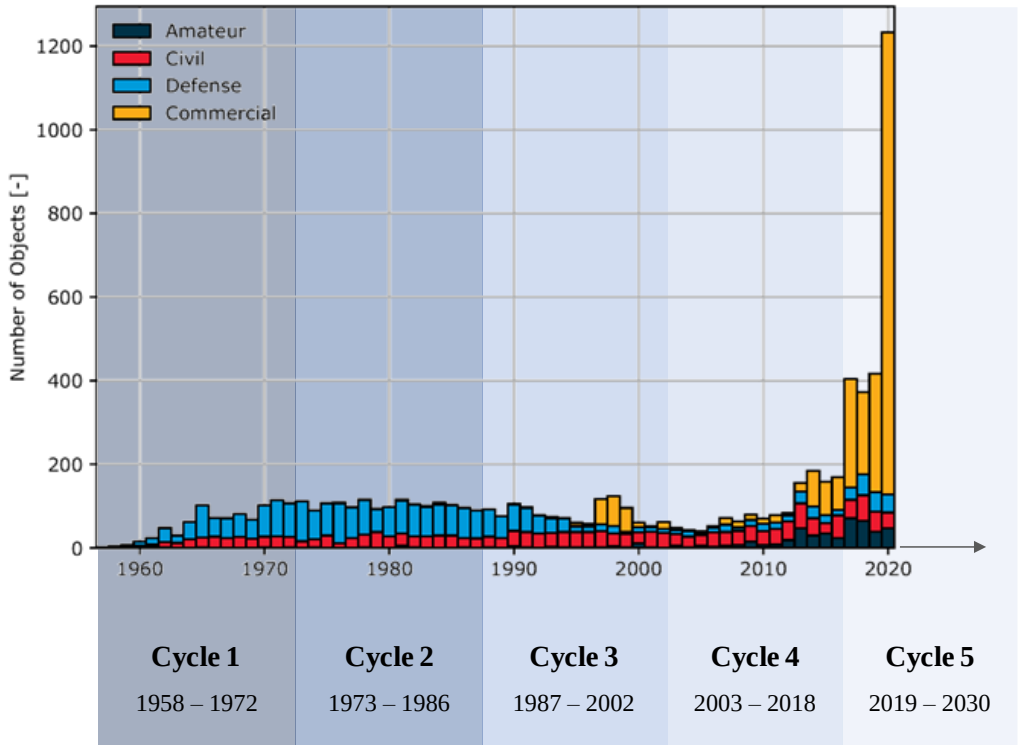

Figure 1.1 – Evolution of the launch traffic near Low Earth Orbit (LEO) per mission funding and the main development phases of the space industry.

With the end of the tensions between Americans and Soviets at the beginning of the 90s, which mainly led to the decrease of the number of military programs, could begin a phase of international cooperation and technology transfers leading to the creation of the second generation of space stations – MIR and the ISS – built in a multilateral way. The first large-scale commercial applications have also emerged thanks to the technological advances made so far for military purposes and the creation of large industrial groups such as Airbus – EADS at that time – in Europe. While on Earth digital tools began to spread at this period and gradually replaced the analogous equipment, the constraints of the space environment, and mainly to the radiative environment that reigns there, did not allow to integrate them as widely in space systems. In addition, access to space was still limited to a few multinational companies at the time, and the cost of launch used to represent a very large part of the budget of satellite projects. For these two reasons, commercial satellite manufacturers developed high-power satellites (several tens of kilowatts) to be placed in geostationary orbit (at about 36 000 km) in order to limit the number of launches required – since each satellite can cover a wide geographical from this orbit – and thus limit the implementation and operating costs. This allowed the development of satellite television and appeared to be a complement to terrestrial infrastructures for mobile applications.

In the 2000s, it is all the same the democratization of the digital technologies in the ground segments, which allowed the trivialization of the use of the space systems in the daily uses by bringing the necessary flexibility to the overall system. In parallel, the advances on microelectronics – not only digital components – material sciences, but also computers, allowed to develop small-satellites, micro-satellites and nano-satellites embedding more and more intelligence. Thanks to the reduction of the size and weight of the satellites, it has been made possible to send several satellites per launch and thus reduce the cost per satellite. This decrease has allowed the emergence of smaller national space programs and accelerated the globalization of space activity, developing a global value chain. It is also at this time that appeared large private groups with their own space program, not acting as a simple spacecraft manufacturer anymore like the industrial groups used to do until then. These actors are well known to the general public and have instilled the upheavals that the sector knows today: SpaceX, Blue Origin, etc.

Although their methods are radically different, going into space is not an easy thing and it took these companies almost 15 years – like almost everything in the sector – to succeed, and they are only now starting to see the fruits of their investment. However, the changes are no less spectacular as shown by the tremendous increase in the number of satellites put into orbit in the last 5 years shown in Figure 1.1. The facilitation of access to space leads to a disruption of the infrastructure in terms of telecommunications. Indeed, the ability to launch more satellites, allows to place them on lower orbits to reduce the latency of communications, with an equivalent geographical coverage, making it possible to provide a fast internet connection – bidirectional link – almost everywhere on Earth, where the distance only allowed broadcasting in GEO systems.

To make this possible, in addition to achieving the digital revolution of the space segment, it has also been necessary to provoke the industrial revolution of an entire sector, while most of satellites are still integrated by hand. This is what is called the New Space trend.

But the New Space trend is not only limited to commercial applications. It has a deep influence on the entire space sector, even on the historical space agencies. These lasts can concentrate their efforts back to exploration missions, whose interest in terms of influence and prestige is revived with the accentuation of international tensions and allow the developments of large scale projects: return to the Moon and set up a permanent base there, create a lunar orbital station as a "gateway" to the rest of the Solar System and of course, go to Mars.

1. 1 Introduction to space systems

Whatever its mission, a space system is always composed of two distinct elements which will be detailed in the following.

1. 1. 1 The ground segment

A spacecraft cannot fully accomplish its mission alone. In the same way that talking on a phone only makes sense if there is someone on both ends of the line, the telemetry has to be sent back to Earth where the data is used, meaning that a ground station has to complete the whole system to receive the data. Ad hoc telecommands can also be sent to support the spacecraft, to update the parameters of the different sub-systems or even update the whole on-board software (OBS).

The ground segment – and thus the humans controlling it – has also the ultimate responsibility to send the passivation command to the spacecraft at the end of its mission, which corresponds to the removal of all the remaining energy contained in the vehicle. In practice, it induces the release of a pyrotechnic charge which bursts the propellant tank as well as the disconnection of the batteries from the rest of the power system after having emptied them. These measures, which are put in place to limit the proliferation of space debris that could result from the explosion of an overloaded battery or a deficient tank, also include the re-entry of the satellite in the atmosphere, when possible. If they are part of the design recommendations of most space agencies, France was the first country to vote a law in 2008 to make them an obligation for every spacecraft operated by French companies [3].

But with the exception of those few functionalities still handled by the ground section due to their criticality, more and more control functions are progressively embedded in the space segment, which is in line with the need to control a larger number of satellites.

1. 1. 2 The space segment

The space segment, which merely refers to the spacecraft in opposition to the ground segment, is a complex interweaving of a multitude of subsystems. However, a multi-level classification of all these subsystems is generally applied. At satellite's scale two main parts can be dissociated.

1. 1. 2. 1 The payload

The payload corresponds to the set of sub-systems and instruments which effectively accomplish the mission of the satellite. The confusion is often done between the payload and the whole spacecraft. Through misuse of language, it is indeed common for a satellite to be named after its payload, as is the case for example with the Hubble Space Telescope or most space capsules – the payload of a crewed spacecraft. Nevertheless, the payload in itself is only an instrument of the satellite and only represent a small part of the systems composing it.

1. 1. 2. 2 The platform

The platform corresponds to the infrastructure gathering all subsystems enabling to operate properly in orbit. Among these system, one can typically find the satellite's attitude and orbit control system (AOCS), the thermal control system (TCS) but also the electrical power system (EPS) on which the present work focuses. All of them are supervised and controlled by the Data Handling System (DHS) which corresponds to all on-board software and hardware resources.

a) The Data Handling System

In conventional space systems, the DHS main component is the On-Board Computer (OBC) which behaves as a central supervisor for all other subsystems. It is responsible to collect data from the on-board systems and payloads, process that data with various type of functions and distribute the commands to the right equipment, in a fully automatic way [4]. In parallel, the centralisation of all the data allows it to send telemetry to the ground. To this respect, the DHS gives the observability and the controllability to all subsystems and makes the link between them, including the ground segment. It is subsequently one of the most critical system of the spacecraft.

Based on this, the basic concept and structure of a space system is not different from a conventional automatic system and the same control theory methods can be applied. It is indeed composed of the same parts as shown in Figure 1.2 to wit: an operator – human or computer – which determines the set points of the system, a command part that computes the control signals, and a controlled system itself which provides feedback telemetry to the command part and the operator to allow them to follow the evolution of the system.

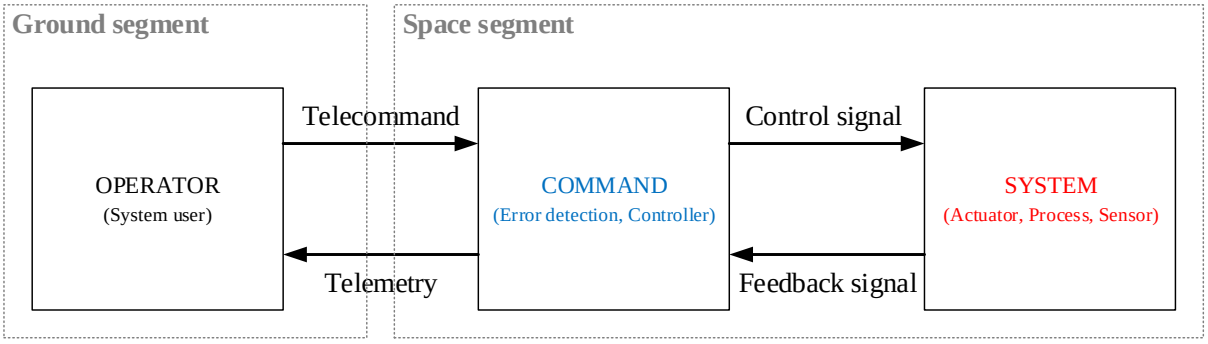

Figure 1.2 – Generic block diagram of an automatic control system applied to a space system.

The control structure can then be assimilated to a fractal tree, repeating this command-actuator bimorphism at each scale of the system, from a systemic point of view to the lowest level of sub-system, in the manner of the DHS-EPS couple which is the subject of the present study.

All these inherent characteristics explain the important contribution of the space industry on control engineering, especially in its early phases of evolution during which the domain had necessarily to be innovative on this subject.

In the current context, the enormous growth in the number of objects in orbit and therefore in the amount of available data, pushes the ground segments to focus on the aspects of data management and its accessibility by a large number of users – bulk-downloading, big data approaches, open data policies, etc. – and to turn away more and more from the control aspects, in favour of a greater autonomy of the space segment.

In order to do so, more “intelligence” has to be embedded but without overloading the OBC and drastically increase its criticality. A solution could be to distribute parts of its functions directly locally in the subsystems such as the EPS. However, this requires to develop a deep understanding of how they are working and of the stakes which drive the way space systems are designed. Thus, before the most widespread EPS systems are presented, and to fully understand the reasons that led to their definition, it is important to define all the constraints that must be taken into account, otherwise, certain choices may seem incomprehensible.

1. 2 Major space systems constraints

Technologically speaking, and quite surprisingly for neophytes, most space systems do not correspond to the most advanced systems, using leading-edge components. This is particularly remarkable when compared to other technological sectors to which we are accustomed, such as automobiles or smartphones, for which the time-to-market of an innovation is very short. The main reason is that the room for maneuver is small and there is no place for doubt in such an environment. It is generally said that on earth stresses add up while in space they multiply among themselves. From this observation, the most notorious performance of space systems is to succeed in overcoming all these constraints to fulfill their function. Thus, in such a context, notions like heritage – feedbacks on flight proven solutions – take a particular importance and each design change must be justified by a significant added value to counterbalance the "risk" induced. To be able to understand the reasons which led to the current EPS architectures both in terms of functional and physical distributions, the definition of performance criteria to be met is essential.

1. 2. 1 Reliability

As maintenance is not possible in space and that the space environment is challenging for the systems, reliability is a major concern of their design to be able to guarantee the proper operation on a given duration, typically defined in the specifications between 5 and 15 years. From this requirement and based on the criticality of every system and subsystem a Reliability, Availability and Maintenance Study (RAMS) is performed. Its aim is to identify actions and precautions to take at design phase on systems architecture as well as components choice in order first to limit the risk of failure and then to be tolerant to faults if they occur anyway.

1. 2. 1. 1 Resistance to environmental stresses

In conventional systems, the limitation of the risk of failure is mainly achieved by the choice of components able to withstand the severe operating conditions that the space environment offers such as the UV radiations, repeated large temperature variations in short laps of time and the operation in the vacuum. Concerning purely electronic systems which can be protected inside of the satellite, the main concern corresponds to the radiative environment. Space typical radiation spectrum is composed of three main types as explained in [5]: electromagnetic particles trapped in the Earth's magnetic field – Van Allen radiation belt –, particles emitted during solar particle events such as solar flares and galactic cosmic rays which are high-energy protons and heavy ions travelling through the universe. Standard integrated circuits and more especially micro processing components are particularly sensitive to these events.

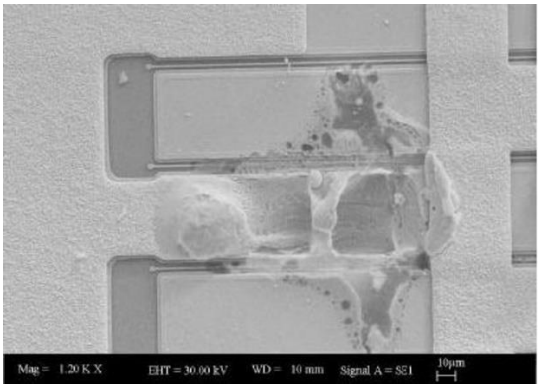

Figure 1.3 – Latch-up caused by an heavy ion [6].

Indeed, [6] details that radiations can induce software upsets, memory bit flips, transistor gate ruptures and runaway short circuit called “latch-up”, as illustrated in Figure 1.3. These phenomena are called Single Event Effects (SEE) since they happen only punctually. To this regard, the miniaturization of electronic components makes them more vulnerable to disruption by incoming charged particles.

In addition to this, a sustained particle bombardment also creates defects within oxides and displacements of atoms in the semiconductor crystal lattice which cause gradual degradation of the components performances.

The particularity of radiations also relies in the fact that the solutions to protect systems from them – such as shielding – have limited efficiency. In order to tackle this challenge, the choice of technologies more robust have been made, such as the FPGA instead of microcontrollers and radiation hardened references have been developed. Screening and the choice of high quality class components complete the solutions which are conventionally used in space systems. However, these methods have a significant impact in terms of cost but also in term of diversity of components available.

Finally, in the case of power electronic subsystems, another challenge is to guarantee their proper functioning throughout the life of the satellite with regard to their electrical environment. Indeed, a sustained operation at high power is source of stress for the materials due to the dissipation – and thus the temperature variations – it induces. The notion of stress, for any component, can be defined in a purely qualitative way as the proximity between its values of use and its maximal values as rated in its specification. Generally speaking, the more a component is stressed, i.e. the more the component is used around its limit values, the faster it will tend to deteriorate, even while remaining within the authorized nominal operating range. Thus, “derating” rules are applied when sizing components to prevent premature aging. This typically corresponds to apply a margin of 20 percent on every characteristic values like the maximum voltage, maximum current, or temperatures.

1. 2. 1. 2 Fault tolerance

In spite of these restrictions the choice of the components, some failure can still occur like in any system which have been working for years without maintenance. To be able to react appropriately to this eventuality, the most likely failure cases for each component and sub-system are studied and in function of the type of component and the criticality of the function it implements, some solutions can be put in place to respect the required level of fault tolerance. The aim is then to reduce the number of single point of failure of the system, defined as the elements on which one fault or malfunction could cause the entire system to stop operating, by introducing adaptation on systems architectures – such as redundancy, cross-strapping or majority voting – to be tolerant to one or more faults simultaneously.

From a hardware point of view, to address the need for rapid response and active reconfiguration between the nominal and redundant modules when an issue is detected, a dedicated function is integrated to the OBS and is composed of three phases: The Fault Detection, its Isolation and the system Recovery (FDIR). An eloquent example of this process happened on June 13, 2021, when the payload computer of the Hubble space telescope experienced a problem which automatically placed the instruments in a safe configuration and suspended science operations. On July 15, the NASA operation team – from the ground – switched the spacecraft to backup hardware which returned it to operational status.

Regarding the software point of view, Time and Space Partitioning (TSP) is employed to segregate concerns between functionally independent software components to contain and isolate execution faults [7], [8]. Indeed, integrating several software functions in the same computing core or without allocating a time limitation to each function’s execution leads to a combinatorial explosion of the number of tests

cases and increases the complexity of the software integration, verification and validation process. To avoid these issues, uncorrelated functions have to be implemented in isolated computing cores (space partitioning) or if not possible, time windows and memory areas have to be allocated to every function executed in a single computing resource in order to avoid a general paralysis caused by a computational lag or bug of one function (time partitioning).

These considerations, specific to digital components, associated with the fact that a centralization of data is often necessary, show the interest of adopting a systemic approach to consider and design the DHS subsystem and justify the fact of considering it as a subsystem in its own right whereas it could, at first sight, be perceived only as the control part of the other subsystems.

This approach of implementing reliability in conventional space systems is deeply challenged by the new space actors. Since some design solutions as simple as components redundancy can be applied and bring sufficient guaranties, and since these solutions are most of the time anyway applied to be compliant with the fault tolerance requirements, the use of COTS appears more cost effective and, in the same time, opens access to a much wider number of references. The flexibility it brings can then be used to tackle the other –numerous – challenges that space systems face.

1. 2. 2 Embeddability

In a spacecraft, the systems have to be able to be integrated in a limited environment, where all physical features are strictly restricted. This ability, called embeddability, corresponds to a combination of characteristics which have to be respected.

1. 2. 2. 1 Volume and weight

The global cost of a satellite – including design, launch and operation – is quasi-proportional to its weight and the maximum volume and mass is limited by the launcher's characteristics.

In these respects, the EPS corresponds to one of the most challenging subsystems since its components are the biggest, at least at the scale of the platform, as it can be observed in Figure 1.4, showing a Myriade platform with its lateral faces open.

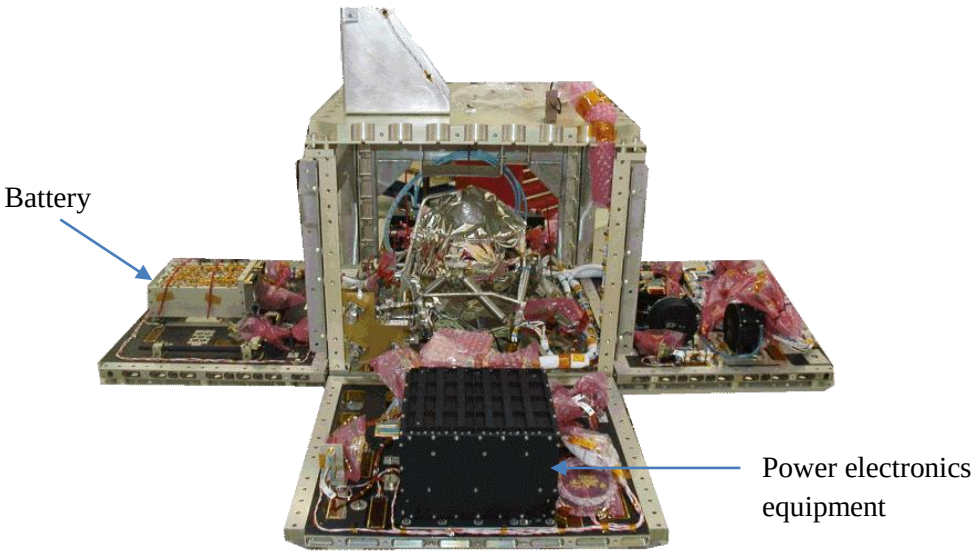

Figure 1.4 – The Myriade platform

1. 2. 2. 2 Thermal dissipation capacity

A second aspect to the evolution in a limited environment is that the effects – or requirements – of the systems operation must be manageable. This is the case of the thermal regulation which is an important concern in satellites and within the equipment. Indeed, a particular attention is paid to the distribution and the homogeneity of thermal load. Convection is a principle which only works in a fluid environment which is not the case in space. Consequently, all the heat produced by power devices has to be channelled by conduction inside satellites to specific heat sinks which dissipate this lost power through infrared radiations in the space environment.

1. 2. 2. 3 Routing complexity

Last, considering the rising number of systems embedded in satellites, the routing of all data and power distribution lines becomes always more complex and very restrictive precautions must be put in place during the integration to minimize the probability of misrouting as shown in Figure 1.5. The proximity of such a number of wires, converging at the same place also induces some challenges in term physical layout as several hundred connectors can be concentrated in very small volumes.

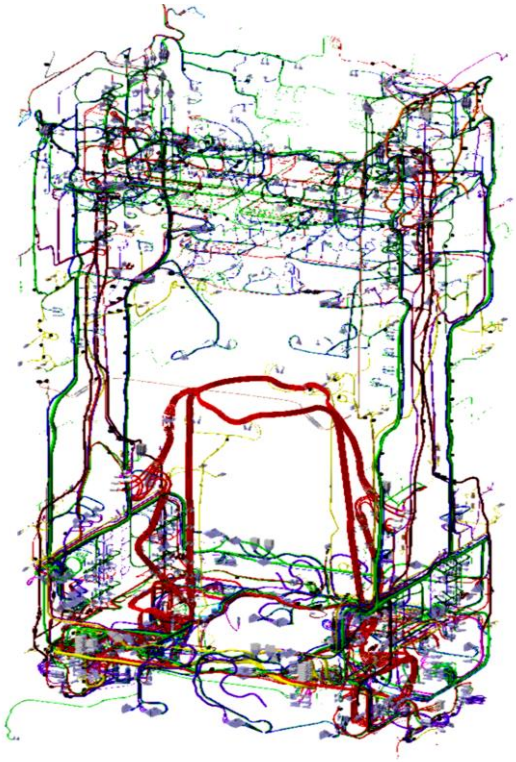

Figure 1.5 – 3D view of the harness bundles in a large telecom satellite.

This three cases are usually the subject of specific studies to clearly define equipment's mechanical, thermal and electrical interfaces. This is generally made at the scale of each sub-systems defining the different modules composing it, which gives a certain modularity and scalability to the system.

1. 2. 3 Modularity

In an industrial context, modularity can be defined as the property of being composed of standardized units making them easy to assemble and flexible to be reused.

1. 2. 3. 1 Modular system

In complex system such as space systems, a modular definition of the systems is generally used since the complexity of the overall requires to split the work into different packages owned by different persons and even different entities. To this respect it can be stated that conventional space system has been developed as modular system, by necessity.

The most common approach is to define modules thanks to functional definitions and to identify the way each module is linked to all others and this, at each abstraction level of the system [9]. To this respect, in opposition to the integral system approach, the modular approach is based on two fundamental elements: modules and interfaces. As detailed in [10], fully modular systems shows three main advantages:

- The final integration and test phases is greatly simplified
- The stabilization of the interfaces allows to swap one module with another easily
- The flexibility it offers in terms of development process by the succession of asynchronous phases – from one module development to another – cadenced with synchronization milestones.

However, this advantages are only fully exploitable if the modular approach is also put in place at the design phase of the systems. Indeed, this classification, which can be defined a posteriori of the system's development, has to be dissociated from a modular approach applied to the system's design.

1. 2. 3. 2 Modular design

The adaptation of the principle of modularity at the design phase corresponds to the taking into consideration of the modular approach at all development phase, and more particularly at early phases of a project development. Two major principles can then be defined as guidelines.

The first one states that, at a given abstraction level of the system, the definition of the different modules should be done in order to reduce their interdependence and tend to be as close as possible to the functional definition of the system. This induces two effects. The first one is the fact that it allows the functional partitioning mentioned earlier which is required for both hardware and software functions to reach the required reliability level.

This also is the prerequisite for the second principle of modular design which states that the interfaces between the modules have to be simplified at maximum. This is generally achieved by the implementation of standards for mechanical, thermal and electrical interfaces in domains such as computing engineering. In the context of space systems, some technological limitations such as the lack of small digital components to be distributed in the different units until recently, did not allow to significantly simplify the interfaces especially concerning the electrical interfaces as no digital data bus was available for a large deployment as it was the case in the car industry for example thanks to the introduction of the CAN bus in the 90s.

In addition to this, in the conventional way of doing in the space industry, "reuse" is generally used instead of standardization, which induces side effects. Indeed, in a context where "heritage" takes a central role in the design of elements, "small" adaptations of existing systems are most of the time preferred to the modification of the overall architecture. But the modification of a so-called modular system, as small as it may be, can result in a system that does not have the advantages mentioned above anymore and thus even if its modular structure may not seem altered and first glance. To assess this in the frame of EPS, the most conventional current architectures are presented in the next section.

1. 3 Conventional EPS

The aim of the EPS is to generate, condition, store and distribute the electrical power to the whole system. In other words, it is the first link in the food chain and if it stops working, the whole system is lost. The resulting need for robustness and reliability in addition to the particularly isolated and hostile environment in which it has to operate have driven the EPS design choices and lead to a very high efficiency system, electrically speaking.

The purpose of a power system is to provide a continuous electrical supply to a set of loads. These include not only the satellite payload, but also all the platform components requiring electrical power. Thus, apart the loads, in a system level approach, three main components can be defined, corresponding to the three main functions given above.

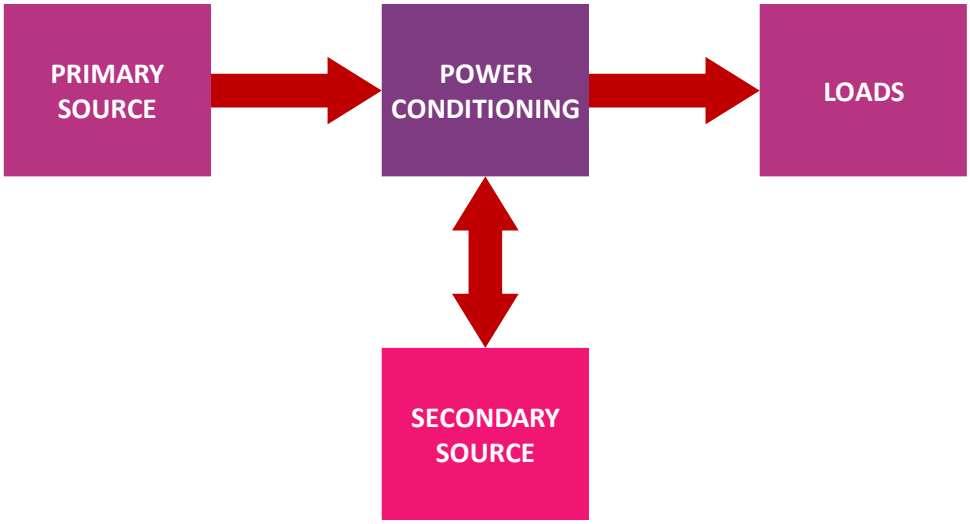

Figure 1.6 – Generic electrical power system representation.

1. 3. 1 Components

1. 3. 1. 1 Primary source

The first component is the primary power source which is the module which produce the electrical power required by the system to operate. However, nothing is created, nothing is lost, everything is transformed. Hence, the primary is most of the time a multi-physical transformer which converts an input resource, such as thermal or mechanical energy for instance, into electricity.

Thus, the choice of the technology of the power production unit is an important concern and is mainly driven by the ease of access to environmental resources. Primary batteries – single-use – made of electrochemical cells as well as Radioisotope Thermoelectric Generators (RTG), which convert heat from radioactive material into electricity, can be used when the access to external resources is too limited.

However, for inner solar system missions, primary sources are conventionally photovoltaic (PV) panels since the relative low distance to the Sun enable to receive an appropriate amount of power from it with an acceptable surface of PV.

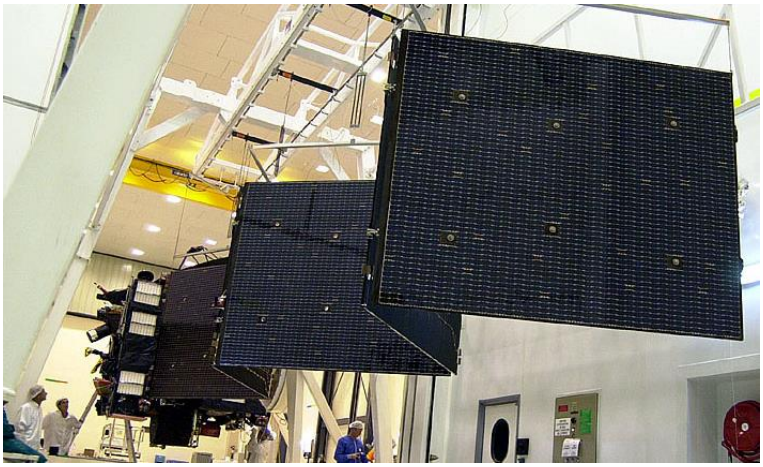

Figure 1.7 – Rosetta probe's solar arrays during deployment test [11].

In the case where the available primary source is not continuous, a secondary source is required: this is a source capable of delivering so-called secondary energy, i.e. directly in the form in which it is used – electricity in the present case. This corresponds to storage components, which are recharged during periods of access to resource by the primary source in order to supply the energy needed to operate the system during periods when such access is no longer available.

1. 3. 1. 2 Secondary source

The aim of the secondary source is to store energy to be able to balance the energy consumed during the period of unavailability of the primary source that is to say during eclipses when PV panels are used.

Most of the time, rechargeable accumulators are chosen. Nickel-Cadmium and Nickel-Hydrogen batteries, used to equip all satellites until 2001. Since, Lithium-ion batteries have gradually replaced them thanks to its good performances and versatility, with the best compromise between power and energy density in particular as shown in Figure 1.8. In some cases, it can also be interesting to combine several types of technologies to meet specific load requirements. Super capacitors, for instance, are particularly well designed for load profiles with very high power peaks.

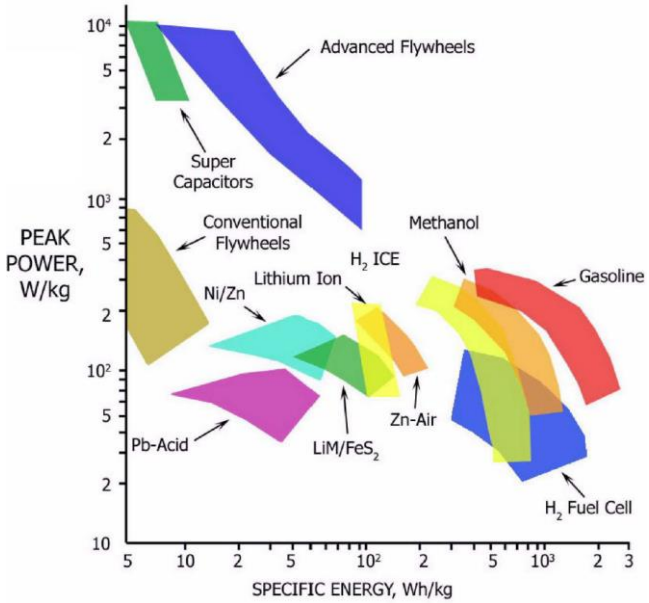

Figure 1.8 – Ragone plot of energy storage technologies [12].

Figure 1.9 – Galileo satellite's battery [13].

1. 3. 1. 3 Power electronics

Finally, in order to interface the primary and secondary sources as well as the loads, power electronics is required. Two main sub-functions can then be defined: the power conditioning and the power distribution functions.

In conventional architectures, these functions are centralized in the Power Conditioning and Distribution Unit (PCDU). As one can observe in Figure 1.10, the PCDU is composed of stacked electronic cards that form 3 sub-units:

- The Power Conditioning Unit (PCU) which gathers all the actuators of the EPS which manage the electricity fluxes and required conversions from one level of the systems to another.
- The Power Distribution Unit (PDU), which is typically composed of Latch Current Limiters (LCL) whose aim is to protect the system from possible short circuits and other faults which could induce over currents on outlets.
- The TM/TC and control units which can be described as the local DHS units, making the link between the On Board Computer (OBC) and the PCU and PDU. In addition, it is also responsible of acquiring all measurements from the battery and the solar arrays as these lasts do not embed any processing capacities.

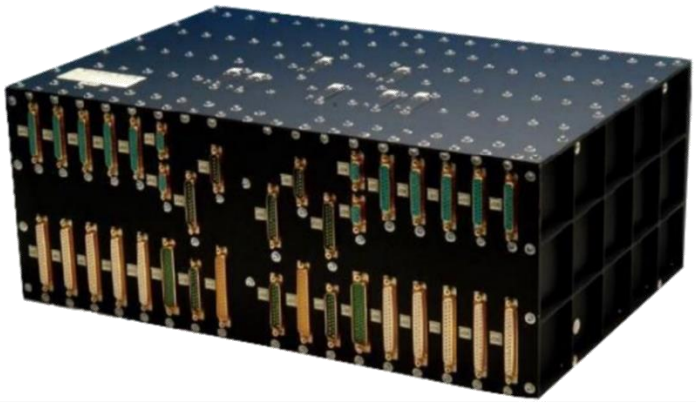

Figure 1.10 – Sentinel-3 satellite's PCDU [14].

It has to be noted that this can slightly differ from one mission type to another. For GEO missions for example, the PCU and PDU units are two separated units. And even if at this level of abstraction the main components are the same, this corresponds in fact to two different approaches in term of electrical architecture of the system.

1. 3. 2 Electrical architectures

Speaking about EPS architectures necessitates to introduce two notions: the distribution network topology on one hand and the power conditioning and distribution functions location in this network, on the other hand. Depending on the chosen distribution network topology, different options are available to integrate the EPS regulation and protection functions. Taking the example of a radial distribution scheme, two possible integrations can be identified and modify the physiognomy of the distribution architecture.

A centralized architecture can be adopted giving the EPS a star shape as shown in inset a) of Figure 1.11. In this functional architecture, all functions are gathered in the same unit and the same place, around the primary power node. Even though the primary power node is most of the time integrated inside the central unit, it is called primary power bus in the literature. It can be noted that, in this architecture, the conditioning and protection devices, which are specific to each distribution lines and each power load or power source, are deported from these lasts.

The concept of distributed architecture is precisely at the opposite, that is to say that it consists in placing the power conditioning and protection functions at the neighbouring of their related power terminals. This implies the primary power bus to be distributed in the whole satellite to interface the distributed modules. As shown in inset b) of Figure 1.11, this results in a distribution scheme which is more likely to integrate distributed energy resources (DER) as the key central component is no longer a power conversion equipment – whose interfaces usually exactly fits to number of distributions lines to provide – but the primary power bus on which any load or source can be connected at all points.

It can be observed that the choice of the type of functional architecture is not independent of the choice of the distribution topology. It is for example impossible to implement a centralized functional architecture to a loop distribution topology and conversely, it is possible to implement any distribution topology with a distributed architecture. In contrast, a modular functional architecture allows to implement both centralized and distributed functional architecture.

It is important here to dissociate the electrical architecture and thus the requirements it induces to electrical power lines introduced above, from the DHS architecture which would rather induce requirements on the data interfaces. It is all the more important to ensure their compatibility, a sine qua non for the proper functioning of the overall system.

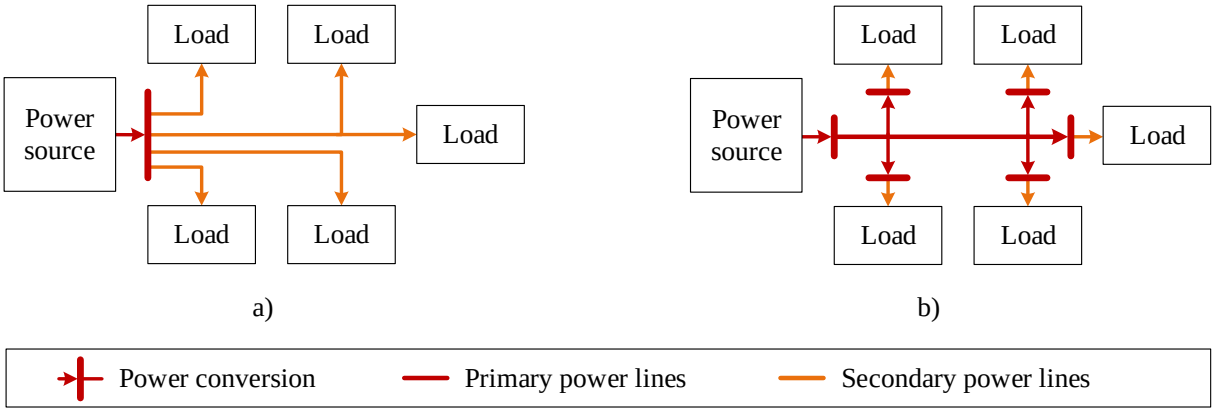

Figure 1.11 - Centralized (a) and distributed (b) radial power conditioning and distribution architectures.

In conventional space EPS, two main alternatives can be found to realize the conditioning and distribution functions [15], [16], [17], [18], [19].

1. 3. 2. 1 Non-regulated primary bus architecture

The non-regulated bus (NRB) architecture, presented in Figure 1.12, is the most common in small and medium-sized satellites. In this architecture, the primary bus is directly connected to the battery which therefore imposes its voltage. Thus, the bus voltage changes depending on the battery State Of Charge (SOC). The PV panels are connected to the primary bus – and consequently to the battery – thanks to a PCU which manages the power production from the PV, to regulate the battery charge as well as the loads power supply. This unit is most of the time composed of Direct Energy Transfer (DET) circuits – sequential shunt composed of a shunt switch and a serial anti-return diode – since there is no need of dynamic response to regulate the bus as the battery imposes its voltage [16]. Near full charge, the PV sections are shunted progressively to avoid overcharge of the battery.

Finally, protected distribution power lines are generated by the PDUs thanks to LCL and allow to connect the different secondary distribution lines to the loads – including the PCDU itself that is self-powered.

The simplicity of design and the low number of equipment required allows this architecture to reach very high reliability both in terms of equipment failure risk and electrical operating stability and for very low costs. In addition, for LEO missions for which the battery cycling is constant and regular all along the satellite's life, there is no interest to dissociate the battery from the primary power bus. These characteristics have made of this architecture the most widely used on low-power satellites for decades.

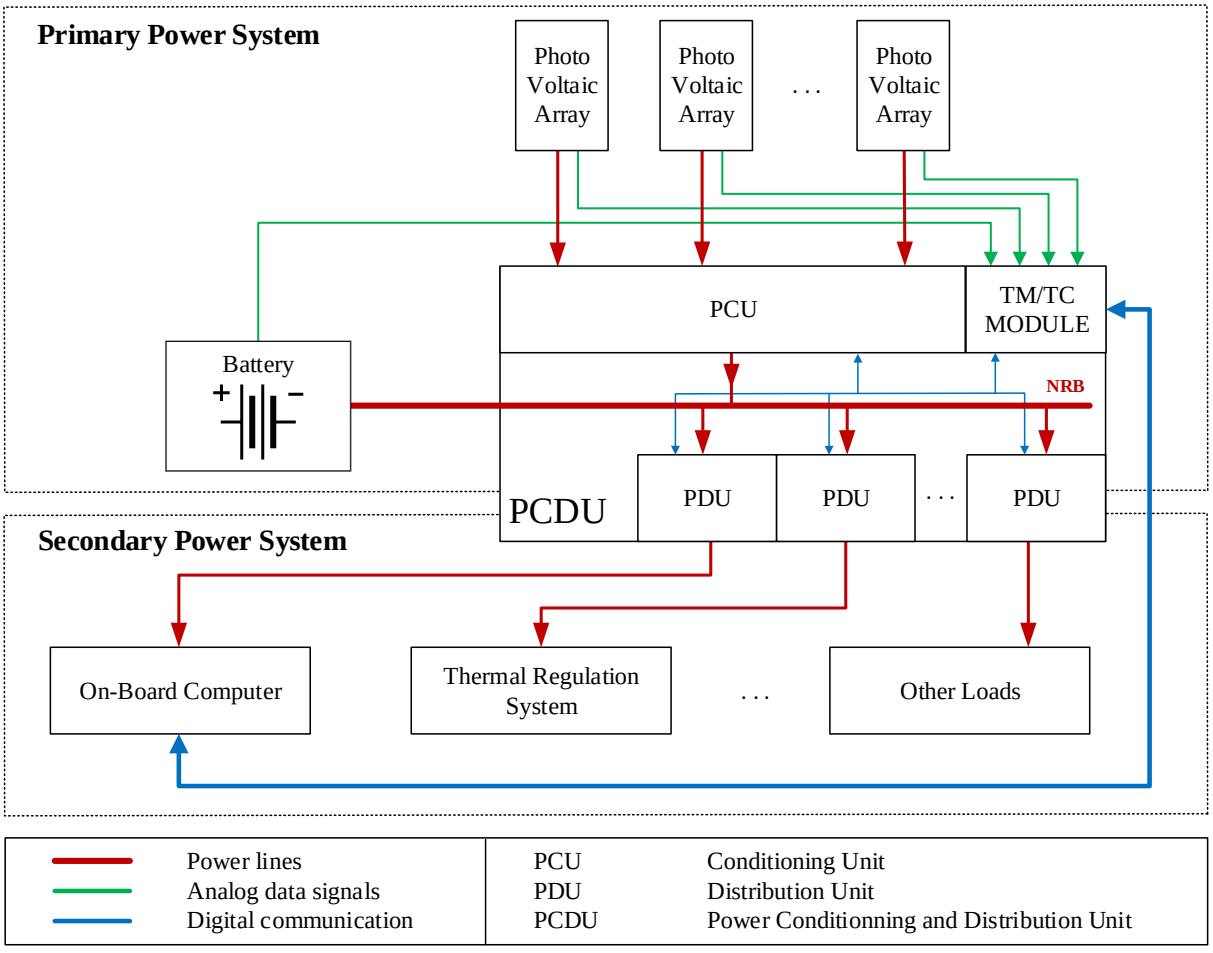

Figure 1.12 - Non-Regulated Bus (NRB) architecture functional diagram.

However, this architecture shows a significant lack of flexibility in use, particularly in terms of battery management and sizing. Indeed, as the battery and the solar panels are directly connected to each other in this architecture, their design and especially their layout needs to be especially determined to be compatible from one to the other, for all possible environmental and electrical conditions. This makes this architecture particularly unadaptable and drives to add margins on every parameters of the system, leading to an overall oversizing in regards to the actual need.

In order to bring a solution to this, while keeping the benefit of the NRB architecture, some derived architecture have implement a power converter in place of the DET. Although the converter induces losses, quasi non-existent with a DET, it generally improves the energy transfers by allowing to control the PV operating point.

With this kind of converter and by the simple addition of a power diode between the battery and the primary power bus, a Semi-Regulated Bus (SRB) architecture can be implemented, regulating the bus voltage directly from the PV serial converter during the illumination phases, and letting the battery impose its voltage during eclipses. However, this architecture requires a specific system for the battery charge. Nevertheless, it has often been implemented in series of satellites whose mission profile included only rare eclipses, or eclipses that were much shorter than the periods of sun illumination such as the first generations of GEO satellites.

1. 3. 2. 2 Fully-regulated bus architecture

For GEO applications in particular, the batteries reach much higher Depth of Discharge which induces wide voltage variations on its terminals. Indeed, in these orbits, eclipses only occur during relatively short periods of the year around the equinoxes which allow to reduce the margins applied to their sizing. In this context it becomes interesting to be able to regulate the power bus to a constant value to reduce all the loads requirements in terms of input voltage operating range. This is what the fully-regulated bus (FRB) architecture implements, as presented in Figure 1.13.

Compared to the NRB architecture, a Battery Charge/Discharge Unit composed of a bidirectional converter could be introduced and integrated to the PCU, decoupling the battery and the bus and allowing to set a constant voltage independently of the battery nominal voltage and of the operating phase – day or night. This improves the use of every terminal since all operating points are decorrelated from each other and can be specifically set to match each terminal's optimum operating point. The sizing of each can thus be realized as close to the need as possible.

In both cases, the modularity in terms of the system scalability is handled at the PCDU level, by adapting the number of sub-modules stacked in it depending on the need of maximum power of the mission. On the battery side, the same approach is used with the definition of cell modules (CM) which allow to adapt the size of the whole battery.

In terms of interfaces, even if the electrical power distribution network is quite simple due to its radial configuration, the data links is much more complex since for every analog link shown in the graphs, several tens – and even hundreds – of electrical signals are actually implemented, requiring recurrent compatibility analysis and increasing the risk of errors at integration. This is mainly induced by the high degree of interdependence between the different modules and that in fact the PCDU not only deal the power conditioning functions but also the acquisitions for the battery and solar panels which is contrary to the principle of function partitioning required in modular systems.

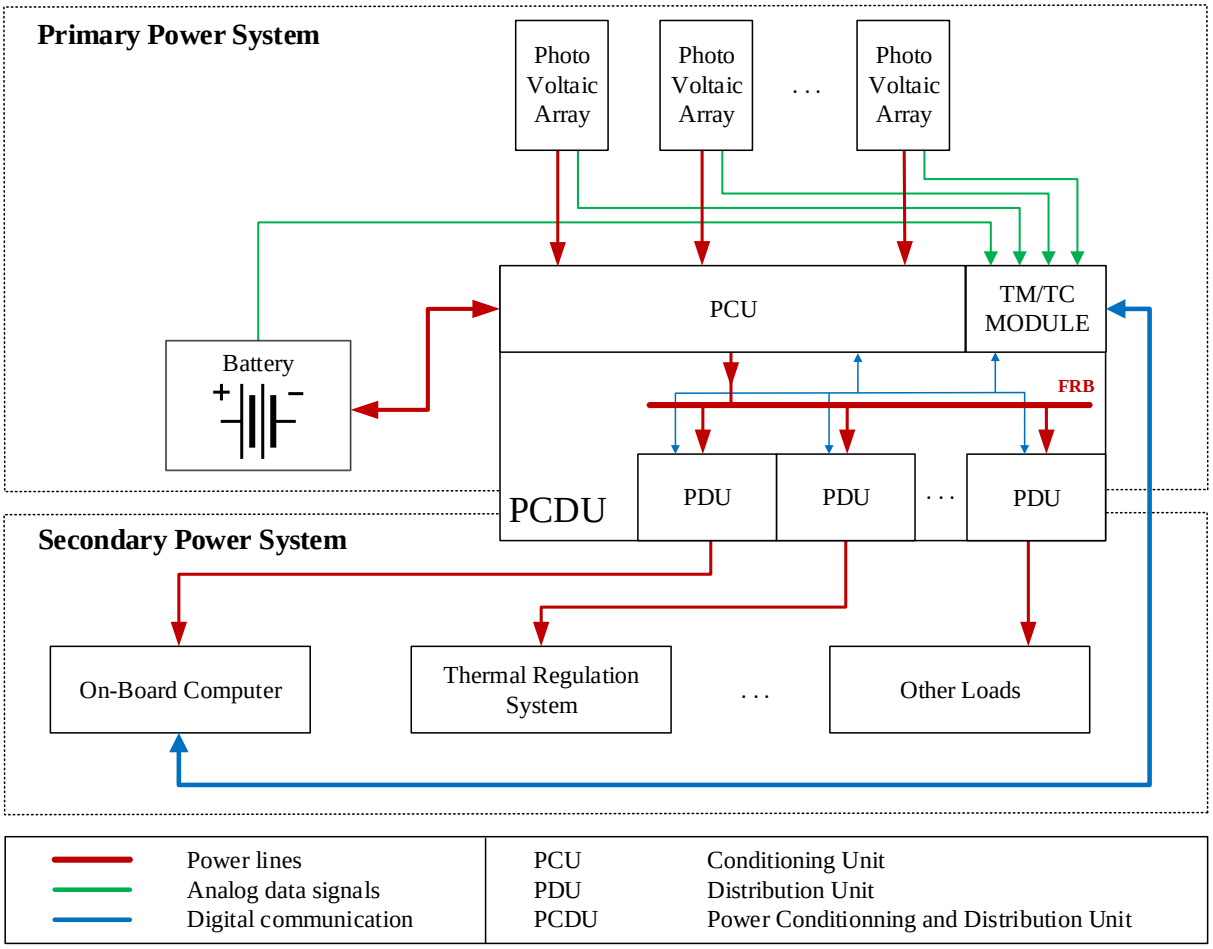

Figure 1.13 - Fully-Regulated Bus (FRB) architecture functional diagram.

In addition, considering new needs, such as In Orbit Assembly (IOA), on line EPS evolution or technology hybridization, this approach suffer from a significant lack of flexibility and modularity inherently due to the centralized feature of their electrical architectures. One of the main objectives of the project in which this work is integrated is to propose a solution to these drawbacks by defining a truly modular architecture.

1. 4 Synergies

When it comes to modularity and flexibility, the design logic is reversed compared to what is presented in the previous section: the spacecraft electrical requirements are not precisely determined and have to be anticipated. The only constant input parameter which is relevant to consider is the fact an electrical network will be needed to interconnect power sources to loads, whose type and number are a priori unknown. It is therefore a completely opposite approach to the conventional one. In this paradigm, the distribution network and in particular the primary power bus, has to be managed separately from the power conditioning and distribution functions which are intrinsically linked to the power terminals they are related to, whether on the source or the load side.

This is typically what happens in the systems which are presented in this section, which are constantly evolving. Whether technologies are for Earth applications or in the space industry, it can be interesting to study them, due to their similarity with satellite's EPS. Two of them are particularly interesting in term of electrical architecture since they already implement modular solutions.

1. 4. 1 The ISS

The ISS EPS gathers all the characteristics of a modular space system but at a very large scale. The total power supplied by the Photovoltaic modules can reach up to 248kW [20] and makes the ISS the world's largest DC power system in space [21]. Due to its size, and because it was impossible to launch such a massive spacecraft at once, IOA technics had to be used. This constraint makes modularity an inherent characteristic of the ISS. The American, Russian, Japanese and European modules have indeed been progressively added to the rest of the station and the EPS had to keep evolving to allow those changes.

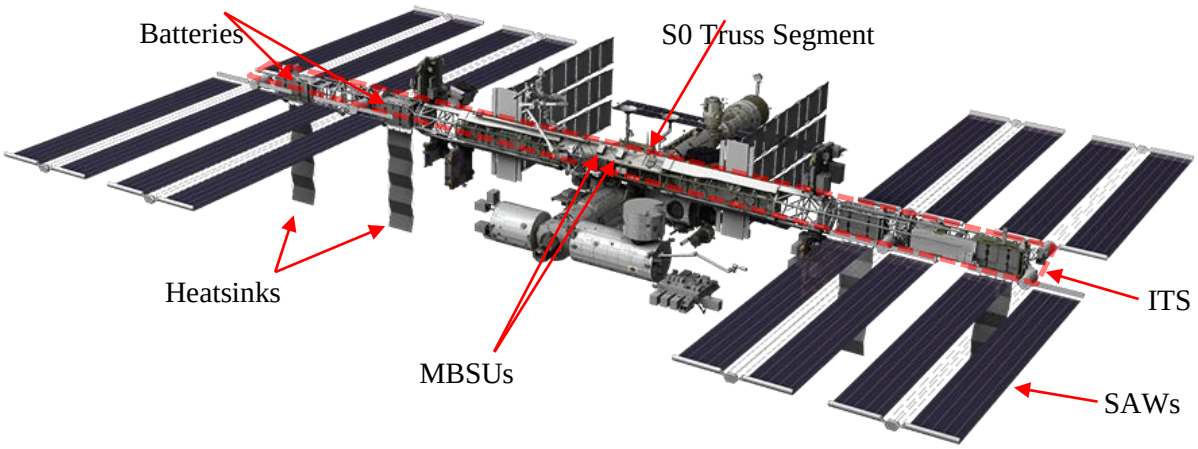

Figure 1.14 - The International Space Station (ISS).

The ISS EPS is composed of 4 PV modules as it can be seen in Figure 1.14. Each PV module contains two Solar Array Wings (SAW) mounted on the Integrated Truss Structure (ITS), the backbone of the ISS. The power system is thus separated in 8 power channels – one per SAW – all composed of the same set of units as illustrated in Figure 1.15 [22]. Most of primary conditioning and distribution power units are fixed outside of the ISS, directly on the ITS, at the neighbouring of the power generators. These modules allow the distribution of the thermal load and are equipped with their own heatsink which can be seen in grey in Figure 1.14, under each pair of SAW. Other elements are located on the S0 Truss Segment, the central structural section of the EPS, which allows the connection with the rest of the ISS modules and more particularly the inhabited parts of the station.

Sequential Shunt Units (SSU) handle the SAW primary power regulation by shunting and un-shunting solar array sections based on the same technique as DET presented previously. The operating set point, provided to the SSU by the OBC, is defined to maximize the power delivered by the solar array during illumination phases. When the SSU power output exceeds the power demand, the bus voltage tends to rise above the set point and that triggers SSU to shunt sections which reduces the power output, and vice versa [23].

Battery Charge/Discharge Units (BCDU) manage the battery charges and discharges. When the solar array can produce sufficient power, BCDUs charge the batteries, by injecting the appropriate amount of current to the batteries. When the solar array is not able to supply all the power anymore, the primary bus voltage drops under the SSU set point, even with all sections connected, and once it reaches the BCDU set point which is slightly lower, BCDUs begin to regulate the power bus by discharging the batteries. This is achieved by bidirectional DC/DC converters in the case of the ISS, making it a FRB architecture [4].

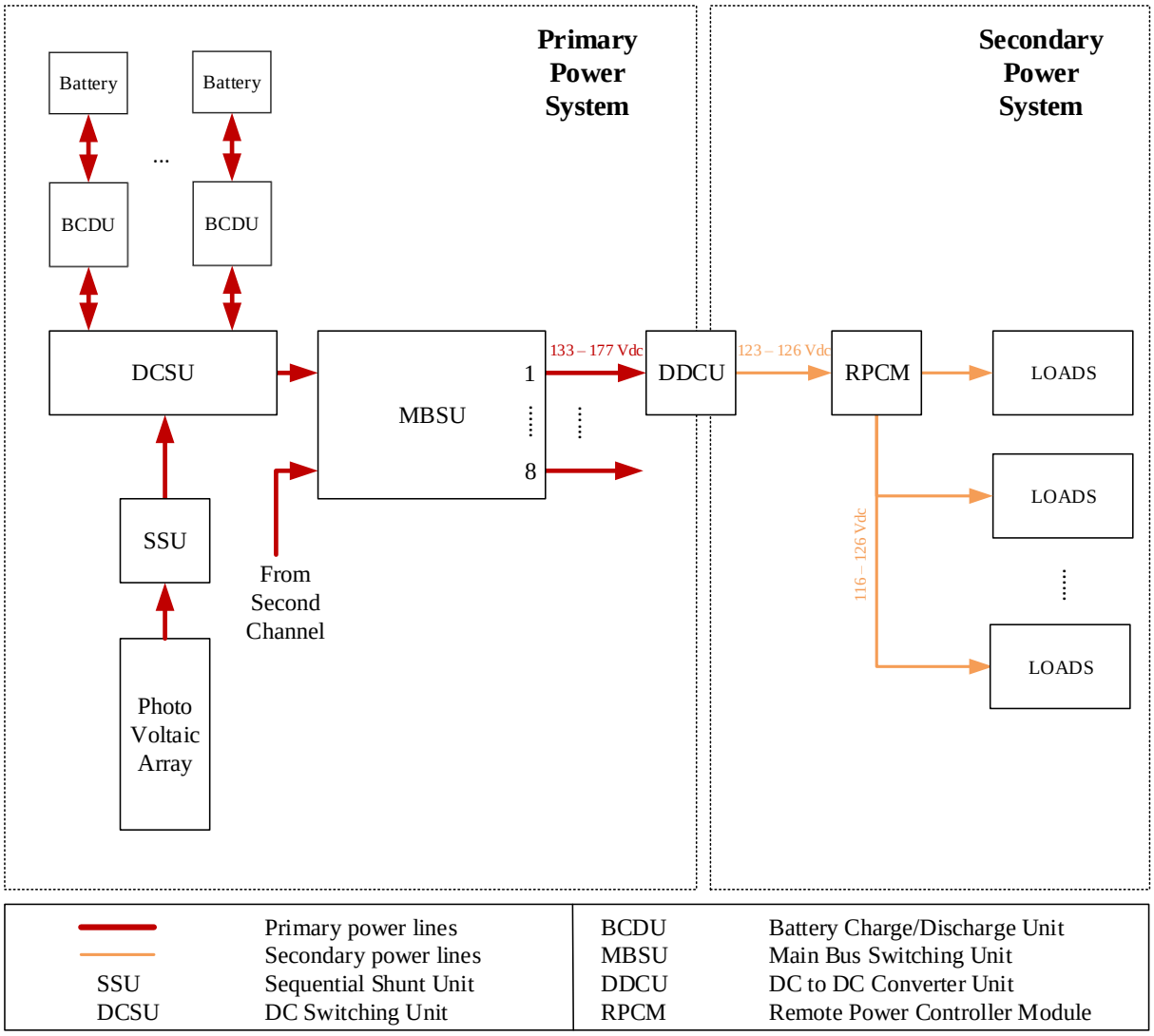

Figure 1.15 - The ISS's EPS architecture.

Main Bus Switching Units (MBSU) and DC Switching Units (DCSU) are the electrical distribution units of the EPS and so are critical parts of the power system. The DCSUs have the aim to route power between each element of a primary power channel and provides fault protection thanks to remote controlled relays. Each of the four MBSUs distributes primary power from two power channels to their associated set of loads thanks to the same type of relays. Every MBSU is however connected to the 8 sets of loads so that each power channel can supply every set of load. This choice is driven by the need of a structural redundancy for the Electrical Power generation. In the case of a failure in a power channel, thanks to MBSUs, loads initially supplied by a channel can be fed by another channel.

Finally, DC/DC Converter Units (DDCU) make the interface between the primary power system and the secondary power system. Thanks to its integrated DC converter, a DDCU can provide a tightly regulated voltage to the loads downstream, simplifying the design of their internal converters – the voltage variations are limited to ±1.5V. Remote Power Controller Modules (RPCM) are the interface between the EPS and all non-EPS equipment on-board the ISS and can either be located inside the pressurized modules or outside of the station to supply the other platform sub-systems. They are multichannel high power circuit breakers and assure the control of the secondary power flow as well as the protection of the upstream EPS devices from downstream faults.

Since the first station elements went into orbit, the ISS has changed a lot and so has the EPS. Be that as it may, most of the changes have been realised thanks to human interventions. Approximately 112 Extra Vehicular Activity (EVA) have been needed to obtain the EPS as it is nowadays. This makes a significant difference between the ISS and the system which is studied in the present document. Re-configurability in the ISS is made possible by the possibility to operate directly on the systems by sending astronauts which is most of the time not possible.

The study of the electrical system of the ISS is rich in lessons for the responses that have been made to the constraints, often common, mentioned in the previous section. Feedbacks of years of ISS's EPS operations are precious for actual developments and makes the system a well-proven technology. It demonstrates that a more distributed power architecture has already been implemented in space and can serve as a precedent.

However, the actual architecture is very similar to conventional ones at the scale of a power channel. The modularity is then brought by the adding of parallel redundant channel and the possibility to reconfigure the loads distribution which requires a specific online reconfiguration to assure the power availability at load level. To this regard, some systems which naturally guarantee the continuity of service – without the need to reconfigure the system – can be studied and used as inspiration. This is the case of the electrical grid on Earth for example.

1. 4. 2 DC Microgrids

Some obvious differences can be identified between ground based and space electrical systems such as the access to resources or the equipment's weight constraints.

The drastic needs in reliability also push to strip as much as possible the space systems of the superfluous and induce choices of design taking advantage of the simplest possible technologies such as the use of DETs instead of a converter to control PV power production modules or the choice of a NRB architecture. Yet again, in a generic ground based electrical system the approach is significantly different, generation and storage units being at the great majority connected to the DC bus through DC-DC converters such as Boost or bidirectional Buck-Boost converters. [24], [25], [26].

In spite of this, some similarities can be found with certain ground based systems such as the Microgrids (MG) or Nanogrids (NG) which are defined as small-scale and local power systems connected – or not – to the utility grid and mostly powered by Distributed Energy Resources (DER) such as PVs, fuel cells or wind turbines [27]. The lower level of constraint applied to these systems associated with the increasing geopolitical pressure making the development of alternative energy systems a strategic issue, makes this research sector an important source of inspiration, as was the space sector during the cold war.

DC distribution is experiencing a resurgence of interest due to its simplicity in regards to AC distribution. This renewed interest is even more pronounced by the fact that most loads and DER are DC terminals which allow a reduction of the number of converter used and thus, a better efficiency for the entire system and a lower cost [28]. DERs give the opportunity to have the power production available in the vicinity of loads, reducing power transmission losses and more generally enable to electrify isolated areas in preserving their independence. This last aspect reinforces the similitude between DC MGs and satellites' EPS. allows the experimentation of very varied solutions. More and more applications are studied in order to make certain systems such as buildings, data centers or electric vehicle charging stations totally autonomous [24], [29], [30], [31].

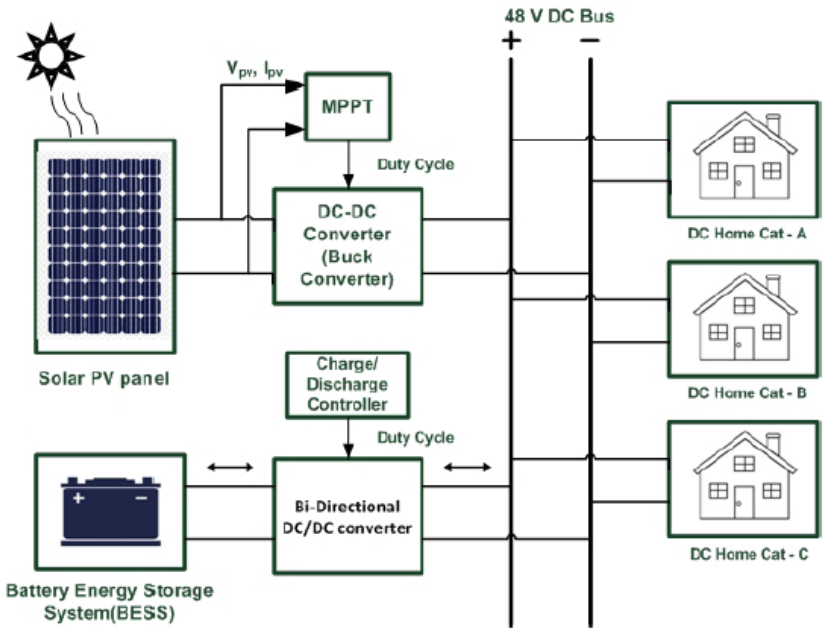

Figure 1.16 – Typical residential PV based DCMG [32].

In their electrical composition, DCMGs based on solar generators coupled with batteries are very similar to a satellite on-board network in its FRB version as the example shown in Figure 1.16. In addition, this type of system is constantly evolving and therefore intrinsically integrates modular functionalities. The building of a house in a residential DCMG like in [33]or the connection and disconnection of one or more electric vehicles to a charging station in [34], [35] are examples that could be used to develop in-flight reconfiguration capabilities in spacecraft.

An important observation which is common to all these systems is that the central element of the system is no longer the power conditioning modules but the distribution network. This characteristic, mainly due to the nature of these systems which spread over large areas obliged to develop the different terminals as peripherals, inherently implemented in a modular approach. A second remark which can be done is that each of these peripherals is composed of three elements:

- The power terminal to be connected to the rest of the system – which can be either a power source, an energy storage system or a load;
- The power electronic which is related to it;
- A capacity to embed control functions and communicate with the rest of the system.

To this regard, it is significantly different to what is implemented in conventional space systems. This difference in the approach of the modules allows to highly simplify the interfaces – both power and data interfaces- at system level.

The study of these two proven systems helps to understand the challenges to be tackle and gives the hindsight needed to design a more generic modular power architecture system. The system implemented on the ISS takes into account the space constraints and is mainly composed of the same hardware as the conventional architectures presented before while bringing solutions to make the system adaptable, notably by separating conversion and conditioning functions from power flow distribution and control functions with the introduction of dedicated modules such as DCSUs. On the other hand, in term of terrestrial applications can be an important source of inspiration in terms of the global design approach and offers interesting solutions to enhance both its modularity and standardization.

1. 5 Proposed Electrical Architecture

Based on this assessment and as a leading player in space on a European and global scale, the CNES – the French space agency – started to work on the future generation of EPS. Figure 1.17 presents the proposed architecture which has been obtained from these preliminary developments.

The proposed EPS architecture, introduced in [16], combines the advantages of NRB and FRB architectures by introducing distributed modules to implement all conditioning and distribution functions at the neighboring of their dedicated terminals, in the same manner as what has been observed on terrestrial systems. This gives flexibility and scalability to the system compared to conventional architecture based on the PCDU.

Functionally speaking, the distributed PCU module, which is dedicated to the PV power conditioning, consists in DETs to connect the PV sections to the bus. The Battery Charge and Discharge Unit is dedicated to the battery and includes a bidirectional converter. Finally, the distributed PDU are equipped with conventional LCL circuits to secure the power distribution.

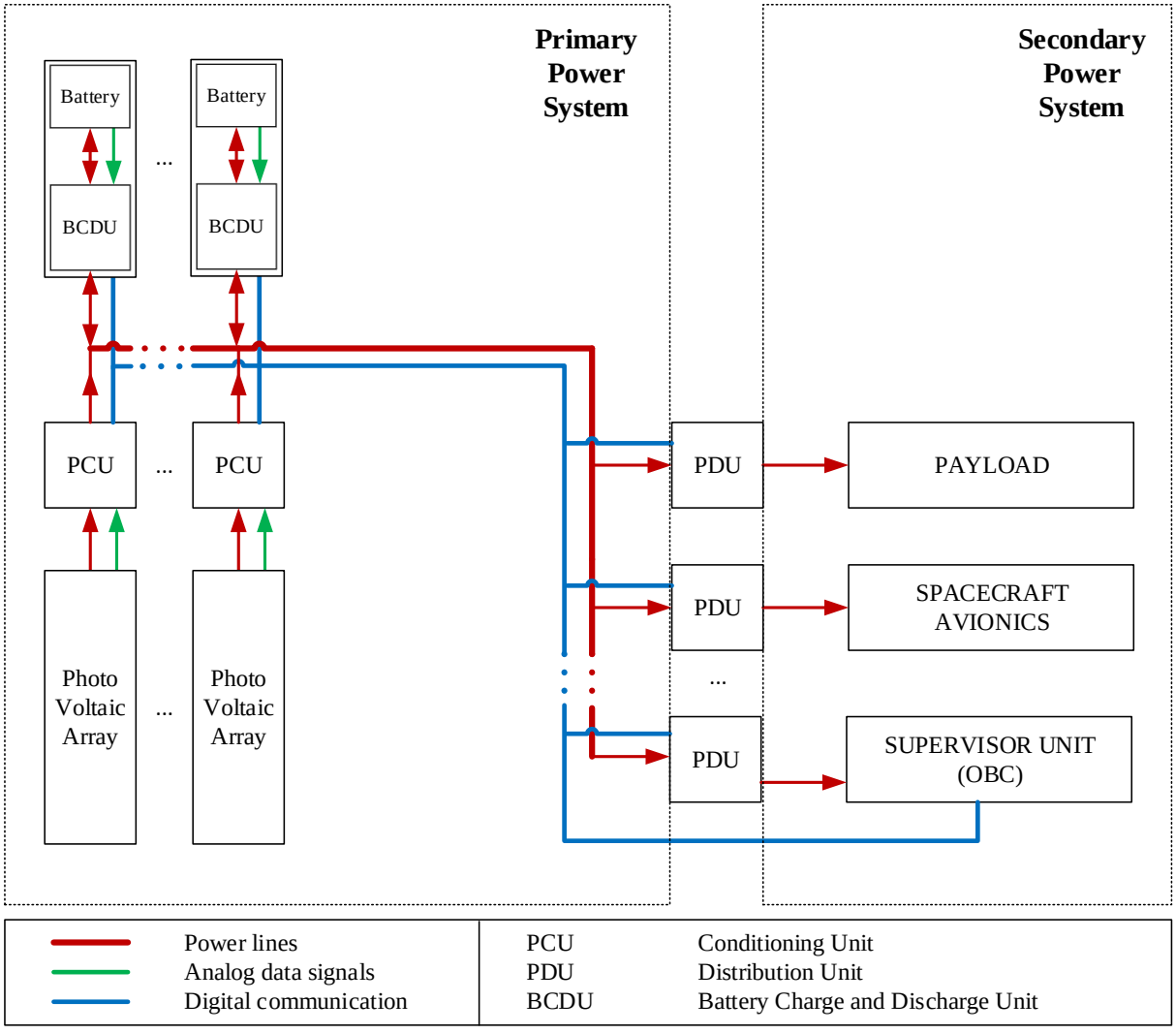

Figure 1.17 – Proposed distributed FRB power architecture overview

From an energetic point of view, this architecture has the advantage of having a very high efficiency during the illumination phase since the part of the power produced by the solar panels which is directly delivered to the loads does not pass through any conversion stage, which therefore induces almost no loss, while assuring a good primary power bus voltage quality thanks to the BCDU which act as parallel regulators.

In addition to this, all types of module are equipped with embedded avionics that enable them to process data autonomously and communicate to each other through a digital data bus. The resulting system is thus strongly modular as each distributed unit strictly corresponds to one function and the interfaces between them is resumed to only two links: a regulated power bus interface and a serial data bus interface.

To develop this solution, the CNES initiated a collaboration with Airbus Defence and Space and the LAPLACE Laboratory in Toulouse in 2018 which started with the development of the distributed modules. In the same time, in order to validate that the proposed system allows a proper regulation of the different battery charge in the same time that the primary power bus is regulated, a detailed study is required.

1. 6 Motivation and scope

This thesis is the fruit of this consortium and aims to study the control component which could be applied to such distributed electrical power systems. The study thus addresses the modelling of the system, the identification of control strategies required to assure its proper operation at short, medium and long term, and finally the analysis of its stability. To cover all these aspects, the present manuscript is articulated as follows.

First in chapter 2, a literature review of the state of the art methods to model, control and analyse the stability of DC electrical systems is presented. In particular, it identifies the main challenges to be tackled in order to assess the stability of multi converter systems and the gaps which may be found in the literature. It also introduces the notion of hierarchical control strategy on which the rest of the document's structure is based. The primary, secondary and tertiary control levels are thus defined.

In the third chapter, after defining the main design choices, hypothesis and conventions used, a focus is done on particular tools as well as on preliminary developments necessary for the understanding and coherence of the elements presented in the following. To do so, a case study is defined on the basis of a typical space mission.

The fourth chapter presents the stability analysis of the system and the impact on it of the implemented primary control. To do this, two methods are used and compared. The first approach corresponds to a conventional small signal study on models obtained by linearization of the average models of the different elements of each module. The second approach proposes an extended modelling of the system to generalize the stability study to all multi converter systems.

Based on these results, which determine the operating ranges of the system, the fifth chapter presents the experimental demonstrator which has been developed to verify the results obtained in term of stability and primary control strategies. It allows to verify the practical feasibility of the proposed primary control prior to the implementation of the secondary and tertiary control strategies.

Finally, these lasts are presented in the last chapter. The secondary and tertiary controls, which respectively correspond to the power and energy management and optimization of the system are thus

tested and validated in simulation. Battery SOC management and PV power injection techniques are first implemented in a unitary way and then integrated and combined in order to complete the global supervision strategy.

CHAPTER 2.

State-Of-The-Art

Summary

In this chapter, the state of the art of the modelling, the control and the study of the stability of modular EPS is performed. First, all the functional components of a power system are presented and their most common models are detailed. In comparison to the elements presented in the first chapter, which mainly focused on the conventional equipment composing it, the various possible topologies of power distribution are here introduced in detail. The most common control methods are then studied. The field of application is extended to terrestrial DCMGs, since they provide an important source of information and innovation, especially for source parallelization methods which have only rarely been studied for space applications. Thus, a focus is done on these methods and a review of possible technics is presented. The different architectures for distributing control functions are then presented. Finally, the most common stability analysis methods used in the frame of electrical power systems are presented. The aim of this general review is thus to set up the tools and present the main challenges which will have to be addressed in the following developments.

2. 1 EPS modelling

Although, generally speaking, a large number of different types of electrical power sources and storage elements exist, this study is limited to a typical space application based on the use of solar panels as the sole primary source and lithium-ion batteries as secondary sources. In addition to these elements, there are the basic components of any electrical power system: the conditioning units, the loads and the distribution network. The latter, although often negligible - and neglected - in terms of its impact on system operation, is no less important for its modeling. Particular attention is therefore paid to it in this section.

For each of these elements, equivalent electrical circuit modeling is used to define the mathematical model as well as their large signals I-V characteristics.

As the aim of this thesis is to study system control laws from a global perspective, the very fast dynamics of certain elements - such as the dynamic model of solar panels - and very low-level control circuits - such as PWM signal generation - are neglected. For elements with dynamic characteristics, the average model is used to obtain characteristic transfer functions in the Laplace domain.

2. 1. 1 Loads

2. 1. 1. 1 Resistive Loads

Resistive loads are the most common type of loads in electrical systems whether they are desired like in the case of the heaters, or induced due to the natural impedance of the electrical components. However, the distinction is done between a simple resistor whose aim is to participate to an electrical function and a Resistive Load (RL), which can either correspond to an actual resistor or an equivalent resistor of a whole circuit, and whose aim is to dissipate power. Nevertheless, this type of loads is equivalent to a mere resistor characterized by the Ohm's law:

$$I_R = \frac{V_R}{R} \tag{2.1}$$

with I_R, the resistive load in receiver convention, V_R, the voltage at the resistive load terminals and R, the nominal resistance of the load.

Its power consumption P_R can be expressed as:

$$P_R = \frac{V_R^2}{R} \qquad 2.2$$

Thus, the power consumption corresponds to the typical power consumption the heaters at their rated voltage. The characteristic I-V and P-V curves of a RL are given below.

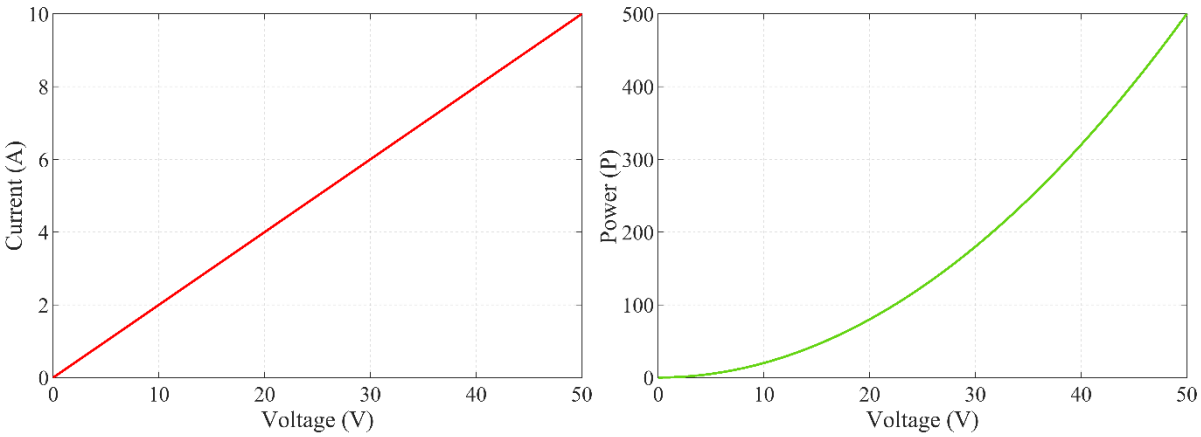

Figure 2.1 – I-V and P-V curves of a typical 5 Ohms resistive load.

2. 1. 1. 2 Constant Power Loads

When considering a RL supplied through a power converter which regulates its output voltage, which can thus be considered as constant, from the converter input point of view, namely the primary bus point of view, the {converter + RL} system has a Constant Power Load (CPL) behavior in the input voltage operating range of the converter.

CPL are characterized by a constant electrical power consumption as expressed by the following equation:

$$I_{load} = \frac{P_{CPL}}{V_{load}} \qquad 2.3$$

with I_{load}, the load current in receiver convention, V_{load}, the voltage level of the primary power bus at the CPL terminals and P_{CPL}, the power consumption of the load.

This equation corresponds to the large-signal behavior of a CPL and can be implemented as follows:

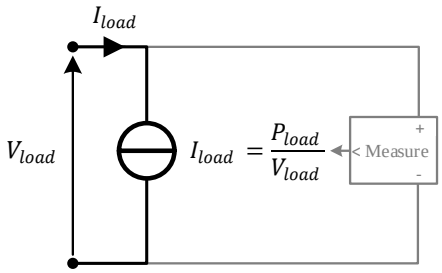

Figure 2.2 – CPL Large-signal model.

From Figure 2.3, it can be noted that the validity magnitude of the small signal model depends on the voltage set point and on the load's power consumption: except in the neighboring of the inflection point of the large signal model, the curve is almost linear. In these regions, the range on which the small signal model is representative of the actual CPL is wider.

It can also be observed from equation 2.3 that the current consumption of an ideal CPL tends to infinity when the voltage tends to 0. However, actual systems are physically limited by the load converter minimum input voltage. Below this limit, the converter operates in open loop, saturating on its maximal duty cycle, applying a static gain between its input and output. From the primary side point of view, the load thus exhibits the same characteristic as the secondary side elements which corresponds to a resistive behavior in most cases whose characteristic resistance is:

$$R_{CPL}{}' = \frac{{V_{min}}^2}{P_{load}} \qquad 2.4$$

Their characteristic curves can be observed on below, validating the aforementioned considerations.

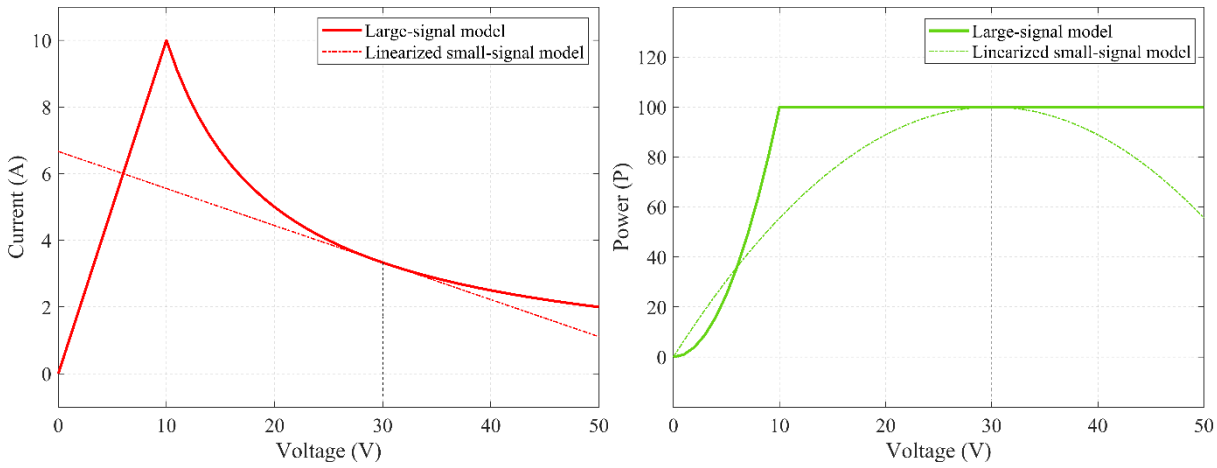

Figure 2.3 – I-V and P-V characteristic curves of CPL with $P_{load} = 100W$ and $V_{min} = 10V$.

As it can be observed in Figure 2.3, the large-signal characteristic of a CPL is non-linear and in order to study it using conventional methods, it can be linearized around an equilibrium point – 30V here. The linearization is usually performed on the $I = f(V)$ characteristic as shown above. In term of power, it results in a parabolic curve in function of the voltage.

2. 1. 2 Solar Generators

In the vacuum of space, solar irradiation can be considered as constant and does not suffer any alteration as it does in the Earth's atmosphere. The solar irradiance passes from 1000W/m² at sea level to 1370W/m² at LEO [36]. The relative simplicity of integration – in term of electrical features – and durability compared to other solutions is also a significant advantage. On the other side of the coin, this has to be qualified by the poor performances in term of efficiency.

Considering the important impact on the cost of a mission of the volume and weight of the different subsystems, big efforts have been made to improve the efficiency and thus the power density of solar arrays. The use of advanced – and often rare – materials as semiconductor and substrate such as Gallium arsenide (GaAs), associated in multilayers structures to make the most of the entire light spectrum as illustrated in Figure 2.4, enables to reach up to 33% of efficiency against 18 to 20% for conventional monocrystalline silicon cells used on Earth.

The solar arrays being external elements their operating temperature varies in a wide range during the orbit. As the temperature impact the cells characteristics in term of available power, it has to be taken into account in the developed models.

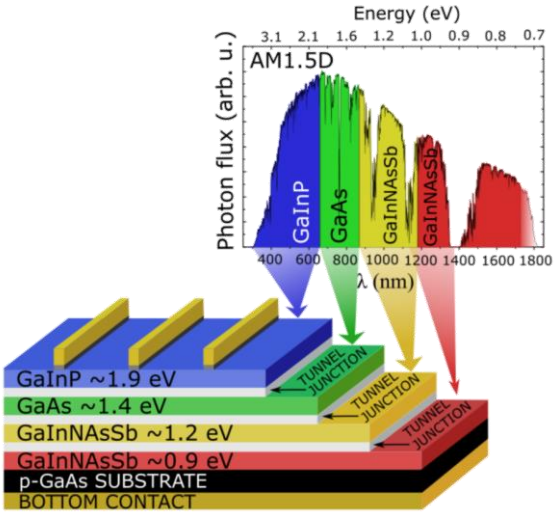

Figure 2.4 – Four layers solar cell structure [37].

Several methods exist to model PVs. Manufacturers often prefer to provide only a few parameters such as V_{OC}, I_{SC} or MPP coordinates. From these parameters, a polynomial approximation of the I-V curve can be realized. This method is widely used in the control of PV emulators.

The electrical equivalent circuit approach is also widely used and allows a better control on the PV parameters as well as the consideration of additional parameters such as line impedances or the equivalent parallel resistance. The solar cell equivalent circuit is given in the following figure.

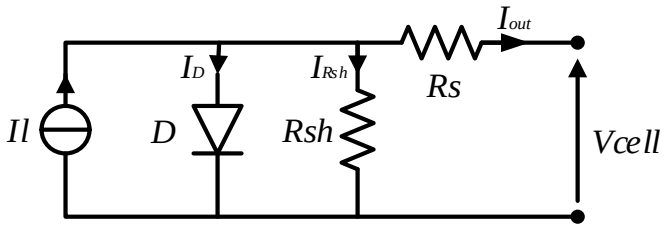

Figure 2.5 – Equivalent circuit of a photovoltaic cell.

Thanks to the output voltage applied to the Solar Wing (SW) the current injection of every section can be calculated.

$$I_{out} = I_l - I_D - I_{R_{sh}} \tag{2.5}$$

The representativeness of the model depends on the identification of these three currents and on their adaptation to the PV environment.

In [38], [39], [40], a method to model these parameters based on the three main points of the I-V curve (open circuit, maximum power and short circuit) is presented. The current injection I_l at the current source corresponds to the light current and is expressed as below:

$$I_l = \frac{S}{S_{ref}}\left(I_{SC0} - \alpha_{I_{sc}} \cdot \left(T_{cell} - T_{ref}\right)\right) \tag{2.6}$$

with S, the solar irradiance in $W.m^{-2}$, S_{ref} and T_{ref}, respectively the reference solar irradiance and temperature in Kelvin at which I_{SC0}, the rated short circuit current of the cell, was

characterised, $\alpha_{I_{sc}}$, the current temperature coefficient of the cell in $A.K^{-1}$ and T_{cell}, the temperature of the cell in Kelvin.

It can be observed that the light current expression takes into account the temperature variations. Nevertheless, as $\alpha_{I_{sc}}$ is most of the time very low, the impact of the temperature on the current generation is minor. Indeed, the temperature variations mostly impact the voltage range of the cells which is characterized by the open circuit voltage. The two characteristic points can thus be expressed in function of the operating temperature.

$$I_{SC_T} = I_{SC0} - \alpha_{I_{sc}} \cdot \left(T_{cell} - T_{ref}\right) \quad 2.7$$

$$V_{OC_T} = V_{OC0} - \alpha_{v_{OC}} \cdot \left(T_{cell} - T_{ref}\right) \quad 2.8$$

with V_{OC0}, the Open Circuit voltage reference of the cell in Volts at T_{ref}, and $\alpha_{v_{OC}}$, the voltage temperature coefficient in $V.K^{-1}$.

The diode current is calculated by the Shockley diode exponential expression [40]:

$$I_D = I_{D0} \cdot \left(\exp\left(\frac{q \cdot V_{cell}}{\gamma \cdot K \cdot T_{cell}}\right) - 1\right) \quad 2.9$$

$$I_{D0} = \frac{I_{SC_T}}{\exp\left(\frac{q \cdot V_{OC_T}}{\gamma \cdot K \cdot T_{cell}}\right) - 1} \quad 2.10$$

with I_{D0}, the diode saturation current in Amps, q, the elementary charge, V_{cell}, the voltage level across the section, γ, the diode ideality factor and K, the Boltzmann constant.

In the expressions above, the serial resistor R_S is neglected allowing to consider that the voltage applied to the shunt resistor, the diode and the light current source is equal to V_{cell}. Indeed, the serial resistor characterizes the connection and transmission lines resistance from the cells pins to the point where the measurements are achieved. Thus at the scale of a single cell, its value is very low. It can also be noted that in multilayers solar cells, as several PN junctions compose the cell, several diodes should be integrated to the equivalent circuit. In order keep an acceptable level of complexity of the models, the single diode model is often used.

Determining the shunt resistor's current by a mere application of Ohm's law, the total characteristic equation of a cell can be obtained.

$$I_{sh} = \frac{V_{cell}}{R_{sh}} \quad 2.11$$

The resulting equation states that the output current of a cell is a function of the voltage at its terminals, its surface temperature and the solar irradiance defined by the mission profile. The angle of incidence is neglected as the solar cells are supposed to be Sun oriented.

Even if all these parameters cannot always be found in solar cell manufacturers datasheets, they can be deduced from the I-V characteristic curve of the solar cell which is easy to obtain either directly in the documentation or by performing characterization tests [41].

For the present study, typical space cell parameters are used giving the following typical I-V and P-V curves.

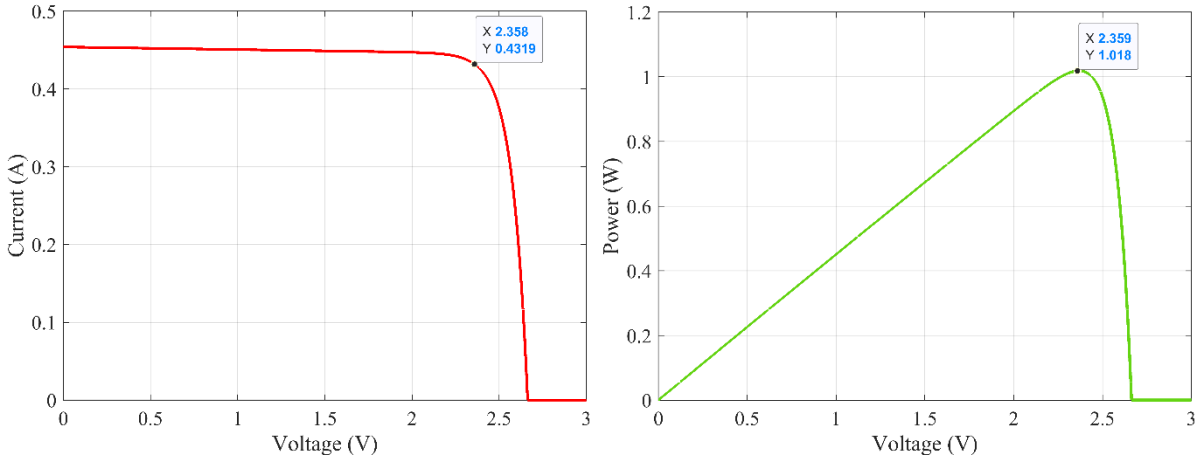

Figure 2.6 – I-V and P-V curves of a single PV cell.

The dynamic behavior of a PV cell is driven by parasitic phenomena which can be added to the equivalent circuit. Two main elements can generally be identified: the wires and connector characteristic inductance and the shunt equivalent capacity between the positive and negative terminals of the cell [42], [43]. The resulting equivalent LC circuit drives the dynamic of the voltage variations at the output of the PV section. However, the value of these parameters are very small – of the order of hundreds of nano-farads for the equivalent capacitor for instance – which implies that the dynamic of the phenomenon, which is inversely proportional, in very important – several kilohertz [44]. This range of frequency being out of the scope of the present study and even if they are mandatory to understand the solar cell behavior in open circuit, the aforementioned elements are not integrated to the models and the solar cells are presumed to have an instantaneous response time.

The behavior of a whole PV section can be deduced in considering that all cells are identical and arranged in N_S cells in series per string and N_P strings in parallel per section.

$$V_{cell} \cdot N_S = V_{section} \tag{2.12}$$

$$I_{cell} \cdot N_P = I_{string} \cdot N_P = I_{section} \tag{2.13}$$

Moreover, in a full PV section, the serial impedance R_S becomes non negligible and has to be taken into account.

$$V_{section} = V_{PV} - R_S \cdot I_{section} \tag{2.14}$$

with V_{panel}, the voltage at the whole solar panel terminals – a solar panel being composed of several PV sections.

On the characteristic I-V curve given below for a nominal sun irradiance and temperature in orbit, it can be noticed that the current and power are limited to positive – or at least null – values, which corresponds to the action of serial blocking diodes. These elements added on actual systems, aim to avoid the panels to operate at reverse current during the mission.

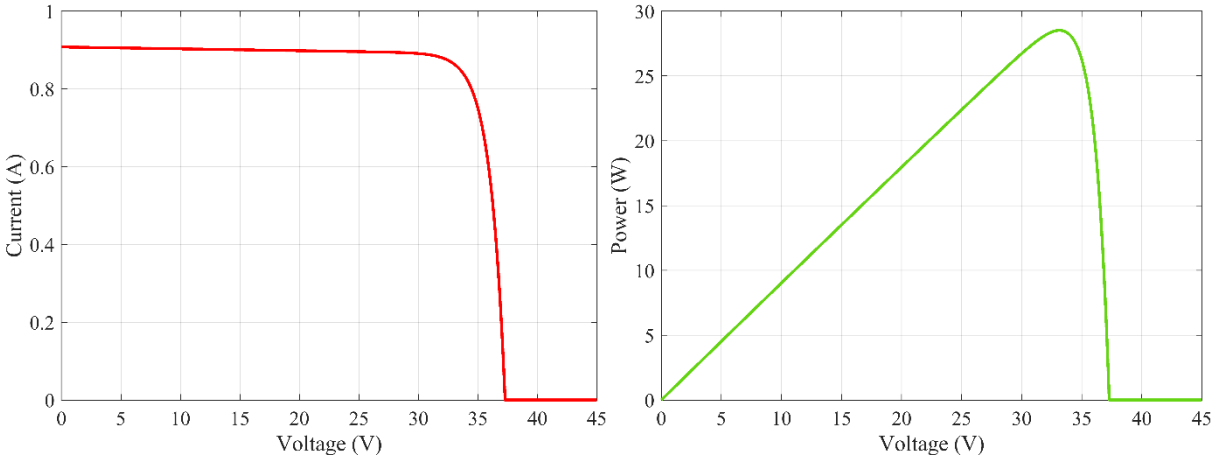

Figure 2.7 – 14S2P PV section I-V and P-V characteristic curves at rated sun irradiance (1370W/m²) and temperature (28°C).

It is also possible to represent the variations of these curves caused by the variation of environmental conditions. Thus, Figure 2.8 illustrates that the temperature mainly impacts the voltage characteristics of the PV sections with a very small effect on the current. The exact opposite remarking is done on Figure 2.9 for the sun irradiance variations which is almost proportional to the available output power.

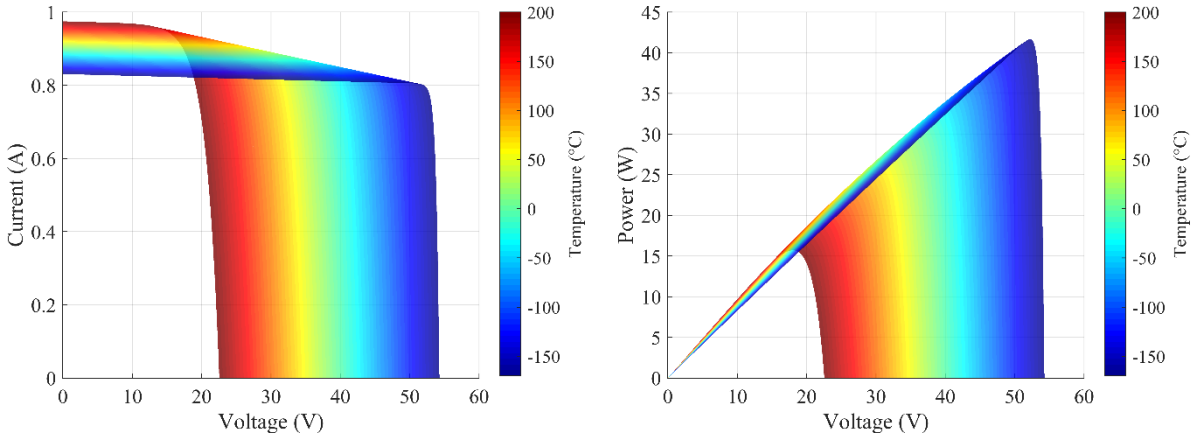

Figure 2.8 – I-V and P-V curves evolution in function of the temperature.

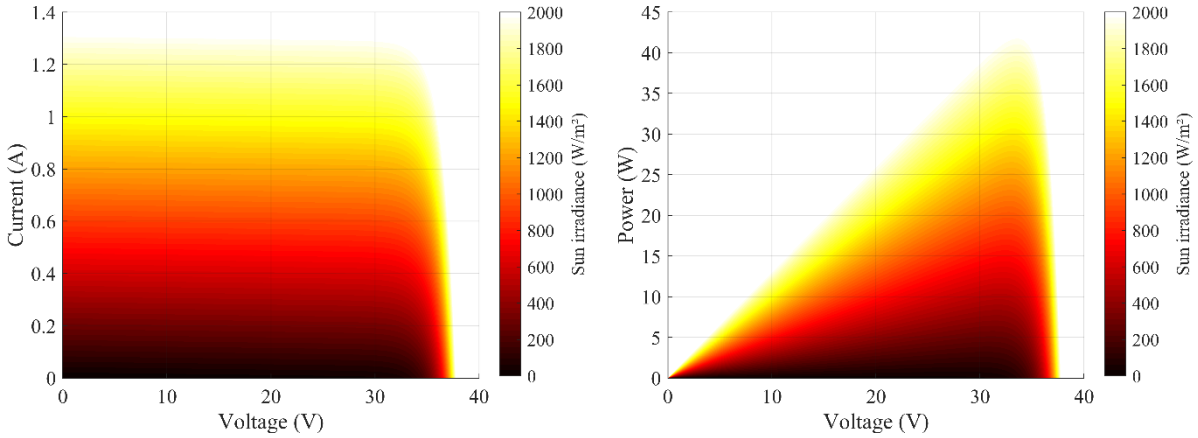

Figure 2.9 – I-V and P-V curves evolution in function of the sun irradiance.

The reverse relation can be obtained by assuming that the shunt resistor R_{SH} is high enough to neglect the current flowing through it.

$$V_{section} = \frac{\gamma \cdot K \cdot T_{cell} \cdot N_S}{q} \cdot \ln\left(\frac{N_P \cdot I_l - I_{section}}{N_P \cdot I_{D0}} + 1\right) - \frac{I_{section}}{N_P} \cdot R_S \quad , \forall\, I_{setcion} < I_l + I_{D0} \qquad 2.15$$

If the assumption that R_{SH} is considered infinite cannot be made, or if a detailed model is needed, the reverse voltage expression can be obtained by the Lambert W function [45]. However, such a detailed model is not required in the present study.

2. 1. 3 Lithium Ion Batteries

In order to be able to easily switch from one battery configuration to another, battery pack models are generally based, like in real batteries, on serial and parallel arrangement of individual cells. In order to obtain a steady-state battery cell model, and as the detailed chemical behavior is very specific, an equivalent circuit based approach is most of the time used.

Electrically speaking, battery cells behave like voltage sources. Their Open Circuit Voltage (OCV) varies from a characteristic low level to a characteristic high voltage, depending on the State-Of-Charge (SOC) of the battery. Only considering the steady state behavior, battery cells can thus be modelled as a resistor – modelling the internal lines and connections impedances [46] – in series with a SOC dependent voltage source as depicted below.

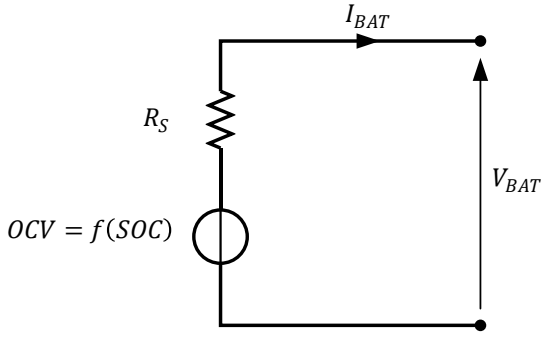

Figure 2.10 – Battery cell equivalent circuits.

However, this equivalent circuit approach requires to be able to estimate the cells SOC. The Coulomb Counting (CC) method, consisting in integrating the current flowing in and out of the battery in regard with the capacity of the battery, is one of the most used methods due to its simplicity of integration and its accuracy for short term calculations [47].

Nevertheless, errors in the initial SOC or in the estimated capacity of the battery, which evolves all along the mission duration, induce a cumulative error which makes the estimation diverge in medium term. In most applications, the SOC estimation is thus periodically reset based on the battery OCV which has the advantage to be independent from the rated capacity and the initial conditions. However, this OCV measure must be achieved at rest, when the battery current is null, in order to avoid to be impacted by the voltage drop due to the internal impedance of the battery, which also varies throughout the aging of the battery.

A lot of other methods to estimate the battery SOC as depicted in [48]. In particular, the estimations based on the Kalman filter method is known for its good accuracy and good immunity to measurement noises and parametric uncertainties as explained in [49].

However, the SOC estimation is used here to a simulation purpose, in order to emulate the battery behavior and not to estimate the SOC of an actual battery evolving in parallel as it is the case for online SOC estimations. The drawbacks mentioned previously concerning the CC method are thus not valid in this case and its simplicity of use makes of it the widest spread method for battery modelling. This is what is implemented in the following:

$$SOC_{cell} = \frac{1}{C_{cell}} . \int (-I_{cell}) . dt \qquad 2.16$$

with C_{cell}, the capacity of the battery here expressed in A.s and I_{cell}, the current flowing through the cell, in A.

By initializing the SOC at the wanted value, it is then possible to determine the battery ElectroMotive Force (EMF). To do so, different methods are proposed in the literature like in [46], based on available internal parameters. Another method is to realize a complete charge and discharge cycle of a real battery to obtain its characteristic I-V curve and then approximate the curve equation thanks to a polynomial equation.

$$E_{cell} = E_{cell0} + E_{cell1} \cdot SOC + E_{cell2} \cdot SOC^2 + E_{cell3} \cdot SOC^3 + E_{cell4} \cdot SOC^4 \qquad 2.17$$

with E_{cell0}, E_{cell1}, E_{cell2}, E_{cell3} and E_{cell4} quadratic approximation coefficients provided by the CNES and determined on actual cells data.

The EMF gives a good representation of the OCV of the battery, and completed with the voltage drop in the serial equivalent resistor, the battery output voltage can be calculated for a given current.

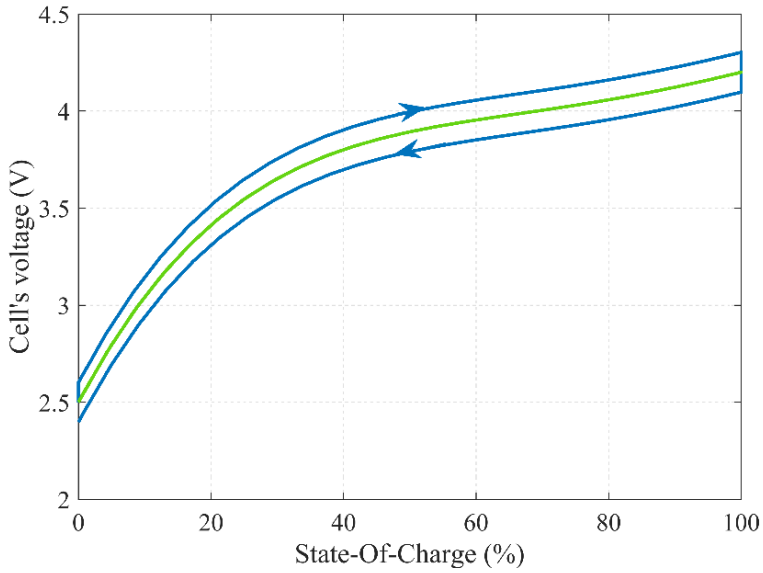

Figure 2.11 – Typical 3.07A.h / 3.6V Lithium ion terminal voltage evolution

On Figure 2.11, the curves obtained thanks to the implemented models are visible. The EMF evolution depending on the cell's SOC is illustrated in green whereas the blue curves show the impact of the serial resistance during charge and discharge for a constant current in both sense.

To simulate a whole battery pack, two options are available. The first one consist in emulating every cells to allow to study the effect of a fault on a single cell of a string for example.

In the present case, this level of complexity is not required and the second option is chosen: to simulate the global behavior of a battery pack composed of cells in series and parallel strings, a global equivalent circuit can be calculated, based on the same model of a single cell by adapting the internal parameters of the model. Thus, equivalent capacity and serial resistance are calculated as following.

$$\begin{cases} C_{bat} = N_P \cdot C_{cell} \\ R_{bat} = R_{cell} \cdot \dfrac{N_s}{N_P} \\ E_{bat} = N_S \cdot E_{cell} \end{cases} \qquad 2.18$$

Applied to a 12S10P battery, the characteristic curve shown in Figure 2.12 is obtained.

It is also possible to observe the battery voltage variation during the battery discharge at different C-rates. Figure 2.13 illustrates the link between the C-rate and full discharge time. It can be seen that at a 3C rate, the battery is discharged in 20 minutes.

Finally, it can be mentioned that the presented model does not take into account the thermal behavior of the battery cells. Indeed, the temperature of the cells is considered as constant thanks to the thermal regulation of the internal elements of the satellite.

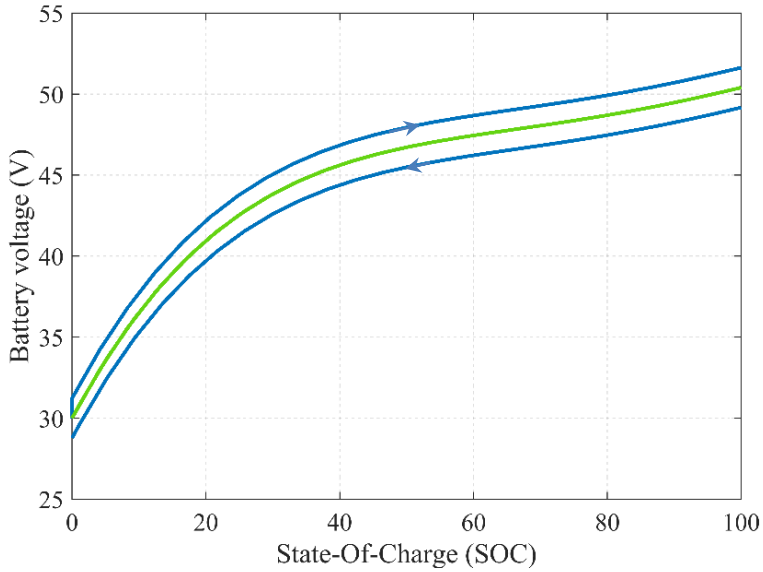

Figure 2.12 – 12S10P battery output voltage in function of the SOC.

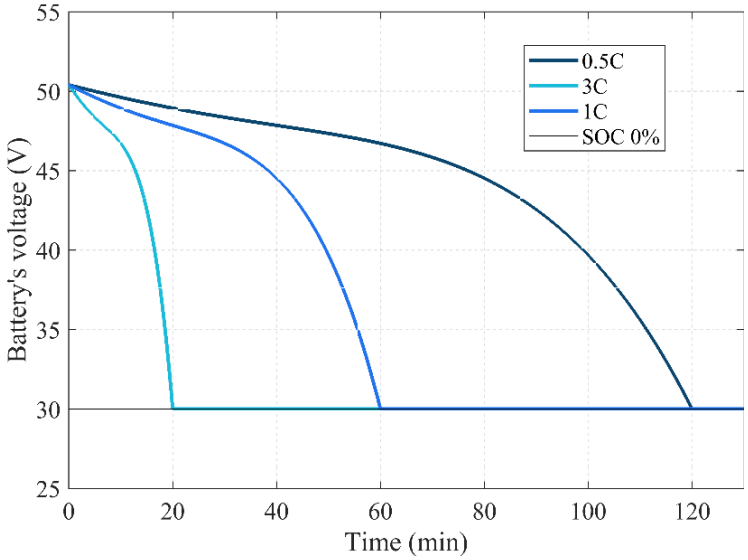

Figure 2.13 – 12S2P battery time of discharge at three different rates.

The battery configuration and the SOC are not the only parameters that influence the battery behavior. As the accumulators are electrochemical devices, their composition and characteristics can evolve with the time. Ageing phenomena thus also has to be taken into account to assure the good working of the system in the worst configuration, that is to say at the End Of Life (EOL) of the satellite.

In general, in the case of a LEO mission, a typical operational life of 5 years approximatively equals to 30 000 cycles which have to be tackled by the batteries which is not the case for example in a GEO mission where eclipses occur only at the autumn and spring equinoxes.

The ageing of a battery can be characterized by a lot of estimators. The capacity fade, defined as the evolution of the available capacity in function of the number of charge/discharge cycle, is the most common. Combining these different estimators, the State Of Health (SOH) can be determined as a global indicator of the battery ageing. The determination of these estimators highly depends on the cells technology but also on the conditions in which they are used, both in term of chemical and electrical aspects. Thanks to [50], within the specified operating ranges of a given cell, the total number of cycles achievable by a cell at 80% capacity can vary of up to thousands of cycles.

As it has already been implied in the previous sections, the temperature for example plays an important role in the ageing of the cells and on both short and long term evolution of their capacity [51]. However, in the present work, this constraint is neglected since it is considered that an accurate temperature regulation is handled by the thermal control sub-systems present in satellites. In more conventional applications such as in electric vehicles, in order to manage the thermal aspects of the battery, an estimator called State Of Temperature (SOT) is determined, taking into account several thermal aspects such as the maximum temperature or the thermal gradient across the battery [52].

All aforementioned elements show the need to have an accurate and exhaustive monitoring of the battery temperatures and voltages both at cells and battery voltage in order to be able to evaluate its global state. In conventional terrestrial applications, specific systems allow to perform this monitoring, called Battery Management Systems (BMS) [53]. According to [54], the BMS plays a major role to ensure a safe and trustworthy battery operation, especially when using Li-ion cells. It also allows to verify that all cells are equally charged and if not, it can perform an autonomous balancing thanks to dedicated systems which could be purely dissipative – by connecting resistors in parallel of the cells to discharge all cells

and get aligned with the lowest charged one – or based on a redistribution of the charge – achieved through an intermediate capacitor which avoids to discharge the whole battery pack at the price of a more complex management.

As for all other systems in space applications, the electronics to perform these measurements are most of the time reduced to the strictest minimum and deported inside the PCDU. In order to limit the number of analogic signals to rout from the battery to the PCDU, only a few temperature acquisitions are performed for the whole battery pack and cell voltage measurements are performed at a low rate to decrease the requirements on the electronics. Finally, the balancing of the different cell strings is performed by the simple dissipative method.

With the proposed modular architecture, a better monitoring of the battery can be possible thanks to the distributed acquisition features provided by the integration of microcontrollers inside the battery modules. In terms of control, the main impact of the introduction of such systems in the battery modules is that it gives a much better observability of the system. In the following, it allows to consider that the actual SOC and SOH of the battery is known and that high accuracy and frequency acquisitions of all battery variables are available. This will significantly facilitate the management of the battery to respect its operating limits such as the maximum battery currents during charge and discharge or the battery voltage to avoid its overcharge at the power conditioning level.

2. 1. 4 Power Conditioning Units

Power conditioning components can be defined as the elements regulating the way the power produced by the solar panels is delivered to the different users of the system among which the battery has a special status. These power electronics which are conventionally concentrated in specific equipment such as the PCDU presented in Chapter 1, can be classified into two categories which are presented in the following.

2. 1. 4. 1 Direct Energy Transfer (DET)

The DETs are based on the circuit presented in Figure 2.14 and take their name from the fact that, when turned ON, they are almost equivalent to a direct electrical connection between their input and their output. They are suitable to interface modules which can be polarized by the same voltage level and allow a unidirectional power transfer.

Although several other topologies exist, the one depicted in Figure 2.14 is especially well adapted for PV section management and is therefore the most common in space system.

During the ON state, the shunt MOSFET of a DET is turned OFF which makes it equivalent to an open circuit. Thus the diode enters its pass band as the voltage at its terminals becomes positive, making it equivalent to a closed circuit – with a typical voltage drop of about 0.6V. The PV section is then polarized at the same voltage level than the primary bus, minus the diode voltage drop, and the current flowing outside of the DET equals to the PV section current.

During the OFF state, the reverse configuration is obtained. The PV section is then put at its short-circuit operating point, the MOSFET conducting resistance being very low and the DET output current is null.

From a modelling point of view, an average model is then sufficient for the study of the system stability. Since, there is neither an input nor an output filter, the dynamic of a DET is a function of its diode and MOSFET dynamical characteristics.

Indeed, during the transitions between the two operating states, for short laps of time both the diode and the MOSFET are conducting – or in open circuit – in the same time. For the OFF state to ON state transition for example, the PV section initial operating point corresponds to its short circuit point $(\sim 0V; I_{SC}A)$. At the opening of the MOSFET, as the diode is still in reverse polarization, namely in blocking state, the output voltage of the PV section is a priori floating.

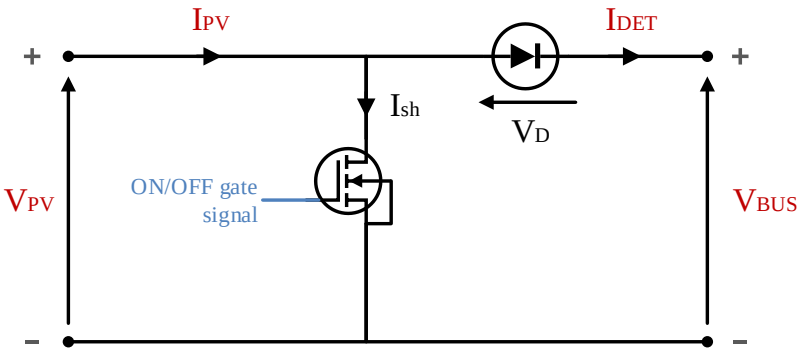

Figure 2.14 – DET electrical circuit.

In the same approach to the PV model, the dynamic behavior of the DET is then related to parasitic elements, and more precisely to the drain to source capacitance in this case which is even smaller than the characteristic capacitance of the cells – of the order of hundreds of pico-farads.

In addition, the aim of the present models is to characterize the modules from a bus side point of view, which allows to neglect the PV section behavior when disconnected from the bus. Thus, the DET components can be considered as ideal and only their steady state parameters are integrated to the models.

The following figures illustrate the behavior of a DET coupled to PV sections with varying inputs. In order to be able to observe the characteristic of the PV panels as well as the controllability that the DET offers, the primary bus input voltage is defined as a sinusoid oscillating around the sections' MPP and the command signal is determined to connect an increasing number of sections.

The measures sent by the TM function of the module are presented in Figure 2.15. As a consequence, the different sections are shunted or connected to the bus and polarized at the oscillating voltage, making them operate all along the equivalent I-V and P-V characteristic curves corresponding to the number of connected sections as shown in Figure 2.16.

It can thus be observed that, at the dynamics considered, i.e. at a control sample period of about 1 second, the system outputs depend only on the bus voltage and the configuration of the solar panel section - layout and environmental conditions.

Generally speaking, if the bus voltage can be considered constant – as regulated from somewhere else in the system – and considering that each sections is coupled with a DET, controlling the number of sections connected therefore amounts to discrete control of the injection of current - power - on the bus.

Thus, it can be noticed that this gives discontinuous properties to the EPS. From this point of view, the overall system could be analyzed as a switched dynamical system as defined in [55].

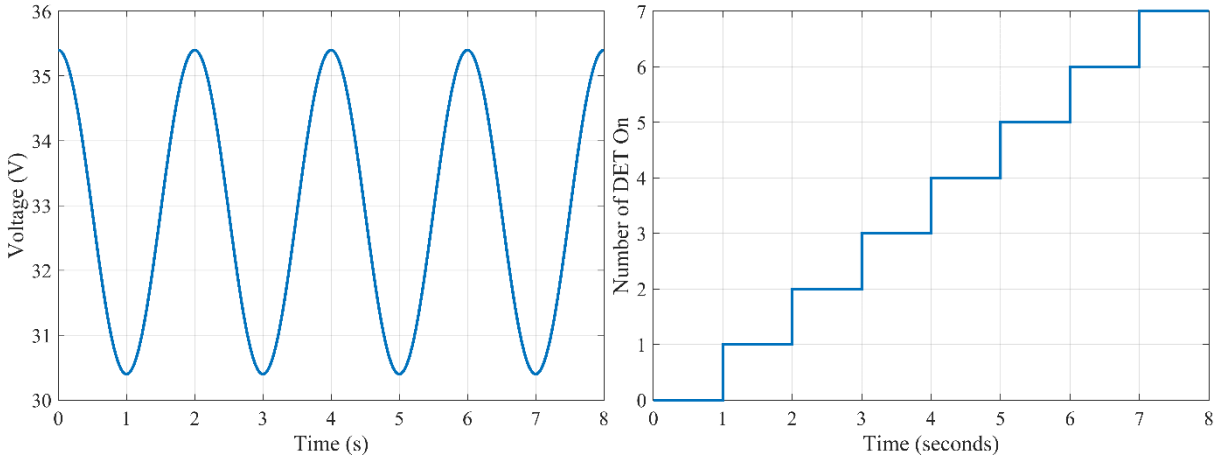

Figure 2.15 – Example of input parameters variations on a 7 DET system.

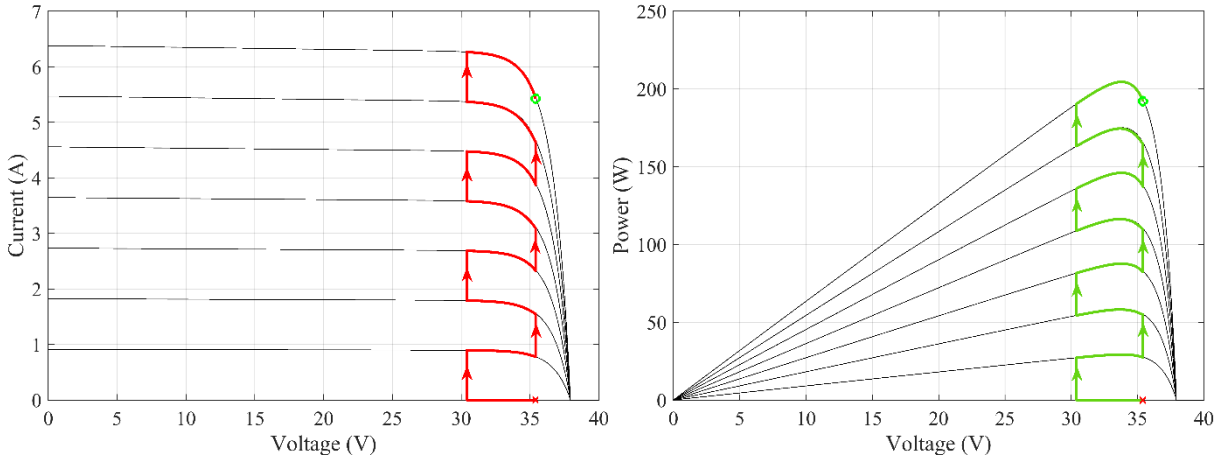

Figure 2.16 – Example resulting output current and power variations in the I-V and P-V plane for a 7 DET system.

If the DET control take an injected power set point as reference signal and that this does not correspond exactly to an integer number of sections – which is most of the time the case – an oscillation between two numbers of sections will then be visible, so that on average, the set point is reached.

On the same principle, on this oscillating section, by sufficiently increasing the refresh rate of the control signal and using it as a PWM signal, it is possible to modulate the voltage on either side of the DET, which then becomes a switching cell.

Although the electrical diagram is exactly the same in this last case, the system is referred to as a Sequential Switching Shunt Regulator (S3R). The advantage of this operating mode is that most of the power is injected by DET, as the first connected sections remain in a fixed position and only one switches, thus inducing very low losses.

However, considering the system made up of a solar panel section and a PWM-controlled DET as a whole, it no longer fully corresponds to a DET since additional losses are induced by the oscillations and can rather be considered as a pseudo DC/DC converter.

2. 1. 4. 2 DC/DC converters

The DC/DC converters are designed to adapt voltage and current levels from their input to their output which are often respectively referred as the source and the load since their basic forms are unidirectional. In the following, only bidirectional implementations of the most basic topologies are presented since it allows to cover all possible uses, and more particularly it addresses the battery charge and discharge applications which cannot be handled by the DET presented above. Be that as it may, the notions of input source and output load can be conserved since it allows to define the sense in which it is control: the load always corresponds to the side for which the current or the voltage – or both – is regulated.

The Buck converter is the most common and basic DC/DC converter. Its principle is detailed in Figure 2.17.

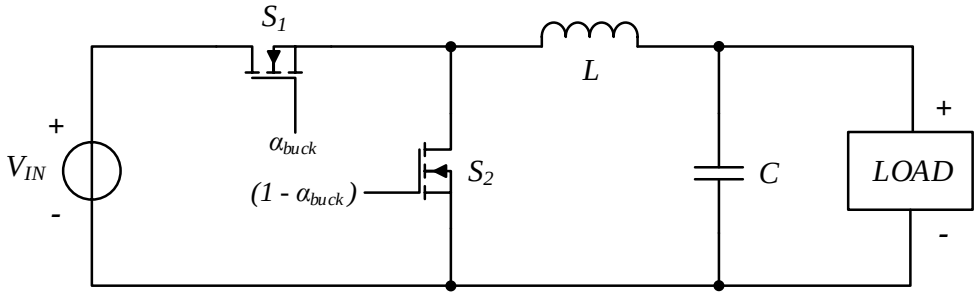

Figure 2.17 – Synchronous buck converter (a) and its equivalent circuit in S_1 ON (b) and OFF states (c).

Let's consider that the load can be represented by a mere resistor, noted R. Using the inductor's current and capacitor's voltage, respectively noted i_L and v_C, as state variables and the PWM signal's duty cycle, α_{buck}, as the command variable, the state equation can be defined as follows:

$$\begin{pmatrix} \dot{\imath_L} \\ \dot{v_L} \end{pmatrix} = \begin{pmatrix} 0 & -\frac{1}{L} \\ \frac{1}{C} & -\frac{1}{CR} \end{pmatrix} \begin{pmatrix} i_L \\ v_C \end{pmatrix} + \begin{pmatrix} \frac{V_{IN}}{L} \\ 0 \end{pmatrix} \alpha_{buck} \qquad 2.19$$

Thus, since on average $\dot{\imath_L} = 0$ and $\dot{v_C} = 0$:

$$\bar{v}_{OUT} = \bar{\alpha}_{buck} V_{IN} \qquad 2.20$$

with $\bar{v}_{OUT} = \bar{v}_C$ and $\bar{\alpha}_{buck} \in [0; 1]$.

This makes of the Buck converter adapted to situations where the desired load voltage is lower than the nominal input voltage.

One other main characteristic which makes of it the most present converter in the literature is that its state representation is fully linear on condition that the load as well as the input voltage can be considered as constant.

The other way round, when the desired load voltage is higher than the actual input voltage, the Boost converter, shown in Figure 2.18, can be used.

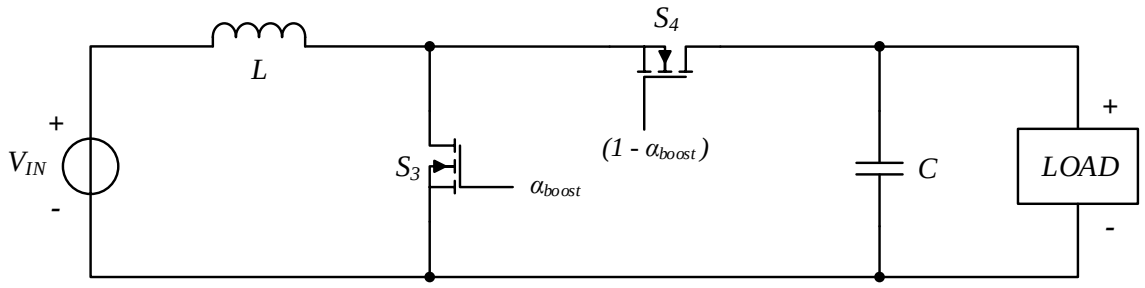

Figure 2.18 – Synchronous boost converter.

Using the same state vector as above, the state representation shows non-linear characteristics since the PWM signal's duty cycle α_{boost} is part of the state matrix:

$$\begin{pmatrix} \dot{i_L} \\ \dot{v_L} \end{pmatrix} = \begin{pmatrix} 0 & -\frac{1}{L}(1-\alpha_{boost}) \\ \frac{1}{C}(1-\alpha_{boost}) & -\frac{1}{CR} \end{pmatrix} \begin{pmatrix} i_L \\ v_C \end{pmatrix} + \begin{pmatrix} \frac{1}{L} \\ 0 \end{pmatrix} V_{IN} \qquad 2.21$$

This is due to the "indirect" nature of Boost-derived converters in contrary to the Buck-derived topologies which are qualified of "direct" converters. Indeed, in comparison with the Buck converter, two charge – discharge cycles can be identified in the boost operation, respectively corresponding to the inductor's charge during the ON state, which discharges into the capacitor to charge it during the OFF state, enabling it to discharge itself to supply the load during the next ON state.

This characteristic makes of its study more complex and explains why its use is avoided in a lot of studies on the topic. However, as its average transfer function below confirms, in contrary to the Buck converter, it allows to step up the voltage which is a useful feature for some applications.

$$\bar{v}_{OUT} = \frac{1}{1-\bar{\alpha}_{boost}} V_{IN} \qquad 2.22$$

with $\bar{v}_{OUT} = \bar{v}_C$ and $\bar{\alpha}_{boost} \in [0;1[$.

The same observation can be made on the last basic topology presented here: The Buck-Boost converter. It allows to step up and down the output voltage compared to the input which makes of it may be the most versatile and useful topology. Indeed, most of the time, these converters are used to interface the primary power bus and a battery whose voltage varies in function of its SOC as introduced earlier. Considering that the DC/DC converters reach their optimum operation point near a transformation ratio of about 1, batteries are generally designed to have a nominal voltage close to the nominal bus voltage. This induces that depending on their SOC, they can either show higher or lower voltage levels than the bus, which shows the relevance of the use of a Buck-Boost topology.

Several possibilities exist to implement it but a special focus on the Four Switch Buck Boost Converter (FSBBC) is proposed since in addition to allow bidirectional operation, it is also conservative in term of polarity compared to conventional Buck-Boost. In term of structure, the FSBBC is basically composed of a Buck converter cascaded with a Boost converter, both sharing the same inductor. Although the number of switches is higher than in the other topologies, its operation remains quite simple.

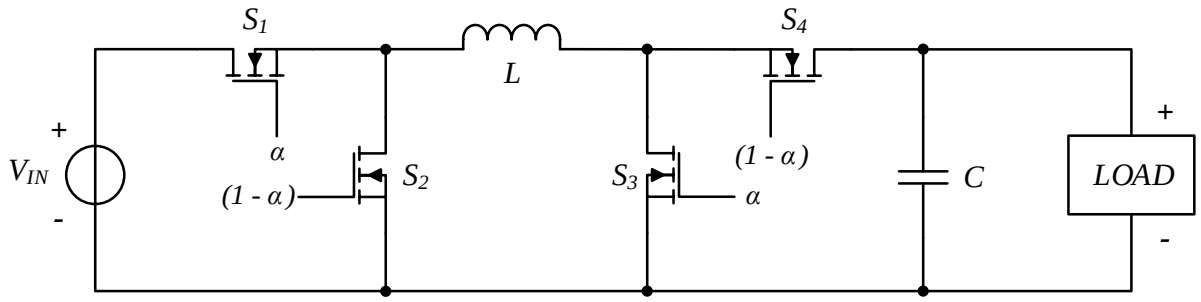

Figure 2.19 – Four-switch synchronous non-inverting Buck-boost converter (a) and its equivalent circuit in S_1 and S_3 ON (b) and OFF states (c).

In a general approach, let's assume that S1 and S3, which are the main switches, are controlled by the same duty cycle α. S2 and S4 which are their respective synchronous rectifiers – equivalent to the diodes in the two switches noninverting topology – are controlled by the complement of α [56], [57], [58]. Its state representation can thus be written as

$$\begin{pmatrix} \dot{\imath_L} \\ \dot{v_L} \end{pmatrix} = \begin{pmatrix} 0 & -\frac{1}{L}(1-\alpha) \\ \frac{1}{C}(1-\alpha) & -\frac{1}{CR} \end{pmatrix} \begin{pmatrix} i_L \\ v_C \end{pmatrix} + \begin{pmatrix} \frac{\alpha}{L} \\ 0 \end{pmatrix} V_{IN} \qquad 2.23$$

Hence, on average

$$\bar{v}_{OUT} = \frac{\bar{\alpha}}{1-\bar{\alpha}} V_{IN} \qquad 2.24$$

From the above developments, it can be observed that all the operating characteristics of a classical buck-boost converter can be identified in this topology, both in terms of its ripple characteristics and its average transfer function, with the exception of its inverting character, which makes the FSBBC easier to sense and control.

Another way to operate the converter can be implemented in which S1 and S3, the main switches, are respectively controlled by the duty cycles α_{buck} and α_{boost} allowing the converter to operate either as a buck or as a boost exactly as depicted above [56], [57], [58]. S2 and S4 which are their respective synchronous rectifiers, are respectively controlled by the complements of α_{buck} and α_{boost}.

This highlights the huge number of possible variations, both in terms of control and topology. In fact, there are a huge number of variants, such as flyback, half-bridge and full-bridge converters. The justifications for choosing one or other of these variants over those presented above are usually based on practical considerations – the need for galvanic isolation, adaptation to the power range, etc. – rather than on the nature of the converter itself. What's more, most of the time it's possible, under certain assumptions, to relate to the three topologies presented, which means that the results obtained on these topologies in the rest of this study will remain mainly applicable to any kind of converter.

2. 1. 5 Distribution Network

Finally, although this aspect has not been mentioned in introduction and is often neglected in the modelling and study of power systems, whether in the space domain or on terrestrial microgrids, a last

component of the EPS is the power harness composed of all distribution lines. Indeed, these lines are generally dimensioned to limit the maximum voltage drop they can induce for a given maximum power, and their impact on overall system operation is thus relatively low. However, just as they are essential to the operation of the actual system, it will be shown later that their modelling is just as essential to the study of systems, so that all possible configurations can be taken into account.

First, the distribution network topology in itself is an influential concern in the design of power harness in space. A trade-off has to be done considering their benefits and drawbacks as it impacts the weight of the overall system, or the integration complexity for example. It is also noticeable that the distribution topology has to be taken into account in the control design to make it the more general possible and thus to be operational in any case which is not trivial. Three types of distribution architecture can be identified as shown in Figure 2.20 and presented in [59].

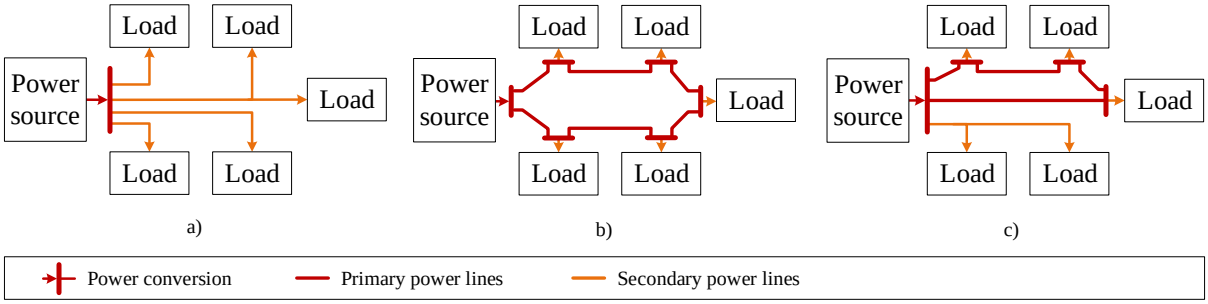

Figure 2.20 – Typical distribution topologies: radial distribution (a), loop or ring distribution (b) and hybrid distribution (c).

The radial distribution is the most widely used topology across the word – e.g. 90% of North American electrical network – regardless of the type of the electrical system. It is recognizable by its tree shape as shown in inset a) of Figure 2.20 below and whose base node corresponds to the primary power bus. In the case of a diversity of sources, it should be noted that the flows being mainly unidirectional, a reversed tree structure – as a root network – will have to be developed upstream of the primary node. Radial distribution is also the most common topology in spacecraft thanks to its ease of implementation and operation and the possibility of sizing the wire gauge specifically to the downstream loads. Indeed, each line is associated to a given equipment and only have to take into account the constraints relative to it. This topology also has some serious disadvantages. As all interconnections are made at the level of the primary node, if a new element has to be added, it is only possible to do so at this position which concentrates a large number of wire for complex systems, as it is often the case in a spacecraft. Moreover, in the case of a failure at some point of the distribution line (defective connector or loose solder), equipment of one side would be totally isolated to equipment of the other side. Nevertheless, this drawback can be minimized by splitting the different lines into several parallel lines which can thus be of smaller gauge as the current flow is shared between the parallel conductors. As a result, the distribution lines are somehow redundant and their equivalent impedance can be significantly reduced, allowing to minimize the distribution power losses.

The second distribution topology is the looped distribution as shown in inset b) Figure 2.20. In this case, the primary power bus is distributed in the whole system in chaining all equipment together which brings an intrinsic redundancy. In spite of this, although the current only flows in one direction at a time, it becomes difficult to predict all operating configuration, especially when several power sources are present in the loop. It follows from the previous assessment that sizing approach is completely different from how it is done with a radial topology: the gauge of the distribution lines is likely to be oversized

to anticipate all possible configurations. This has to be balanced by the gain of reliability and modularity as it simplifies the integration of extra load or even Distributed Energy Resources (DER).

The last distribution mode is a combination of the two firsts and is presented in inset c) of Figure 2.20. This kind of topology emerges as the size of the power system increases and the needs of different loads become more diverse. It can also appear spontaneously in systems that are constantly evolving as the network is adapted to new terminals. In multi-source networks, by connecting the different sources – primary or secondary sources – in a loop and the loads in radial distribution, a variation of electrical production or a loss of a transmission line can be overcome and a production unit can replace another. In this case, the isolation of deficient units and transmission lines is needed to be possible and controllable.

If these two last kind of distribution topologies seem to be well suited for Lunar or Martian bases, or more globally in a cooperation framework, it is important to note that they have to be avoided in LEO orbital systems. Indeed, in these systems, all topologies that are likely to generate current loops are prohibited. The main reason is that a current loop generates electromagnetic fields which could disturb other subsystems by coupling phenomena and even disorient the whole satellite by its interaction with the earth magnetic field which is used to ensure the attitude and orbital control of the spacecraft.

In a general way, a wire – or any other kind of electrical link such as flat cables – can be characterized by a C-RL-C circuit as shown in the figure below, called π-section model in reference to its shape.

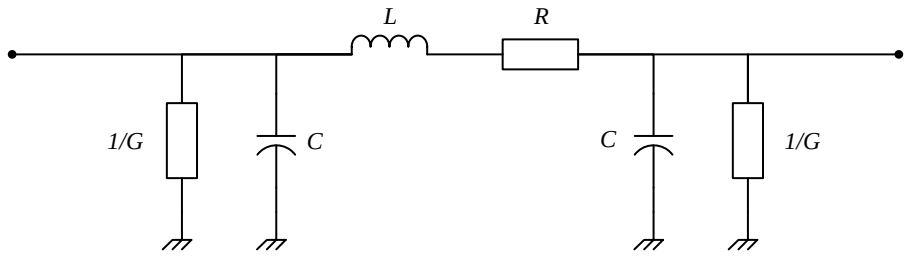

Figure 2.21 – Electrical wire π-section model.

In this model, R and L are characteristic of the wire material whereas C and G characterize its insulation toward the electrical reference – the structure or the $0V$ line. For given material and wire type, the value of the different parameters mostly varies as a function of the wire length and temperature.

This representation which is widely used in power line modelling is directly derived from Heaviside's transmission line's model [60]. It allows for any section of cable to determine its characteristic impedance, z_0, as follows:

$$z_0 = \sqrt{\frac{R + j\omega L}{G + j\omega C}} \qquad 2.25$$

with j, the imaginary unit and ω, the pulsation of the electrical signal.

In order to model a whole network, the nodal admittance matrix representation can be adopted. Generally used in massive AC networks in which the above parameters can have an important impact on grid synchronization and frequency management, it can also be applied to DC networks as shown in [61].

In this context, man call buses the different nodes which can be identified in the network. A minimum, a network is thus composed of at least the same number of buses – nodes – than the number of modules composing it.

In order to illustrate the method, an example of a 4-buses network is presented below.

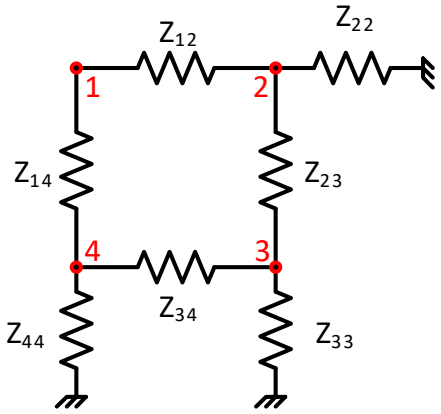

Figure 2.22 – Example of a 4-bus network.

The objective of the admittance matrix is to link the currents injected to the different nodes, marked in red in the figure above, and the voltages at these same nodes.

The determination of the nodal admittance matrix is based on the well-known Kirchhoff's law, applied to all buses of the distribution network.

In the example above, for bus 1, it gives:

$$I_1 = I_{21} + I_{41} = \frac{(V_1 - V_2)}{Z_{12}} + \frac{(V_1 - V_4)}{Z_{14}} \qquad 2.26$$

However, in order to be fully complete and to be the most general possible, it is also possible to express also the link between bus 1 and 3 and between bus 1 and the voltage reference, even if the respective characteristic impedances, Z_{13} and Z_{11}, are infinite in this example.

$$I_1 = \frac{V_1}{Z_{11}} + \frac{(V_1 - V_2)}{Z_{12}} + \frac{(V_1 - V_3)}{Z_{13}} + \frac{(V_1 - V_4)}{Z_{14}} \qquad 2.27$$

By considering the characteristic admittances instead of the impedance – $y_{ij} = 1/Z_{ij}$ – and by factorizing the expression above by the different bus voltages, the following expression is obtained.

$$I_1 = V_1(y_1 + y_{12} + y_{13} + y_{14}) + V_2(-y_{12}) + V_3(-y_{13}) + V_4(-y_{14}) \qquad 2.28$$

Applied to each bus and concatenated in matrix form, it comes

$$\begin{bmatrix} I_1 \\ I_2 \\ I_3 \\ I_4 \end{bmatrix} = \begin{bmatrix} y_1 + y_{12} + y_{13} + y_{14} & -y_{12} & -y_{13} & -y_{14} \\ -y_{21} & y_2 + y_{21} + y_{23} + y_{24} & -y_{23} & -y_{24} \\ -y_{31} & -y_{32} & y_3 + y_{31} + y_{32} + y_{34} & -y_{34} \\ -y_{41} & -y_{42} & -y_{43} & y_4 + y_{41} + y_{42} + y_{43} \end{bmatrix} \begin{bmatrix} V_1 \\ V_2 \\ V_3 \\ V_4 \end{bmatrix} \qquad 2.29$$

Knowing the voltages at each node of the system, it is thus possible to calculate the current injected at each of them thanks to the 4^{th}-order matrix thus defined. This is this matrix which is called the nodal

admittance matrix of the system, noted Y_{BUS}, and it allows to model a distribution network including its resistive, inductive and capacitive characteristics.

However, in the present study a simplified model will be used. From [62] it can be defined that since in DC systems, serial inductances and shunt capacitances are negligible compared to the converters' output filters elements, this modelling can be reduced to only taking into account the line series resistances R from the equivalent circuit above. For small-signal stability studies, this type of cable and filter modelling is appropriate, since the impact of the DC transmission lines still is represented correctly. In this context the admittance matrix becomes a conductance matrix and instead of being noted Y_{BUS}, the notation Q is adopted. This simplification does not impact the capacity of the conductance matrix to represent how all the modules are connected to each other which completes the modelling of the EPS components.

2. 2 Control

In the first part of the chapter, only the system's actuators were presented, which represents only half of an automatic system. In this part, an overview of existing control methods is then proposed, no longer concentrating solely on the control strategies conventionally used in space equipment, but extending the study to all types of control methods and in particular DCMGs.

Of course, the control functions implemented depend on the type of system to be controlled. In the case of an unregulated bus configuration, for example, control of the bus voltage is equivalent to control of the battery charge - the voltage being the image of the SOC in the case of a Li-ion battery. In this case, no high-frequency bus voltage regulation is required to ensure system stability, since the battery imposes its voltage. On the other hand, in the case of a regulated bus architecture, battery charge control is independent of bus voltage, and is therefore linked to control of the power produced by the solar generators. In this case, specific high-frequency regulation is required to ensure stable system operation at all times and in all possible configurations.

At the same time, it is important in the long term to ensure that the system is capable of balancing itself, i.e. that the energy stored in the battery is sufficient to power the system during future eclipses, without exceeding the maximum load. This involves controlling the power injected by the solar generators.

Finally, in the case of a modular system where several storage modules are connected in parallel to the system, in order to control balancing between modules - as with balancing between cells within a single battery - it is necessary to control the sharing of currents between them. This control must also ensure that the current capacities of each module are respected, which requires a relatively high level of dynamics.

From the elements presented above, it is possible to classify the dynamics of the various control functions by order of magnitude. This gives rise to a hierarchy of control laws, very widespread in the field of terrestrial applications, as illustrated in [63], [64], [65], but also in the space domain such as in the ISS as detailed in [4], or in [66].

Figure 2.23 illustrates this hierarchical structure which is generally composed of three levels of control. As it can be seen, their definition can defer from one application to another since the constraints but also the degrees of freedom of the systems intrinsically depends on their nature – electrical architecture, operating context and environment, etc.

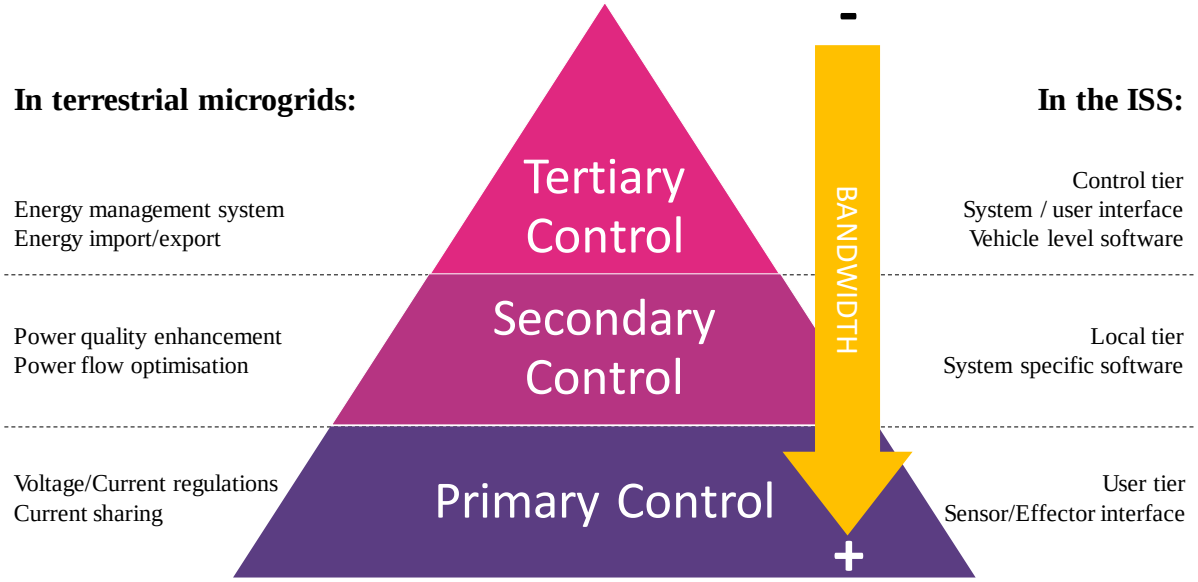

Figure 2.23 – Hierarchical control categories as presented in [63] and their equivalence with the ISS control “tiers” as defined in [4].

The definition of these levels are thus adapted to the present application and each of them is defined in the following subsections. For each level, a study of the existing and most significant control methods is performed thus listing the objectives which will have to be handled by control strategy proposed in the following.

2. 2. 1 Primary control

The primary control is the lowest level of control and corresponds to basic and high speed regulation loops such as individual voltage and current regulations or current sharing management introduced earlier. Most of the time, these functions are achieved locally as the characteristic response time is required to be as low as possible in order to get good dynamic performances [67].

2. 2. 1. 1 Bus voltage regulation

In the case of a regulated bus architecture, a proper bus voltage regulation has to be achieved. In conventional space systems, it is still customary to perform this control in an analog way while in most terrestrial systems digital controls are the majority and allow a greater variety of types of correctors.

Regardless of how it is implemented, voltage regulation represents the first challenge in ensuring system operation and is a critical function of the power system. In [30] and [31], units regulating bus voltage are described as "generous", as in keeping the main power within its operating range, they allow the other modules to concentrate on other aspects of the system. In opposition, these units are said to show a “selfish” behavior. Like in social relations, an EPS always needs at least one “generous” module to assure the common voltage regulation which is the guarantor of the proper operation of the whole rest of the system.

In the light of this assessment, two widely used methods are presented and compared below.

a) Main Error Amplifier

The analog bus voltage control implemented on most space systems is known as the Main Error Amplifier (MEA). It is in fact a simple analog Proportional Integral corrector, as illustrated in the figure below, based on the star point bus voltage measurement – usually inside the PCDU.

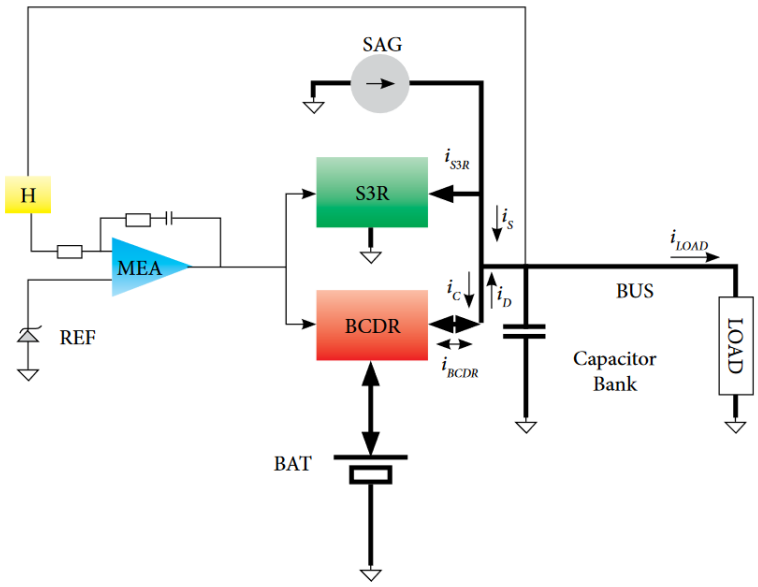

Figure 2.24 – Typical fully regulated control components [69].

As detailed in [70], the MEA manages the power regulation either from the Solar Array Generators thanks to the S3R regulator, from the battery thanks to the BCDR regulator – DC/DC converter – or from both in the same time, depending on the available power in comparison to the consumption and in order that the unit injecting the power always perform the regulation.

This way of doing is inherited from former systems, where BCDRs were not yet bidirectional, and in fact consisted of two top to tail DC/DCs in parallel, one for the discharge phase and the second for the charge phase. As in the latter case the converter is controlled in a selfish way to regulate the battery side variables, another system is required to perform voltage regulation, i.e. operate in generous mode. In most cases, the S3R is used to performs it.

This requires the MEA – analogous – signal to be reliably distributed to all power regulators in order to keep high dynamic performances for the bus voltage regulation loop. Thus in order to avoid to make the satellite's harness more complex, this has logically lead to the centralization of all units in the PCDU.

This strategy shows that only one power module is operating in "generous" mode at the time. Even if the transitions between the three operating modes presented in Figure 2.25 are automatic and lead to negligible transients to the main bus voltage as explained in [70], other solutions of control exist in order to limit the number of transition to deal with. Indeed, mode transition brings discontinuities to the system and are often critical phases of the operation.

From the strategy detailed above, it can be deduced that the S3R and the BCDR have to embed processing capacities in order to determine the appropriate response to give to a given level of the MEA signal and thus generate the corresponding control signal – switch gates PWM signals for example – to get along with the developed strategy.

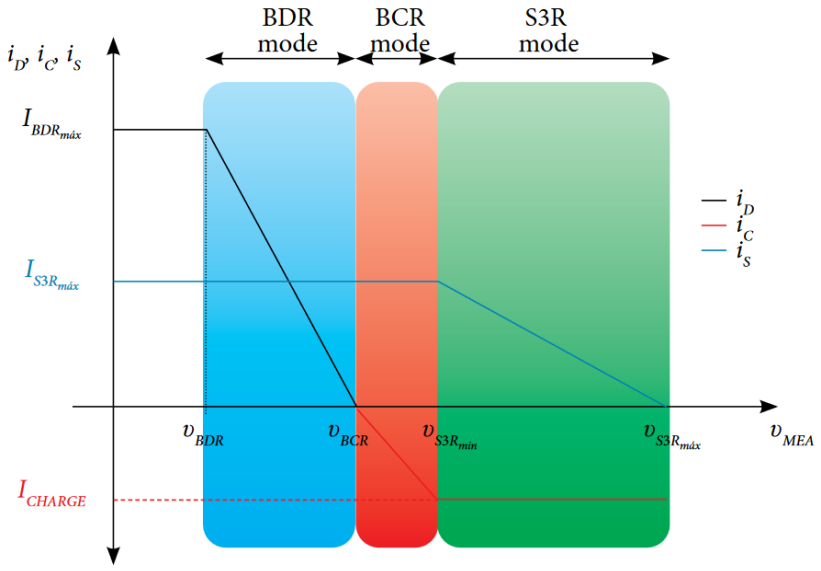

Figure 2.25 – Typical fully regulated three-domain control diagram: Battery Discharge Regulation (BDR), Battery Charge Regulation (BCR) and S3R modes [69].

Although the processing capacities in question is generally limited to simple analog OpAmp-based and signal modulation circuits, this shows that more local control, at the individual unit level, is possible. This is usually the case for terrestrial systems, which are often far apart. Indeed, in this case, it is not adequate to distribute analog signals to all units.

b) Current & voltage cascaded inner loops

In the vast majority of terrestrial applications, control is performed digitally. The ease of implementation that this brings, together with the choice of using local measurements – avoiding the need to share signals between modules – makes it possible to achieve great flexibility and therefore to implement the most comprehensive control laws possible.

Thus, in order to take into account the operating limits at the level of each module, either depending on the performance of the conditioning units, or that of their attached terminals – such as batteries or solar panels – two cascaded control loops are generally implemented, as illustrated in the figure below.

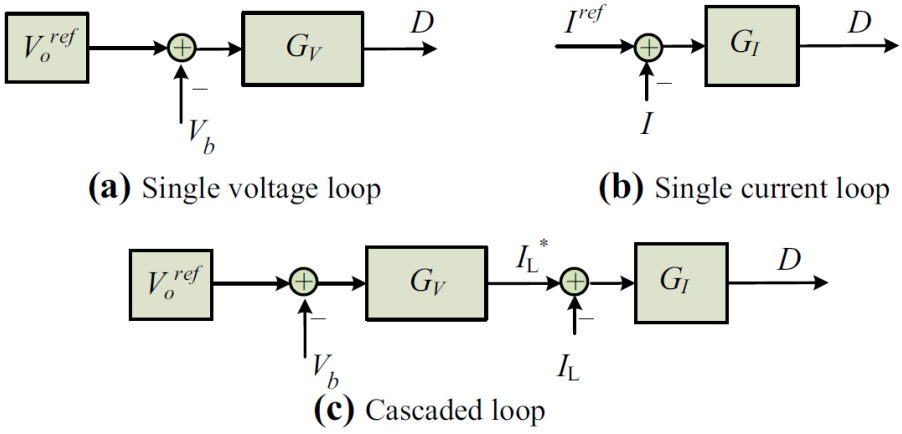

Figure 2.26 – Inner current and voltage regulation loops [71].

The bus voltage loop is then combined with a current control loop, which generally operates a decade faster, so that they can be implemented in cascade, as illustrated by inset c above. In this case, the reference signal generated by the voltage loop is homogeneous with the current used as feedback and the variable to be controlled by the current loop [72]. By simply adding saturation to this reference current, a current limitation can be implemented in the controlled system – a converter in the above case, taking a duty cycle D as the control signal.

Other methods such as robust control approaches based on Linear Parameter Varying (LPV) systems modeling can also be used to implement the DC voltage regulation, like in [73]. In [74], this method is used to implement a fully decentralized voltage control ensuring the robust stability and optimal performance of an islanded DC microgrid under different sources of uncertainties. One other advantage of this method is its ability to optimally control nonlinear systems such as DC electrical power systems by allowing the definition of equivalent polytopic-LPV models on which robust control can be applied.

The design and analysis of these so-called "inner" loops are fundamental, and are the subject of a large number of studies on DCMGs [32], [71], [75]. However, basing these regulations on local measurements, particularly for voltage, means having to manage the sharing of currents between modules. This challenge must be dissociated from internal current regulation – which only takes into account the module's own current – since it must not override the bus voltage regulation capability of modules operating in this mode.

2. 2. 1. 2 Current sharing management

The challenge of current sharing arises precisely when several modules regulating the same voltage are connected in parallel. The phenomenon can be summed up as a problem of current sharing between equivalent Thévenin sources, as shown in the example below.

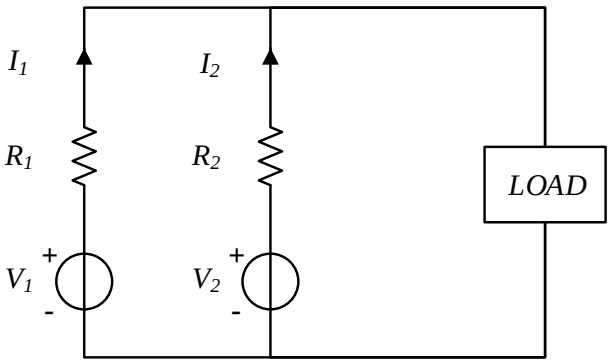

Figure 2.27 – Current sharing introductive example with two parallel Thévenin sources feeding a load.

Let's consider two bus voltage-regulating converters, modelled as ideal voltage sources V_1 and V_2 in the figure above, feeding a load through a distribution network characterized by two resistances R_1 and R_2. If the same reference voltage is applied to the two converters, that is to say that $V_1 = V_2 = V_{REF}$ the current sharing between the two converter is defined by the two line impedances as expressed below:

$$I_1 = \frac{R_2}{R_1} I_2 \qquad 2.30$$

In a purely centralized architecture, as is the case in space applications within the PCU or PCDU, this constraint is often considered negligible and therefore goes unaddressed. Indeed, based on the fact that

industrially manufactured boards are used – with very good repeatability between boards and very close performance from one to another – and that all secondary sides – outputs – are connected as close as possible most of the time, the sharing of currents between converter cells is considered to be naturally balanced since $R_1 \approx R_2$. In the field of power supply manufacturer, this way of – not – dealing the CS problem is known as « brute-force » CS [76]. Moreover, in centralized architectures, all the primary sides – inputs – are interconnected too, which means that any current imbalance between two modules cannot translate into an imbalance in different battery modules and therefore in their respective SOCs.

On the other hand, in a distributed architecture, where each element is not connected to exactly the same point on the network, and therefore where $R_1 \neq R_2$, a current imbalance appears. Moreover, in this case, the various modules are generally connected to different batteries, which leads to a progressive divergence of SOCs and generally makes it impossible to control these current shares which can cause some sever issues [77].

In addition to the line impedances, other phenomenon can induce an unbalance in the CS, such as inaccurate voltage reference values or measurements uncertainties [78].

In a first approach, individual converters should share the load current equally and stably [79] and none of the modules should sink current from the others [80]. It can also be desirable to control the current contribution of every module to implement optimized control at a system level – aim of secondary and tertiary controls. Indeed, the different power supplies may not have the same capacities and considerations have to be made to ensure a proportional current sharing.

A variety of methods exists with different complexity and performances and can be classified in two categories: active current sharing and passive current sharing methods [77], [79].

a) Active current sharing methods

Active CS methods are based on the presence of a specific loop in addition to the conventional inner voltage and current loops which uses an active circuitry to measure and compare the different modules output current [77]. A feedback signal is then distributed to all parallel units in order, most of the time, to adjust the output voltage of the different units in order to balance the CS. Indeed, based on the example studied in introduction, if V_1 and V_2 are different to each other, it can be deduced that the CS is given by the following expression:

$$I_1 = \frac{1}{R_1}(V_1 - V_2) + \frac{R_2}{R_1} I_2 \qquad 2.31$$

Thus, the difference between all active CS methods mainly corresponds to the choice of the feedback variable shared to all modules and used in each of them to compute the appropriate V_1 and V_2 values [79].

One common solution is the average current-programming. It consists in determining the average load current by gathering all converters individual current and in using it as the current reference. A weight function is used to moderate the proportion of the current rating of each converter [79], [81]. It allows accurate current sharing and load regulation. Depending on the communication link used to share the average current information, a fast dynamic response and a good flexibility can be reached with the possibility to add new units without reconfiguration required – “plug and play” feature.

A second well known active CS is the Master-slave method [79]. It corresponds to a configuration where there is one Master module, responsible of the bus voltage regulation, and the other modules are its slaves, operating in current regulation mode. The principle is that the current reference in output of the voltage control loop of the master module is shared to the slaves which use it as their own current reference. In general, as the master is the only module to operate in voltage mode, it is the first to detect load variations. This principle can be implemented in various way but in the most common one, the module which has the highest current automatically becomes the master by a system of diodes on a sharing bus. Thus, instead of determining the average current of all modules, the maximum current serves as reference which is simpler to implement. Other implementations are possible where the master module is determined and fixed and where the current reference is shared by a variety of communication technics such as radio-frequency transmission or CAN bus [82].

The common drawbacks of these active methods is the need of high speed communication lines to share the current reference to all converters. Indeed, in active CS methods, a too low-bandwidth communication link may cause instability issues due to its lags which moderates their good dynamic performances [82], [83]. Thus, the use of analogue communications is still widely common nowadays.

In view of the elements discussed in the previous section, this makes them particularly suitable for centralized architectures. On the other hand, in the case of distributed architectures, the choice of relying solely on local measurements for bus voltage regulation has been made so as not to depend on communication lines. Thus, the same consideration is generally applied to CS methods, making active methods less widespread.

b) Passive current sharing

Passive current sharing methods, also called droop control methods, are based on the principle of relying solely on local measurements [80]. They generally consist in adding a virtual resistor in series with the module to intentionally give it a Thévenin source behavior and use the phenomenon presented in Figure 2.27 to control the CS by acting exactly in the same manner than the line impedances.

In practical, it can be implemented by merely adding a gain in an extra outer loop to modulate the voltage reference as shown below.

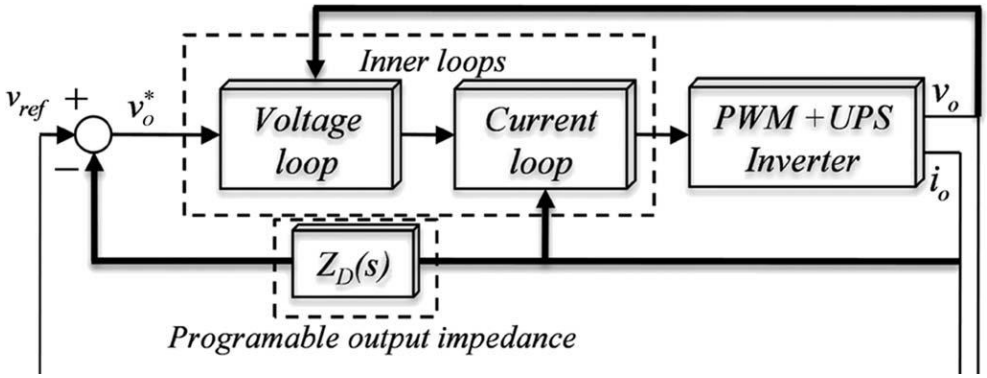

Figure 2.28 – Droop control with virtual impedance [63].

In a first approach, considering the inner loops as ideal and the programmable output impedance as a constant value noted R_D, the large-signal characteristic curve presented in Figure 2.29 are obtained based on the following expression:

$$V_{OUT_i} = V_{REF_i} - R_{D_i} \cdot I_{OUT_i} \tag{2.32}$$

In the frame of DC systems, the output impedance is in the great majority of the time implemented as a mere gain which explains that it can also be called virtual resistance as in [27] or droop resistor / droop coefficient such as in [84].

Considering three units with the same parameters, and provided that the line resistances are negligible compared to the droop resistances, current sharing naturally balances out. In practice, if one of the modules supplies more current, the voltage at its output decreases, which is detected by the other modules which, through the action of their voltage loop, automatically inject more current until a balance is found [85] [86].

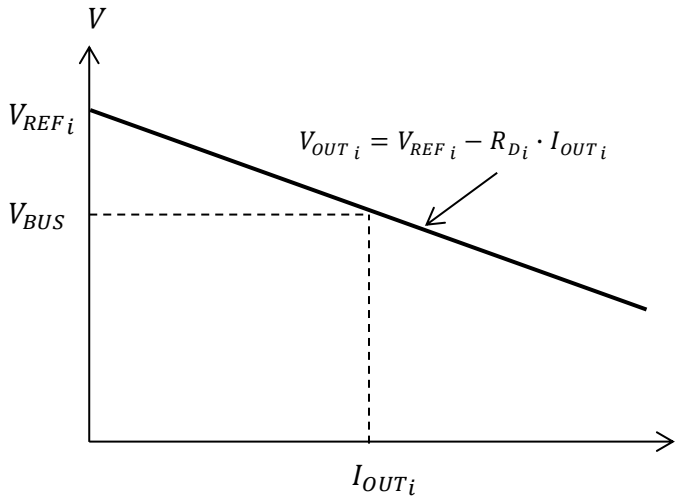

Figure 2.29 – Droop control large-signal characteristic curve.

It also comes that by varying the different values of V_{REF} and R_D, the current sharing is changed in consequence as it is shown in Figure 2.30.

First considering an identical voltage reference for every module and different values of droop resistances, the one with the highest R_D value will supply less current than the others as shown in inset a. The induced CS difference can then be expressed as a proportional relation and constant ratios between the currents as expressed below:

$$I_{OUT_1} : I_{OUT_2} : I_{OUT_3} = \frac{1}{R_{D_1}} : \frac{1}{R_{D_2}} : \frac{1}{R_{D_3}} \tag{2.33}$$

Base on this behavior, an adaptation of the different R_D of the system is thus proposed in [87] in order to balance the different battery contributions consistently with their respective capacities.

It can also be deduced from the equation above that the CS stays unchanged if all droop resistors are shifted up or down by the same value. The only impact is on the voltage drop induced for a given load and the validity of the hypothesis previously done on the neglectability of the actual line impedances

with regard to the droop resistance. Thus, the selection of droop resistors corresponds to a tradeoff between the maximum acceptable voltage and the required CS accuracy.

Considering now an equal serial resistor for every module and different voltage references, the one with the highest voltage reference will supply more current as shown in inset b below. However, in this case, the induced CS difference is constant in function of the load and can be expressed as in the following equations:

$$I_{OUT\,1} - \frac{V_{REF\,1}}{R_D} = I_{OUT\,2} - \frac{V_{REF\,2}}{R_D} = I_{OUT\,3} - \frac{V_{REF\,3}}{R_D} \qquad 2.34$$

In the same way than for the droop resistors, it can be observed that the CS stays unchanged if all reference values are shifted up or down by the same value. This property can be useful in order to compensate the voltage drop induced by the droop control without changing the droop resistors in order to keep the appropriate current sharing during transients at load steps, as proposed in [88], [89], [90], [91].

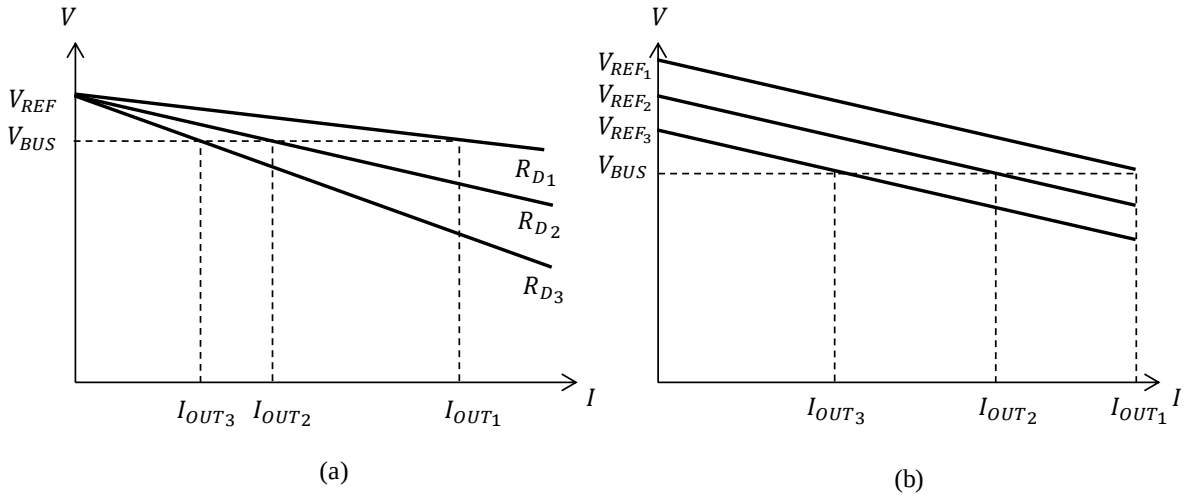

Figure 2.30 – Droop control characteristics with different droop resistors (a) and different voltage references (b).

In addition to its strong establishment in DC microgrid applications thanks to its ability to operate without any communication lines, droop control is also used in small scale systems, like in multicellular converters, to avoid central controller and increase their scalability [92].

However, these benefits have to be balanced by the reduced accuracy and dynamic response in comparison to active methods and bus voltage deviation – voltage drop caused by high load's current [88]. Two main phenomena can impact the accuracy which are the serial line impedances of the different converters – which have to be added to the droop virtual resistors value to precisely calculate the actual current sharing balance – and disturbances and inequalities on feedback measurements or voltage reference signal generation.

Even though, enhanced droop controls have been proposed to reduce these drawbacks. For example, a dynamic droop control is proposed in [65] in order to enhance the conventional droop control dynamic response. However, most of these proposed methods to improve the overall performances of conventional droop control are based on adaptations of the presented primary level parameters by secondary controllers. Some of them are thus detailed in the following subsection.

2. 2. 2 Secondary control

Secondary control handles the synchronization and the homogenization of the responses computed by the primary control to the whole system. It also ensures that the electrical levels into the system are within the required values [63]. In other words, in guaranty the good power quality and balance in the system.

In order to manage the power balance of the system, the different parameters of the primary control – reference signals as well as control parameters such as the droop coefficient – are used as output signals. To do so, even though a wide number of methods exists, adaptive control and cascaded control loops are most of the time implemented [26], [93], [94], [95]. This explains that in terms of dynamic, the characteristic time of the secondary control is generally one order of magnitude slower than for primary control. As a result, the use of communication lines is less critical since the delay it could induce would at worst only impact the general performance of the system but could not call into question its stability.

In the present study context, three main functions can be identified as secondary control components. In the following, each of them is presented and a quick review is performed on the available control strategies presented in the literature.

2. 2. 2. 1 Power sharing accuracy

First, in the case of the use of droop control as primary current sharing method – equivalent to power sharing between the different modules when considering a constant voltage – it is possible to use the droop control properties in order to enhance its accuracy in steady state.

Concerning inaccuracies induced by serial line impedances, two possible approaches can be adopted. The first one consists in adapting each droop coefficients to take into account these intrinsic – and static – disturbances. Thus, in [87], [93], adaptive droop controls are successfully implemented on the droop coefficients in order to enhance its accuracy. The second approach to limit the impacts of the line impedances is the increase of the droop coefficients in order to makes the line impedances negligible. However, in this case, the voltage deviation induced by the droop control is increased. As an element of solution to this issue, non-linear droop control is proposed in [96] to limit the voltage drop in light load condition and optimize the CS accuracy for heavy load conditions.

Nevertheless, in any case, a particular attention has to be given to the impact of these methods with regard to power quality in the system.

2. 2. 2. 2 Power quality

In the frame of DCMGs, power quality generally refers to the voltage regulation quality. Although this includes a large number of elements such as the management of current harmonics, inrushes and grounding constraints, as detailed in [97], [98], only the aspects of load regulation and, more generally, the accuracy of the bus voltage level are studied in the present study. Indeed, most of the above-mentioned elements are the subject of numerous measures specific to the space domain, which could not all be detailed here. On the other hand, it has been observed that most of the methods used to realize the CS induce variations in the regulated voltage level.

In the case where the power bus serves as an intermediate bus to supply multiple distributed Point-Of-Load (POL) converters, the voltage deviation is less of an issue [99]. However, considering the ECSS

specifications for regulated power buses given in [100], the voltage should not be vary of more than $\pm 0.5\%$ at the main regulation point.

In the frame of droop controlled microgrid a very common method to tackle the power quality issue is the voltage restoration method as presented in [71], [101]. The most conventional method to implement the voltage restoration is the adding of a second external voltage loop, at lower dynamic than the inner loop such as in [88]. This enables to reach very good voltage regulation accuracy and by taking into consideration the voltage level directly at load's input, the voltage drops induced by distribution lines can even be compensated. In order to also limit the transient voltage drop and rise at load variations, voltage restoration is implemented in [90] in combination of the non-linear droop control presented previously. Based on the same principle, an adaptive control is presented in [102] to compensate the voltage deviation in increasing the voltage reference in high loads conditions. In the context of space system, voltage restoration is proposed in [91] as a solution for manned lunar base microgrid.

As part of the power architecture chosen for this study, it should also be noted that the bus voltage also applies to the solar panel sections. Thus, a variation in bus voltage has an impact on the operating point of the panels. This is the principle used by the popular Maximum Power Point Tracker (MPPT) method [103]. However, in this case, fine control of the bus voltage no longer follows power quality constraints, but rather corresponds to power generation management.

2. 2. 2. 3 Power Production management

The last aspect to guarantee the global power balance is the management of the power production, that is to say, in the frame of a satellite's EPS, the control of the power injection and production from the solar generators.

The EPS of a satellite is equivalent to an islanded microgrid, so its objectives are slightly different from what can be done in grid connected microgrids. In these lasts, PV panels are generally operated at their Maximum Power Point (MPP) to supply as much power as they can, to make the most with renewable power sources, the general power balance and grid regulation being performed by other controllable terminals as detailed in [104]. The MPPT is indeed a well-known solution used in the operation of solar arrays to reach the operating point where the power production is maximized [105], [106], [107], [108].

Even though the objective is most of the time not to reach the MPP in space systems, the same principle can be used to modulate the power production of the solar generators by adapting their polarizing voltage. [68] and [69] present a method, directly derived from the conventional MPPT, called Limited Power Point Tracker (LPPT). Its aim is to regulate the output power of solar generators to a defined value by the same approach than for MPPT. In order to be able to perform this while limiting the voltage variations it induces, an operation on the voltage source zone of the PV characteristic is preferred.

If the system's specifications on the primary bus performances allow such variations, it is possible to perform it by adaptations on the voltage set point and thus use DETs as conditioning units. However, the access to the appropriate operating point is highly dependent on the PV sections configuration and environmental conditions which may vary a lot during operation. Thus, in the large majority of the applications, MPPT or LPPT are achieved by the use of DC/DC converters such as in [32] and [58].

For solar generators conditioned with DET units, the most common control consists in operating at a constant voltage at the left of the MPP – where PV behaves as constant current sources – in order to manage the power injected to the system by connecting and disconnecting the different sections, as

introduced earlier and detailed in [108]. A typical regulation loop can thus be implemented using the number of PV sections to connect as control signal and the required power as reference signal.

In any of these power production management strategies, the choice of the process variable – and thus the definition of the reference signal – is an important concern and depends on the primary objective of the function. An intuitive choice is to perform this regulation based on the loads total power demand. However, this requires to precisely know the actual power demand which can vary in large ranges depending on the application and requires to have the observability on all these data. In addition, this requires to integrate to this power needs inventory the power required to charge the batteries, which are then considered as loads from a PV panel point of view.

However, in an islanded system, the main objective of solar generators could be redefined as simply recharge the energy storage systems. Choosing the total battery charging power as feedback value thus allows to reduce the number of communication to share the required data between the different modules. Furthermore, doing so allows to consider the other loads power consumption as disturbances if a proper regulation, including an integral component, is implemented.

Finally, in this last solution, the choice of the power setpoint is much more convenient to determine since it based on the charging requirements of the different batteries composing the systems. As this corresponds to energy considerations, the definition of this value thus falls to the tertiary control

2. 2. 3 Tertiary control

The tertiary control level corresponds to the last control level considered in the present study and aims to manage slow evolutions to optimize the global efficiency of the system and long term energy balance. This is why it is also sometimes referred as supervisory control in some works such as in [111]. Like for the secondary level, it is achieved by adapting lower level control loop parameters such as control loop references, saturation limits, or even controller coefficients such as the virtual resistor of the droop control for example.

2. 2. 3. 1 Battery management

In the frame of the present study, the energy management is the ultimate control function required to allow a sustainable operation of the system in the time and in order to pass the eclipse cycles autonomously. Based on this and considering li-ion batteries as unique energy storage systems type, the state-of-the-art charging method is defined as a Constant Current, Constant Voltage (CCCV) sequence performed by an outer battery voltage loop implementing a saturation on the battery current [50], [112]. The constant current phase allows to charge the battery at its fastest rate up to approximately 95% of SOC. The actual value in fact corresponds to the value for which the electromotive force of the battery plus the voltage across its equivalent internal resistor equals the maximum allowed voltage, also called End Of Charge voltage and noted V_{EOC}.

$$E_{bat} + I_{charge} \cdot R_{bat} = V_{EOC} \tag{2.35}$$

The constant voltage phase – also called taper-current phase – is performed at V_{EOC} and allows to complete the charge of the battery by letting the current naturally tend towards 0 as full load approaches and thus avoiding any risk of overcharging the battery. The choice of the I_{charge} and V_{EOC} is mainly driven by their impact on the battery lifespan as explained in [113].

A battery C-rate is defined as the average current at which it is charged or discharge, expressed as a fraction or a multiple of its nominal capacity, noted C. Applying high C-rates induces capacity losses, especially during the charging phase [114]. Most of the time these losses are temporary and the capacity can be recovered if the rate is lowered but systematically applying high C-rates can induce long term effects and reduce the efficiency of the cells as presented in Figure 2.31.

Based on this, the manufacturers determine typical charge and discharge C-rates to optimize the balance between the electrical performances of the batteries and the evolution of their capacity in the time. $I_{charge} = C/2$ is generally applied for the charging phase.

On the other hand, as detailed in [115], the more the battery is used at a high average SOC, the faster the capacity of the battery decreases. However, limiting the usage of a battery to the a SOC of 50% for example amounts to store half as much energy and thus induces to oversize the battery for the same usage. A tradeoff between these two constraints has to be performed and in practical, it is avoided to cycle the battery above 90% of SOC – and sometimes even 80% depending of the cells performances.

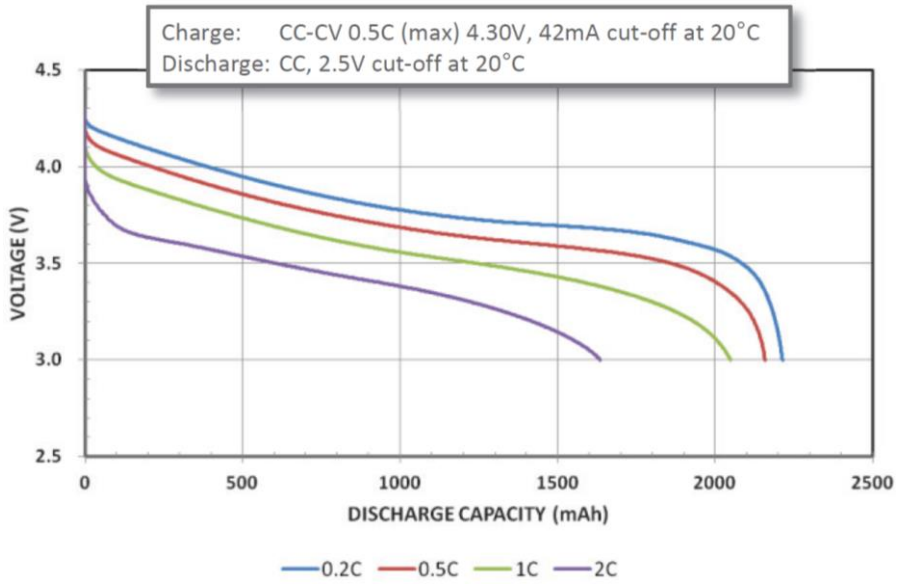

Figure 2.31 – Typical discharge curves at different C-rates [116].

Based on this and depending on the cells characteristics, the corresponding V_{EOC} is determined.

2. 2. 3. 2 Operating mode management

Finally, in the case of a system composed of PVs, batteries and a set of loads, and based on the aforementioned secondary and primary controls, the main modes can be defined as following:

- *Mode 1 - Normal operating mode*: PVs generate enough, or almost enough, power to cover the total power consumption of the system and depending on the power balance, batteries are charged or discharged to absorb or supply the power difference between the production and the consumption.
- *Mode 2 - Battery charging mode*: The SOC of a battery (or more) drops below a defined low threshold and, provided that power production allows it, the battery in question begins a regulated charge cycle.
- *Mode 3 - Full SOC mode*: All batteries are fully charged and the total power production is modulated to inject on the power bus the same amount of power consumed by the set of loads.

These system-level operating modes can slightly vary in the different papers, the principle staying the same. A “Load shedding” can indeed be introduced in the case of an absence of power primary and secondary production. The idea is, in this particular case, to shut down the less important loads to decrease as far as possible the power consumption. The most used method to represent this mode switching is the use of State-machines [117]. By using such a method, clear relationship between the operation modes and the power balanced conditions is established.

The implementation can be achieved by several ways. The first of them is the use of a mode-adaptive droop control to control subsystems [117]. It is based on the concept that if the droop control enables the different modules of the same type to achieve current sharing between each other, by defining voltage mode interval corresponding to operation modes, it is possible for the modules to determine in which mode it has to operate [68].

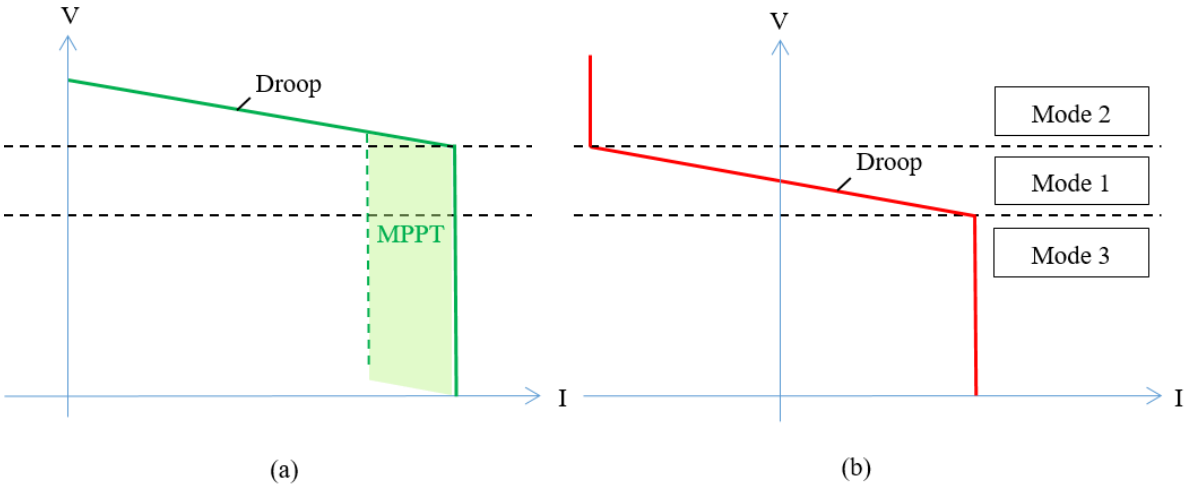

Figure 2.32 – Mode-adaptive droop control curves for PVs (a) and batteries (b)

The mode switching supervision can also be handled by a central controller which gathers feedbacks from all modules and choose the best configuration to operate [104].

The total power equation which is easily calculated, is the control law of the power flow management and, thanks to a predefined priority order between distributed generators type, the algorithm assigns power references, droop VR and operating modes to every module [118]. A centralized supervisor even allows to segregate the sections of every solar wings and to be able to identify every one of them specifically, knowing for example its location relatively to other units. Optimization problem formulation is then simplified since the global knowledge of the configuration allows to define a cost function to minimize the energy cost of the system [119] [120].

In this case, fuzzy logic supervisor is well adapted and can be used. The difficulty to predict some external or internal events such as load variations or PV power decrease due to a maneuver, makes the use of fuzzy logic interesting for smooth mode switching [121].

In the same way than in this example, an important number of researches uses the tertiary control to optimize the global operation of power systems with regards to fluctuating contexts. In [122] an electrical vehicle charging station powered by PV sources is thus studied and an energy cost optimization problem is formulated, using a mixed-integer linear programming. This allows to take into account the intermittent arrival and departure of vehicles, real-time adaptation of the power management based on meteorological predictions as well as the physical limitations of the system. The same approach

is used in [123], [124], [125], [126] to optimize load shedding, reduce the dependence on the grid – for grid connected systems – or enhance the DC power supply on islanded systems.

Even if these methods would not be fully replicable for space applications since both solar power production and loads power consumption are much more deterministic and constant and since the energy cost fluctuation is for example not a constraint for islanded systems, the method could be used to anticipate and better manage events such as attitude control loss or components failures.

2. 2. 4 Control architectures

The study of the different hierarchical control levels logically introduced considerations on the way these controls are implemented and their dependence with regard to communication lines is often taken into consideration. Thus in order to conclude this part, a quick review on the existing control architectures is performed. Indeed, in the same manner as for power distribution architecture, various control architectures exist and of the physical integration of the DHS units, directly depends the choice of data sharing protocols and communication technologies, which are highly critical for automotive control since they are the links which allow to close the control loops. The access to data is thus essential for the units which execute the control algorithms and the way it is achieved determine the type of command architecture.

2. 2. 4. 1 Centralized control

The more widespread control architecture which also is the simplest to implement – in term of control methods – is the centralized control. This architecture is based on a single “omnipotent” controller – typically the OBC – which gathers all the measurements and transmits commands to every subsystem via a data bus or dedicated analogous communication lines [67].

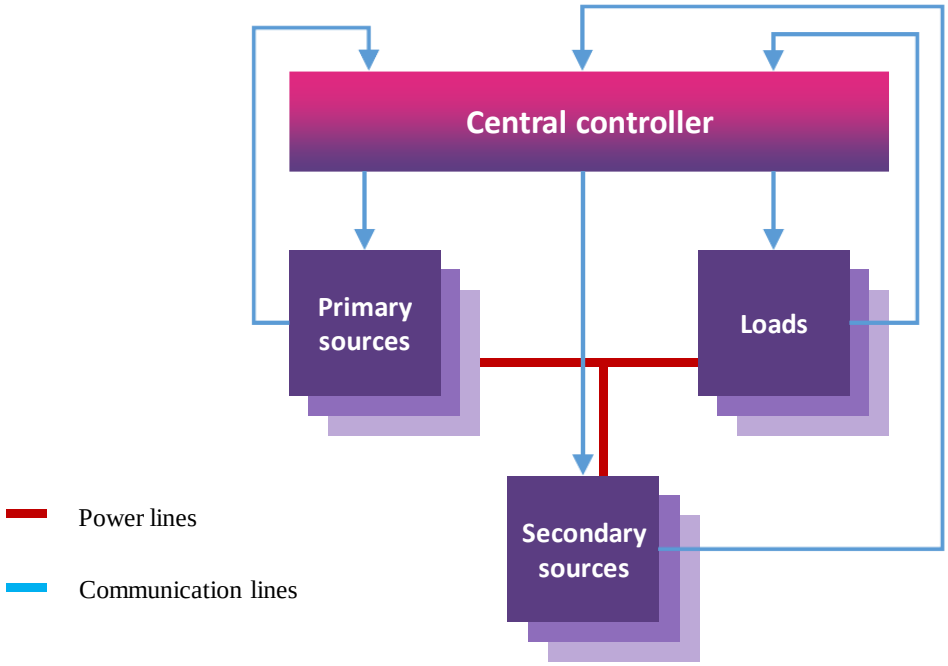

Figure 2.33 – Centralized control architecture.

The central controller has an accurate estimation of the state of every module and, by this open access to every variables of the overall system and a global view on the actual configuration of it. It makes it easy to compute the different commands to send to the modules and this is why it is often the chosen

solution for simple applications. There are two main drawbacks of this solution. The first one is the fact that the reactivity of the system is dependent on the communication speed. The bandwidth needs to be wide enough to collect measurements and send commands for high speed regulation loops. This constitutes a significant limitation in the design of control loops. The second aspect is the vulnerability of the central controller and the induced lack of robustness.

Although solutions are available like those presented in the introduction of the chapter, they are only palliative solutions to a lack of robustness which is inherent to the implemented system. In order to limit the need to implement these solutions as much as possible, which are generally costly in terms of weight, it is essential to take these constraints into account in the design choices of the systems. Indeed, in this case, if a failure happens, not only in the central controller but also in the different communication interfaces, the whole system is impacted and potentially becomes out of order.

2. 2. 4. 2 Distributed control

Distributed control is based on a series of control nodes operating independently but able to share data [67]. It means that every module can access to every data of from every module as shown in Figure 2.34. This allows each module to compute a partition of the global control strategy and share the results with other in a sort of "democratic" control system. In this sense, the execution time and the global reliability is thus enhanced as the C&C functions are distributed in several control units. Yet, the same weakness as in centralized control is observed due to the fact that the good functioning is very dependent on the communication lines.

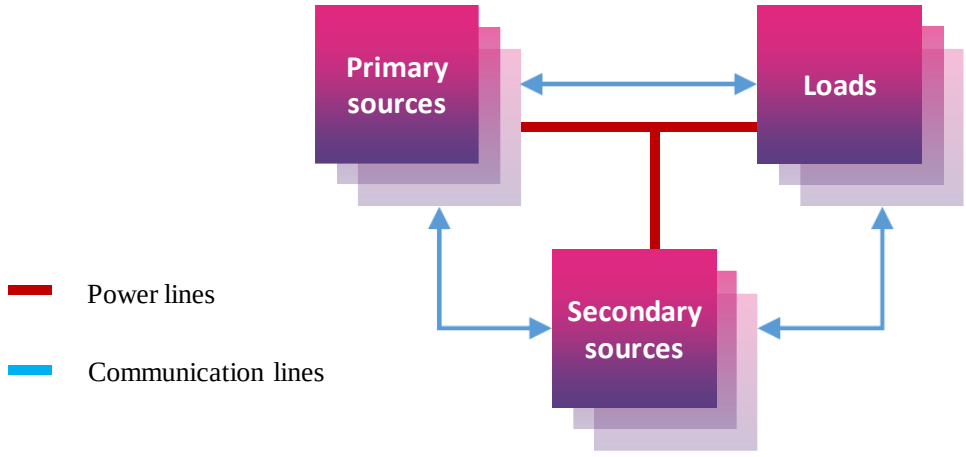

Figure 2.34 – Distributed control architecture.

2. 2. 4. 3 Decentralized control

Decentralized control is similar to distributed control in the sense that it does not have any central controller as presented on Figure 2.35 (b), but it differs by the fact that there are no communication lines between the modules to achieve their control algorithms which are thus specifically based on local measurements and an incomplete knowledge of the system [27]. Initially, this control architecture was developed to tackle the control of systems which were too large and/or too complex for being simply achieved by fast computers with large memories [127].

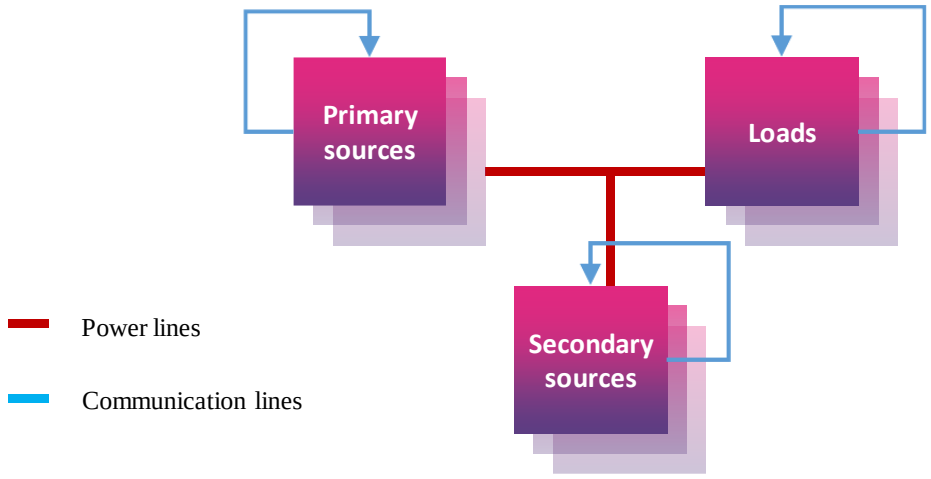

Figure 2.35 – Decentralised control architecture.

The principle is then to divide the analysis, synthesis and control of the overall system into independent – or almost independent – sub-problems. This enables an important gain of modularity because the control does not rely on communications and makes the interface constraints easier to satisfy. It also induces limitations in global optimization because the only view on the rest of the system is what can be measured at the module's terminals. In this case, every modules of the same type generally execute the same program.

The different control architectures are combined in a lot of complex systems to handle the different control functionalities and especially match their need of a global or local knowledge of the system which is the overriding criterion in the choice of the type of architecture. Indeed, these systems are often made as a mere assembly of several independent subsystems based on the fact that all these subsystems are independent. Nevertheless, it is likely to be more an assumption than a fact, and from this point of view, the overall systems can be seen – at least partially – as decentralized controlled systems, although they were not designed as such.

It is also interesting to observe that these notions of control architectures are as valid at the satellite scale as at the level of a subsystem such as the EPS. This highlights its fractal structure which can also be found in automation when several cascaded loops are employed. For this vision to be valid, it is necessary to make the same assumption as before is made, i.e. that the different successive fractals can be considered as independent of each other, but this time not by segregating different type of functionality but rather by identifying different time scale which allow to consider the input parameters of the lower scale fractal as constants.

The choice of input parameters is therefore crucial in the design of a system and is not unique and depends on the logic with which the problem is approached. Paradoxically, the more precise and detailed the parameters are, the easier the system is to design. This is the reason why it is easier at first to develop a very specific system and only then to make it evolve to a more universal version. From this point of view, ensuring a continuous power supply in an environment as isolated as the space environment is not an easy task.

Proceeding like this, the border between primary and secondary control is identified as whether the algorithm is processed in local controller or in the central one [128]. Two types of control architecture thus coexist in the system and improves system's reliability thanks the intrinsic controller redundancy it induces. However, the impact in terms of stability of all these interleaved and cascaded control loops has to be properly addressed.

2. 3 Stability analysis

According to [68], the stability and operating capacity of a power system depends on the capacity that the different conditioning modules have to regulate the power flow in the system. As a consequence, in the case of a DC system, this power balance stability can be assessed by studying the overall system's bus voltage stability. Indeed, an excess of power injected to the primary power bus induces the charge of the equivalent bus capacitor – composed of the parallel association of all converters bus side filtering capacitors – and thus the rise of the power bus voltage. Reversely, a deficit of power injection will induce a drop of the primary power bus voltage.

However, the notion of stability also induces to take into consideration the dynamic of the different phenomena impacting this balance. In this respect, fastest phenomena are often considered as the most impacting in terms of stability. This is why only the closed loop system composed of the primary control loops are most of the time taken into considerations in studying the stability [87], [129]. In order to assure that the system is still stable while secondary and tertiary control are implemented, variations on reference signals and parameters can then be considered at primary level such as in [130]. To do so, a large number of stability analyzing methods and criteria can be used.

All of these methods and criteria are based on the general stability criteria of a linear time-invariant (LTI) dynamical systems which states that a closed loop system is asymptotically stable if its transfer function does not have any positive real part poles. In the case of state space representation, the same condition applies to the eigenvalues of the state matrix A. However, even if the system would be stable if this condition is fulfilled, its performances would not be identical depending on the real and imaginary parts values of the roots of the system.

The classical Gain Margin and Phase Margin (GMPM) criterion is the most rigorous and complete approach to assess a system's stability, not only in the frame of EPS. It allows to identify precisely the range of validity of the stability criterion as well as study the related time-domain performances of the system [96]. This method has been used for long in the frame of academic studies on DCDC converters such as in [19] and [87]. In the frame of space systems, it is used in [132] in order to design a S3R for high-power applications. However, the GMPM's results validity are highly dependent on the system model accuracy and this last is most of the time obtained through successive simplifications. In order to reach a wider validity range and to guarantee the desired performances, the whole system should be considered, which makes the analysis more complex.

Based on this assessment, it is usual that the system's controllers are designed considering a nominal or worst case operating point, with the desired performances and that only then, the stability is assessed on the whole range of operation. To do so, some simpler criteria can be identified by derivation of the general stability criterion.

In the frame of EPS, the Middlebrook criterion is one of the most common. It states that in a system composed of a single source and a load, the stability is guaranteed if the source's output impedance $|Z_o|$ is always – much – lower than the load's impedance $|Z_i|$ as presented in [133]:

$$|Z_o| \ll |Z_i| \tag{2.36}$$

The criterion is also known as the impedance criteria [134]. As explained in [128], this criterion is derived from the Nyquist stability criterion with the aim to provide a simple and conservative criterion

to apply for power converter systems design. In addition to terrestrial applications, it has been widely used for space systems, including for the ISS stability analysis as detailed in [21].

However, the Middlebrook criterion only apply to very simple systems and does not allow to study the stability across a whole complex system [135]. In addition, considering complex impedances, the condition may be too conservative and can be released in some frequency ranges [128].

In this sense, the Routh-Hurwitz criterion allows a more precise assessment. It defines that a necessary condition for a system to be stable is that the coefficients of the characteristic polynomial should be positive. It also stated that a sufficient condition is that all the elements of the first column of the Routh array should have the same sign. It is applied in [135] to a DC network connected to the AC grid. In [136], the Routh-Hurwitz criterion is applied to aircrafts EPS in the frame of the development of the More Electrical Aircraft (MEA) project.

All the methods presented above correspond to analytical methods based on small-signal approximations, which require the manipulation of the transfer functions or state representation matrix, and a deep understanding of the models. In the case of time evolving or non-linear system the same analytical approach should be repeated for each configuration which is not feasible by hand.

In the study of nonlinear systems, the Lyapunov stability theory can be applied [134]. In [86], it is used to analyze the stability of a droop controlled DCMG implementing bidirectional Boost converters. A Lyapunov stability analysis is also performed in [137] on an AC system implementing a H_∞ controller. However, due to its relatively complex implementation – in comparison to other methods – it is rarely applied in industrial projects. Indeed, for large scale applications, the ease of use and implementation are the main parameters which drive the choice of the stability analysis method.

In such cases, which in fact corresponds to almost every practical system, numerical methods based on computing can be used. This mainly consists in defining a parametric model of the system, a range of variation for each parameter and numerically compute the poles and the zeros. The computing capacities thus allows to take into account very detailed system models and a wide range of parameter variations. To visualize the results two main graphical representations are used which allows to easily determine the system's stability.

The first one is the Nyquist plane. Also called W-plane, it enables to represent, in the complex plane, the harmonic response of the corresponding open-loop of a system for a pulsation ω varying from 0 to infinity, called the Nyquist plot. In this representation, the graphic interpretation of the general stability criteria is that the number of unstable closed-loop poles is equal to the number of unstable open-loop poles plus the number of encirclements of the point $(-1, 0)$ [128]. It is used in [96] to study the stability of a DCMG composed of an hybrid resistive and constant power load controlled with a nonlinear droop characteristic. In [21], it is combined to the Middlebrook criterion in order to analyze the stability of the ISS JEM module EPS. Complex, high-order multi-converter systems can also be studied with this method such as in [138] where it is combined to the admittance matrix modelling of the system to study the impact of the physical location of the different converters on the system's stability margins.

The second common graphical representation is the Laplacian plane, called S-plane in reference of the Laplacian variable s. The S-plane is a complex plane with an imaginary and real axis which allows to simply plot the roots – poles and zeros – of a system thanks to their respective imaginary and real parts. When mapping poles and zeros onto the plane, poles are conventionally denoted by an "x" and zeros by an "o". The position on the complex plane also gives information on the system performances thanks to the argument to the origin and the angle from the positive, real axis around the plane of the dominant

roots. In this plane, the graphic interpretation of the general stability criteria is trivial: when plotting the poles of the system, for it to be stable, all of them have to be in the left half plane, corresponding to the negative real parts.

A practical property on this plane is the possibility to observe the changes of the root locations with regard to a given parameter variation. For a given system, the lines on which the roots move for a given parameter variation are called the root locus. It is widely used in order to study the stability sensitivity to some changes, either at modelling level, due to non-linearity for example, or at parameter level. This is particularly useful when adaptive controls are used such as in [87], [96] or at design phase in the determination of components values such as in [139].

However, even if these graphic methods allow to address merely more complex systems, it can be difficult to interpret their outcomes practically. In order to do so, their combination with large signal analysis can be performed. Indeed, thanks to the computing capacities of numerical solvers, it is easy to determine the reaction of a system in any configuration in which it might be. Thus, in [140], [141], [142], the stability of a typical spacecraft's EPS is assessed thanks to phase plane trajectories representation, as defined in [143]. In addition to sometimes allowing to understand the origin of stability boundaries determined analytically, it also allows to determine if the different equilibrium points of the system are reachable in function of the defined initial state.

The combination of several methods is an interesting principle for a systemic approach in terms of stability analysis. It allows to evaluate it with regards to different phenomenon and dynamics. However, the increasing complexity of the systems studied often leads to simplifying the models, which generally results in a drop in representativeness if the justification is not precisely studied or if it is not valid over the entire operating range taken. into account.

The most common example of this is the global trend to always simplify all systems to unitary systems, composed of a single equivalent converter and a single equivalent load in order to be able to apply basic stability criteria, and systematically consider linear systems such as the Buck topology in terms of converters.

This simplification of the system is most of the time justified by the fact that the consideration of CPL mode operation of the different converters corresponds to a worst case in term of stability. However, this assumption is not always true as demonstrated in [144].

Thus an important challenge is to adopt a more generalized approach to study these systems in their most complete form. This is what is done in [65], [129] using the matrix formalism based on the admittance matrix representation of the distribution network. It allows to develop in [111] a detailed analytical stability analysis of DC systems and opens new perspectives in the way these systems are studied.

2. 4 Conclusion

In this chapter, the state of the art of the different aspects studied in the following were presented which enable to identify gaps in the literature.

First, the study of the electrical power components used in classical satellite's EPS allowed to realize that with the exception of resistive loads, all of them are nonlinear which makes their formal modelling more complex. In most of the cases, the small signal approach is then used by linearizing the system around operational points to be able to study it. However, this also have the effect of focusing the global

attention on the simplest systems as the large number of publications on the Buck topology shows. Indeed, this last's linearization is trivial which makes it more regularly studied than others. Finally, at this step of the development, as the components are treated as individual units, only low attention is paid to distribution lines which are most of the time neglected.

In a second part the hierarchical control structure was introduced and allowed to detail the different components composing the full system's control. This showed the relation which could be made between the different way of implementing control features: secondary and tertiary controls are usually implemented in a centralized way since they require a more systemic point of view, based on data coming from all over the system, while the primary control is preferred decentralized in local units based on local measurements to guarantee good dynamic performances with no dependence on communication lines. This structuration of the control features allows to treat each unit composing the system independently and thus enhance the overall modularity at least at primary level. However, and as the short term stability of the system indeed mainly relies on the primary control functions, this observation is often used to justify the simplification of the system in order to study its stability.

Indeed, in the review of the existing stability analysis methods and criteria performed in the last part, it was demonstrated that in most of the cases, the stability analysis performed on EPS relies in the application of a criteria designed for unitary systems. This observation explains the need of simplification of the system which pushes to consider all converters separately. Nevertheless, this "need" is more dictated by the lack of an appropriate formalism to simply model multi converter systems than a real requirement imposed by such system's physical properties.

Questioning the neglect of line impedances in this context goes a long way towards feeling this gap. One of the aims of the next chapter is thus to demonstrate how taking the line impedances into account enables us to simply set up a formal representation of a system that also allows us to study its stability and performance in a more complete and rigorous way. As such, it will show how these hitherto neglected elements due to their low impact on systems performances, become of prime importance in terms of systems modeling. In addition to this, the main hypothesis, conventions as well as design choices will also be detailed.

CHAPTER 3.

Study case definition and preliminary developments

Summary

The purpose of this chapter is to set up the tools and main hypothesis necessary for the developments presented throughout the rest of the thesis.

In the first section, a reference system used to test the theoretical developments by their application to a realistic case is presented. Based on assumptions of LEO mission profiles, key parameters and main components operating ranges are defined following a similar approach to what is actually done for satellite's design. The system is then simulated in a unitary way, with only one module of each type like in conventional applications, in order to define a benchmark on which the results obtained with the proposed control can be compared.

In the second section, the global strategy proposed for designing the system's control is presented. Based on the elements presented in the state of the art, a particular emphasis is done on the chosen current sharing method and the control functions allocation strategy with regard to their hierarchical level and degree of dependence to communication links. This allows to present the general guiding principles which have been followed all along the project.

The two last parts introduce some key methods and preliminary developments used to tackle the two main challenges of studying distributed power systems. Thus, the hypothesis used in the present work to handle nonlinearities is first presented and justified. A specific focus is done on the nonlinear components which are directly connected to the primary power bus: the electrical power converters and the loads. Finally, a method to generalize and formalize the representation of the overall system is introduced. Its aim is to present a solution to accurately and simply represent the system in its entirety, including all control functions, in order to avoid excessive simplifications to study its stability and performances.

3. 1 Reference system

The reference system introduced in this first section aims to provide a realistic case to apply the theoretical results obtained and quantitatively evaluate the performances in comparison to conventional system. The definition of a reference model basically amounts to the same exercise than the EPS preliminary sizing achieved in the phase A or B of a mission lifetime cycle – early development phases. It consists in choosing and sizing the different power terminals, namely the production and energy storage devices, needed to achieve the mission.

It has to be noted that the sizing of the EPS has an important impact on its performances as presented in [145] for terrestrial applications. However, up to now, the reliability requirements applied for space applications have been met by taking into account the worst cases in terms of systems operating conditions and applying important margins at the sizing phase of the EPS. This has led to a general oversizing of the different elements which is even more important considering the NRB architecture for which the mismatch of components actual operating point with regards to their optimal operating point is significant. The proposed architecture could thus allow to redefine the sizing process of the EPS to implement optimal sizing by enhancing the interdependence of the different terminals. Several works have been undertaken in this sense such as in [146], in which a statistical approach is implemented to design the EPS. Nevertheless, these sizing aspects are not covered by the present thesis since it focuses on the control aspects of the EPS.

Thus, a conventional scenario of a LEO orbit mission is chosen for the case study. At an average altitude of 400 kilometers which corresponds to the operating orbit of the ISS, it corresponds to the most common orbit for current and future missions. The orbit type has an important impact on the sizing of

the EPS since it defines the available Solar flux as well as the illumination and eclipse duration and frequency.

The precise sizing procedure which was performed to determine the study case and justifications are presented in Annex A. Its main characteristics are presented in the table below.

Table 3.1 - Use-case parameters.

Description	Symbol	Values	Units
Mission profile			
Orbit duration of which day of which eclipse	D D_{day} D_{night}	93 62 31	min
Solar flux average	S	1370	$\mathrm{W.m^{-2}}$
External temperature range	T	$[-170\,;\,125]$	$°C$
Power consumption			
Average power consumption	P_{avg}	110	W
Maximum power consumption	P_{max}	230	W
Primary power bus			
Primary power bus voltage setpoint	V_{ref}	28	V
Energy storage			
Cycled energy	E_{cycled}	60	$W.h$
Maximum depth of discharge	DOD_{max}	20	%
Battery required energy capacity	E_{req}	328	$W.h$
Power production			
Solar panels required power	P_{req}	205	W
Number of PV sections	N_{sec}	10	-
Sections short circuit current @28°C	I_{SC}	0.9	A
Sections open circuit voltage @28°C	V_{OC}	35	V

In accordance to the chosen mission orbit, a scenario of an Earth observation microsatellite based on a Myriade platform [147]. Typical power consumption profiles are often composed of a constant component and a variable one. The constant component corresponds to the basic power consumption needed by the overall system to operate properly, payload and platform combined, and also corresponds to the safe mode power consumption. The variable component of the power consumption is induced by the sub-systems whose mission requires them to respond to specific events, mostly related to the location of the spacecraft in its orbit.

Based on these power consumption parameters, the operating voltage of the primary power system is chosen in accordance with the rules determined by the European Cooperation for Space Standardization and listed in [100].

These standards have been defined to reach the best tradeoff between the electrical performances – especially in terms of distribution losses – and the constraints applied on the power systems – which rise with the increase of the operating voltage in the space environment. This standard determines the voltage

levels to be respected and associates to it a determined power range in order to respect a balance between voltage withstand – which is particularly constraining in the space environment – and conduction losses as can be found on all power distribution systems. Thus, for a regulated bus voltage of 28V, the maximum specified power is 1500W, which is sufficient for the determined power budget.

Taking into account the maximum eclipse duration as well as the determined power consumption during this phase, the cycled energy can then be determined. This energy corresponds to the minimal energy capacity required for the system to operate. However, in practical, margins are applied to it to size the storage elements in order to be able to overcome situations after faults in which the system would lose its Sun pointing functionality.

Indeed, the sizing of the solar panels are highly related to the battery. The required power production is directly deduced from the power required to recharge the battery during illumination phases. In combination with the power consumption and the available solar flux, the solar panel configuration can thus be determined.

Implemented in a unitary, fully centralized and conventional way, with only one PCU composed of the 10 DETs connected to the 10 PV sections, one equivalent load and more particularly one battery with a single battery charge discharge regulator, as shown in Figure 3.1 below.

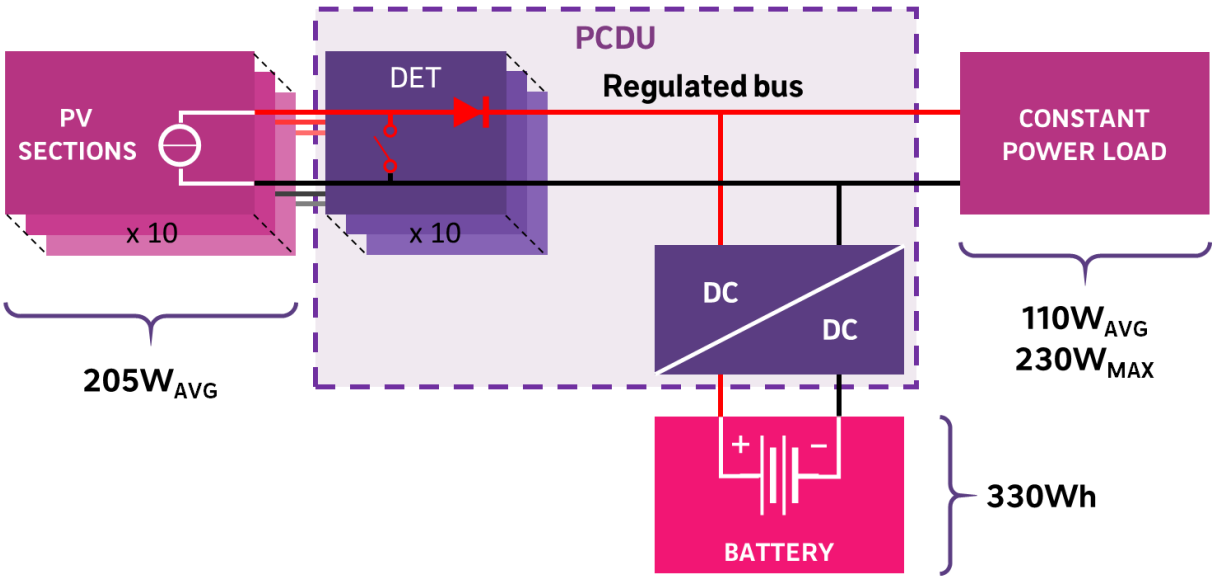

Figure 3.1 – Conventional centralized implementation the reference use case.

The results presented in Figure 3.2 are obtained for a 6 orbits-long simulation.

Inset a) shows the power consumption profile obtained by the parameters characteristic given above. It is constructed with a random duration offset compared to the actual orbit duration in order to vary the consumption profiles in eclipse from one orbit to another. This explains that the DOD observed in inset f) is not constant all along the simulation. In this inset, it can also be observed that the battery is initialized at 70% of SOC. It allows to check that the solar panels are able to recharge it properly even if the discharge is more important than expected. Insets b) and d) show the battery voltage and current. On these curves, the classical constant current, constant voltage charge cycle can be observed. This is obtained by the DET control which connect or shunt the appropriate number of PV sections depending on its power production as shown in insets c) and e).

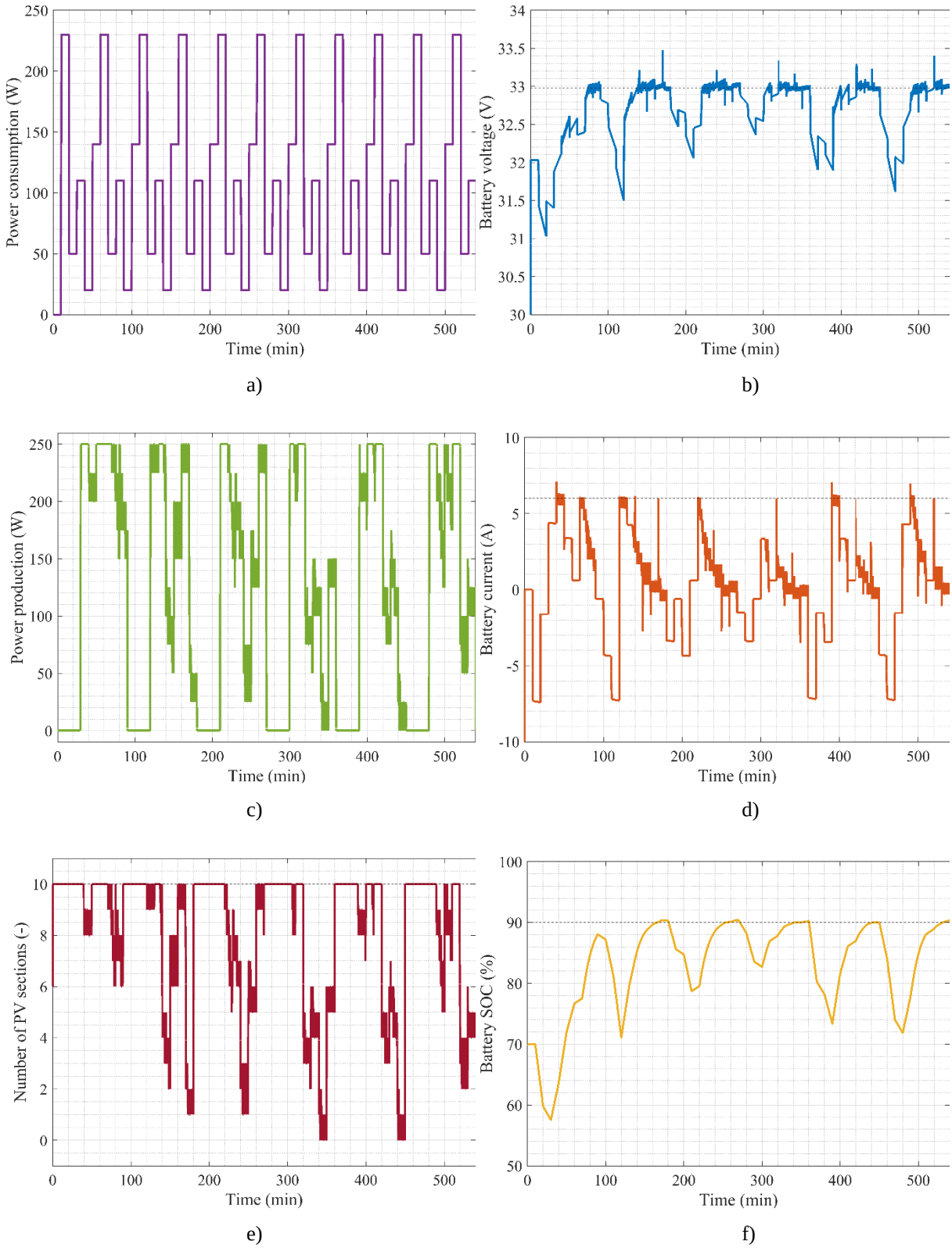

Figure 3.2 – Reference system centralized implementation simulation results: loads power consumption (a), battery voltage (b), PV total power production (c), battery current (d), PV sections control signal (e) and battery SOC (f).

This simulation will be used in the following as a point of comparison and more generally allows to better understand the operation of such systems. Its main objective is indeed to give an example of possible application and the results obtained in the present work does not limit to it. The following sections in particular aim to propose the most suitable methods and justifications to homogenize and formalize the modeling of the proposed electrical architecture, regardless of its configuration – number of modules, distribution network topology, etc – as shown in the figure below.

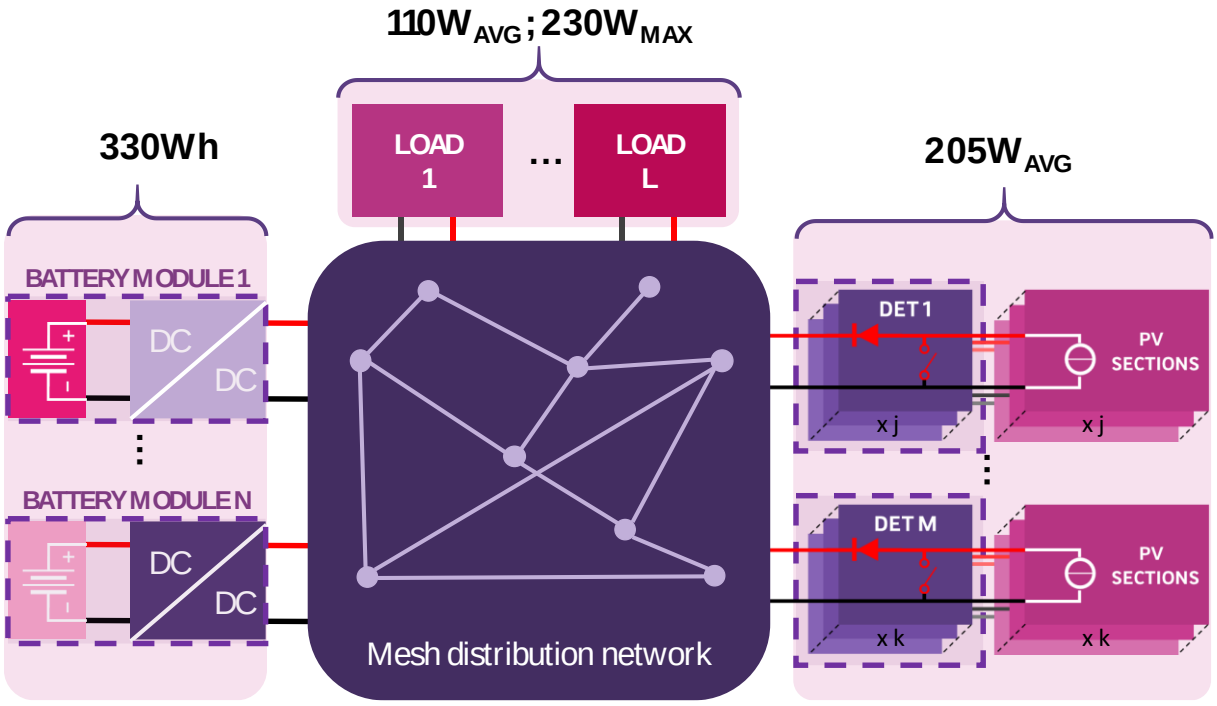

Figure 3.3 – Modular implementation of the reference use case based on a set of L loads – resistive and constant power loads – M sets of PV sections and respective DET modules and N battery modules interconnected by a distribution network implementing any possible distribution configuration – mesh topology chosen for a general approach.

3. 2 Proposed control design strategy

In order to define some general guiding principle for the development of the global control strategy for the proposed electrical power system architecture an important trade-off is necessary. These design choices have to take into consideration an important number of parameters starting with the capabilities the proposed electrical power architecture aims to provide.

The study of the state of the art concerning electrical power systems control architecture introduced the concept of hierarchical control and shew how it is already de facto implemented in space systems. This way of structuring the control functions is indeed particularly well adapted to systems which have to combine the constraints of modularity and the need of data centralization. Indeed, in the case in space segments since the data must be downloaded to the ground segment to allow the spacecraft remote monitoring and control, a central controller is required. However, the distributed processing resources the proposed electrical architecture embeds to enhance its modularity, both in term of functional segregation and interfaces simplification, offers opportunities to reallocate a certain number of functions as well as introduce new ones as detailed in [148].

Based on this, the principle of subsidiarity is introduced as the major rule to design and allocate the control functions in the different modules. Subsidiarity, most of the time applied to political systems, can be defined as the principle of devolving decisions and responsibilities for performing some actions to the lowest practical level able to do it. A corollary deduction of the strict application of the subsidiarity principle is that for each level of operation, the strategy inducing the lower level of modules interdependence and need of communication has to be defined to be compliant with the requirements of a modular space system in the same time.

At primary level particularly, this assessment justifies that each converter should implement its own inner current and voltage regulation loops. Furthermore, it makes of the droop control the most suitable current sharing method since its main advantage is to rely on local resources to operate. Indeed, this goes along with the want to avoid any discrete analog signal distribution between modules for control purpose. Moreover, the implementation and working principle of the droop control is relatively simple. Precisely, in addition to making it more likely to be actually implemented in an industrial context, the definition of a system as simple as possible also limits the necessary increase of the risk of failure induced by a more complex system. To this regard, the high autonomy and independence of the different modules processing the function gives it an intrinsic redundancy and functional partitioning which makes the fault isolation much more simple to handle since no module is a priori essential for the rest to operate. Lastly, the apparent good compatibility to actual conventional systems, as it can be implemented as an "add-on" to inner control loops that already exist, minimizes the changes to perform at these level which is an important concern in the space industry in which heritage plays a predominant role.

At secondary and tertiary levels which respectively handle the power and energy management and thus require a more global knowledge of the system, outer cascaded – and thus slower – control loops as well as adaptive control are favored. At this level of dynamic, which makes of the related control functions less critical for the system's short term stability, and considering the targeted objective of each control component, communication line can be used and several practical allocations can be defined. However, here again, the subsidiarity principle applies.

Finally, in the design of the all control functions, it has to be guaranteed that the system stays in its nominal operating range and limits of operation thus have to be precisely identified at each level. This is usually done by the introduction of saturations on output control signals. For most primary controls, the operating limitations correspond to the physical or practical limits of the components such as the maximum voltages or currents for power switches or the duty cycle of converters which is bounded by definition between 0 and 1 for examples. At secondary and tertiary levels which provide as output control signals the input setpoint of the primary levels, these limitations are dictated by two main aspects.

The first one is the stability boundaries of the inner loops which have to be guaranteed and for which specific conditions on setpoint operating range could be defined. This aspect which comes up from primary control performances is studied in depth in the next chapter. However, to do so, and to limit the frame of the study to consistent cases, the conditions of existence of equilibrium points, which constitute the second limiting aspect, have to be defined, coming down from the secondary and tertiary perspectives. Indeed, these limits can be defined by the study of the large-signal characteristics of the systems as they would be from a high level point of view if all lower level control would be implemented. Nevertheless, these characteristics are most of the time nonlinear which makes them more difficult to study.

3. 3 Nonlinearity management

In addition to characterize the large-signal characteristic of certain subsystems, nonlinearities are also present in the model of some others, despite the fact that their large-signal characteristics are linear. Thus, more than just changing the conditions of existence of equilibrium points, in these cases it also makes it impossible to apply the conventional control theory methods which only apply to linear systems for most of them. From this, the linearization of the systems appears as the keystone of their study.

In the conventional way of doing, the linearization is often done once the whole system is represented. However, for system combining a large number of nonlinear subsystems, the mere initial nonlinear model determination can become complex as some modelling formalisms only rely on linear operations.

Thus, in the present work, in order to facilitate the modelling and thus enable the study of the entire system, it is proposed to perform its linearization at subsystem level. The resulting bi-level system model especially allow to specifically define an individualized linearization strategy for each type of module.

3. 3. 1 Power converters model homogenization

In the frame of power converters, in order to overcome nonlinearities, the Buck converter – whose average model is linear when considering a constant input voltage – is often used as a standard application. Although it may lead to a lack of representativeness and accuracy, this is driven by the difficulty to have an homogenous representation, easily applicable to any kind of converter, which is an important need in order to apply classical analysis methods.

Starting from this postulate, and in order to propose an adequate solution while keeping a similar approach toward towards comprehensive coverage of different converter topologies, the state feedback linearization's implementation like in [149], [150], in the control of all converters composing the system, is suggested as a simplifying prerequisite to its study.

This hypothesis, which may seem coercive, is nonetheless essential in order to justify the use of a homogenized model and made always more easy to implement with the generalization of high-performance digital controls.

In a general way, nonlinear systems can be expressed as

$$\begin{cases} \dot{X} = f(X) + g(X,u) \\ Y = h(X) \end{cases} \tag{3.1}$$

Taking the example of the Boost – as introduced in Chapter 2 – to illustrate the method, when considering the load as a perturbation and focusing on the state equations, it comes:

$$\dot{X} = \begin{pmatrix} 0 & -\frac{1-\alpha}{L} \\ \frac{1-\alpha}{C} & 0 \end{pmatrix} \cdot X + \begin{pmatrix} \frac{1}{L} \\ 0 \end{pmatrix} \cdot v_{IN} \tag{3.2}$$

with $X = \begin{pmatrix} i_L \\ v_C \end{pmatrix}$

3. 3. 1. 1 Current loop linearization and control

Focusing first on the inner current loop, a sub-system of degree $n = 1$ can be expressed in the following form, considering α as the input variable and i_L as output:

$$\begin{cases} \dot{i_L} = \dfrac{1}{L}(v_{IN} - v_c) + \dfrac{1}{L} \cdot v_c \cdot \alpha \\ y = i_L \end{cases} \tag{3.3}$$

Which is equivalent to

$$\begin{cases} \dot{i_L} = f(X) + g(X) \cdot \alpha \\ y = h(X) \end{cases} \tag{3.4}$$

with $f(X) = (v_{IN} - v_c)/L$, $g(X) = v_C/L$ and $h(X) = i_L$

The relative degree $\boldsymbol{r}$ of the current sub-system can easily be determined thanks to Lie derivatives:

$$\begin{aligned} L_g h(X) &= \frac{\partial h(X)}{\partial X} \cdot g(X) = \frac{v_c}{L} \neq 0 \\ L_f h(X) &= \frac{\partial h(X)}{\partial X} \cdot f(X) = \frac{v_{IN} - v_c}{L} \neq 0 \ \forall v_{IN} \neq v_C \end{aligned} \quad \Rightarrow \boldsymbol{r} = 1 \tag{3.5}$$

It is then possible to exactly linearize the inner current sub-system, the state vector staying unchanged:

$$\alpha = \frac{\delta - L_f^r h(X)}{L_g L_f^{r-1} h(X)} \tag{3.6}$$

$$\Leftrightarrow \ \alpha = \frac{L\delta + v_c - v_{IN}}{v_C} \tag{3.7}$$

In the present case, the new control signal δ is then homogeneous to the derivative of the inductor's current. It is also possible to concentrate the linearization only on the nonlinear part of the system, that is to say, in the case of the current sub-system, to the duty cycle to inductor's voltage transfer function. In this case, it corresponds to a linearization by inversion of the average model. The result is the same, except for the *L* parameter:

$$\alpha = \frac{\delta + v_c - v_{IN}}{v_C} \tag{3.8}$$

Thanks to this linearization, it is possible to implement any linear control method to regulate the current. Taking the example of a PI controller, the current sub-system becomes as below.

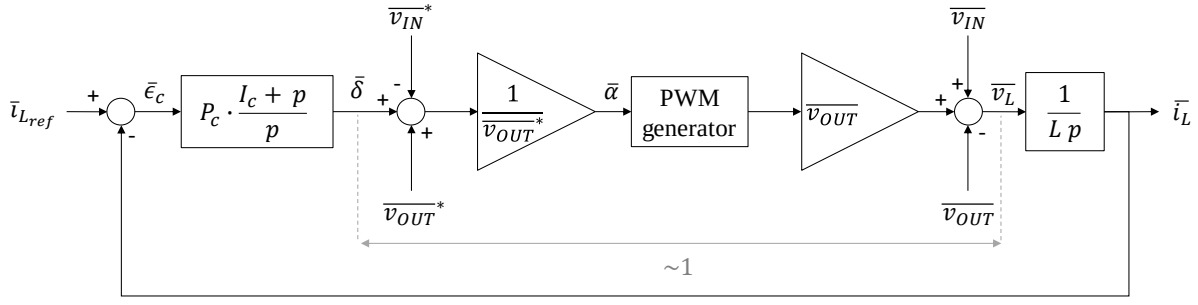

Figure 3.4 – Boost converter linearized inductor's current regulation loop.

An interesting property of the resulting control variable δ is that it is now homogeneous to the inductor's voltage. This ability to give a physical interpretation to a control signal is useful to the global understanding of the system but also gives the possibility to control to a certain extent this variable. This possibility is particularly interesting when studying the voltage subsystem.

3. 3. 1. 2 Voltage loop linearization and control

Let's assume that the aforementioned inductor's current control strategy is applied, and that the closed loop performances of the regulation allows to simplify the current loop by a unitary gain, the voltage subsystem can then be expressed as follows:

$$\begin{cases} \dot{v_C} = \dfrac{1}{C} \cdot \dfrac{v_{IN}}{v_C} \cdot i_L \\ y = v_C \end{cases} \tag{3.9}$$

$$\begin{cases} \dot{\imath_L} = f'^{(X)} + \dfrac{1}{C} \cdot g'(X) \cdot \alpha \\ y = h'(X) \end{cases} \tag{3.10}$$

with $f'(X) = 0$, $g'(X) = v_{IN}/(v_C)$ since $i_{L_{ref}} \approx i_L$ is the new control variable, and $h'(X) = v_C$

Since the relative degree of the subsystem is 1, it is possible to determine the linearizing control variable γ:

$$i_{L_{ref}} = \frac{\gamma - L_f^r, h'(X)}{L_g, L_{f,}^{r-1} h'(X)} \tag{3.11}$$

$$\Leftrightarrow \; i_{L_{ref}} = \frac{v_{IN}}{v_C} \cdot \gamma \tag{3.12}$$

Integrating this expression to the state equation:

$$C\dot{v_C} = \gamma \tag{3.13}$$

Reintegrating to this equation the load's current i_{OUT}, the expression becomes:

$$i_C + i_{LOAD} = \gamma \tag{3.14}$$

However, at steady state, since the capacitor's voltage average is constant:

$$\gamma = i_{LOAD} \tag{3.15}$$

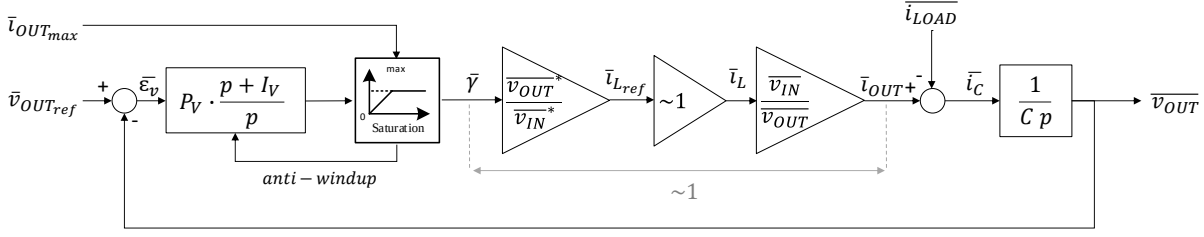

Figure 3.5 – Boost converter linearized output capacitor's voltage regulation loop.

Thus, γ is homogeneous to the average output current of the converter which allows to introduce a limitation of this variable by merely add a saturation on it, at the output of the voltage controller, upstream of the feedback linearization as shown in the figure above.

This feature is mandatory for a battery charger for example in order to achieve a constant current / constant voltage charge cycle and considering that the method is totally adapted to bidirectional converters.

The same method can be applied for any type of converter leading to the same closed loop system:

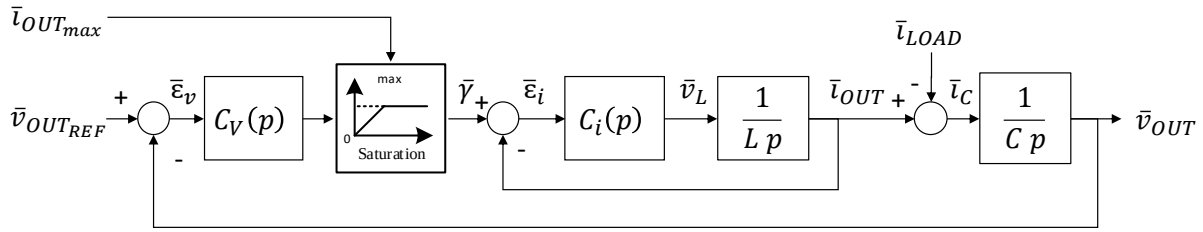

Figure 3.6 – Block diagram of the homogenized DC/DC converter and local primary controls – current and voltage regulations.

The main advantages of considering this equivalent system are its linearity, its independence to input or output voltages, its relative simplicity while keeping both current and voltage dynamics as well as a physical interpretation for each of its component.

Thus, in the rest of the study, this homogenized converter representation will be considered under the assumption that a linearizing control by state feedback is implemented. It is important to remember that the objective of this thesis is not to determine the optimal control for converters in microgrids but to study the mechanisms and behaviors from a systemic point of view and that the application of this method allows to simplify the approach. It should be noted, however, that the majority of the controls can be implemented, making the application of the proposed approach more complex but no less possible.

3. 3. 2 Loads characterization

The loads and more especially the CPL, are one of the nonlinear subsystems of the EPS. In addition to this, their combination with resistive loads results in an even more nonlinear system in spite of the fact that the lasts are linear when considered alone.

In the frame of the proposed electrical power architecture, since the conditioning units of the PV sections are controlled by DET, designed to be managed at low frequency, they are not able to regulate the primary power bus. From this observation, they can thus be considered as a load of the system from a primary control level point of view and their parameters as constants. Indeed, the notion of load is studied in a control theory sense in the following which has to be distinguished from its electrical meaning which rather refers to power sinks.

Based on this, the EPS in open loop, that is to say without any regulating module, can be modelled as presented in Figure 3.7 under proper sun irradiation, as studied in [15]. This simplified model proposed in [17], [140], [151], was often used to describe spacecraft EPS in the past. In the present study, it is proposed as a representation of the systems load as seen by the regulating modules.

The particularity of this equivalent load in comparison to what is usually studied is thus that it includes power sources in combination of classical electrical loads where usually the power sources are considered as controllable. It comes from this remark that the system does not necessarily stay at rest when no proper regulation is performed.

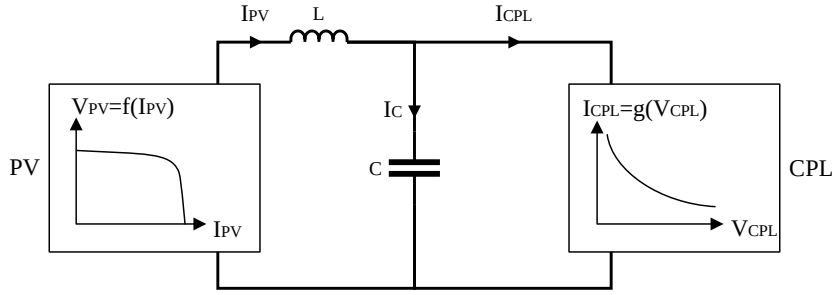

Figure 3.7 – Simplified equivalent circuit of the EPS loads under Sun illumination.

The LC circuit which interfaces the PV and the CPL modules, represents the actual equivalent input filter of the different CPL POL switching regulators and the equivalent line impedance of the distribution network [140]. They determine the dynamic of the system and thus enable to analyse its stability. The assumption to neglect the line resistances in this representation makes of it a "worst case" in terms of stability since it would damp the system.

3. 3. 2. 1 Open loop stability

The equivalent load can be modelled using a second order system based on the characteristic differential equations of the bus equivalent inductor and capacitor

$$\begin{cases} C \cdot \dfrac{dV_{CPL}}{dt} = I_{PV} - I_{CPL} = I_{PV} - g(V_{CPL}) \\ L \cdot \dfrac{dI_{PV}}{dt} = V_{PV} - V_{CPL} = f(I_{PV}) - V_{CPL} \end{cases} \quad 3.16$$

where $f(I_{PV})$ and $g(V_{CPL})$ are respectively the characteristic nonlinear functions of the solar array and the CPL.

These functions also depend on two system input variables: I_{SC}, the PV short circuit current and P_{CPL}, the CPL operating power consumption. Hence

$$\begin{cases} C \cdot \dfrac{dV_{CPL}}{dt} = F(V_{CPL}, I_{PV}, P_{CPL}, I_{SC}) \\ L \cdot \dfrac{dI_{PV}}{dt} = G(V_{CPL}, I_{PV}, P_{CPL}, I_{SC}) \end{cases} \quad 3.17$$

F and G can be approximated to first order linear functions using small signal formalism on the state and input variables. In open-loop operation, the input variables can be considered as constant and taking the first-order approximation of the Taylor series, a linearized system is obtained

$$\begin{cases} C \cdot \dfrac{d\widetilde{v_{cpl}}}{dt} = F(X_0, U_0) + \left[\dfrac{\partial F}{\partial V_{CPL}}\right]_{X_0,U_0} . \widetilde{v_{cpl}} + \left[\dfrac{\partial F}{\partial I_{PV}}\right]_{X_0,U_0} . \widetilde{i_{pv}} \\ L \cdot \dfrac{d\widetilde{i_{pv}}}{dt} = G(X_0, U_0) + \left[\dfrac{\partial G}{\partial V_{CPL}}\right]_{X_0,U_0} . \widetilde{v_{cpl}} + \left[\dfrac{\partial G}{\partial I_{PV}}\right]_{X_0,U_0} . \widetilde{i_{pv}} \end{cases} \quad 3.18$$

Considering these equations, the dynamic response of the system at each point of the state-variables plane I_{PV}-V_{CPL} can be expressed as a vector given by $\left(d\widetilde{v_{cpl}}/dt\,;\,d\widetilde{i_{pv}}/dt\right)$. Extending it to every point of the plane, the state-plane trajectories can be represented from the resulting vector field, and give a qualitative representation of the system dynamic response as shown in Figure 3.8. The same approach can easily be applied for a system only composed of a PV with a resistive load as depicted in Figure 3.9.

State-plane trajectories are particularly adapted to the study of resonant systems – the LC bus model in this case – since it allows to observe the nature of the different equilibrium points of the system and can also be used to improve the system's control laws like in [141]. In addition, the method is also particularly useful to identify how the different operating points can be reached – or not – by representing the trajectories of its state variables from any initial point of the state plane.

The definition of an equilibrium point is that at this point $F(X_0, U_0)$ and $G(X_0, U_0)$ equal to zero. The coefficients multiplying the state variables correspond to the partial derivatives of f and g which can be identified as the tangential slopes – respectively R_{PV} and R_{CPL} – of their corresponding characteristic curve at the neighboring of the equilibrium point.

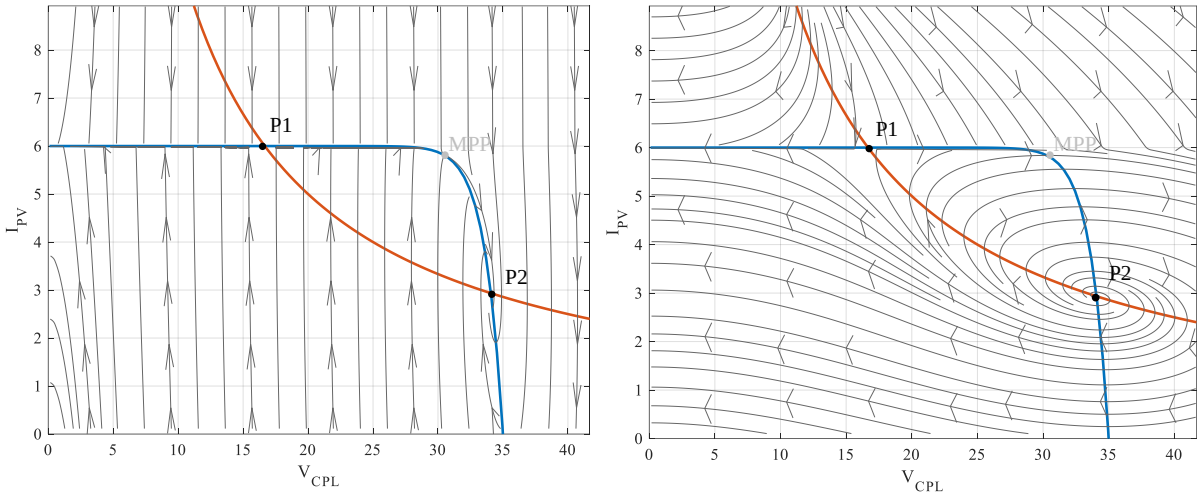

Figure 3.8 – State-plane trajectories in two configurations: (a) P2 is a stable node ($C = 380\mu F. L = 10\mu H$). (b) P2 is unstable ($C = 380\mu F. L = 2mH$).

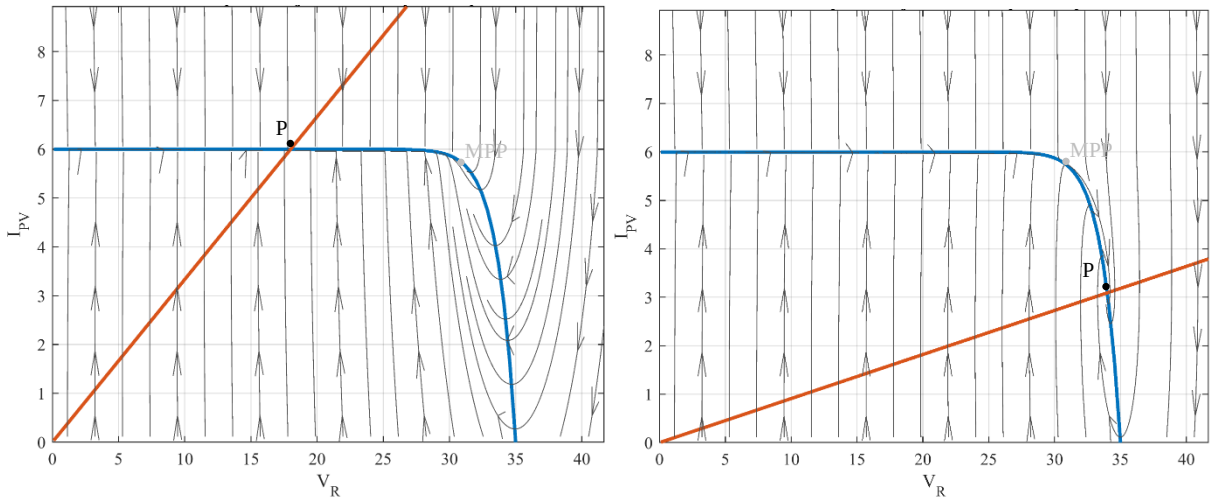

Figure 3.9 – State-plane trajectories for two values of resistive load: 3ohms on the left and 11ohms on the right.

If in the case of the solar panel the expression of this value is tough, the linear approximation of a CPL around a given voltage set point V_{set} is straightforward:

$$\tilde{\imath}_{CPL} = -\frac{P_{CPL}}{V_{set}^2}\tilde{v}_{CPL} + 2\frac{P_{CPL}}{V_{set}} \tag{3.19}$$

This equation can be interpreted as an equivalent electrical circuit composed of a negative resistance R_{CPL} in parallel with a constant current source I_{CPL} as expressed below.

$$\tilde{\imath}_{CPL} = \frac{\tilde{v}_{CPL}}{R_{CPL}} + I_{CPL} \quad with \quad \begin{cases} R_{CPL} = -\dfrac{V_{set}^2}{P_{CPL}} \\ I_{CPL} = 2\dfrac{P_{CPL}}{V_{set}} \end{cases} \tag{3.20}$$

Introducing these notations in the system's state equations, the following matrix form is obtained

$$\dot{\tilde{x}} = \begin{pmatrix} -\dfrac{1}{C \cdot R_{CPL}} & \dfrac{1}{C} \\ -\dfrac{1}{L} & \dfrac{R_{PV}}{L} \end{pmatrix} \cdot \tilde{x} \tag{3.21}$$

with the state vector $\tilde{x} = (\widetilde{v_{cpl}} \quad \widetilde{i_{pv}})^T$. The eigenvalues of the system are thus expressed as following.

$$\lambda_1, \lambda_2 = \frac{1}{2}\left[\left(\frac{R_{PV}}{L} - \frac{1}{CR_{CPL}}\right) \mp \sqrt{\left(\frac{1}{CR_{CPL}} - \frac{R_{PV}}{L}\right)^2 - \frac{4}{LC}\left(1 - \frac{R_{PV}}{R_{CPL}}\right)}\right] \tag{3.22}$$

In Figure 3.8, two equilibrium points can be identified at the intersection of the characteristic curves of the PV panel and the CPL: P1 at the left of the PV MPP and P2 at the right.

1. At the left of MPP: $R_{CPL} < 0, R_{PV} < 0, |R_{CPL}| < |R_{PV}|$
   The system is unstable and P1 is a saddle since the two eigenvalues are real but of opposite signs.
2. At the right: $R_{CPL} < 0, R_{PV} < 0, |R_{CPL}| > |R_{PV}|$
   The system stability and the nature of P2 depends on the value of L and C as shown in Figure 3.8 inset a) and b):
   - if $\frac{L}{C} < R_{CPL}R_{PV}$ the system is stable and P2 is a stable node or a focus.
   - if $\frac{L}{C} > R_{CPL}R_{PV}$ the system is unstable and P2 is an unstable node.

These results confirm the fact that the operating point of the open-loop system essentially depends on the PV open-circuit voltage – and thus on the temperature. It also shows that even without any voltage regulation, the system can still reach a stable operating point and thus operate in a "degraded mode" that is to say at a voltage level which is not regulated but which could allow to maintain a power supply to

the most critical sub-systems. This behavior is an interesting feature in case of anomalies during operation.

Performing the same development with a resistive load, that is to say with a positive equivalent impedance in place of the negative CPL equivalent impedance in the developments presented above, it can be determined that the system is always stable at its unique equilibrium point, called P in Figure 3.9.

From the above analysis, it can be deduced that in terms of loads, the stability of an operating point mainly depends on the sign of the ratio between the power sources linearized small-signal impedance and the one of the power sinks – which is consistent with the Middlebrook criterion.

Concerning the worst case which is obtained with a pure CPL, the condition for which the system becomes unstable even at the right of the MPP is unlikely to be met in practice, since it would imply nonrealistic values of L and C. In addition to this, the characteristic time of the observed behavior which is defined by $\sqrt{LC}$ – less than $1\mu s$ – is much lower than the characteristic reaction time of the lowest level control functions which are within the scope of the present study. Based on these observations, the inductive component of the line impedances can reasonably be neglected in the following.

From system point of view and in order to study the system stability, only the small-signal impedances of the different loads can thus be considered. Two approaches are then applicable. The first one consists in considering all loads individually and to linearize them all. This represents the most rigorous approach however it results in an increase of the model complexity. Another approach is then to combine the large-signal characteristics of each loads to determine a unique equivalent load.

3. 3. 2. 2 Loads equivalent large-signal characteristic

Calculating the equivalent load's large-signal characteristic enables to quickly evaluate all possible loads configurations that a single regulating system could face.

However, the representations usually used are heterogeneous since they differ according to the type of terminal considered, which can lead to confusion. Indeed, most of the time when a solar panel is characterized, since it is generally operated as a current source, the I-V plane – current in ordinates and voltage in abscissae – is used. Conversely, when studying droop control methods as in the present study, as it applies to parallel voltage sources, the use of the V-I plane – ordinate voltage and abscissa current – is preferred.

As an example, seen from the output of a droop controlled unit equipped with a bidirectional converter, Figure 3.10 synthesizes all the characteristics of the different components of the system.

Since the PV are considered as loads in this representation, their current convention is changed to receptor convention, which explains that they are represented in the negative currents half-plane. A corollary of this modification is that their standalone linearized small-signal impedance is always positive in comparison to the study performed previously.

On the graph, the different physical limits of the droop controlled power converter have also been represented: the minimum and maximum bus voltages and currents, which are mainly dictated by the voltage holding limitations of all the terminals connected to the bus, and the maximum charge and discharge powers which could be induced by the battery side limitations.

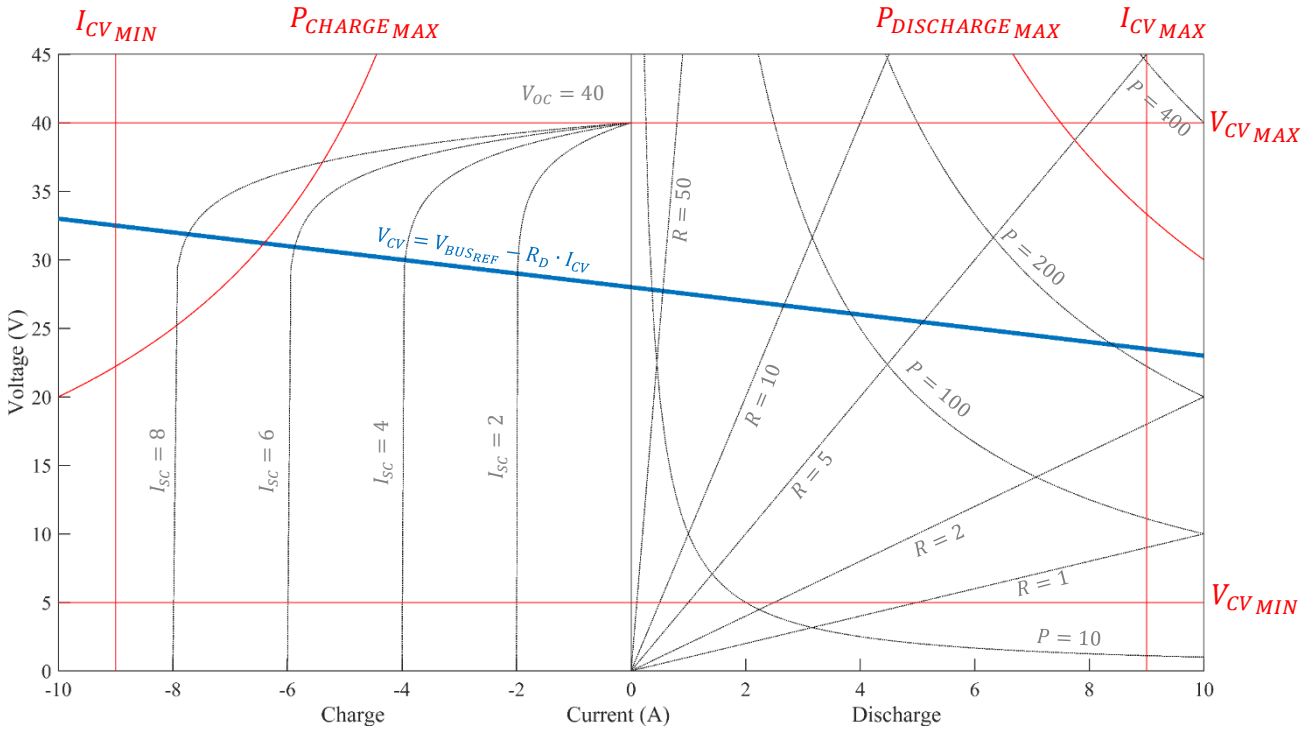

Figure 3.10 – Loads and droop controlled converter large-signal characteristics on the V-I plane.

Focusing on the loads however, only individual characteristics are represented and in order to characterize the load observed from a power converter point of view, it is possible to determine a single equivalent load based on the combination of the PVs, CPLs and resistive loads characteristics. Considering typical ranges of values for the different loads parameters as defined by the reference system introduced in the first section, the graph presented in Figure 3.11 can thus be constructed.

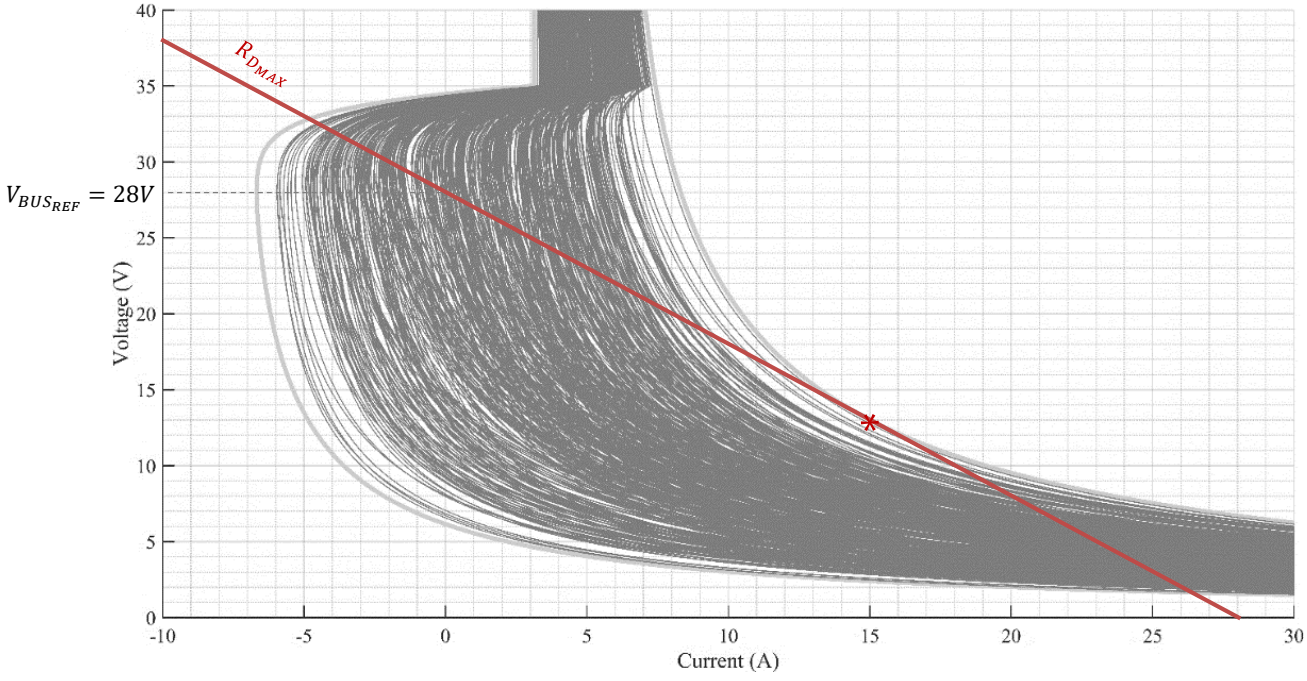

Figure 3.11 – Equivalent load's large-signal characteristics with random variations of power consumption and production.

It can be observed that below the PV's MPP voltage, the loads characteristic impedance is mainly determined by the CPL. Above, between the MPP and the open circuit voltage, the PV characteristic is dominant. Even further toward high voltages, not represented in the graph, the resistive loads shape the equivalent characteristic waveform.

The determination of the set of possible equivalent loads characteristics as represented in Figure 3.11 also allows to identify the large-signal limitation of the droop coefficient in function of the reference function. This limitation corresponds to the condition of existence of at least one operating point, that is to say the condition to respect to guarantee that the droop control large-signal characteristic crosses all possible loads large-signal curves. This configuration is represented by the red line in Figure 3.11 and corresponds to the configuration where the load is only composed of CPL and resistive loads and for which the power consumption is at its maximum. Solving the equation described above results in the following condition:

$$R_{D\,MAX} = -\frac{R}{2} + \sqrt{\frac{R^2}{4} + \frac{V_{REF}^2 \cdot R}{4P_{CPL}}} \qquad 3.23$$

To this first limitation, a second one is most of the time added of the droop coefficient in order to avoid a too important voltage drop.

$$R_{D\,MAX}{}' = \frac{V_{REF} - V_{MIN}}{I_{MAX}} \qquad 3.24$$

$$\Leftrightarrow R_{D\,MAX}{}' = \frac{V_{REF} - V_{MIN}}{\frac{V_{MIN}}{R_{MIN}} + \frac{P_{CPL\,MAX}}{V_{MIN}}} \qquad 3.25$$

It results that from a system point of view, depending on the operating voltage, a wide range of equivalent linearized small-signal impedances – slopes of the characteristic curves – can be encountered. Figure 3.12 represents the resulting equivalent loads small-signal impedances considering a realistic voltage range around a nominal value of 28V – one of the standard power bus voltage in conventional satellites.

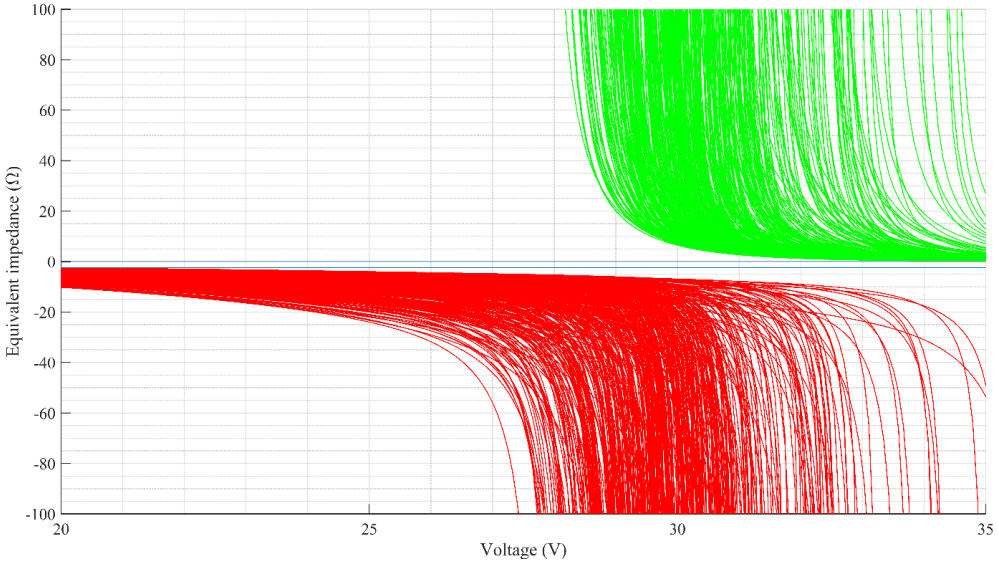

Figure 3.12 – Loads incremental impedance obtained by the linearization of the equivalent load large-signal characteristic in function of the primary bus voltage.

Applying the methodology presented above to characterize the loads of the system thus allows to define a range of reachable small-signal impedance which is particularly interesting for the study of power converters stability. Thus, based on the values determined for the reference system, it can be deduced that for a voltage range of $[20V\,;35V]$ the equivalent load's impedance belongs to $]-\infty\,;\,-2.4\Omega] \cup [0\Omega\,;+\infty[$ as visible in Figure 3.12.

A sensitivity analysis with the impedance variations determined by the above method indeed assures to cover all possible operating points and configurations – electrically but also thermally speaking considering for example the PV characteristics deviation within a temperature range. In term of small-signal modelling particularly, only resistive loads can thus be considered which greatly facilitates its manipulation and further its analysis.

3. 4 Multi converter systems modelling

Based on the developments presented in the previous section which introduced an homogenized power converter model and detailed that all loads of the system – electrical power sinks as well as PV sections – could be modelled by a mere resistor for small-signal stability analysis the nonlinearities are no longer an obstacle to the consideration of all individual elements while studying the system's stability.

The state-space matrix representation is the most appropriate formalism to deal with systems with varying dimensions as it is the case for modular EPS.

3. 4. 1 Matrix dimensions' analysis

Let's consider a system composed of N voltage regulating converters, with $N \in \mathbb{N}$. Based on the homogenized power converter model and focusing on the voltage loop, the following expression can be determined:

$$\dot{V}_{OUT} = C^{-1}[I_{OUT} - I_{LOAD}] \tag{3.26}$$

with $\dot{V}_{OUT}$ the converters bus side voltages derivatives vector, C a diagonal matrix composed by the converters output capacitors, I_{OUT} the converters output currents vector and I_{LOAD} the vector of the converters individual contribution to the loads regulation.

Yet, if I_{OUT} can easily be expressed by each converter internal parameters and state variables, it is not the cases of I_{LOAD}. Thus in order to construct the full state-space representation, it has to be expressed in function of either V_{OUT} or I_{OUT}.

A solution to do so is to use the nodal conductance matrix Q_{BUS} which is also able integrate the loads characteristic impedances as it allows to link the input voltages and currents at each of its nodes as follows:

$$I_{LOAD} = Q_{BUS} \cdot V_{OUT} \tag{3.27}$$

However, considering a random electrical network as illustrated in Figure 3.13 the nodal admittance matrix does not necessarily comply with the requirements in term of matrix dimensions.

Indeed, from the above equation, it appears that Q_{BUS} must be a $N \times N$ matrix in order to be integrated to the state-space matrix.

A key method to solve this issue is the Kron reduction of the general conduction matrix.

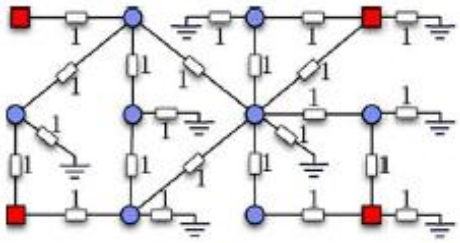

Figure 3.13 – Example of electrical network interconnecting 4 active components. In this representation the red nodes represent the boundary nodes on which the actives components are connected and the blue nodes represent internal nodes at the interconnection of several distribution lines.

3. 4. 2 Reduced conductance matrix

The Kron reduction of an electrical network consists in segregating in the conductance matrix the boundary nodes of the network – in which a current is effectively injected – from the interior nodes – in which reversely no current is injected – and to perform a matrix transformation in order to reduce it to a n-order system – n being the number of boundary nodes – without losing any accuracy in term of modelling at the boundary nodes.

This method, introduced by Gabriel Kron in 1939 [152], is very powerful because it allows to start from a very accurate modelling of the distribution harness, able to integrate practical subtleties such as wire splices, and to keep a reasonable size to the problem to solve.

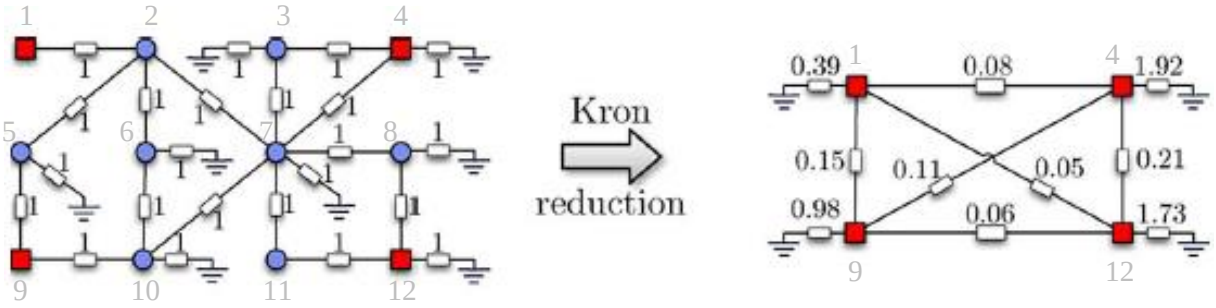

Figure 3.14 – Electrical network identified with 4 boundary nodes – in red – 8 interior nodes – in blue – and unit-valued branch and shunt conductance. Kron reduction of the interior nodes results in a reduced network among the boundary nodes [153].

Taking the example of the network presented in Figure 3.14, the conductance matrix Q can be expressed as following :

$$\begin{pmatrix} i_1 \\ i_2 \\ i_3 \\ i_4 \\ i_5 \\ i_6 \\ i_7 \\ i_8 \\ i_9 \\ i_{10} \\ i_{11} \\ i_{12} \end{pmatrix} = \begin{pmatrix} 1 & -1 & 0 & 0 & 0 & 0 & 0 & 0 & 0 & 0 & 0 & 0 \\ -1 & 4 & 0 & 0 & -1 & -1 & -1 & 0 & 0 & 0 & 0 & 0 \\ 0 & 0 & 3 & -1 & 0 & 0 & -1 & 0 & 0 & 0 & 0 & 0 \\ 0 & 0 & -1 & 3 & 0 & 0 & -1 & 0 & 0 & 0 & 0 & 0 \\ 0 & -1 & 0 & 0 & 3 & 0 & 0 & 0 & -1 & 0 & 0 & 0 \\ 0 & -1 & 0 & 0 & 0 & 3 & 0 & 0 & 0 & -1 & 0 & 0 \\ 0 & -1 & -1 & -1 & 0 & 0 & 7 & -1 & 0 & -1 & -1 & 0 \\ 0 & 0 & 0 & 0 & 0 & 0 & -1 & 3 & 0 & 0 & 0 & -1 \\ 0 & 0 & 0 & 0 & -1 & 0 & 0 & 0 & 2 & -1 & 0 & 0 \\ 0 & 0 & 0 & 0 & 0 & -1 & -1 & 0 & -1 & 3 & 0 & 0 \\ 0 & 0 & 0 & 0 & 0 & 0 & -1 & 0 & 0 & 0 & 2 & -1 \\ 0 & 0 & 0 & 0 & 0 & 0 & 0 & -1 & 0 & 0 & -1 & 3 \end{pmatrix} \cdot \begin{pmatrix} v_1 \\ v_2 \\ v_3 \\ v_4 \\ v_5 \\ v_6 \\ v_7 \\ v_8 \\ v_9 \\ v_{10} \\ v_{11} \\ v_{12} \end{pmatrix} \quad 3.28$$

Considering that a current can only be injected or absorbed at the four boundary nodes – corresponding to nodes number 1, 4, 9 and 12 – the previous equation can be reorganized in order to dissociate these nodes from the others.

$$\begin{pmatrix} i_1 \\ i_4 \\ i_9 \\ i_{12} \\ i_2 \\ i_3 \\ i_5 \\ i_6 \\ i_7 \\ i_8 \\ i_{10} \\ i_{11} \end{pmatrix} = \begin{pmatrix} 1 & 0 & 0 & 0 & -1 & 0 & 0 & 0 & 0 & 0 & 0 & 0 \\ 0 & 3 & 0 & 0 & 0 & -1 & 0 & 0 & -1 & 0 & 0 & 0 \\ 0 & 0 & 2 & 0 & 0 & 0 & -1 & 0 & 0 & 0 & -1 & 0 \\ 0 & 0 & 0 & 3 & 0 & 0 & 0 & 0 & 0 & -1 & 0 & -1 \\ -1 & 0 & 0 & 0 & 4 & 0 & -1 & -1 & -1 & 0 & 0 & 0 \\ 0 & -1 & 0 & 0 & 0 & 3 & 0 & 0 & -1 & 0 & 0 & 0 \\ 0 & 0 & -1 & 0 & -1 & 0 & 3 & 0 & 0 & 0 & 0 & 0 \\ 0 & 0 & 0 & 0 & -1 & 0 & 0 & 3 & 0 & 0 & -1 & 0 \\ 0 & -1 & 0 & 0 & -1 & -1 & 0 & 0 & 7 & -1 & -1 & -1 \\ 0 & 0 & 0 & -1 & 0 & 0 & 0 & 0 & -1 & 3 & 0 & 0 \\ 0 & 0 & -1 & 0 & 0 & 0 & 0 & -1 & -1 & 0 & 4 & 0 \\ 0 & 0 & 0 & -1 & 0 & 0 & 0 & 0 & -1 & 0 & 0 & 2 \end{pmatrix} \cdot \begin{pmatrix} v_1 \\ v_4 \\ v_9 \\ v_{12} \\ v_2 \\ v_3 \\ v_5 \\ v_6 \\ v_7 \\ v_8 \\ v_{10} \\ v_{11} \end{pmatrix} \quad 3.29$$

$$\Leftrightarrow \begin{pmatrix} I_{bond} \\ I_{int} \end{pmatrix} = \begin{pmatrix} A & B \\ C & D \end{pmatrix} \cdot \begin{pmatrix} V_{bond} \\ V_{int} \end{pmatrix} \quad 3.30$$

with

$$I_{bond} = \begin{pmatrix} i_1 \\ i_4 \\ i_9 \\ i_{12} \end{pmatrix} \qquad V_{bond} = \begin{pmatrix} v_1 \\ v_4 \\ v_9 \\ v_{12} \end{pmatrix}$$

$$I_{int} = \begin{pmatrix} i_2 \\ i_3 \\ i_5 \\ i_6 \\ i_7 \\ i_8 \\ i_{10} \\ i_{11} \end{pmatrix} = \begin{pmatrix} 0 \\ 0 \\ 0 \\ 0 \\ 0 \\ 0 \\ 0 \\ 0 \end{pmatrix} = O_{8\times1} \qquad V_{int} = \begin{pmatrix} v_2 \\ v_3 \\ v_5 \\ v_6 \\ v_7 \\ v_8 \\ v_{10} \\ v_{11} \end{pmatrix}$$

$$A = \begin{pmatrix} 1 & 0 & 0 & 0 \\ 0 & 3 & 0 & 0 \\ 0 & 0 & 2 & 0 \\ 0 & 0 & 0 & 3 \end{pmatrix} \qquad B = C' = \begin{pmatrix} -1 & 0 & 0 & 0 & 0 & 0 & 0 & 0 \\ 0 & -1 & 0 & 0 & -1 & 0 & 0 & 0 \\ 0 & 0 & -1 & 0 & 0 & 0 & -1 & 0 \\ 0 & 0 & 0 & 0 & 0 & -1 & 0 & -1 \end{pmatrix}$$

and

$$D = \begin{pmatrix} 4 & 0 & -1 & -1 & -1 & 0 & 0 & 0 \\ 0 & 3 & 0 & 0 & -1 & 0 & 0 & 0 \\ -1 & 0 & 3 & 0 & 0 & 0 & 0 & 0 \\ -1 & 0 & 0 & 3 & 0 & 0 & -1 & 0 \\ -1 & -1 & 0 & 0 & 7 & -1 & -1 & -1 \\ 0 & 0 & 0 & 0 & -1 & 3 & 0 & 0 \\ 0 & 0 & 0 & -1 & -1 & 0 & 4 & 0 \\ 0 & 0 & 0 & 0 & -1 & 0 & 0 & 2 \end{pmatrix}$$

Rewriting Equation. 3.30 in two equations, it comes

$$\begin{cases} I_{bond} = A \cdot V_{bond} + B \cdot V_{int} \\ \\ O_{8\times1} = C \cdot V_{bond} + D \cdot V_{int} \end{cases} \quad 3.31$$

$$\Leftrightarrow \begin{cases} I_{bond} = A \cdot V_{bond} + B \cdot V_{int} \\ \\ V_{int} = -D^{-1} \cdot C \cdot V_{bond} \end{cases} \quad 3.32$$

Thus

$$\Leftrightarrow I_{bond} = (A - B \cdot D^{-1} \cdot C) \cdot V_{bond} \quad 3.33$$

By defining the reduced conductance matrix as

$$Q_{red} = A - B \cdot D^{-1} \cdot C \quad 3.34$$

Since $size(A) = 4 \times 4$, $size(B) = 4 \times 8$, $size(D) = size(D^{-1}) = 8 \times 8$ and $size(C) = 8 \times 4$, a reduced order model of the network with $size(Q_{red}) = 4 \times 4$ is obtained and the full network can be expressed as follows, seen from its boundary nodes as shown in Figure 3.14 from [153]:

$$Q_{red} = \begin{pmatrix} 0.68 & -0.08 & -0.15 & -0.05 \\ -0.08 & 2.32 & -0.11 & -0.21 \\ -0.15 & -0.11 & 1.31 & -0.07 \\ -0.05 & -0.21 & -0.07 & 2.03 \end{pmatrix} \quad 3.35$$

And finally

$$I_{bond} = Q_{red} \cdot V_{bond} \quad 3.36$$

Equation 3.34 which gives the reduced conductance matrix Q_{red}, corresponds to the Schur complement of the complete conductance matrix Q. This equation is valid for any type of network, subject to having previously organized the conductance matrix by placing the boundary nodes at the top.

This is particularly powerful in the framework of the analysis study of electrical systems since it provides the missing piece for modelling multi-converter systems by generating the required $N \times N$ matrix which links all converters together. In addition, by integrating the equivalent loads impedances to the full network configuration this solution allows to develop a very accurate representation of the system in the same time to provide a practical and very efficient formalism to model the entire system without requiring to simplify it.

3. 5 Conclusion

This essential propriety is used in the next chapter to study the systems stability by taking into account all possible parameters variations and thus integrating the interactions between the parallel converters which is most of the time not taken into account in the studies on the topic.

Together with the notions and tools presented previously in this chapter, it helps to understand to global orientation of the following developments and justifies the major hypothesis done in the project. This essential work will thus allow in the following chapter to study the impact of the primary control taking into account all reachable configurations and thus to define the stability criteria of systems implementing such architecture and controls.

CHAPTER 4.

Primary Control & Stability Analysis

Summary

The primary control's aim is to tackle the regulation concerns at the modules level in order to assure the best trade-off between the accuracy and time response of the different implemented control loops while assuring the stability of the overall system [63]. While the inner current and voltage regulation loops are considered as handled at equipment level and are supposed to be properly fitted and invariant from a systemic point of view, the droop control – which has been chosen to assure the current sharing between modules – may have an impact on the global stability and subsequently, the adaptation of its parameter R_D by upper level controls.

In this chapter, the stability aspects of the electrical power system primary control are studied taking as example the use case defined before. In a more general point of view, the impact of different parameters on the stability is assessed like for instance the adding of modules in parallel – which is one of the big concerns of the present work – as well as the droop control virtual resistor R_D. Thus, the main objective of the present chapter is to establish a method to determine the stability criteria of modular and distributed power architectures and thus determine an operating range for each parameter being likely to be adapted by the secondary and tertiary controls. The second objective, corollary of the first, is to evaluate the possible advantages of implementing this type of architecture regarding stability constraints in comparison to conventional systems.

First, a single-converter system is studied, corresponding to a conventional architecture. The impact of the bus impedance on this system is evaluated through the representation of its root locus. This graphical method allows to examine in the complex s-plane how the roots of a system change with variation of a given parameter. The transition to distributed architectures is initiated by analyzing the impact on the same system of implementing droop control. Based on the observations done thanks to root locus analysis, an analytic stability criterion is then determined, then used as a basis for more complex systems.

In a second step, the stability study is extended to multi-converter systems, first on an ideal system, then by generalization on a more complete model allowing to treat all converters individually, thanks to the tools introduced in the previous chapter. The necessary increased complexity of the resulting model no longer making it easy to analytically determine a generic stability condition, the root locus method is directly used as a stability criterion, by combining it with a pseudo Monte Carlo analysis to cover all possible configuration.

4. 1 Single-converter system

The first system under consideration is depicted in Figure 4.1. It is composed of a unique battery module connected to a unique load.

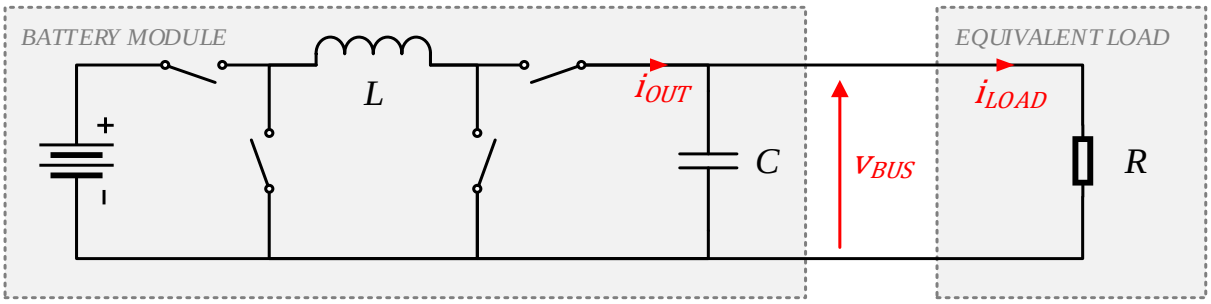

Figure 4.1 – Ideal single-converter electrical power system feeding a resistive load. Based on the loads characterization performed in the previous chapter, the resistive load can represent either a purely resistive load, a CPL, a PV section or a combination of all these elements.

4. 1. 1 Sensitivity to equivalent load impedance

In order to study this system, the battery module is modelled using the homogenized converter model introduced in the previous chapter. Since the aim of the present analysis is to focus on small-signal behavior of the system, and thanks to the load characterization also performed in the previous chapter, the load is modelled as a mere resistor. The line impedances are neglected. In term of control, only the current and voltage loop of the homogenized converter model presented in the previous chapter are considered. These assumptions lead to the definition of the following block diagram.

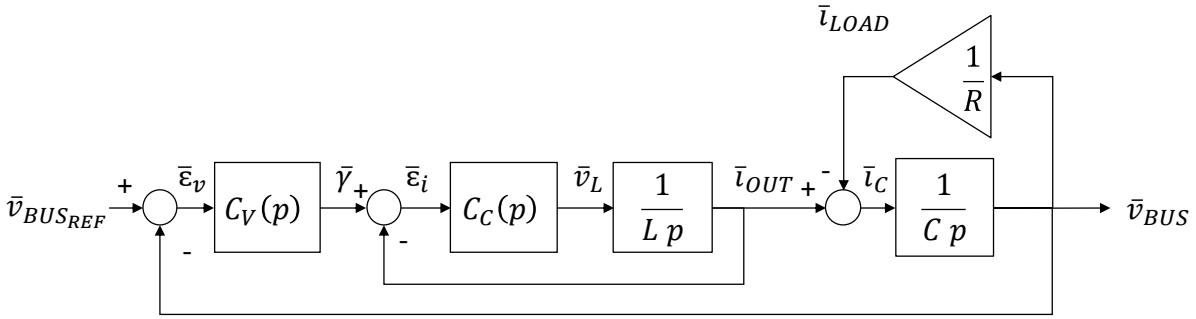

Figure 4.2 – Block diagram of the homogenized converter model feeding a linear – resistive – load.

Although particularly simple, the developments carried out in the previous chapter have shown that this system can represent a large number of configurations in a small-signal approach. In the case of satellites EPS, it covers all the configurations combining solar panels, resistive loads and constant-power loads that might be encountered, both during night and day phases which makes it particularly powerful.

The resulting closed loop transfer function of the system can be expressed as follows:

$$\frac{\bar{v}_{BUS}}{\bar{v}_{BUS_{REF}}} = \frac{RP_VP_C \cdot s^2 + (RP_VP_CI_C + RP_VP_CI_V) \cdot s + RP_CP_VI_CI_V}{\begin{aligned} &RLC \cdot s^4 \\ &+(L + RCP_C) \cdot s^3 \\ &+(P_C + RCP_CI_C + RP_VP_C) \cdot s^2 \\ &+(P_CI_C + RP_VP_CI_C + RP_VP_CI_V) \cdot s \\ &+RP_CP_VI_CI_V \end{aligned}} \qquad 4.1$$

with P_C, I_C, P_V and I_V respectively the proportional and integral coefficient of the current and voltage loops

Using typical values from the use case, the sensitivity of the system to its different parameters can be studied. The following sections will particularly focus on the impact of both positive and negative load impedance as well as of droop coefficient R_D.

In order to study the sensitivity of the system to different values of output impedance and study how the poles change depending on it, the root locus can be drawn.

Using Matlab, it can be obtained using the *rlocus()* function which takes as input $G(s)$, the open loop transfer function of a system and returns the closed-loop pole trajectories as a function of the feedback gain, usually noted K.

This is achieved by solving the characteristic polynomial of the system for every possible value of K :

$$1 + K \cdot G(s) = 0 \qquad , \forall\, K \in [0; +\infty[\tag{4.2}$$

Thus, if the parameter to focus on does not act as a feedback gain, the equation has to be rearranged to match this formalism in order that K corresponds to the wanted parameter.

Based on the aforementioned assessment, in order to study the impact of load impedance variation on the behavior of the system, the denominator of equation 4.1 is put to the appropriate form by factorizing it by R, the equivalent load impedance.

The input open-loop transfer function for the *rlocus()* function is then defined as:

$$G(s) = \frac{LC \cdot s^4 + CP_C \cdot s^3 + (CP_C I_C + P_V P_C) \cdot s^2 + P_V P_C (I_C + I_V) \cdot s + P_C P_V I_C I_V}{L \cdot s^3 + P_C \cdot s^2 + P_C I_C \cdot s} \tag{4.3}$$

It is important to note that this transfer function behaves differently to the one described in equation 4.1 when responding to forced inputs due to the fact that the numerator has not been taken into account. But both system will behave exactly in the same way stability aspects since the denominator has just been rearranged.

4. 1. 1. 1 Positive impedances

This allows to draw the root locus for positive equivalent load impedance – see Figure 4.3.

It can be observed that the system is always stable, for any value of $R > 0$. It can also be observed that the lower the load (i.e. the higher the impedance), the less the system is damped, but without becoming unstable.

On the other side, for low values of impedances, the root locus goes toward the origin along the real axis which tells that for high level of load – low impedance – the system gets slower but never reach the right half plane, synonym of instability.

In addition, this representation does not take into account the current limit that a real converter might have.

Taking into account the power limit of $1.5kW$ defined by the ECSS in [100] for 28V buses – worst case compared to the use case – and considering a fully resistive load, a minimum resistance of approximately 0.52Ω is obtained, visible in Figure 4.3 thanks to a green tick on the real axis.

This means that in practical, the region at the right of this tick is never reached which gives an adequate margin both in term of stability and system's dynamic with a minimum characteristic pulsation of about $5.81 \times 10^3\ rad.s^{-1}$.

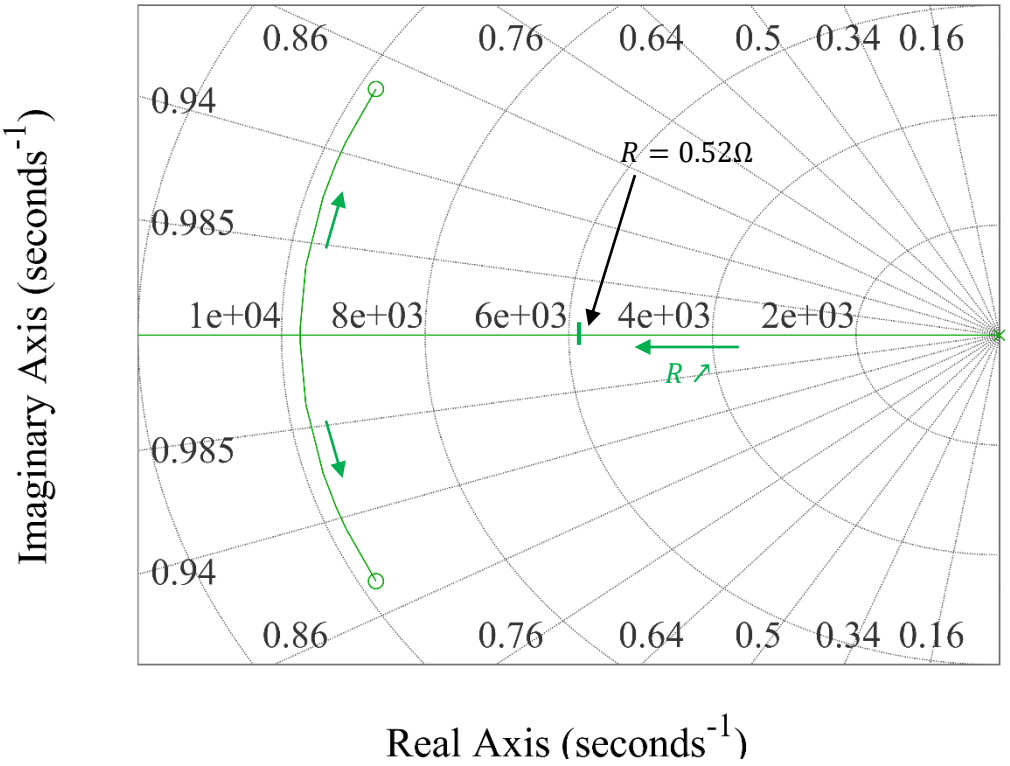

Figure 4.3 – Dominant poles root locus for positive equivalent load impedance – resistive load or linearized PV panel. The arrows give the sense in which the impedance rises.

These results can also be interpreted through the prism of the solar panel which can also be characterized by their positive linearized impedance when considered as loads of the system in terms of stability analysis, at all point of the large signal characteristic since this last is monotonous. From this perspective, the operation of a converter with a pure solar panel is always stable but operating in the current source zone of its characteristic – which corresponds to a high linearized impedance – is less damped than in the voltage source zone – inversely corresponding to a low equivalent linear impedance.

4. 1. 1. 2 Negative equivalent load impedances

Considering the impact of a CPL on the system, the same $G(s)$ transfer function is used, adding a negative sign to the function. It can be observed from Figure 4.4 that the obtained curves are the complements of the ones observed on Figure 4.3 for positive impedances – also visible in the present figure in dot lines. Indeed, the poles and the zeros are the same and only the sign of K changes.

From the curves below, it can be observed that the root locus can pass to the right half plane which means that the system may be unstable. This is the case for low absolute values of impedances which corresponds to high level of power consumption or lower bus voltages since the CPL small-signal impedance is defined by:

$$R_{CPL} = -\frac{V_{BUS}^2}{P_{CPL}} \qquad 4.4$$

In the present case, the system becomes unstable when the load impedance reaches -0.148Ω, which corresponds to approximately $5.3kW$ for a $28V$ bus system. More generally, it appears that the value of the load impedance mainly impacts the damping of the system, keeping the characteristic dynamic unchanged.

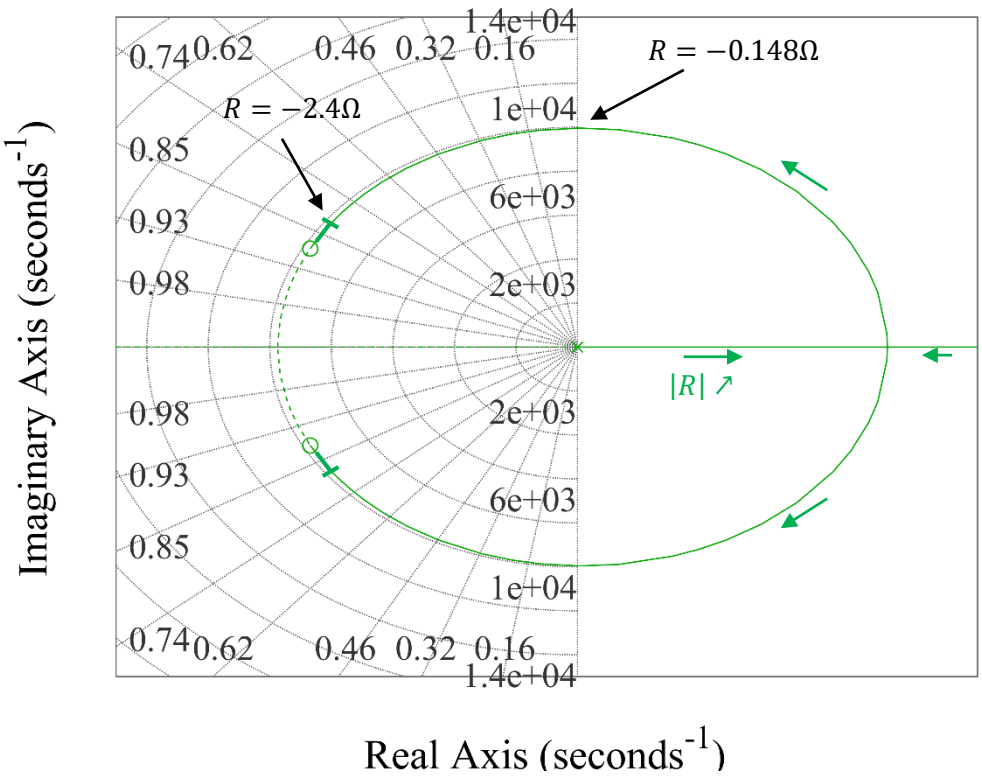

Figure 4.4 – Dominant poles root locus for negative equivalent output impedance – linearized CPL.

It can be observed that these values correspond to relatively important power consumptions, all above the use case maximum power which is represented by a green tick and for which the system stays stable.

In spite of this, these first results confirm that the configuration taking into account a pure CPL as load corresponds to the worst case in term of stability. The following developments are therefore based on this configuration which thus covers all the others.

4. 1. 2 Sensitivity to droop coefficient

On the same ideal system, the droop control is implemented in order to evaluate its impact at the scale of a unique system.

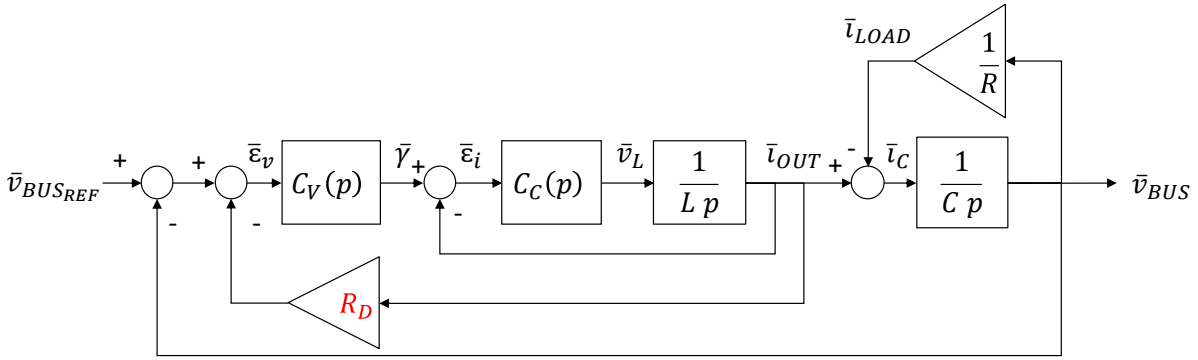

Figure 4.5 – Block diagram of a droop controlled converter feeding a linear load.

Thus, Equation 4.1 becomes

$$\frac{\bar{v}_{BUS}}{\bar{v}_{BUS_{REF}}} = \frac{RP_VP_C \cdot s^2 + (RP_VP_CI_C + RP_VP_CI_V) \cdot s + RP_CP_VI_CI_V}{\begin{aligned} &RLC \cdot s^4 \\ &+(L + RCP_C + RCR_DP_VP_C) \cdot s^3 \\ &+(P_C + R_DP_VP_C + RCP_CI_C + RCR_DP_VP_CI_C + RCR_DP_VP_CI_V + RP_VP_C) \cdot s^2 \\ &+(P_CI_C + R_DP_VP_CI_C + R_DP_CP_VI_V + RCR_DP_CP_VI_CI_V + RP_VP_CI_C + RP_VP_CI_V) \cdot s \\ &+(R_DP_CP_VI_CI_V + RP_CP_VI_CI_V) \end{aligned}} \quad 4.5$$

Applying the same method than previously, the transfer function is written in the correct form as shown in equation 4.6 by factoring the denominator by R_D which allows to draw the root locus presented in Figure 4.6.

$$1 + R_D \cdot \frac{\begin{aligned} &CRP_VP_C \cdot s^3 \\ &+\left(P_VP_C + RCP_VP_C(I_C + I_V)\right) \cdot s^2 \\ &+(P_VP_C(I_C + I_V) + RCP_VP_CI_VI_C) \cdot s \\ &+P_CP_VI_CI_V \end{aligned}}{\begin{aligned} &RLC \cdot s^4 \\ &+(L + RCP_C) \cdot s^3 \\ &+(P_C + RCP_CI_C + RP_CP_V) \cdot s^2 \\ &+\left(P_CI_C + RP_VP_C(I_C + I_V)\right) \cdot s \\ &+RP_CP_VI_CI_V \end{aligned}} = 0 \quad 4.6$$

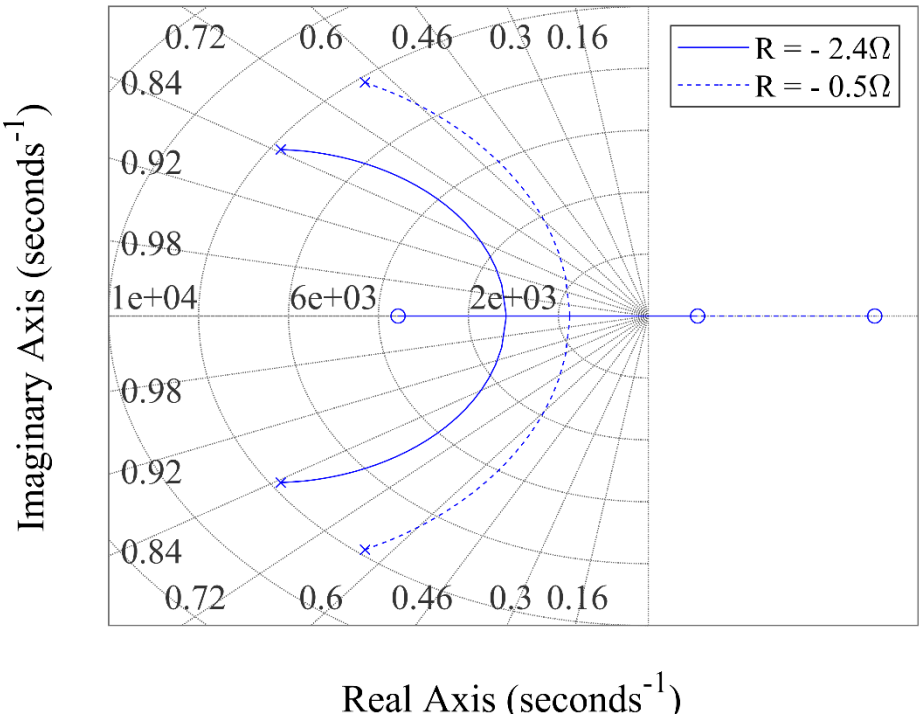

Figure 4.6 – Dominant poles root locus for R_D considering two negative load impedances.

The graph presents the root locus for R_D variations considering two values of negative impedances, -2.4Ω and -0.52Ω, respectively corresponding to the use case maximum value of negative impedance and to the maximal allowed power consumption for a $28V$ bus as defined by ECSS. Based on this, the following observations can be done:

- A limit above which droop control makes the system unstable exists and equals to the absolute value of the load equivalent impedance mentioned above.

- Below this limit, droop control tends to make the system slower and increase the damping, the curve tending to reach the real axes towards low absolute values as R_D rises.

Up to now, the previous results focused only the dominant poles of the system, relative to the voltage loop. But the poles relative to the faster inner current loop were also present further to the left in the S-plane, as shown in Figure 4.7, this last being indeed integrated in the model described by equation 4.1

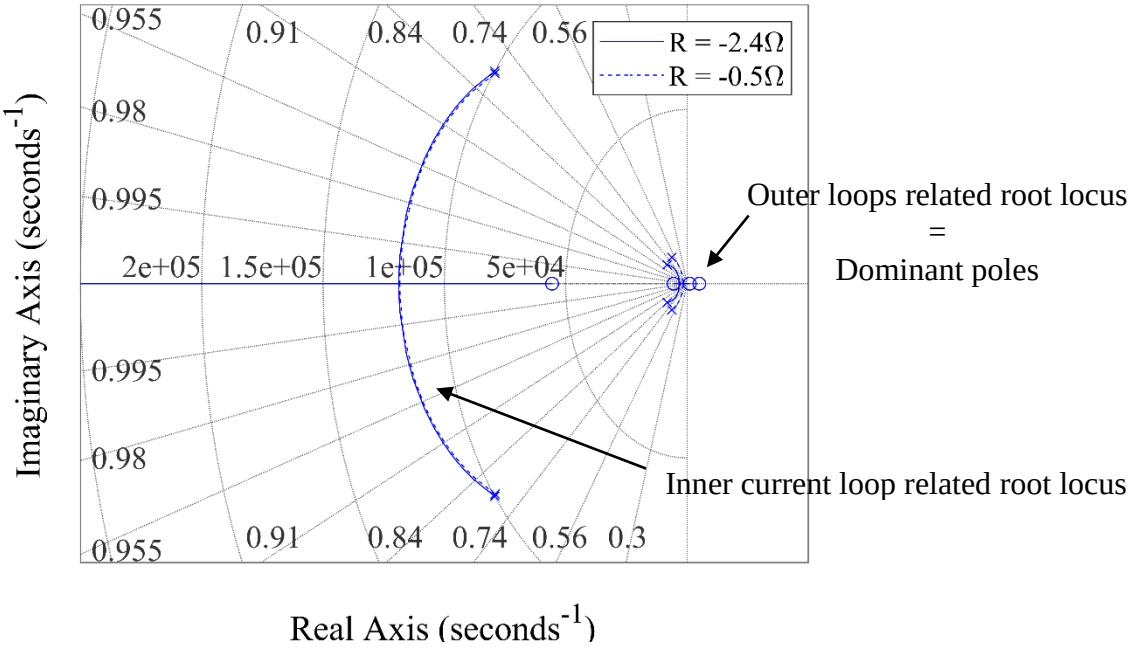

Figure 4.7 – Global view of all root locus for R_D variations considering two negative load impedances

Droop control tends to make the current loop more damped, so that its dynamic performance is maintained or even improved.

4. 1. 3 Stability criteria

The last observation enables to simplify the model by neglecting the current loop. Based on this assessment the following closed-loop transfer function is obtained:

$$\frac{v_{BUS}}{v_{REF}} = \frac{RP_V \cdot s + RP_V I_V}{(RC + RCR_D P_V) \cdot s^2 + (RCR_D P_V I_V + R_D P_V + RP_V + 1) \cdot s + (RP_V I_V + R_D P_V I_V)} \qquad 4.7$$

Since the resulting system has a degree of 2, it becomes easier to determine a stability criterion analytically. Hence, the poles of the system:

$$\lambda_1, \lambda_2 = \frac{-b \pm \sqrt{b^2 - 4ac}}{2a} \tag{4.8}$$

with

$$\begin{cases} a = RC + RCR_D P_V \\ b = RCR_D P_V I_V + R_D P_V + RP_V + 1 \\ c = RP_V I_V + R_D P_V I_V \end{cases}$$

According to the general stability criterion for linear systems, for the system to be stable, all its poles must have a strictly negative real part. In the case of a negative equivalent load impedance R, considering that $2a < 0$ is always true, this condition is reached if and only if the two following conditions are filled.

- Condition 1:

$$4ac > 0 \tag{4.9}$$

$$\Leftrightarrow 4(RC + RCR_D P_V)(RP_V I_V + R_D P_V I_V) > 0 \tag{4.10}$$

$$\Leftrightarrow R_D < |R| \tag{4.11}$$

- Condition 2:

$$-b < 0 \tag{4.12}$$

$$\Leftrightarrow RCR_D P_V I_V + RP_V - R_D P_V - 1 < 0 \tag{4.13}$$

$$\Leftrightarrow |R| < \frac{R_D P_V + 1}{CR_D P_V I_V + P_V} \tag{4.14}$$

Which can also be expressed as a condition on R_D

$$R_D < \frac{1 - |R| P_V}{C|R| P_V I_V - P_V} \tag{4.15}$$

However, for the values of the case study, and in particular for the values of |R| considered, this condition is always covered by Condition 1 – see Figure 4.8 below.

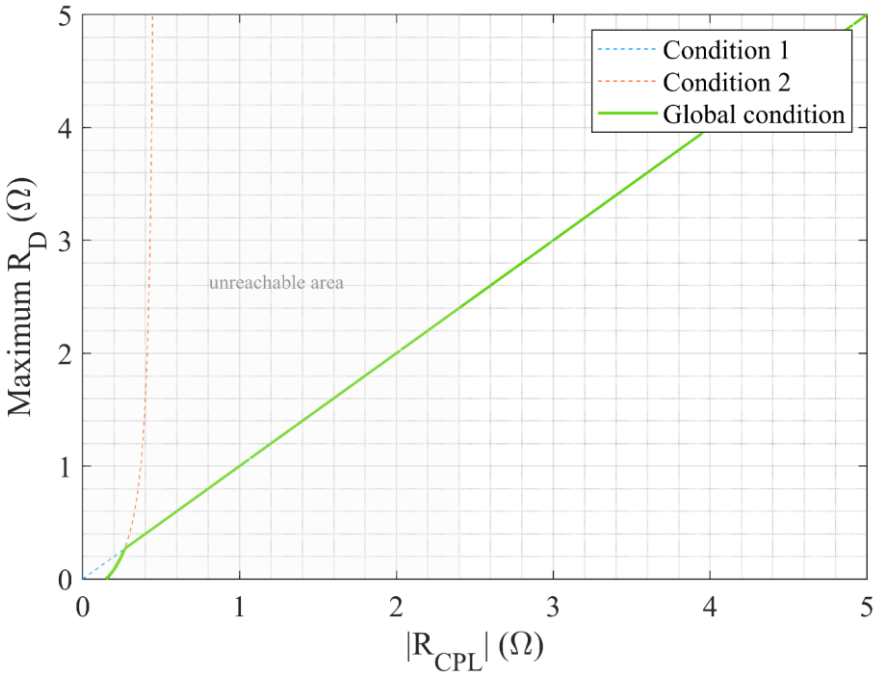

Figure 4.8 – Stability criteria on R_D in function of the equivalent load impedance considering the worst case configuration in terms of stability – loads set only composed of a CPL.

Condition 1 is therefore the necessary and sufficient condition for the system to be stable. It is possible to interpret this result from the point of view of large-signal non-linear characteristics, as was done in the previous chapter for the characterization of loads and the analysis of their open-loop equilibrium points.

To do this, let's recall that for an operating point to exist, the following condition must be satisfied:

$$R_{D\,MAX} = -\frac{R}{2} + \sqrt{\frac{R^2}{4} + \frac{V_{REF}^2 \cdot R}{4P_{CPL}}} \tag{4.16}$$

In the case of a pure CPL, it becomes

$$R_{D\,MAX} = \frac{V_{REF}^2}{4P_{CPL}} \tag{4.17}$$

The large-signal characteristic of a converter using droop control corresponding to this limit, applied to the case under study, is shown in Figure 4.9. Clearly, this line is tangent to the CPL characteristic at maximum power and, together with the $R_D = 0$ characteristic, delimits the zone for which points of equilibrium exist.

In this zone, it is possible to identify 2 distinct parts separated by the line of equation $V = I$:

- For every equilibrium point at the right of this separation, $R_D > |R|$ which means that the system is unstable.
- On the contrary, at the left, the condition $R_D < |R|$ is satisfied and the system is stable .

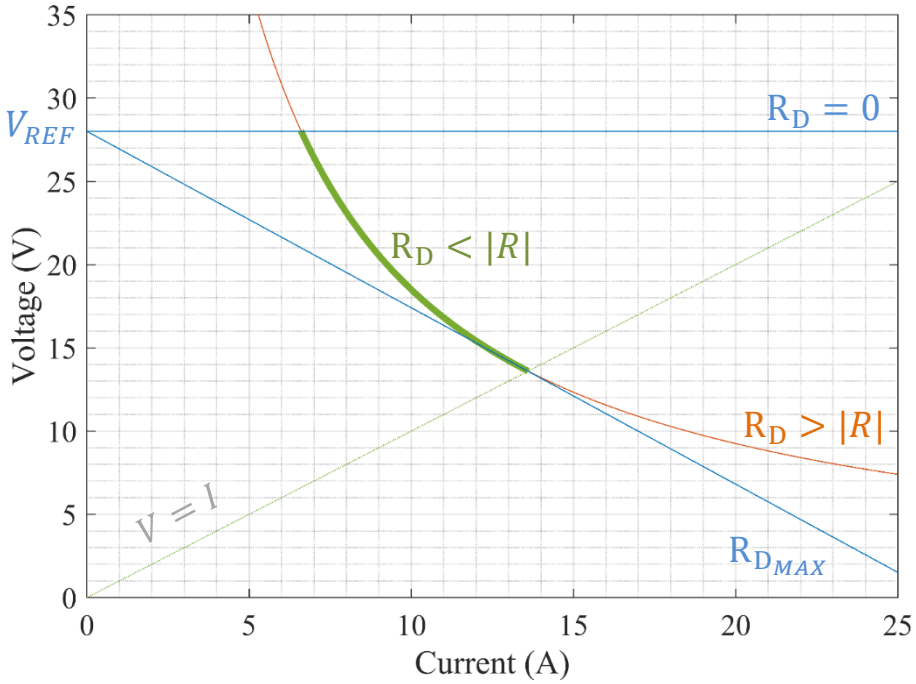

Figure 4.9 – Representation of the stable operation region on the I-V large signal characteristic curves of a system composed of a droop controlled converter supplying a CPL.

It can thus be deduced that the necessary condition on R_D for the existence of an operating point is also sufficient to guaranty the stability of the system, under the conditions considered so far: an ideal system consisting of a single converter coupled to a set of loads.

In order to determine how these results could be applied to modular and distributed power architectures, multi-converter systems will now be studied, based on these elements.

4. 2 Multi-converters systems

The transition to a multi-converter analysis is not straightforward, as it attempts to combine two contradictory objectives.

On the one hand, in a more complex system, a large number of parameters that can generally be neglected can take on new importance as a result of interactions between modules. For example, current sharing can be significantly altered by line impedances in steady-state equilibrium, so it may be worth checking their impact on stability aspects and incorporating them into the model. It is also rare for all the modules making up an assembly to be truly identical, and in order to study the impact of variations in parameters from one converter to another, it is necessary to individualize them in the modelling. As a result, the model to be studied becomes much more complex.

On the other hand, a major challenge in systems analysis is to control and reduce as much as possible the complexity of the models used to simplify their analysis.

The method presented in this section therefore proposes to overcome this contradiction by using a reference model based on the previous models, which will make it possible to determine the main dynamics of a multi-converter system, combined with a more complete model. The latter will make it possible to take into account a larger number of parameter variations and, by comparison, to study how this brings it closer or further away from the performance observed on the reference system.

4. 2. 1 Reference model

To define the reference model, let's first assume that all the converters are identical and that the line impedances are negligible. The previously used model is extended by the introduction of a parameter, noted N, defining the number of modules in parallel, as depicted below.

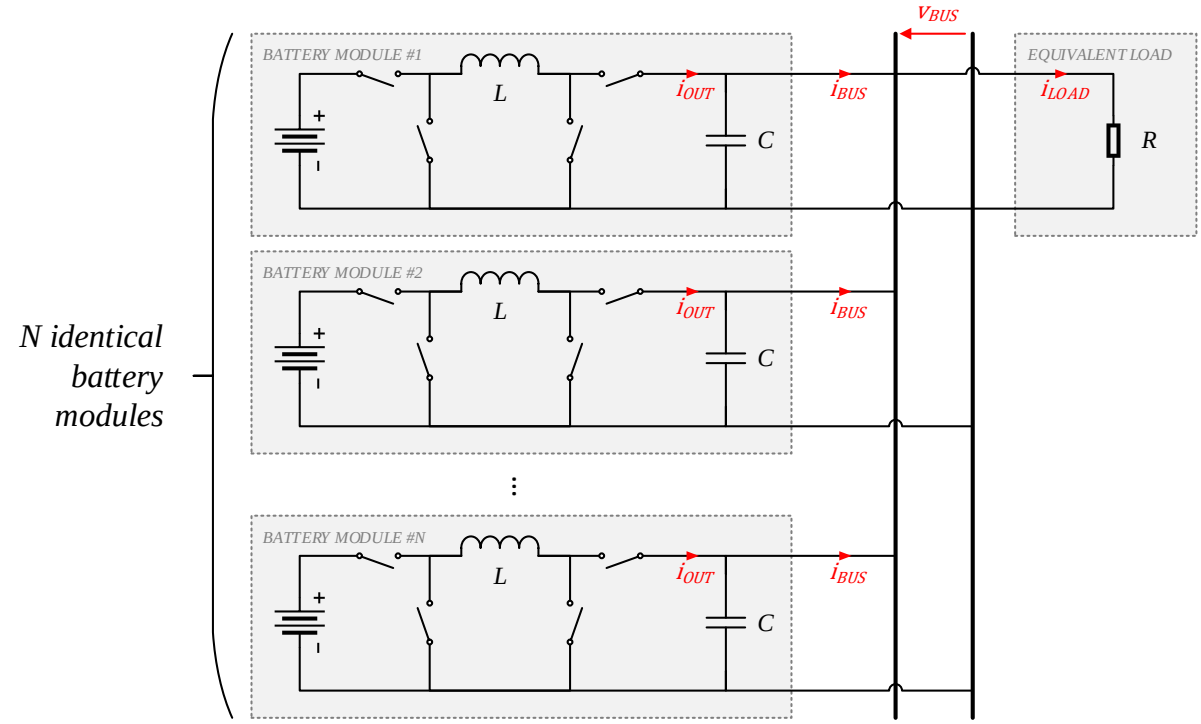

Figure 4.10 – N parallel droop controlled converters feeding a resistive load.

All converters being exactly identical and their output voltage being in common, their respective output currents are also considered as equals. Thus, the model can be defined as a unique equivalent converter as follows.

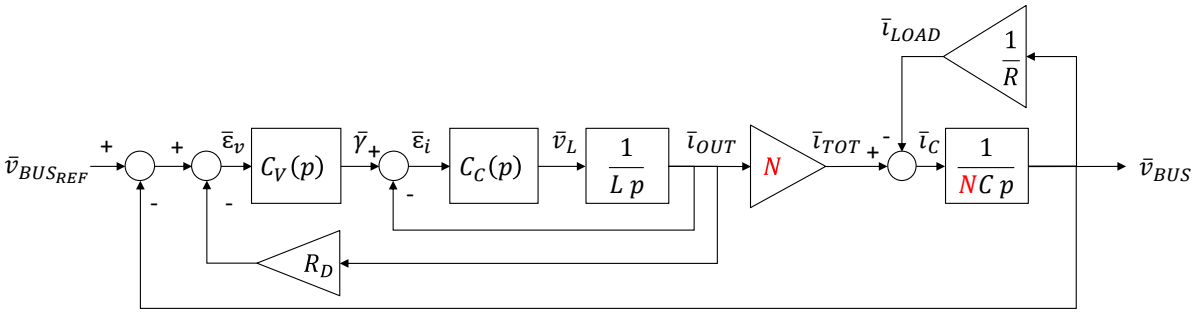

Figure 4.11 – Block diagram of a system composed of N ideal battery modules – considered as identical – implementing local current and voltage regulations as well as droop control.

The transfer function then becomes

$$\frac{\bar{v}_{BUS}}{\bar{v}_{BUS_{REF}}} = \frac{NRP_VP_C \cdot s^2 + NRP_VP_C(I_C + I_V) \cdot s + NRP_CP_VI_CI_V}{\begin{aligned} &NRLC \cdot s^4 \\ &+(L + NRCP_C + NRCR_DP_VP_C) \cdot s^3 \\ &+(P_C + R_DP_VP_C + NRCP_CI_C + NRCR_DP_VP_CI_C + NRCR_DP_VP_CI_V + NRP_VP_C) \cdot s^2 \\ &+(P_CI_C + R_DP_VP_CI_C + R_DP_CP_VI_V + NRCR_DP_CP_VI_CI_V + NRP_VP_CI_C + NRP_VP_CI_V) \cdot s \\ &+(R_DP_CP_VI_CI_V + NRP_CP_VI_CI_V) \end{aligned}} \qquad 4.18$$

And the root locus can be plotted.

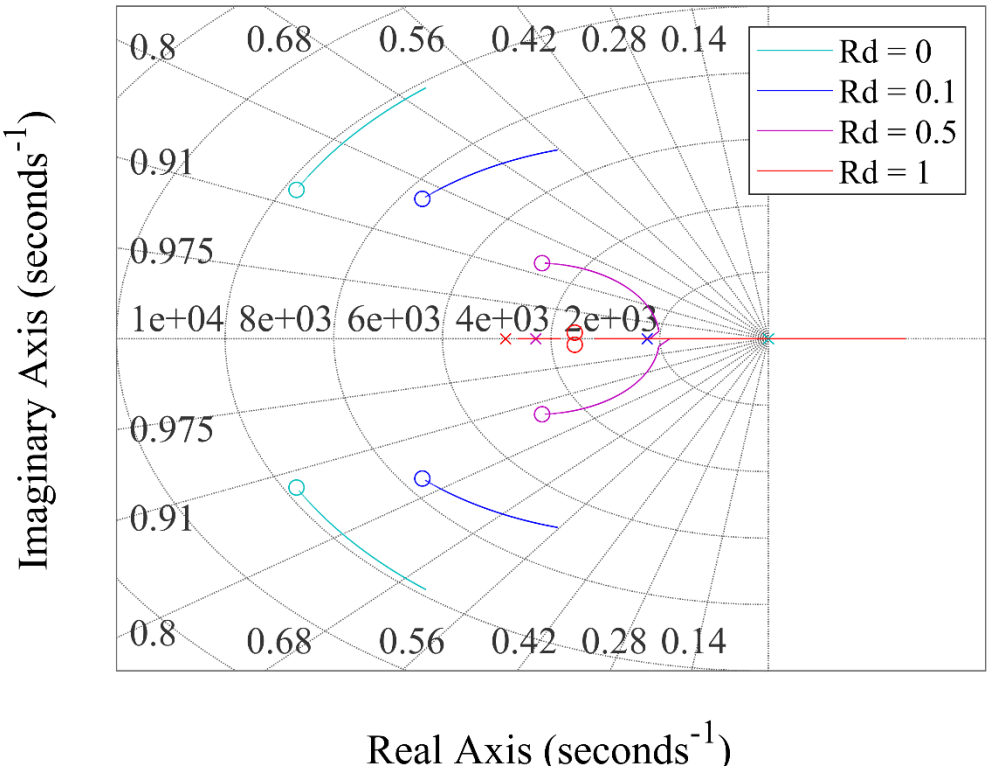

Figure 4.12 – Multi-converter ideal model root locus for $N \in [1\,;50]$ and $R = -2.4\Omega$ – corresponding to the maximum negative impedance defined by the use case.

It can be seen that the number of modules in parallel acts exactly inversely to the load's equivalent impedance. As a result, for a fixed value of R, a larger number of modules in parallel means that higher R_D can be implemented at the level of each converter. For instance, at $R_D = 1$, the system becomes unstable for $N < 2$ and although the value does not satisfy the stability condition determined above. This is due to the fact that this condition applies to $R_{D_{SYS}}$ the equivalent droop resistance of the system, which is obtained by paralleling all the individual droop resistors, since a droop-controlled converter is similar to a Thévenin source.

Considering the present reference system, as the droop coefficients are considered as equal, $R_{D_{SYS}}$ can be determined

$$R_{D_{SYS}} = \frac{R_D}{N} \tag{4.19}$$

Hence, the maximum value of each converter's droop coefficient can be calculated based on equation 4.17

$$R_{D_{MAX}} = \frac{V_{BUS}^2}{4P_{CPL}} \cdot N \tag{4.20}$$

It can be noted that the reverse logic can be adopted depending on the parameter chosen as input. Indeed, it is also equivalent to say that for a given value of R_D, a larger number of modules in parallel means that higher power consumption levels can be supplied by the system.

In both cases, this allows to take account of practical limitations that may arise when implementing the system, such as the current sharing error induced by line resistors, as mentioned above. However, these elements may also impact the stability of the system and are not taken into account by this simplified model. It is also impossible to consider the impact of setting different coefficients in each converter, particularly for droop control.

4. 2. 2 Detailed model

The complete model consists of considering all the converters individually to evaluate how it could impact the stability as shown in Figure 4.13.

Very few studies on electrical architectures, particularly those controlled by droop control, actually take several modules into account in their model. Equivalences or worst cases are generally identified in order to carry out stability analyses, as it has been done so far in the present work, with all the limitations it implies and that have just been discussed.

Even if most of the results following this method are interesting and allow to demonstrate the system's stability at a point, the justifications given for simplifications are often incomplete and these make it impossible to study the impact of some parameters.

As we said earlier, the complexity of analyzing systems with degrees greater than 2 is not easy and explains most of the above statement. Added to this is the fact that establishing the model itself is not trivial either. Indeed, in order to do so, in the present section, and based on the preliminary developments presented in Chapter 3, several methods are used to define a model which can take into consideration any number of modules, treated independently, any distribution network configuration and any type of load.

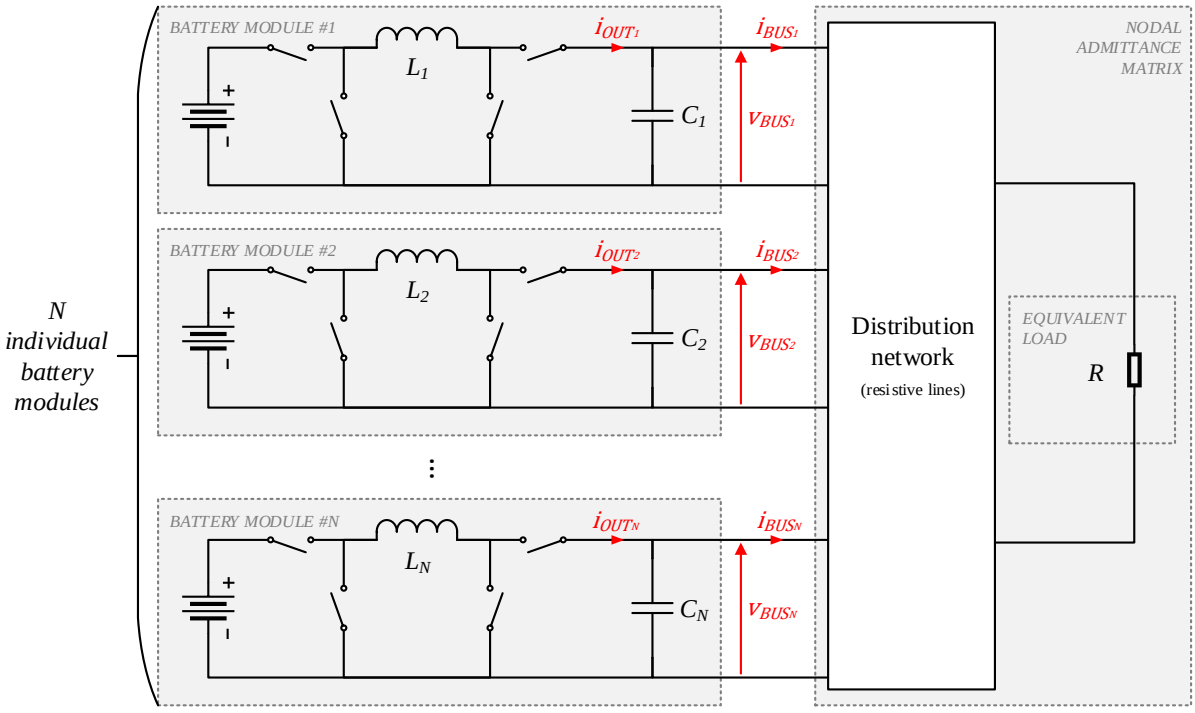

Figure 4.13 – *N* parallel individual droop controlled converters feeding a load through a common distribution network.

4. 2. 2. 1 Model definition

In order to limit the complexity of manipulation of the model, matrix modelling is used and each converter is individually defined using state variable formalism.

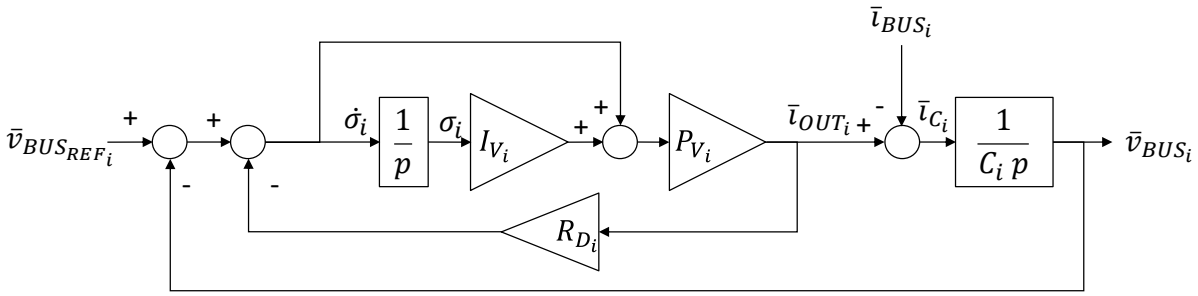

Figure 4.14 – Droop controlled converter's block diagram for state-variable modelling.

Let $\dot{\sigma}_i$ and $\dot{v}_{BUS_i}$ be the state variables. Based on Figure 4.14, it can be stated that:

$$\dot{\sigma}_i = -\frac{R_{D_i}P_{V_i}I_{V_i}}{1+R_{D_i}P_{V_i}}\cdot\sigma_i - \frac{1}{1+R_{D_i}P_{V_i}}\cdot v_{BUS_i} + \frac{1}{1+R_{D_i}P_{V_i}}\cdot v_{BUS_{REF}i} \tag{4.21}$$

$$\dot{v}_{BUS_i} = \frac{1}{C_i}\left[\frac{P_{V_i}I_{V_i}}{1+R_{D_i}P_{V_i}}\cdot\sigma_i - \frac{P_{V_i}}{1+R_{D_i}P_{V_i}}\cdot v_{BUS_i} + \frac{P_{V_i}}{1+R_{D_i}P_{V_i}}\cdot v_{BUS_{REF}i} - i_{BUS_i}\right] \tag{4.22}$$

Line resistances as well as loads – through their characteristic impedance – are modelled through Q_{red}, the reduced conductance matrix obtained using the Kron reduction introduced in Chapter 3. This gives the following expression:

$$I_{BUS} = Q_{red}\cdot V_{BUS} \tag{4.23}$$

with $I_{BUS} = \left[i_{BUS_1} \ \dots \ i_{BUS_N}\right]^T$ and $V_{BUS} = \left[v_{BUS_1} \ \dots \ v_{BUS_N}\right]^T$.

Even though the equivalent impedance of the load is used since the beginning of the present Chapter, this takes on a completely different significance here, since linearizing the components before the model is set up means that they can be integrated into the conductance matrix without having to increase the size of the system, as the Kron reduction integrates them into the reduced matrix Q_{red}.

Defining i as $i \in [1;N], i \in \mathbb{N}$, the system can be written in matrix form

$$\Sigma = [\sigma_1 \ \dots \ \sigma_N]^T \tag{4.24}$$

$$V_{BUS_{REF}} = \left[v_{BUS_{REF_1}} \ \dots \ v_{BUS_{REF_N}}\right]^T \tag{4.25}$$

$$C = diag(C_i) \tag{4.26}$$

$$P_V = diag\left(P_{V_i}\right) \tag{4.27}$$

$$I_V = diag\left(I_{V_i}\right) \tag{4.28}$$

$$R_D = diag\left(R_{D_i}\right) \tag{4.29}$$

The result is a system of order $2N$

$$\begin{pmatrix} \dot{\Sigma} \\ \dot{V}_{BUS} \end{pmatrix} = \begin{pmatrix} -R_D P_V I_V (I_n + R_D P_V)^{-1} & -(I_n + R_D P_V)^{-1} \\ C^{-1} P_V I_V (I_n + R_D P_V)^{-1} & -C^{-1} P_V (I_n + R_D P_V)^{-1} - C^{-1} Q_{red} \end{pmatrix} \cdot \begin{pmatrix} \Sigma \\ V_{BUS} \end{pmatrix} + \begin{pmatrix} (I_n + R_D P_V)^{-1} \\ P_V (I_n + R_D P_V)^{-1} \end{pmatrix} \cdot V_{BUS_{REF}} \tag{4.30}$$

This concludes the modelling of the complete system.

4. 2. 2. 2 Introductive example

Although this model alone corresponds to a linearization of the system, it is easy to add the non-linear terms in order to carry out simulations in the time domain by dealing the loads – non-linear – independently from the line resistances – linear terms. This is particularly useful for verifying the consistency of the results. An example is given here, based on a system made up of 4 modules feeding a network composed of constant power loads – no PV panels are considered in this example.

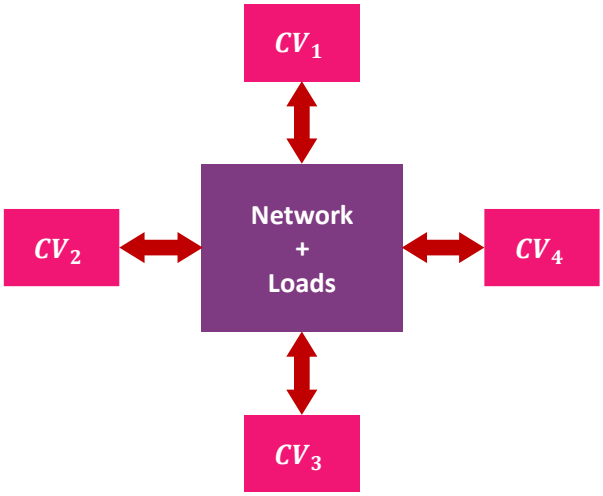

Figure 4.15 – Example system composed of 4 battery modules feeding a set of load through a resistive distribution network.

The voltage loop parameters are all kept identical, in accordance with the homogenized converter model.

In order to cover more cases and for the phenomenon to be observed in the following to be more visible, the power limit for 28 volt buses of 1500 watts of power consumption is considered as load power, noted as P_{LOAD}.

The line resistances forming the distribution network are generated randomly according to a uniform distribution in a determined typical range of 0 to 50 milliohms:

$$R_{line} = \begin{pmatrix} \infty & 0.0082 & 0.0099 & 0.0360 \\ 0.0082 & \infty & 0.0348 & 0.0326 \\ 0.0099 & 0.0348 & \infty & 0.0190 \\ 0.0360 & 0.0326 & 0.0190 & \infty \end{pmatrix}$$

In the same manner, the droop coefficients are defined randomly according to a uniform distribution law:

$$R_D = \begin{pmatrix} 0.2169 & 0 & 0 & 0 \\ 0 & 0.4109 & 0 & 0 \\ 0 & 0 & 0.4505 & 0 \\ 0 & 0 & 0 & 0.2875 \end{pmatrix}$$

In order to obtain a stable system – or at least one that is assumed to be stable in the sense of the study carried out on the reference system – the satisfaction of the condition set out in equation 4.20 is verified :

$$R_{D_{SYS}} = 1/sum\big(diag(1./R_D)\big) < R_{D_{SYS_{MAX}}} = V_{BUS_{REF}}^2/4P_{LOAD}$$

$$\Rightarrow R_{D_{SYS}} = 0.0785 < 0.1176$$

This allows to calculate the equivalent load impedance thanks to the following expression:

$$R = -\frac{\left(V_{BUS_{REF}} + \sqrt{V_{BUS_{REF}}^2 - 4R_{D_{SYS}}P_{LOAD}}\right)^2}{4P_{LOAD}} \qquad 4.31$$

It is then randomly distributed to the 4 nodes of the system which gives the conductance matrix:

$$Q_{red} = \begin{pmatrix} 249.4830 & -121.2423 & -101.2308 & -27.7757 \\ -121.2423 & 179.9483 & -28.7720 & -30.6985 \\ -101.2308 & -28.7720 & 182.3026 & -52.5519 \\ -27.7757 & -30.6985 & -52.5519 & 110.7013 \end{pmatrix}$$

However, in order to simulate the system in the time domain, the equivalent load impedances are removed from Q_{red} and the power consumption is directly calculated at each node with the large signal expression of a CPL, conforming the random distribution defined above. This allows to perform steps between full and half load.

Based on this, the graphs given in Figure 4.16 are obtained.

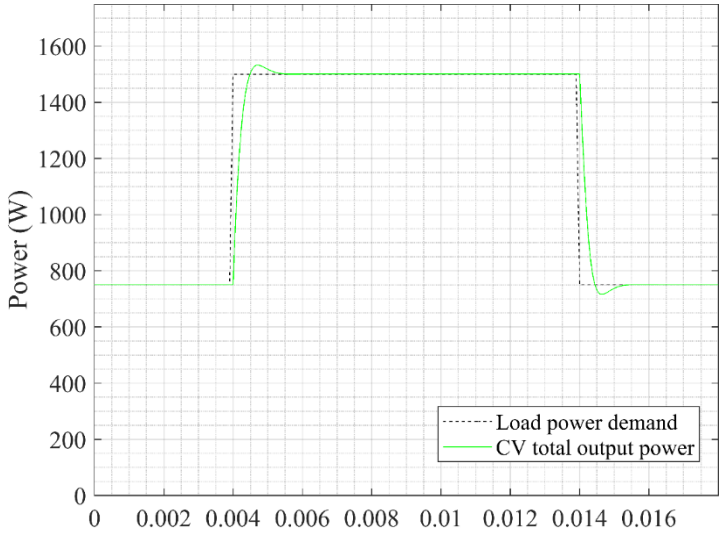

a)

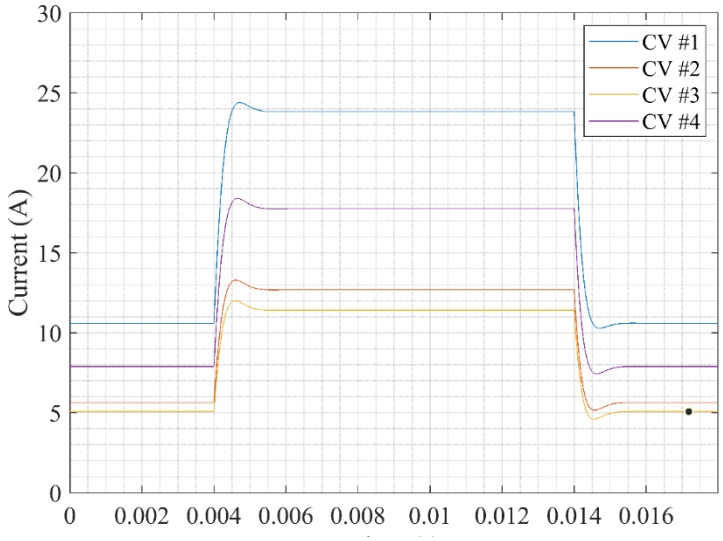

b)

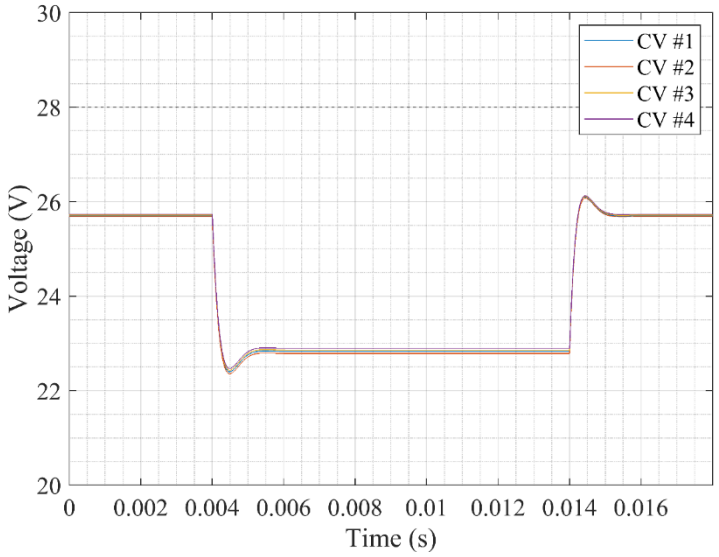

c)

Figure 4.16 – 4 modules example system simulation results: (a) power consumption profile, (b) converters individual currents and (c) converters individual bus voltages.

It can be noted that the system is indeed stable and operating in accordance with the parameters determined above.

This is for instance the case for current sharing, where we find a ratio of approximately 2 between converters 1 and 3, as expected given their respective droop coefficients.

In term of voltage regulation, since, the $R_{D_{SYS}}$ is relatively high in comparison with its maximum possible value, it is not surprising to see that the voltage drop induced by the droop control is significant. Based on this observation, it will subsequently be necessary to add an additional limitation in order to control this voltage drop, but it is important to note that the present randomly generated system does not have any practical meaning in terms of an optimized electrical operation.

Focusing on stability aspects, an overshoot of 17% and a stabilization time of 1.25ms are observed.

By way of comparison, the figure below shows the voltage variations for a system where $R_{D_{SYS}}$ equals 0.0298 – also generated randomly – which allows to verify the validity of the phenomena predicted by the sensitivity analysis carried out earlier.

In this second system, the voltage response presents an overshoot of about 73% for a stabilization time of 0.9ms. Thus for a smaller equivalent value of R_D the system is faster but less damped as expected.

Thus, although it is difficult to analyze the sensitivity to each parameter as it has been done so far with such a complex system, it is still possible to observe their consequences.

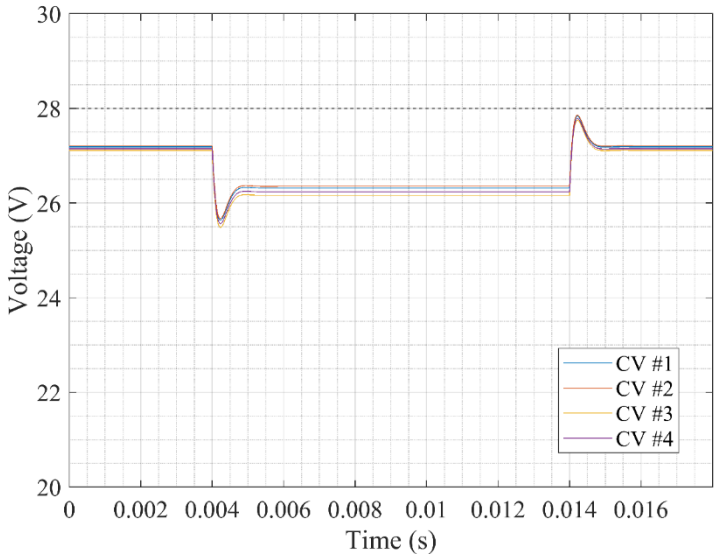

Figure 4.17 – Example system simulated voltages on battery modules bus side with $R_{D_{SYS}} = 0.0298$.

Moreover, the most significant interest of the proposed model, is that it is easy to calculate the poles of the system by calculating the eigenvalues of the matrix A, defined as follows thanks to equation 4.30.

$$A = \begin{pmatrix} -R_D P_V I_V (I_n + R_D P_V)^{-1} & -(I_n + R_D P_V)^{-1} \\ C^{-1} P_V I_V (I_n + R_D P_V)^{-1} & -C^{-1} P_V (I_n + R_D P_V)^{-1} - C^{-1} Q_{red} \end{pmatrix} \quad 4.32$$

But calculating the poles for each configuration is a tedious task and does not allow to deduce anything other than stability at each point.

However, by performing a Monte Carlo analysis on this model using the ability to generate configurations randomly as introduced above, and computing the poles of each particular system, it is possible to approximate the root locus of the system.

As a summary and verification of the applicability of the previous analyses conclusions to multi-converter systems, Figure 4.18 presents the results obtained by considering the variations in the table below.

Table 4.1 – Parameters variations for Monte Carlo analysis on EPS root locus determination.

Parameter	Min	Max	Unit
Power consumption P_{LOAD}	0	230	W
Number of module N	1	20	-
Droop coefficients R_{D_i}	0	$0.8522 \times N$	Ω

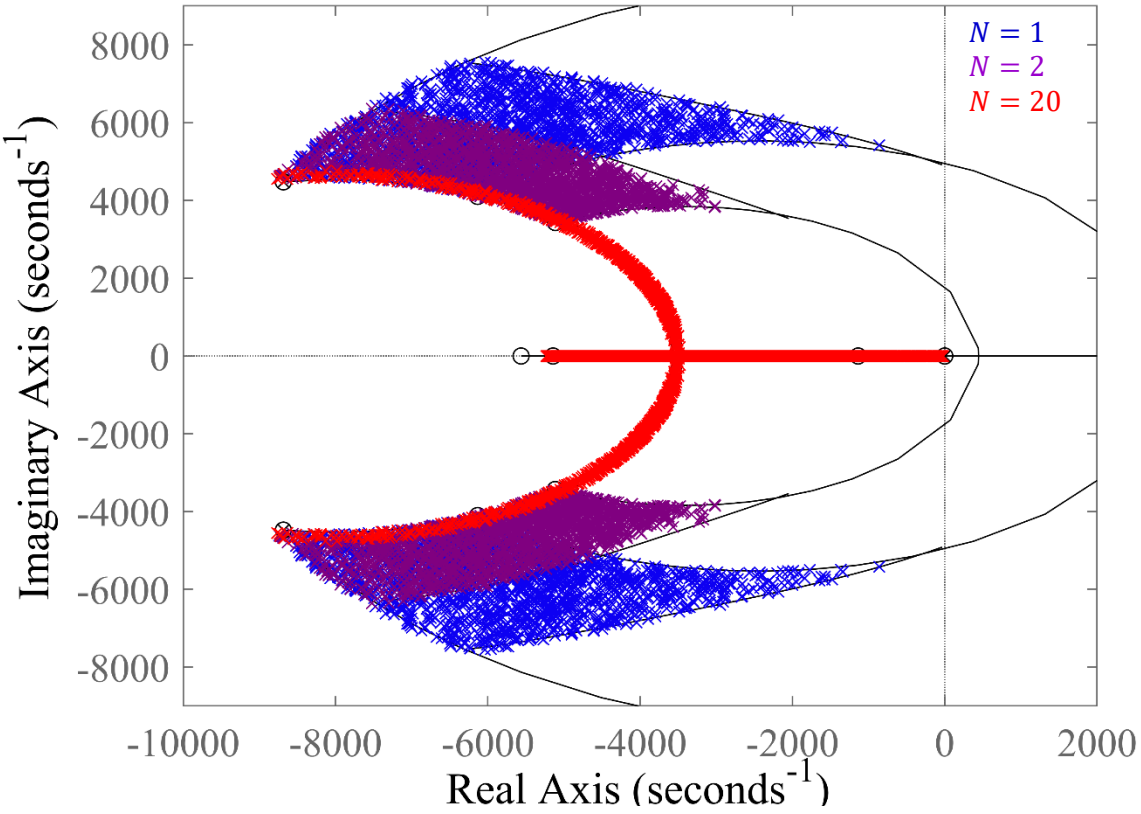

Figure 4.18 – Detailed model root locus for three different number of battery modules connected in parallel, N, and considering identical droop coefficients and typical line impedances.

On this graph, the following boundaries can be identified, based on the root locus observed during the reference system study:

- At the left the poles are bounded by the root locus on R with $R_D = 0$.
- At the right the poles are bounded by the root locus on R with $R_D = R_{D_{MAX}}$ as defined in equation 4.20.

- Towards high absolute values of imaginary part limit (top and bottom), the poles are limited by the root locus on R_D with maximum power consumption and R defined as defined in 4.31.
- Finally, towards low imaginary part limit (near real axis) the identified boundary is the root locus on R_D with minimum power consumption.

These deductions which exactly correspond to the behavior observed on the reference model, together with the previous time domain simulation, allow to validate the proposed detailed model.

In the last sections of the present chapter, this probabilistic method is used to study the sensitivity of the system to the parameters which were neglected so far.

4. 2. 2. 3 Sensitivity to line impedances

Although the conclusions may seem trivial, taking account of line resistances is a sine qua non for establishing the system's conductance matrix, which is the cornerstone of the model proposed here.

This significant dependence on these parameters for the establishment of the model made it necessary to study their impact.

As the impact is relatively low for small variations and the number of variable parameters is relatively large, the two following figures are based on the same parametric variation than in the previous section but for two extreme values of line resistance.

Figure 4.19 presents the results obtained for a maximum line resistance of $1 \times 10^{-12}\ ohm$. It can be observed that for $N = 1$, the results are similar to what was observed previously. In the contrary, for several converters in parallel, the results are highly affected. If it seems that the system stays stable for $N = 2$, it is not the case for $N = 20$.

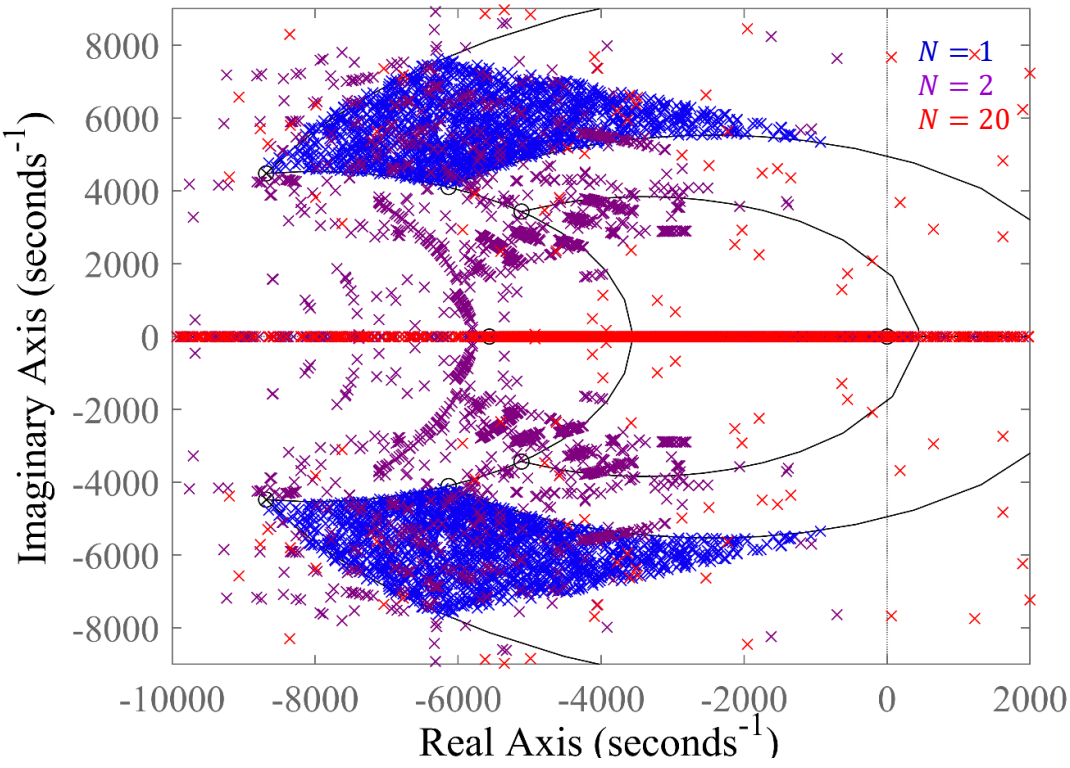

Figure 4.19 – Detailed model root locus for three different number of battery modules connected in parallel, N, and considering small line resistances: $1 \times 10^{-12}\ ohm$.

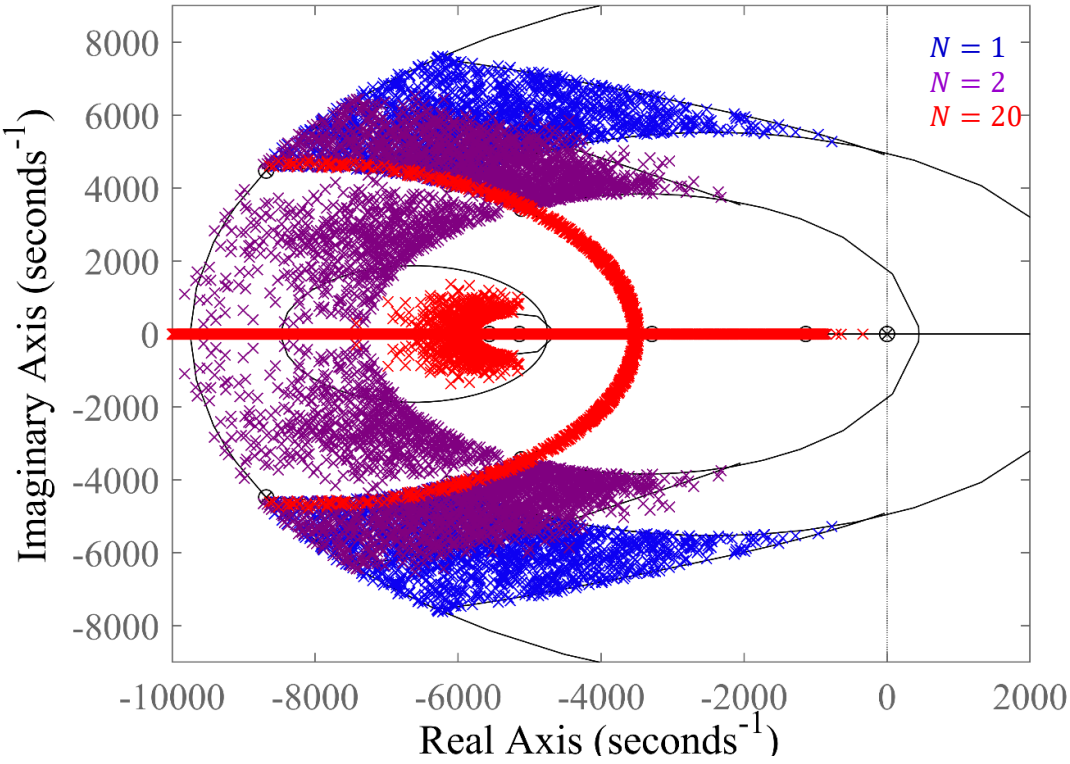

Figure 4.20 – Detailed model root locus for three different number of battery modules connected in parallel, N, and considering large line resistances: 10 $ohms$.

This could be caused by the correlation of the different regulation loops which could then disturb each other. Indeed, bigger line resistances together with converter output capacitors act as an isolator between the different dynamics.

Fortunately, the phenomenon only appears for very low values of resistances which are not reachable in practical, to the contrary of large values.

Figure 4.20 presents the curves obtained for values of line resistances of up to 10 $ohms$ while keeping the same parameter variations as above. As suggested in 4. 1. 1. 1 , it can be seen that it behaves like a resistive load to the system.

Thus, even if it is not desirable in term of electrical system performances, it may not induce any issue in term of stability.

4. 2. 2. 4 Sensitivity to droop coefficient differential variations

The last aspect studied is the impact of setting different values of droop coefficients to each converter.

Indeed, the only condition determined so far is a condition on the equivalent droop resistance, but there are an infinite number of possible combinations that satisfy it. Furthermore, it has been shown that variations in droop control coefficients have a very significant impact on the stability and performance of the system, and it is therefore essential to analyze this phenomenon, which has received little or no study in the literature.

The root locus taking into account an individualized variation in the droop coefficients, while respecting the general condition, are shown in Figure 4.21. The maximum value of coefficient reachable by each

converter is nevertheless limited as a function of the number of modules, so that if one module is lost, the other modules can ensure the operation of the system and therefore stabilize it.

It can be seen that for a small number of converters in parallel, no significant change is observed. However, this does not exclude to obtain very high ratios of coefficients between modules – up to ratios of $1:1000$ for $N = 2$ – and consequently an important controllability in terms of current sharing.

On the other hand, for a large number of converters, the root locus is evolving in a different way, and is moving away from the reference root locus.

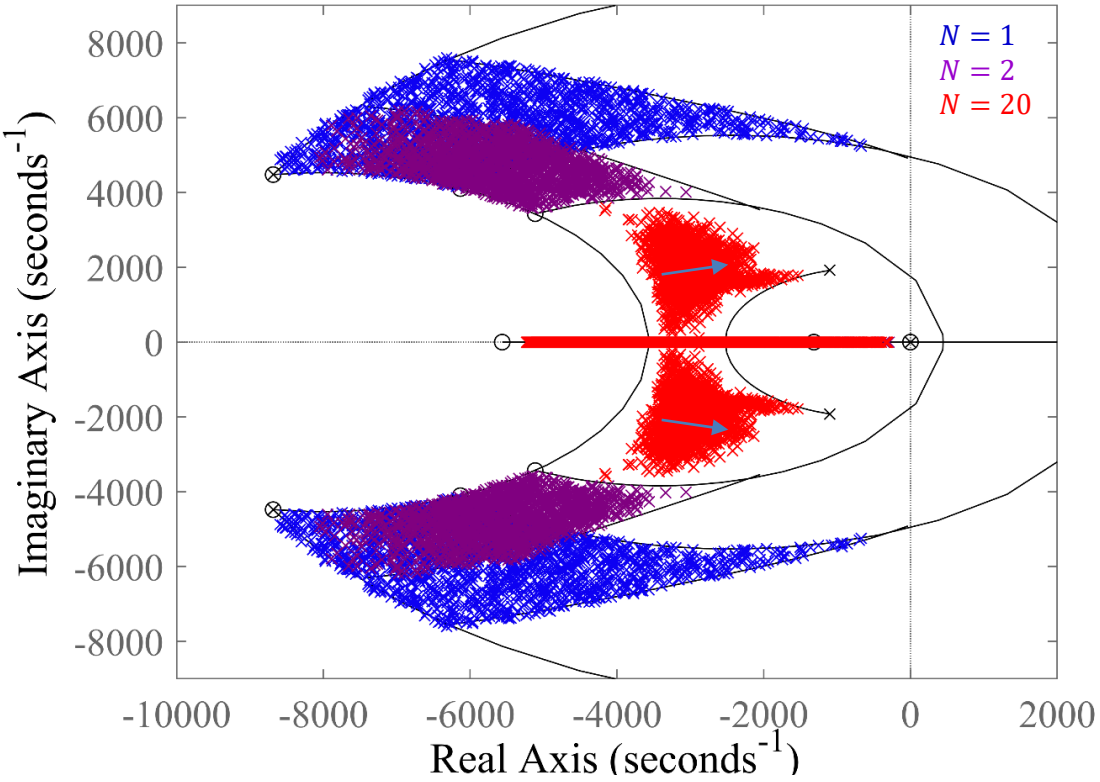

Figure 4.21 – Detailed model root locus for three different number of battery modules connected in parallel, N, and considering individualized droop coefficients. The different droop coefficients are determined randomly and verify the condition on system equivalent droop coefficient, $R_{D_{SYS}}$.

The first and most important observation is that this deviation from the reference trajectory remains limited and does not induce instability in the system under the conditions described above.

The blue arrows on the graph indicate the direction of variation of the dominant poles of the system when only a few of the N modules have low droop coefficients and most have relatively high coefficients. This corresponds to the situation where a small number of modules concentrate the majority of the current contribution and the others, because of their high coefficients, make only a small contribution to current supply, i.e. to bus regulation.

However, it is possible to limit this deviation, as shown by the curve to the right of the red cluster representing the root locus for $N = 20$. By identification, this corresponds to the root locus of the worst-case situation presented just above, i.e. the root locus which covers all the variations of R_D for a single converter regulating the bus and whose output capacitor would have a value equal to N times its nominal value.

This can be explained by the fact that whatever the value of the droop coefficient and therefore the contribution of a converter to bus regulation, its output capacitor is connected to the distribution network and influences the operation of all the others. From a system point of view, it is therefore necessary to consider the total load as the set {capacitors + loads} – at constant power or purely resistive. It is this set that is distributed by the droop control.

So, rather than just being a method of current sharing, droop control is a method of load sharing in its most global sense.

While from a system stability and robustness point of view, the phenomenon can be seen as an advantage, from a system performance point of view, it should be noted that it tends to make the system slower and less damped.

In order to limit this drop of performance, it is proposed to add a limitation on the maximum sharing ratio to be allowed between two converters. In practice, although it may be interesting to adopt very high ratios, particularly for managing mode changes such as at the end of a battery charge, for example, it is still possible to reduce it to a certain extent.

Furthermore, a fairly loose restriction can significantly limit the phenomenon, as can be seen in Figure 4.22, where the same root locus as before are given but by limiting the maximum ratio to $1:20$.

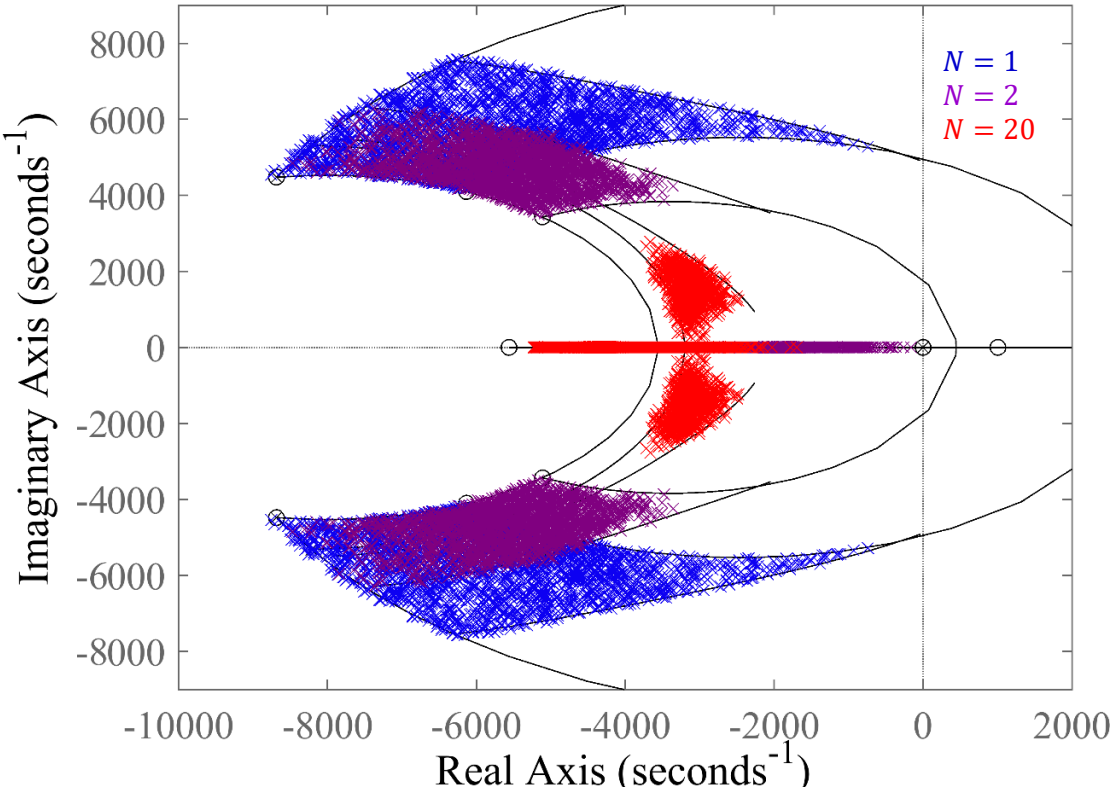

Figure 4.22 – Detailed model root locus for three different number of battery modules connected in parallel, N, and considering individualized droop coefficients with maximum differential ratio limitation of $1:20$.

Finally, it should be borne in mind that in order to highlight these characteristics, the highest achievable power for a 28V bus was chosen. In most cases, and particularly for the use case, these phenomena are naturally limited to acceptable levels as shown in Figure 4.23.

4. 3 Conclusion

As a conclusion to this chapter, which aimed to study the stability of modular electrical systems in as general a manner as possible and see how the droop control could impact it, the method developed here is applied to the case study.

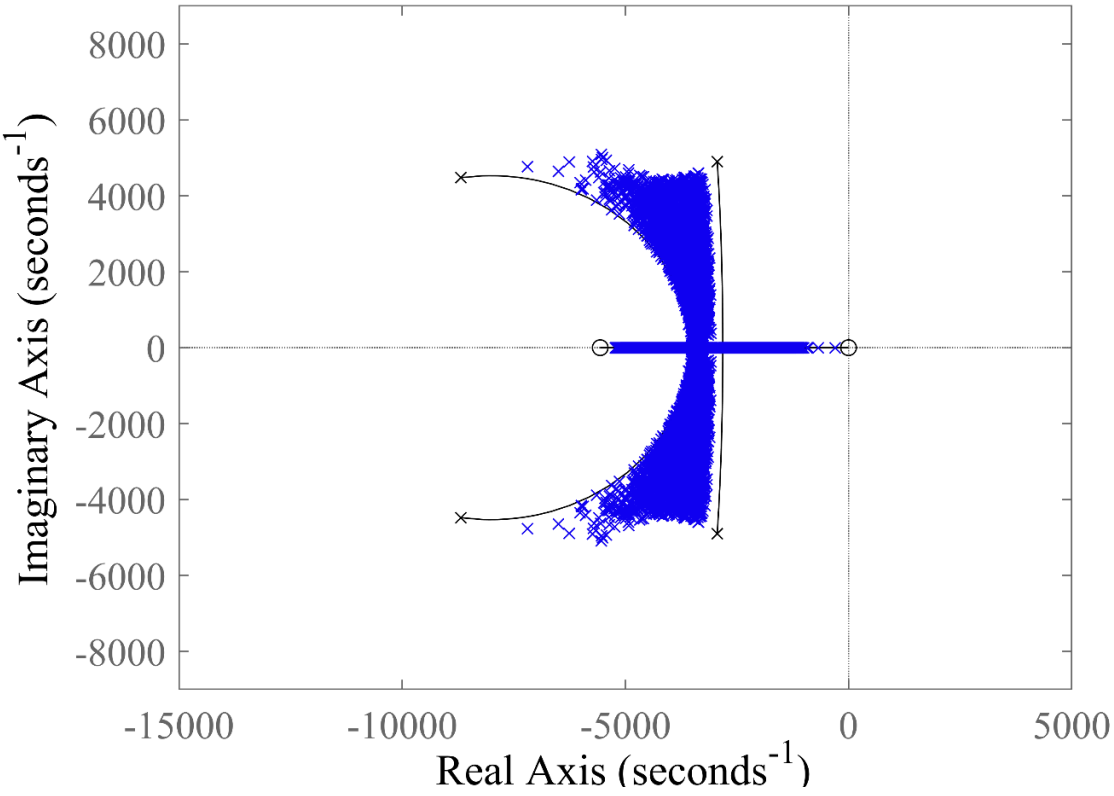

Figure 4.23 – Use case detailed model root locus: $N = 3$, $P_{LOAD} = 230W$, $R_{D_{MAX}} = 0.85$.

This validates the initial tuning approach that enabled this case study to be determined, since it shows a stable system in any configuration, thanks to the conditions determined during the chapter.

It has been shown that, provided the condition of existence of equilibrium points in terms of the large signal characteristics is met, there is a stable operating point. It has also been shown that the closer one gets to this limit value, the more the system's stability margins are reduced, which means that a margin should be kept in relation to this condition. It was also established that increasing the number of modules in a system enabled higher droop coefficient values to be achieved individually.

More generally, these results provide a framework on which to base the implementation, experimentation and interpretation of the results obtained and presented in the following, as well as for the definition of the secondary and tertiary control strategies by defining the possible ranges of variation of the various parameters adaptation, in particular the system level equivalent droop virtual resistance $R_{D_{SYS}}$. This work has also enabled us to gain a better general understanding of the rules governing modular systems and to identify the characteristics that differentiate them from single-converter systems.

CHAPTER 5.

Experimental results

Summary

In the previous chapters, after a detailed study of the different types of existing electrical systems, in terms of both control and power system aspects, in the space domain but also for similar more conventional applications, a new distributed and modular EPS architecture has been proposed and its stability studied. This has made it possible to establish theoretical criteria for its proper operation and to understand its behavior in comparison with that of more conventional systems. In order to test these results and confirm them, a demonstrator was set up. The object of this chapter is thus to present the work undertaken to achieve this objective.

Based on the use-case defined in Chapter 3, the demonstrator takes the form of a “flat sat”, which can be generally defined as a high fidelity electrical and functional representation of a spacecraft, reduced to only the EPS in the present case as presented below.

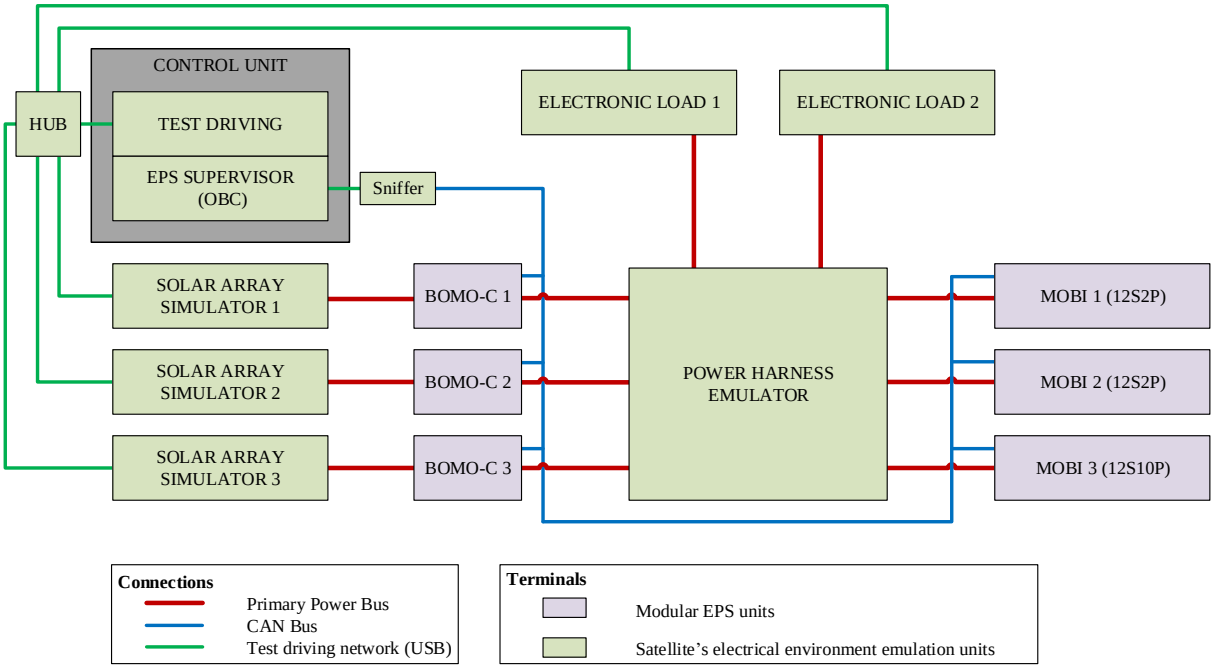

Figure 5.1 – Experimental setup.

The high degree of representativeness required is conditioned by the important constraint of space system reliability mentioned in Chapter 2. Thus, in the space domain, in order to verify the results obtained on a system as completely as possible, without significantly limiting their field of validity, it is the practice to use equipment that is as close as possible to flight equipment, both in terms of the functions implemented and the manufacturing processes used. This is why simple experimental equipment have not been used for all of the units in the setup presented above, and why it is necessary to distinguish between two types of component:

- The units represented in green correspond to the components necessary to emulates the environment in which the System Under Test (SUT) would evolve in an actual satellite, both from a power electrical and data handling point of view, as if it were in orbit. They aim to representatively generate and process the input and outputs signals of each SUT interface. For these elements, laboratory devices were used.
- The units in blue on the other hand, called MOBI and BOMO-C, correspond to the devices composing the actual SUT, that is to say the power electrical part of the proposed EPS. The BOMOs have been developed as part of the CNES roadmap for the development of future architectures to which this study relates. The MOBI have been the object of a co-design

throughout the thesis in order to integrate in a decentralized way the functionalities of the primary control as detailed in Chapter 2.

In this chapter, in order to present the extensive work that went into setting up this experimental set-up, a detailed presentation of these devices will first be provided. This will allow in a second time to develop their practical integration in the demonstrator. Finally, the results obtained thanks to it in order to validate the practical implementation of the proposed primary control will be presented and interpretations that can be drawn from them will be discussed.

5. 1 SUT components

5. 1. 1 The BOMOs

The BOMOs (BOîtier MOdulaire, modular box in French) was developed at the instigation of the CNES to realize the conditioning and distribution functions previously done by the PCDU as closely as possible to the need. The design of the module also tackles the necessity to meet industrial objectives such as low recurrent prices by the use of COTS components. Taking these aspects into consideration makes the project not only technically relevant, but also economically in an increasingly competitive environment.

In a concern of standardization, the concept which is intended to be adaptable, is built around a "base brick" [154]. This standard core is composed of a primary power bus interface, a microcontroller, a Controller Area Network (CAN) bus interface, temperature, voltage and current measurements as well as an internal power supply generated from the power bus. Data buses such as the CAN, already used in massive geostationary telecommunication satellites, allows drastic harness simplifications compared to traditional point to point protocol.

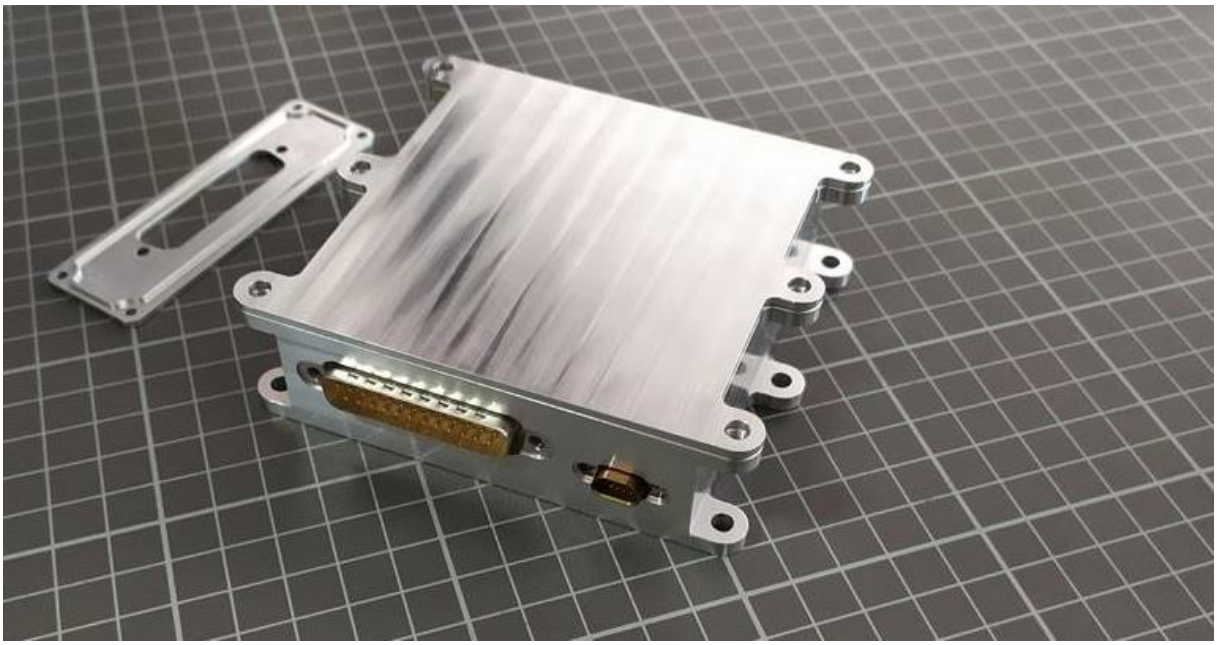

Figure 5.2 – BOMO front panel with standard interfaces.

Considering the number of different functions to address, the choice has been made to develop specific BOMOs for every one of them.

5. 1. 1. 1 BOMO-C

The BOMO-C is dedicated to the Conditioning functions initially done by the PCDU and interfaces solar arrays with the primary power bus. Thus in addition to the standard common interfaces, it disposes of a specific power connection to the PV side. Based on DET performed by MOSFETs, a single BOMO-C allows to shunt, or connect in parallel to the power bus up to 7 PV sections independently. An extra switch, present on the output power line, allows to connect or passivate the whole module.

Figure 5.3 – Stacked BOMO-Cs rear panel with specific interfaces.

As it can be seen on the picture above, in order to address more PV sections and give scalability to the system or to implement redundancy, it is possible to stack the units together.

5. 1. 1. 2 BOMO-D

The BOMO-D is dedicated to the Distribution of the electrical power to the equipment of the satellite and thus interfaces them to the power bus. The distribution function is realized by 7 LCL. The specific part of the module is dedicated to safety and equipment's protection and not to the control of the supply, managed by the OBC with the equipment itself. Nevertheless, measurements processed by the base brick can be used for the overall control of the EPS which makes of it a key unit to give the observability of the system to the OBC.

5. 1. 1. 3 BOMO-PSP

The BOMO-PSP is initially dedicated to the detection of the Pyro actuators and of the Separation strap to connect the main battery to the power bus during the launch of the spacecraft. At the end of life of the satellite, it also handles the Passivation of the satellite. Electrically, it is mainly composed of a switch between the two sides of the module. Thus, it can also be used on the different branches of the power harness to (re)configure the global harness architecture during the satellite's operation life to redirect the power flux.

Other types of BOMO are under development, their possible applications even going beyond the scope of the EPS. The BOMO-M or the BOMO-I can be cited, respectively dedicated to Motor drive and I/O management applications.

The one already developed and presented above allows to implement a modular NRB architecture as shown in Figure 5.4 and presented in [155]. In order to fully replace the former PCDU, it has been evaluated that16 BOMO are necessary for a satellite of approximatively 300W [156].

As it can be seen on the architecture overview, reliability of the system is enhanced by integrating a partial redundancy which are not concentrated in a unique location anymore. A cold redundancy – one entity is operating and the others are powered off – of each BOMO is also implemented at equipment level in the same manner of a conventional architecture. Compared to the ISS EPS, no routing module such as the DCSU is needed as each BOMO is specifically designed to be propagation failure free on this external interface.

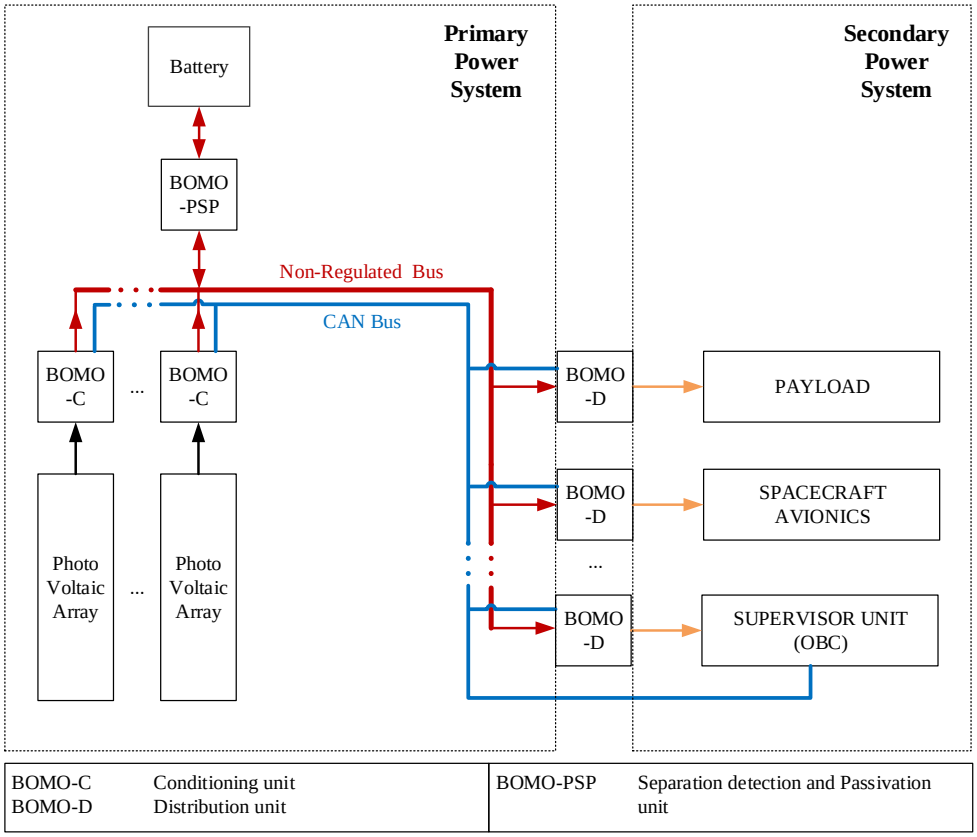

Figure 5.4 - NRB modular architecture based on BOMO [156].

All the variants are space qualified which makes them good candidates to fly. The Morpheus program, a multi-mission platform under development at Thales Alenia Space, based on the aforementioned architecture could be the first opportunity to make the BOMOs fly in the next few years. In this architecture, the BOMOs are used in order to make it scalable: the architecture would be the same from one mission to another but the number of the different BOMOs could evolve easily. However, in this case, this scalability only applies to PV and loads. The battery will have to be resized specifically for each mission.

The BOMOs, which are designed to be autonomous and able to be used as a unitary piece of equipment, are compatible with any type of power bus configuration, battery driven as presented above or regulated as in the architecture proposed in the present work. The possibility to use the BOMO-C in the demonstrator was therefore in the same time an opportunity to use space qualified equipment as conditioning units and to validate its proper functioning in such a configuration.

5. 1. 2 The MOBI: the last step to a fully-regulated modular architecture

As mentioned earlier, the design of the MOBI – MOdule Batterie Intelligent meaning smart battery module in French – which started in 2018, at the very beginning of the present works and which has been done jointly with Airbus Defence and Space, consisted of an important collaborative work since it aimed to design the main element of the proposed architecture.

As described in [157], the module is composed of a battery, a bidirectional converter and an adapted version of the base brick present in the BOMO to be compatible with it in term of communication and power interface. Its overall architecture is presented in Figure 5.5 and detailed below.

5. 1. 2. 1 Li-ion battery pack

The battery is the central component of the MOBI. One of the major objectives is to be able to connect several batteries to the same primary bus, so as to be able to easily modulate the storage capacity of a system while keeping costs relatively low. COTS cells in 18650 format were chosen, and two module sizes were proposed: a $12S2P$ module – i.e. around $270Wh$ – and a $12S10P$ – i.e. around $1.35kWh$ – in order to demonstrate their interoperability.

The idea behind proposing two module sizes is to be able to meet as close as possible the different needs of each mission by varying the combinations. It would also be possible to vary the cells technology used from one module to another. It would then be possible to obtain power or energy modules, depending on the mission profile. This has however not been tested in the present study.

In order to facilitate the storage of the module but also to secure its manipulation during investigations and tests, the battery can be disconnected to the rest of the module thanks to a power strap. This could be a significant benefit during battery integration at the Assembly Integration and Tests (AIT) phases.

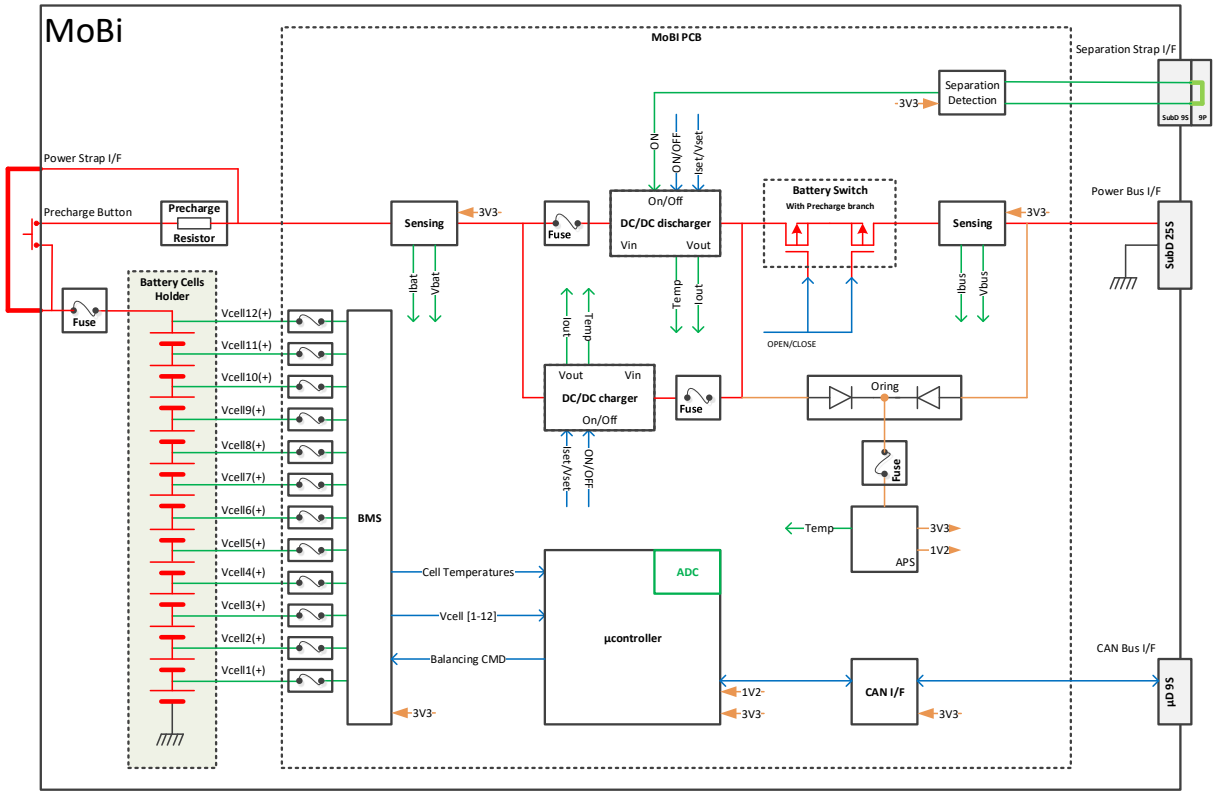

Figure 5.5 – MOBI architecture (courtesy of Airbus Defence & Space).

5. 1. 2. 2 Battery Management Systems

The first function and also the most basic one is the Battery Management System (BMS) which is implemented thanks to a dedicated Integrated Circuit (IC) which performs cells balancing. It also enables to acquire individual cells voltage and temperature which gives a good observability of the battery state during operation. The cell balancing method is a conventional passive balancing: on the reception of a command signal, the cells are successively discharged to align with the least charged one.

5. 1. 2. 3 DC/DC Power conversion

The bidirectional DC/DC power conversion is achieved by two top to tail unidirectional COTS converters which can be assimilated to a non-inverting buck-boost converter as presented in Chapter 2.

The charge and discharge current of each module can be controlled independently on request which corresponds to a battery driven mode also called selfish mode. This could allow to perform state-of-the-art CC/CV charging but also to implement advanced functions such as embedded impedance spectroscopy methods. Indeed, an AC signal can be added to the charge or discharge currents. More conventionnally, it makes also possible to perform full charge / discharge cycles in order to update the estimations of the module's capacity and other estimators while the other modules continue to provide the required energy reserve and regulate the primary bus – bus driven mode.

The converters also integrate fast voltage regulation loops which only require reference values as input signals to operate. This enables to regulate their respective output voltage corresponding to the bus voltage for the discharger and the battery voltage for the charger. In order to operate as a fully bidirectional conversion stage, able to regulate the bus voltage also during charge – corresponding to the generous mode – an additional voltage regulation loop is implemented and uses the charger current reference signal as command signal.

5. 1. 2. 4 Embedded microcontroller

The generation of these different control signals as well as the management of all aforementionned operating modes are handled by an embedded microcontroller. Called Master BMS (MBMS) it also realizes the following functions.

a) Telemetry acquisition

Its numerous ADC interfaces allow to acquire an important number of signals:

- Battery current and voltage
- Bus current and voltage
- PCB temperatures

A serial link allows to get all BMS acquisitions such as cells individual temperature and voltage. This provides an enhanced observability of the battery and enables to take the most of it.

b) Battery monitoring and protection

The access to the set of data mentioned above allows to generate more precise estimators such as SOC and SOH. Based on this, a Fault Detection, Isolation and Recovery (FDIR) policy has been determined and integrated to the module. For each monitored variable, three level of alert have been defined, from nominal condition to critical alert. For each level of alert, a set of actions is autonomously launched, up

to complete isolation of the module. This allows to react as quickly as possible in the event of a component failure, and to prevent the faults propagation. However, before reaching this level of criticality, supervisory units are alerted via dedicated messages.

c) Data Handling management

To do so, a CAN bus interface allows the communication with supervisory controllers such as the OBC. This function is the milestone of the interfaces standardization of the battery modules and can be presented as the DHS counterpart to the power converter for the EPS.

Thanks to it, the OBC is always aware of the state of the battery thanks to housekeeping frames concentrating the most relevant and useful data such as the battery voltage or current. On demand, it can also query detailed data and thus access to the whole set of variable acquired by the module.

This function alone represents a major step forward, not only in terms of the new functionalities it makes possible at the scale of the battery, but also by significantly simplifying all the design in the early stages of development at system level.

d) Start-up management

Finally, a separation strap interface allows to maintain the battery OFF before and during launch and to be automatically set in discharge mode at launcher separation to switch ON the spacecraft according to the following logic:

At the separation strap disconnection, the MOBI is put in master mode. In this state, the battery feeds the power bus – discharger ON, charger OFF and main switch closed. After a fixed time, the MOBI switches to slave mode. Consequently, the On Board Computer must use this time slot to send the commands in order to maintain the MOBI in the desired state.

If the separation strap stays connected, the MOBI also stays in slave mode. In this state, no power is provided by the battery (discharger and charger are OFF, main switch is open). The electronics is supplied the main power bus and after the master switch on, it can be commanded via the CAN interface.

Figure 5.6 – MOBI prototypes with power and data interfaces visible on the front face.

The initial hardware design phase was completed at the end of 2020 with the delivery to CNES of the 3 prototypes shown in the picture above. Software development continued until November 2021 in co-

engineering thanks to successive iterations in order to implement and improve the regulation and droop control functions of the system's primary control as defined by the proposed control strategy.

5. 2 Demonstrator setup

In order to tune and validate these control laws and then to be able to obtain experimental results with those obtained by simulation, the test bed presented in introduction of the chapter has been set up. The objective of this section is therefore to give an overview of the equipment used in this demonstrator, named Octobus and with which the results presented below have been obtained.

5. 2. 1 Electronic loads

The different loads of the system are emulated by two electronic loads – or dynamic loads (DL) – which are able to operate either in Constant Resistive (CR), Constant Current (CC) and Constant Power (CP) modes and whose main features are summarized in the table below.

Table 5.1 – Electronic Loads main features.

Brand	Kikusui
Model	PLZ334W
Voltage operating range (V)	1,5 to 150
Maximum power (W)	330
Maximum current (A)	66
Operating modes	CR, CC, CP
Communication standards for remote control	GPIB, RS232C, USB

Each load is able to handle the maximum power load defined for the study case of 230W which enable to test different configurations with two CP at different location of the system or with a combination of CP and CR loads.

5. 2. 2 Solar Array Simulator

Solar Array Simulators (SAS) are used to emulate the electrical behavior of actual PV panels. Indeed, solar generators are very specific equipment for space systems and it was difficult and restrictive to consider using real generators.

In the maximum configuration of the demonstrator, it can manage 5 SAS of 2 channels each in order to emulate the 10 PV sections defined for the use case. Two different references are used and their main features are given in the table below.

Table 5.2 – Solar array simulators main features.

Brand	Keysight Technologies	
Model	E4361A	E4362A
Voltage operating range (V)	0 to 65	0 to 130
Maximum power (W)	510	600
Maximum current (A)	8.5	5
Operating modes	Fixed, Table, SAS	
Communication standards for remote control	USB, GPIB, LAN (Ethernet)	

Compared to conventional DC power supply, SAS have a very low output capacitance that simulates the high speed constant current characteristics. The fixed operating mode corresponds to a rectangular I-V characteristic of a standard power supply. The table mode allows to specify the I-V curve through a table of up to 4000 points. This enable to set very accurate curves while assuring a fast computation of the response since the points are processed offline. Finally, the SAS mode generates the I-V characteristic curve thanks to an exponential model of solar array based on the four characteristic parameters: the short circuit current (I_{SC}), the open circuit voltage (V_{OC}) and the maximum power point ($V_{MP}; I_{MP}$).

Considering that the characteristic curve is subject to online changes during a test session – to emulate the variation of solar irradiance and temperature during an orbit for instance – and in order to limit the amount of data to be sent – and to generate – the SAS mode is used.

The electronic loads and the SAS are connected to the central control unit via USB through a USB hub. This enable to control these units remotely and in a synchronized way since the power consumption is intrinsically related to the orbit phase – day or eclipse – as it dictates the thermal variations and the imagery shooting time for example.

5. 2. 3 Power harness emulator

In the same approach as for the stability study in the previous chapter, the need to be able to emulate any type of distribution network resulted in the development with ADS of the BODI – for BOîtier de DIstribution meaning distribution box in French – based on the conductance matrix model.

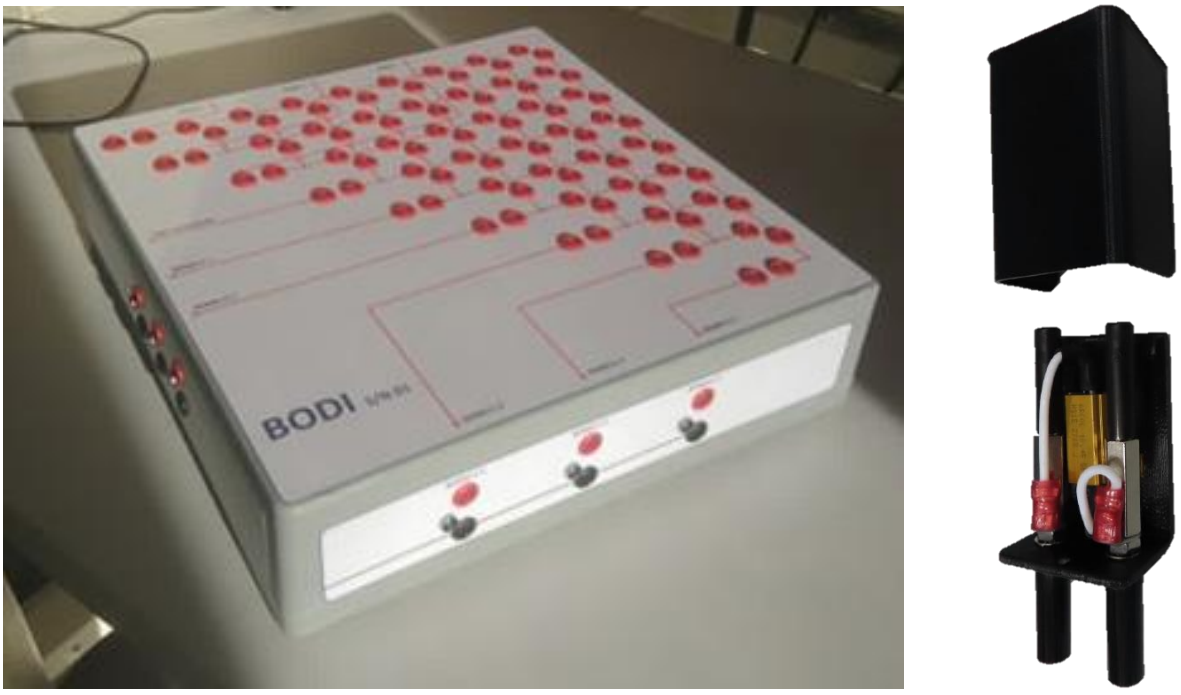

Figure 5.7 – Distribution box (BODI) and a resistive plug.

The upper face of the module is a 9 by 9 physical implementation of the nodal admittance matrix. It enables to interconnect up to 9 units – 3 BOMO-C, 3 MOBI, 2 DL, 1 spare – by plugging resistive elements to characterize the distribution lines. The value of the equivalent resistor of a link R_l is the serial association of the resistances of the connectors, R_{con}, at both end of the link and the equivalent resistance of the wire, R_{wire}.

The BODI is also particularly practical merely used as a high power breakout box in order to instrument the different signals to be monitored.

5. 2. 4 CAN bus

In order to interconnect all devices equipped with a CAN interface, a 'bus-shaped' type harness is put in place - in contrast to chain links or star distribution. The CAN bus being renowned for its robustness to disturbances and the harness length being limited to approximately $2m$, a ribbon cable and D-Sub 9 pins connectors with clips are used to create the main bus. A connector at each end allows connection of 120Ω terminating resistors put in plugs. Connectors can be easily added to any location on the cable by adding a clipped connector. This allows to place the different required interface as close as possible to each piece of equipment and connect them via stubs – short adapters between micro D-Sub and D-Sub connectors – which must not exceed 0.3m for operation at $1Mbit.s^{-1}$.

Figure 5.8 – USB to CAN adapter.

Finally, a Korlan USB2CAN adapter is used to connect all SUT equipment to the test conduit computer which will also have the role of emulating the on-board computer.

5. 2. 5 Control & Protections

Indeed, in order to simplify the control and observation of the state of the demonstrator, the supervision and test management functions are performed by a single computer. This makes it easier to drive the demonstrator and to integrate error and safety management using all the available elements. It is thus possible to define 4 main functions that the supervision unit must support:

1. HMI management
2. Emulation of the OBC and management of communications on the CAN bus
3. Execution of test conduct and management of USB communications
4. Emergency stop management and data monitoring

These functionalities were implemented during two internships in ICARES, a python multi-threaded supervision software, providing a general overview of the state of each component and allowing to easily control the demonstrator by launching pre-defined test scripts.

Among the many possibilities offered by the software, it is as possible to merely configure power profiles to send to DL and SAS in a planned manner as to execute completely automated test sequences for which all data are monitored and saved thus allowing full exploitation of the test bench.

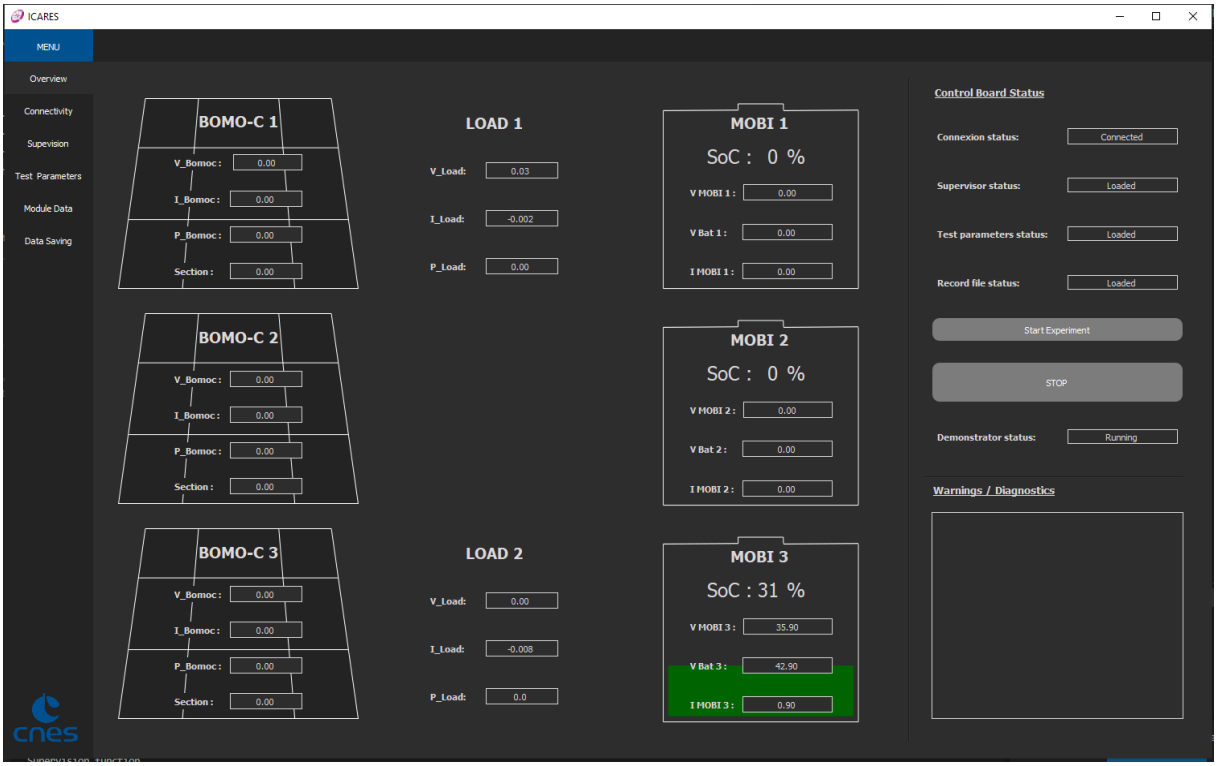

Figure 5.9 – ICARES supervision software main window.

An important aspect implemented by ICARES is the taking into account of the alerts that MOBIs can send. Indeed, working on systems using batteries involves implementing certain safety measures. So as soon as an alarm is triggered on a MOBI – due to excessive temperatures or dangerous voltage levels for example – the experimenter is immediately notified by a pop-up window.

5. 2. 6 Demonstrator overview

Thus all of the elements presented above have been successively integrated into the test bench in CNES electrical laboratory at the Toulouse space center, which resulted in the setup presented in Figure 5.10.

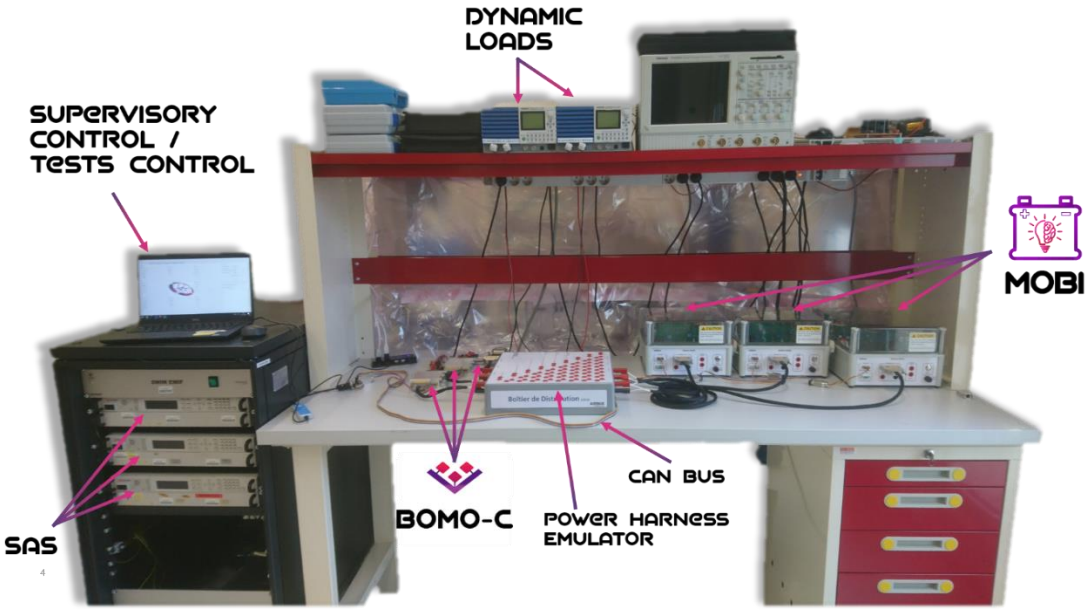

Figure 5.10 – The Octobus demonstrator.

It should be noted that the simple implementation of this demonstrator made it possible to verify a certain number of the advantages expected for this type of architecture. One of them is the simplification of routing which is perfectly visible in the photo below.

At the power harness level, this is achieved thanks to the distribution of the primary power bus while at the DHS harness level, the huge observable difference compared to conventional systems is achieved thanks to the integration of the CAN bus replacing all discrete signals usually used.

5. 3 Experimental results

The implementation of the demonstrator has enabled this study to meet two objectives, which are detailed in this third part of the chapter.

The first and most important is to validate the operation of the modules in an environment representative of a real system, while implementing the proposed primary control. This means checking that the stability of the primary bus voltage is guaranteed and that all the distributed components of the primary control, in particular current sharing, are functional.

The second objective, which follows directly from the observations made to achieve the first, is to identify the obstacles and other practical constraints to the implementation of the complete system in order to be able to define the major points of attention for the development of future systems and in particular for the next steps towards the specialization of a MOBI.

The results presented below propose a step-by-step validation of the various points studied, starting with the unitary validation of functions.

5. 3. 1 Droop control unitary implementation

The first element to be validated prior to the module parallel connection is that, on each of them, the primary functions present nominal performances.

To do this, the operating ranges of the various modules were scanned in discharge using a DL and in load using an SAS. Figure 5.11 and Figure 5.12 respectively show the results of these two tests for the MOBI 3 – $12S10P$ – for different droop resistance values. In order to obtain these characteristics representing the steady-state performance of the modules, the signals are filtered at $100Hz$.

For the discharge characteristic, which is obtained by varying the power of a DL in CP mode, the maximum droop coefficient value tested is set by considering the maximum power defined by the use case – 230 watts for a bus regulated at 28V – with a slight margin to take account of the additional line resistors. Although the power rises to this limit value, no instability is observed, since the module's current is limited to 9.5 A before reaching it.

It can also be seen that, as the droop coefficient increases, oscillation around the ideal characteristic appears to be increasing, although this does not appear to be a problem at this stage.

With regard to the load characteristic, as the measurements were carried out by varying a SAS characteristic with a positive characteristic impedance, no particular limit was taken into account for the tested R_D values. Thanks to the wide range covered, it is therefore possible to observe two characteristic curves at the operating limits.

The first, plotted in red, corresponds to the module's battery charge current limitation, which translates into a constant power characteristic from a bus point of view: in load limitation, the module behaves like a PLC. The behavior described in Chapter 3 when characterizing the load is then observed: for all the characteristics shown, when this limitation is reached, the voltage rises to stabilize at the point of intersection with the second visible characteristic curve. This one corresponds to the SAS characteristic at full power.

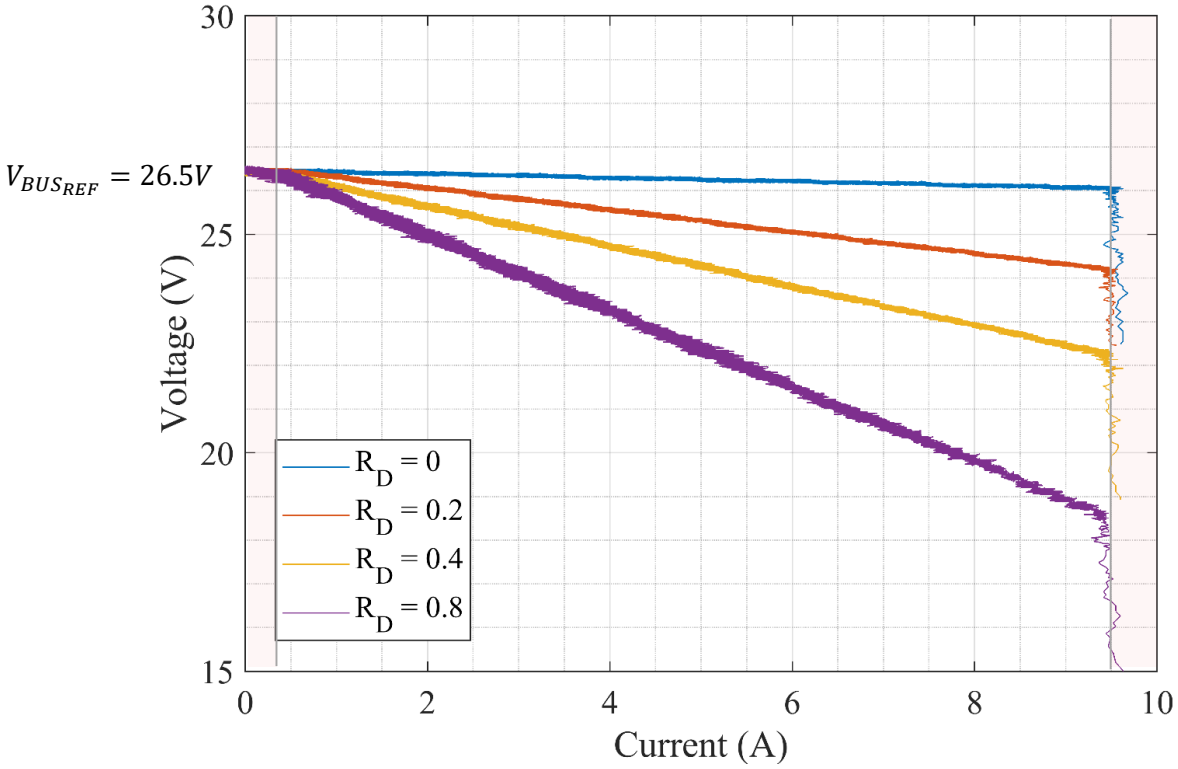

Figure 5.11 – Experimental large-signal droop characteristics of one MOBI during discharge.

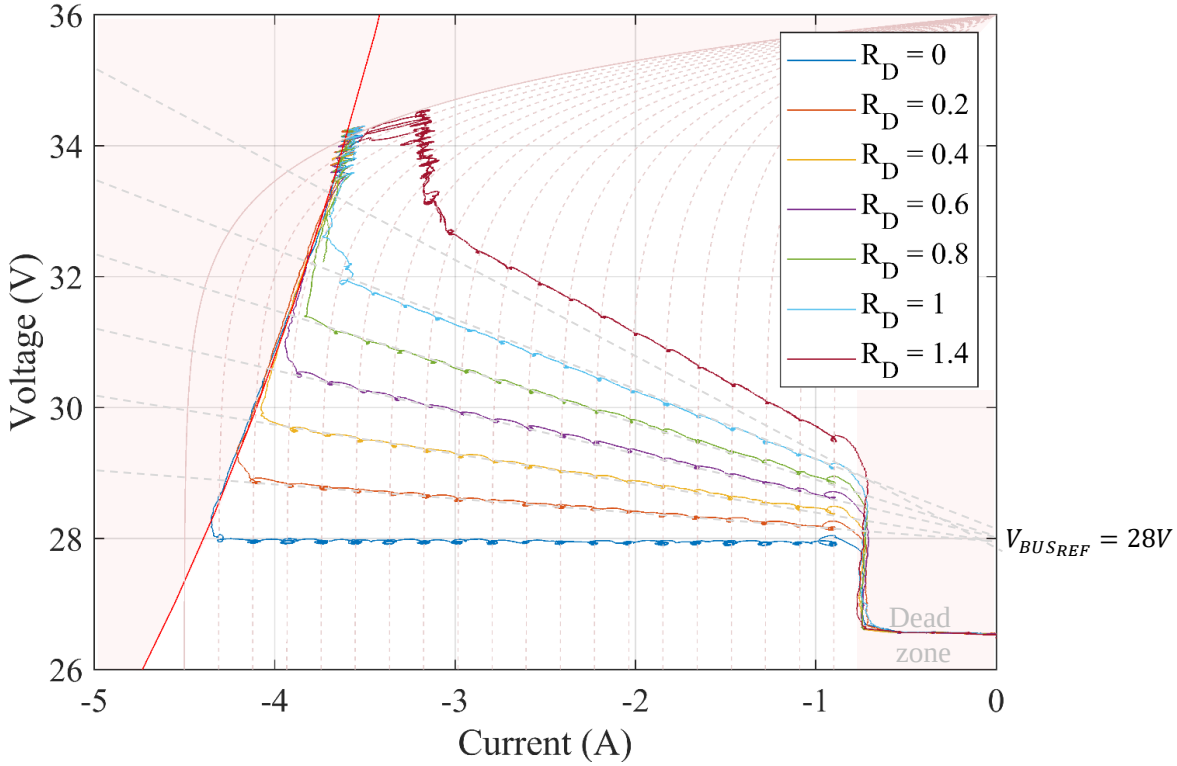

Figure 5.12 – Experimental large-signal droop characteristics of one MOBI during charge.

It is also close to this characteristic that a certain distortion of the droop control characteristics can be observed for high coefficient values. More generally, it seems that as soon as it passes to the voltage source region of the PV characteristic, the voltage is imposed by the PV. Although this has not been validated with certainty, it is assumed that this behavior is exacerbated by the fact that SASs are used. Indeed, as has been mentioned, although SASs have outputs with the characteristics of current sources like actual PVs, they are still switching power supplies which, in this type of circumstance, can conflict with and disrupt the operation of other equipment present. However, as this only happens in fairly specific configurations, the phenomenon is not considered to be problematic. Indeed, BOMO-Cs are meant to be operated to the current source region of the PV characteristic.

Another point which can be observed is that throughout the characteristic curve in charge, points are visible at regular intervals. These points correspond to the stabilization points with the SAS characteristics set successively to sweep the operating range and show that the voltage regulation loop during charging is slower than that during discharging, where these steps are not visible. This is because the bus voltage regulation in battery charge configuration is not natively present in the converters used, unlike that in discharge configuration. To add it, it has been implemented inside the MOBI microcontroller and is therefore necessarily slower.

Although this may seem problematic, given that the load during the battery charge phase is generally characterized by a positive impedance, the system is generally quite stable in this configuration. In addition, this difference in dynamics made it easier to define a strategy for the transition from charge to discharge.

This transition phase represents a twofold challenge. The first, which is specific to the converter configuration implemented in the MOBI, is that close to no load, the charge and discharge converters could interfere. To a certain extent, droop control reduces this risk because, by its nature, it manages the sharing of currents between parallel units. It is with this aim in mind that an offset noted $\Delta V_{BUS_{REF}}$ is applied between charge and discharge voltage set points as shown in Figure 5.13.

However, the second challenge makes this insufficient. Indeed, in order to control the system as well as possible and to be able to manage the charging and discharging behaviors independently, the coefficient applied in these two modes is not the same. In addition to the offset on the voltage reference, and to avoid oscillations that could be problematic in low-load operation, a dead zone is set up, for which no coefficient is applied. In this way, combined with the fact that the discharger's bus voltage regulation is faster than that of the charger and therefore that the former takes control of the regulation in the dead zone, the system is able to switch smoothly from one operation to the other autonomously, as shown in Figure 5.13.

It is important to note that the impact of setting up a dead zone is very small, as only prolonged operation at very low currents could induce sufficient imbalance to unbalance the batteries SOC.

In conclusion, based on the observations made above, and in purely qualitative terms, the large-signal characteristics obtained seem to correspond to expectations and make it possible to envisage tests with several modules.

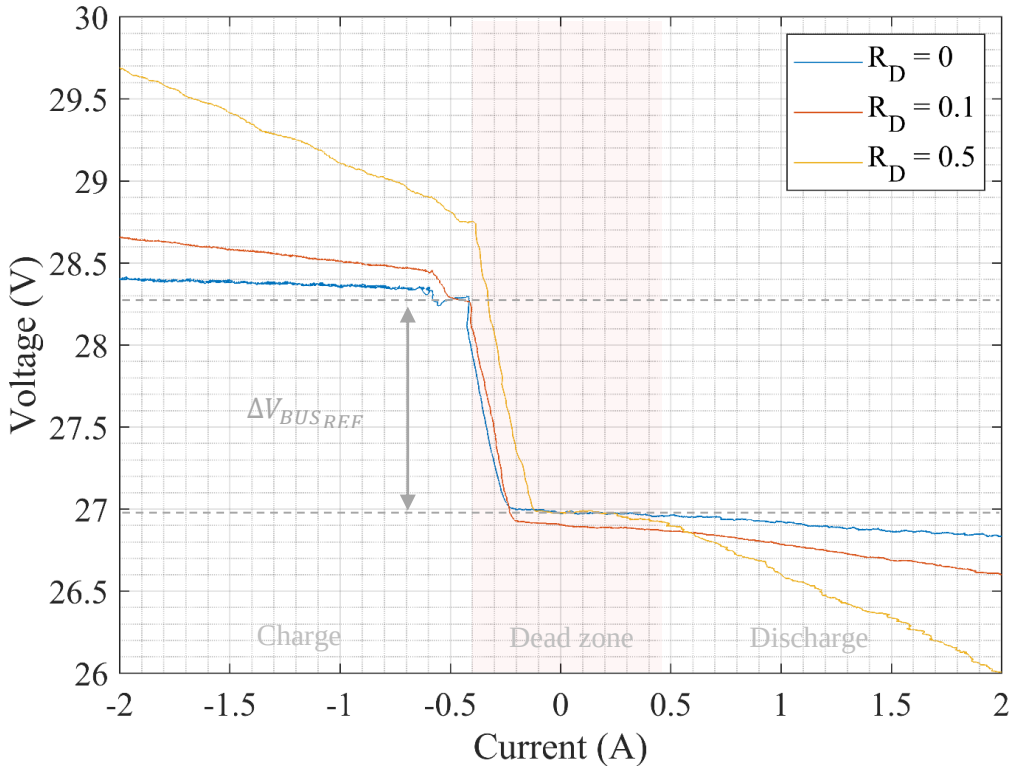

Figure 5.13 – Experimental large-signal droop characteristics of one MOBI at transition.

5. 3. 2 Modules parallel operation

For simplicity purpose, and having verified that the principle presented were fully extendable to more complex systems, the following only focuses on the CS between two MOBIs – MOBI2, 12S2P, and MOBI3 12S10P.

5. 3. 2. 1 Primary bus voltage regulation

The first aspect to verify is the stability of the voltage regulation with several modules in parallel. In order to do so, the power profile presented in Figure 5.14 is applied to two MOBIs in bus regulation droop mode. The resulting voltage variations are shown in Figure 5.15 while considering R_D values of 0.1 and 0.5 – equal for both MOBI.

As a result, it appears that the bus voltage shows good stability performance without taking into account the variations induced by the droop control.

It is possible to observe the impact of the variation in R_D on the performance of the voltage regulation in accordance with the results of the stability study carried out in the previous chapter.

Indeed, in the zoomed view of the load impact at $22.3s$, it can be seen that the system is slower and more damped at $R_D = 0.5$ than at $R_D = 0.1$.

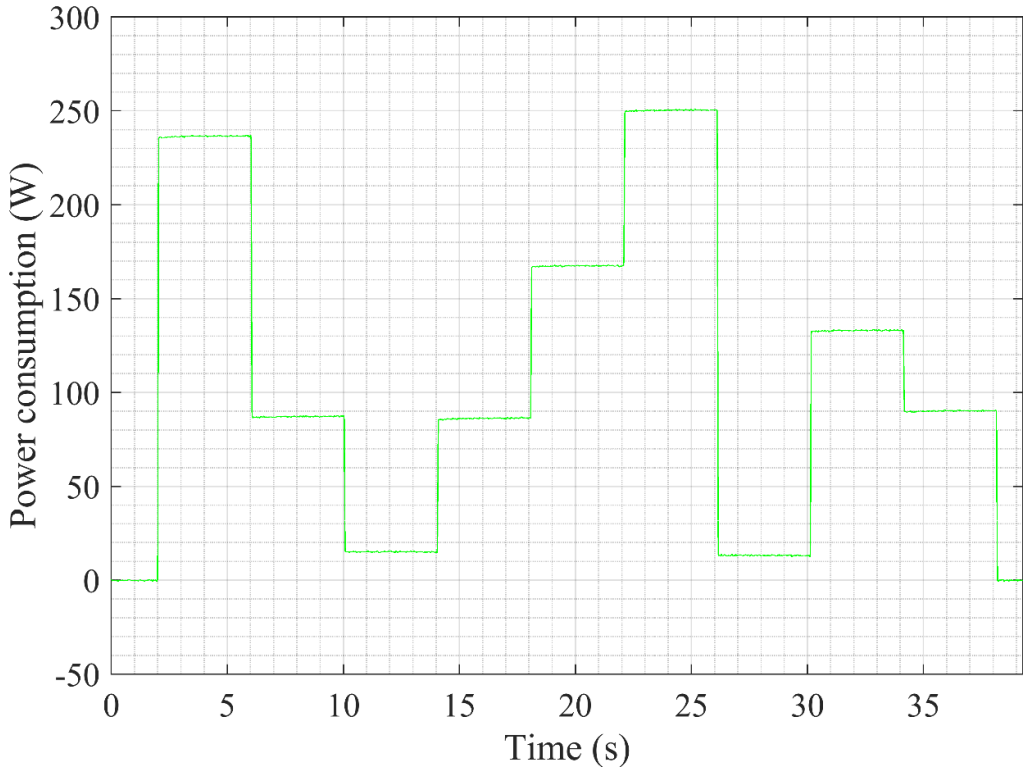

Figure 5.14 – Experimental power consumption profile.

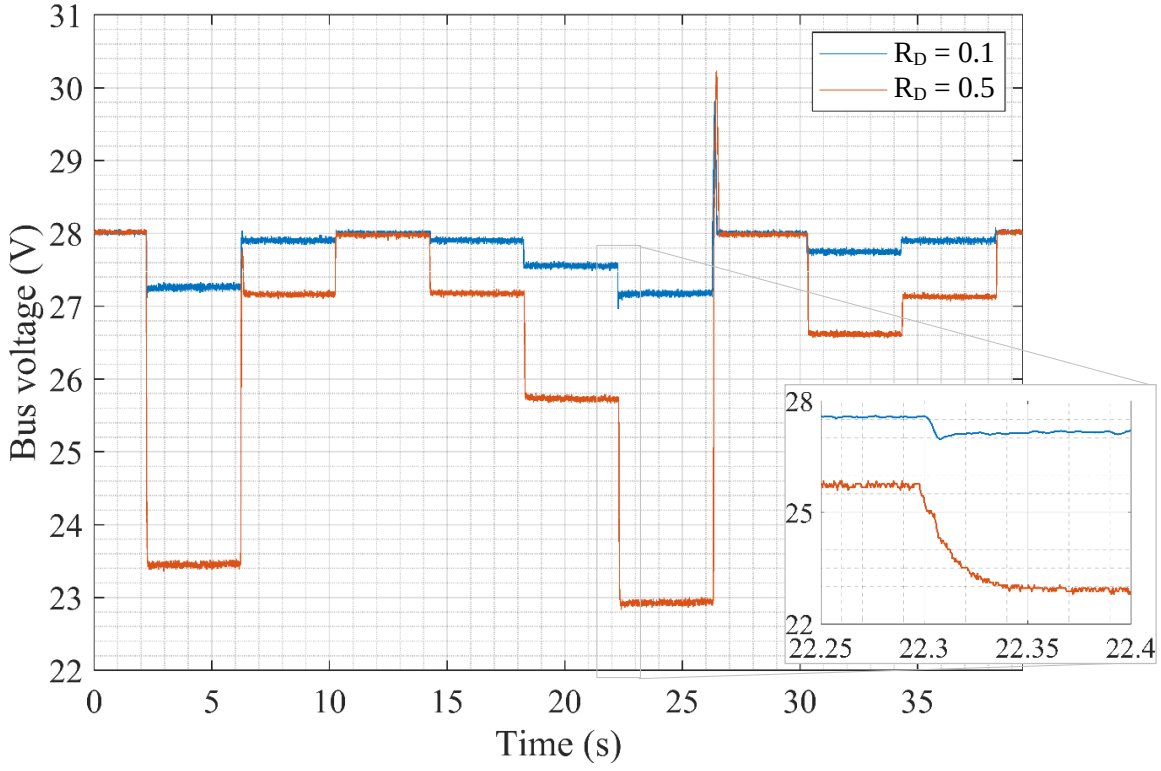

Figure 5.15 – Experimental bus voltage variations in function of droop coefficient.

For the reasons exposed later in 5. 3. 3. 1 , the curves presented here correspond to the moving average values of the currents observed.

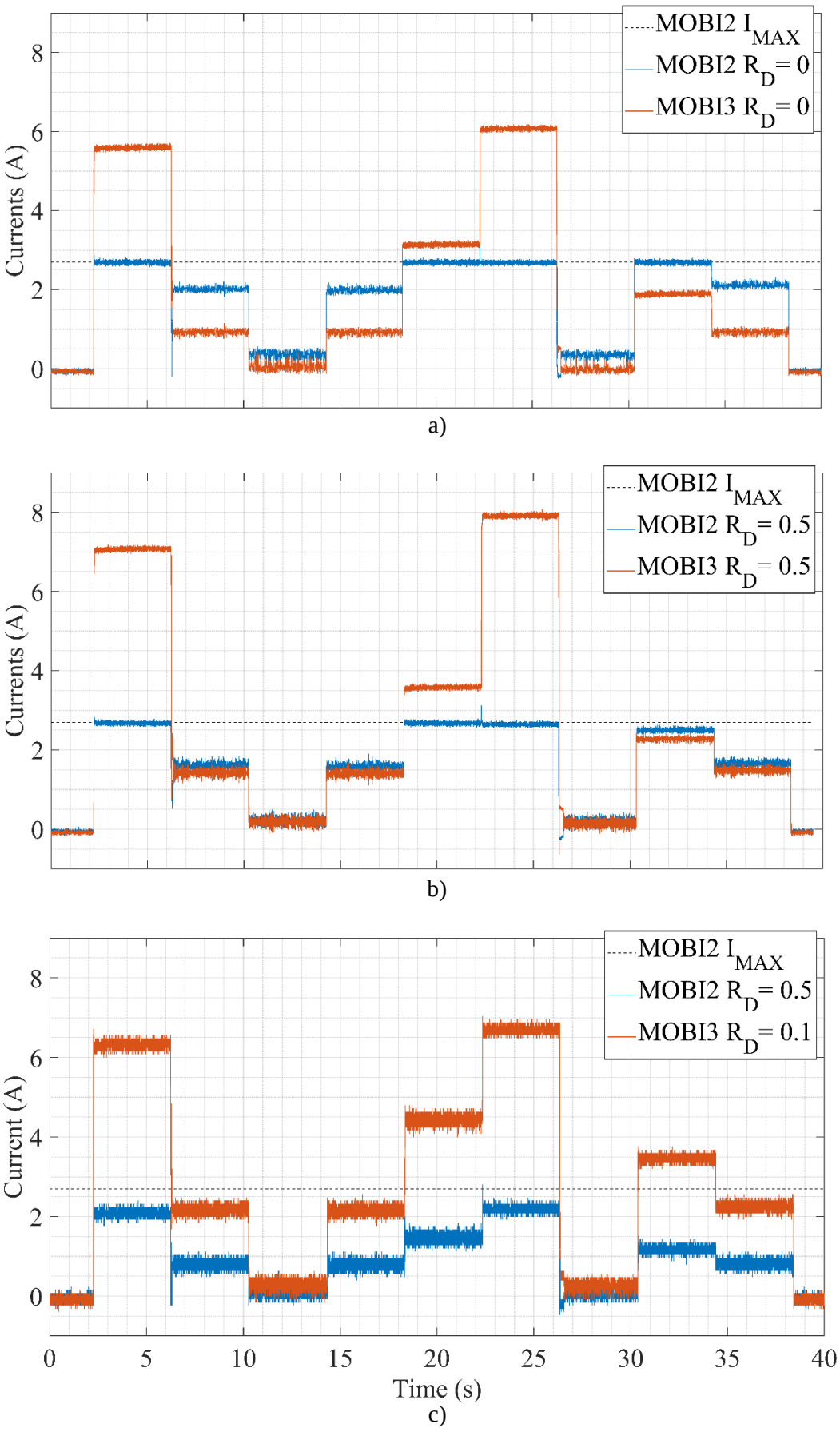

Figure 5.16 – Experimental results of 2 parallel MOBIs for different droop coefficients.

5. 3. 2. 2 Current sharing

Figure 5.16 gives the MOBI currents in response of the power profile defined above, considering different droop coefficient configurations.

As it can be seen on inset a), without any droop control – $R_D = 0$ – the CS balance is only imposed by the line impedances. In order to show this, unequal impedances are intentionally used in the harness: MOBI 2 and MOBI 3 are respectively connected to the primary power bus via harnesses of $35m\Omega$ and $70m\Omega$ of characteristic impedance.

It can be observed that, when no module is at its current limitation, MOBI 2 supplies twice as much current as MOBI 3. Since MOBI 3 is five times bigger, a $1:5$ ratio should be applied reversely instead. It can also be noted that when MOBI 2 reaches its current limit – deliberately set at a relatively low current – MOBI 3 supplies all the remaining current. In this case, only MOBI 3 regulates the bus voltage which decreases the stability margins of the overall system.

Inset b) shows the results in the same configuration but with equivalent droop coefficients on both modules. It can then be observed that below MOBI 2 current limit, the currents of each module can be considered as balanced.

Finally, inset c) shows the results when different values of R_D are parametrized in MOBI 2 and 3 in order to be consistent with their respective size as mentioned above. It can be observed that the proportion is indeed reversed in comparison to inset a) which validates the correct operation of the method even if the ratio does not exactly coincide with the expected one.

This can be explained by the neighboring of the R_D values and the line impedances introduced above and illustrates the limitation of the droop control in term of precision. The CS ratio can indeed be expressed as follows:

$$\frac{I_{MOBI3}}{I_{MOBI2}} = \frac{R_{MOBI2}}{R_{MOBI3}} = \frac{R_{D2} + 0.035}{R_{D3} + 0.07} \approx 3.15 \qquad 5.1$$

Finally, it should be noted that in this last case, compared to the others, the MOBI 2 never reaches current saturation. However, it can be remarked that it was in this configuration that the difference in performance has been seen on the voltage curves. This illustrates the need to take these limitations into account when assigning the different values of droop coefficients.

5. 3. 2. 3 Current and power limits

To do this, as was done for the modules individually, let's observe the equivalent large-signal characteristics obtained as a function of the droop coefficients and limitations of each module.

Figure 5.17 shows the individual large-signal characteristics of each module for load and unload configurations, considering different configurations.

For the first three cases, it can be observed that either the individual characteristics cross when one of the two modules reaches its power limit, or the characteristics are coincident until a limit is reached. These graphical observations reflect the fact that the module with the lowest current or power limitation – for discharge and load respectively – is also the one with the lowest R_D value.

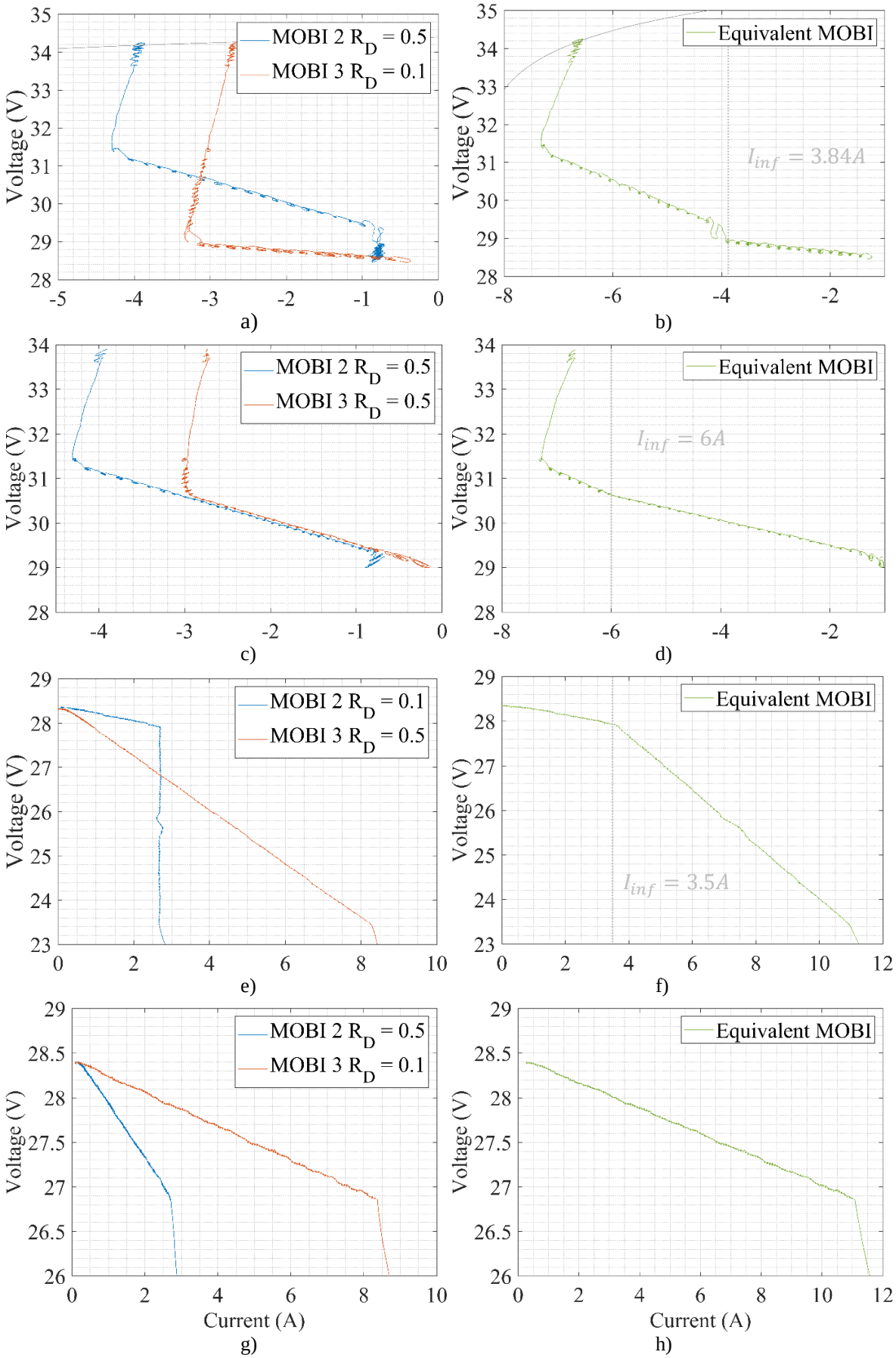

Figure 5.17 – Experimental equivalent large-signal droop characteristics of two parallel operating MOBIs for different configurations.

This induces an inflection in the equivalent characteristic, corresponding to the transition from one equivalent droop coefficient to another.

This transition occurs when the equivalent load current reaches the following value:

$$I_{inf} = I_{MOBI2} + I_{MOBI3} = \frac{V_{BUS_{REF_3}} - V_{BUS_{REF_2}}}{R_{D_3}} + \frac{R_{D_2} + R_{D_3}}{R_{D_3}} I_{MOBI2_{MAX}} \quad 5.2$$

While in the present case, the equivalent characteristic is still easy to define, it becomes much more complex when the number of MOBI increases.

Furthermore, in general, it is not desirable to accumulate the number of modules passing under limitation because, as it has been determined earlier, this reduces the margins of stability of the overall system.

As shown in inset g) and f), it is possible to keep the two modules outside their limit over the entire power range of the system. This is ideally achieved when the inverse ratio to the current limits is applied to the droop coefficients.

Assuming, as in the present case, that the respective batteries in each module are of the same type, their maximum charge and discharge rates, which therefore define these limitations, are proportional to the size of the battery. It is therefore consistent to aim for this configuration to be respected so that all the batteries charge and discharge at the same rate from the point of view of their SOC.

This last observation lays the foundations for the conclusions that can be drawn from the experiments carried out on the demonstrator and constitutes an element to be taken into account for the development of secondary and tertiary control strategies. These are based directly on the intrinsic characteristics of droop control and the limitations imposed by higher-level control constraints – battery power management in this case. In the same way, other factors that have a direct impact on primary control performance can be identified.

5. 3. 3 Performance factors

5. 3. 3. 1 Droop voltage reference accuracy

The measurements presented in Figure 5.18 were done during one of the first parallel connection of two droop controlled MOBIs. In response of the power profile which was sent to the DL given in inset a and considering $R_{D_1} = R_{D_2} = 0.2$, $V_{BUS_{REF}} = 28V$ and $\Delta V_{BUS_{REF}} = 1V$, inset b and c respectively show the bus voltage and modules output currents.

The first observation is that large oscillations in the MOBI output currents are visible. However, these disturbances, with an amplitude of around 3A, do not seem to affect the voltage regulation, since the latter is stable and the voltage drops observed correspond to the expected theoretical performance as defined below:

$$V_{BUS_{MIN}} = V_{BUS_{REF}} - \Delta V_{BUS_{REF}} - R_{D_{SYS}} \cdot I_{LOAD_{MAX}} \approx 26V \quad 5.3$$

On the zoomed-in view of the MOBI currents, it can be seen that the oscillations of the two modules are in perfect phase opposition to each other around equilibrium values, which explains why, seen from the load, a constant current is observed and therefore the quality of the voltage regulation is preserved.

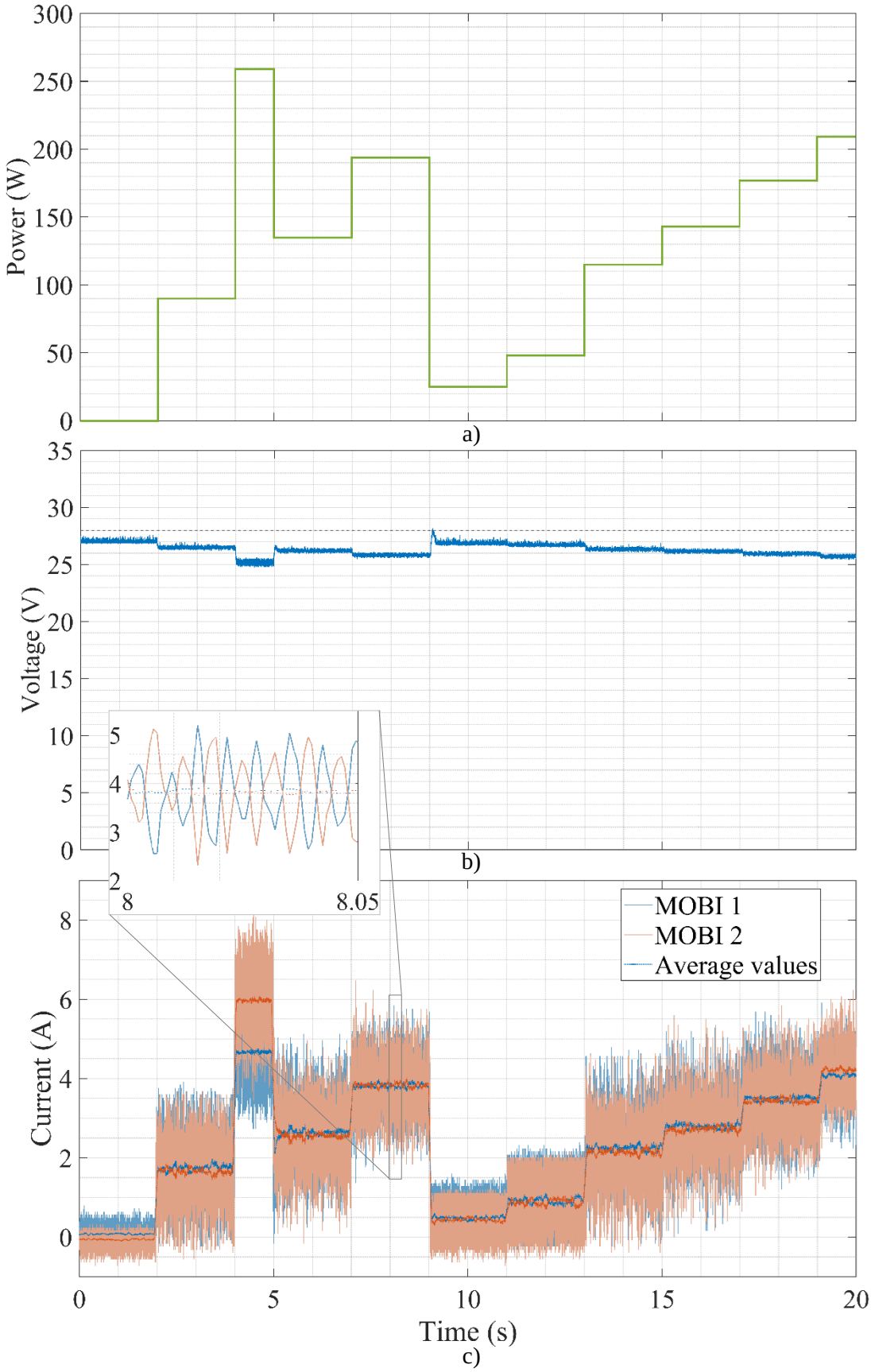

Figure 5.18 – Experimental results of 2 parallel MOBIs with primitive droop control implementation: dynamic load's power profile (a), bus voltage measurement (b), MOBI currents measurements (c).

Also, if only the average values of the currents are considered, it can be remarked that droop control does indeed balance them.

It turns out that the observed current oscillation is due to the precision of the voltage control signal generated by the MOBI microcontroller. Indeed, as shown in Figure 5.19, given that no current sharing method is natively implemented in the converters used, the implementation of droop control consisted of adding an external loop executed within the microcontroller. Although this digital implementation is very practical in terms of the flexibility it provides, it does require the addition of analogue-to-digital conversion stages and signal discretization.

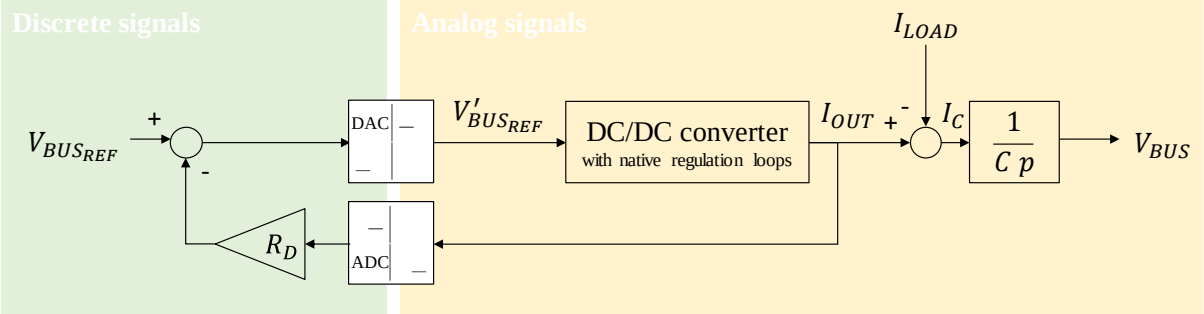

Figure 5.19 – MOBI droop control practical implementation

These two elements directly influence the quality of the current sharing balance. Indeed, it is important to consider that in an open loop, the balance of currents between two modules regulating two voltages $V'_{BUS_{REF_1}}$ and $V'_{BUS_{REF_2}}$ is governed by the following equation:

$$\Delta I = \frac{1}{R_s} \cdot \left(V'_{BUS_{REF_1}} - V'_{BUS_{REF_2}} \right) \qquad 5.4$$

with R_s the serial line resistance between the output of the modules and their point of interconnection, considered as equal for the two modules.

Note that the gain of this function is inversely proportional to the value of the line resistors, which implies that, as these are generally very low, a small variation in the voltage set point calculated by droop control will have a significant impact on current sharing. This is particularly the case if the resolution of the digital to analogue conversion employed is too low.

In this first case, with line resistances characterized at around $50m\Omega$ and a DAC resolution of $200mV$, the maximum observable current variation is estimated at $4A$. In practice, as the period of the droop control loop is shorter than the settling time of the voltage loop, the amplitude of the variations observed is smaller. There are therefore two possible solutions to limit this phenomenon: increase the resolution of the conversion and increase the speed of the droop control loop.

In the case of the MOBI, this made it possible to reduce the oscillations observed by a factor of 7. Although this still represents an oscillation of the order of $400mA$, which is not acceptable for a real application, it validates the explanation of the phenomenon and illustrates the importance of precision in the generation of the voltage reference signal by the droop control.

In order to overcome this hardware limitation, the values averaged over 10 sampling periods of the droop control loop have been systematically taken into account in the measurements. Since voltage stability is

still guaranteed and the average values seem to validate the overall operation of current sharing, this enabled the experimentations to continue.

5. 3. 3. 2 Parameters calibration

The last element identified as having a very significant impact on droop control performance is the dispersion or corruption of its parameters.

It has already been mentioned a number of times that the series line resistances of the modules add to the droop resistance in establishing the ratio of currents. Nevertheless, this limitation is well known and can be tackled by several ways. The first possibility to enhance the droop precision is to choose higher coefficients so line impedances become negligible in regard to it. It is also possible to integrate the line impedances to the droop coefficients definition thanks to a calibration.

This solution is also possible to solve the second issue considering the droop parameter dispersion: the differences from one module to another regarding their voltage reference signal. Indeed, for a given voltage set point, the actual regulated voltage at the output of the module can differ due to practical reasons such as hardware modifications inducing different gains on the voltage feedback for example.

To limit the impact of these phenomena, a calibration procedure can be applied at first switch on of the system as proposed in Figure 5.20 and following the steps detailed below. The sequence aims to identify the different elements which affect the droop performances by checking the current sharing in several configurations.

1) The First module is switched on in bus regulation mode, the loads being off. The second module turns on since the bus voltage rises –which explains the non-zero values of the currents on the figure – but stays in standby. R_{D_2} and R_{D_3} are set to 0.

2) The CPL is turned – 70 watts in the present case.

3) Keeping the droop resistors at 0, MOBI 3 is passed to bus regulation mode too. The resulting current sharing ratio is then the result of the serial resistances due to the distribution lines at the error of voltage reference.

4) Both droop coefficients are set to a relatively high value – 0.5 in this case. This configuration limits the impact of line resistances and a voltage reference offset can be determined. In the case presented, there seems to be no difference.

5) Both droop coefficients are set to a relatively law value – 0.1 in this case – in order to determine the line resistor amplitude combined with previous results.

6) and 7) aim to verify that the correct parameters have been identified by performing a rate inversion taking into account the identified bias. The calibration is successful if the inversion is symmetrical.

8) The calibration is terminated. MOBI 2 is put back in standby mode waiting for further commands from the supervisor.

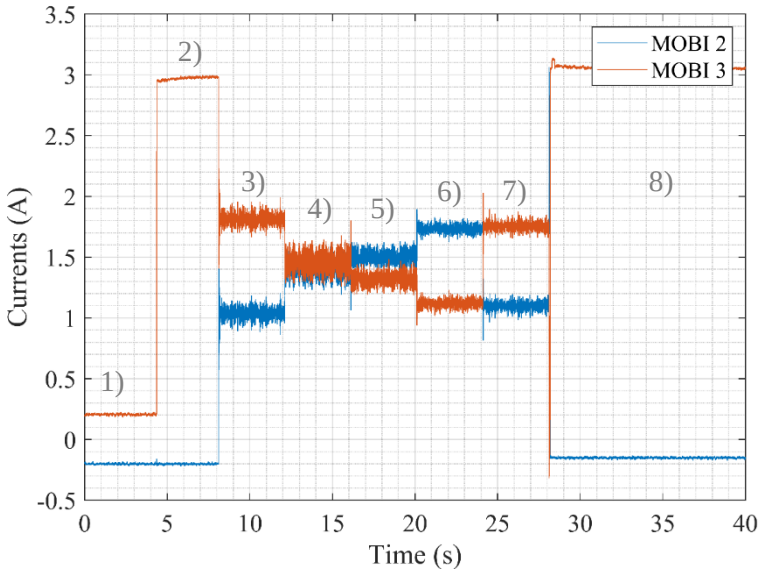

Figure 5.20 – Experimental results of 2 parallel MOBIs droop control parameters after calibration.

Although this procedure significantly improves the accuracy of current sharing, the validity of this calibration is limited insofar as certain parameters are not fixed and may change over time, particularly if the distribution network is modified. Generally speaking, these observations show that it is more interesting, in terms of current sharing accuracy, to position all the parallel modules as close together as possible in order to limit the parasitic phenomena induced by series line resistors in particular by making them negligible.

If it cannot be achieved, in order to be more robust and more flexible to these changes, an online adaptation of the droop coefficients to precisely compensate these errors – at low frequency – can significantly improve the observed performances. However, this would be a matter of secondary control.

5. 4 Conclusion

In this chapter, the work carried out to set up a demonstrator aimed at testing control strategies for electrical systems with a distributed and modular architecture has been presented. The experiments that it enabled to be carried out in order to validate the interest of the proposed primary control have been detailed. In addition to confirming the power bus stability under the conditions determined in the previous chapter, these experiments enabled to understand the strengths of droop control – relative simplicity of implementation, independence from communication links – and to identify its limitations. In order to optimize its performances, solutions have been put in place and the key factors have been detailed.

In order to obtain the best possible performance in terms of the stability of currents between modules, it has been shown that a high level of precision in voltage regulation is required. This precision must take into account all aspects of implementation, particularly the resolution of the digital to analogue conversions applied to the control signals. To achieve this, and although it has been shown here that it is possible to add droop control as a plug-in to the voltage and current control loops, it seems preferable that these are integrated at the same time during the upstream design of the system.

It has also been shown that taking into account the impact of line resistances when determining droop coefficients is essential in order to be able to control current ratios between modules accurately. Measures can therefore be taken to limit this impact, in particular by arranging all the modules as close

together as possible, thus forming a sort of module bank, or by arranging the layout in such a way as to take advantage of these line resistances in line with the respective size of the modules which is generally where the system naturally tends to go.

Finally, although the stability of the power bus has been confirmed, the variations in bus voltage induced by droop control mean that the system cannot currently be considered as a regulated bus architecture as defined by the ECSS, and the solutions available at primary control level are limited.

However, it is possible to remedy these problems by implementing secondary and tertiary controls, which aim to optimize the operation of the entire system over the medium and longer term. To this end, a supervision strategy has been validated in simulation and is proposed in the last chapter.

CHAPTER 6.

Secondary & Tertiary Control

Summary

In Chapters 1 and 2, the main components and topologies of modular and distributed architectures have been studied, enabling to propose a system adapted to the challenges of the space industry. In Chapters 3 and 4, an in-depth study was carried out to model the system as faithfully as possible, and to define the criteria governing its stability. These results were finally verified by experimentation in Chapter 5.

Based on these elements, in this final chapter, a global strategy for secondary and tertiary controls is established, with the aim of balancing the system's operation over the medium and long term.

Although the implementation of the demonstrator presented in the previous chapter should ultimately validate this overall strategy, this was not possible during the course of the present work. The results presented in this Chapter are therefore based on the following MATLAB Simulink simulation models.

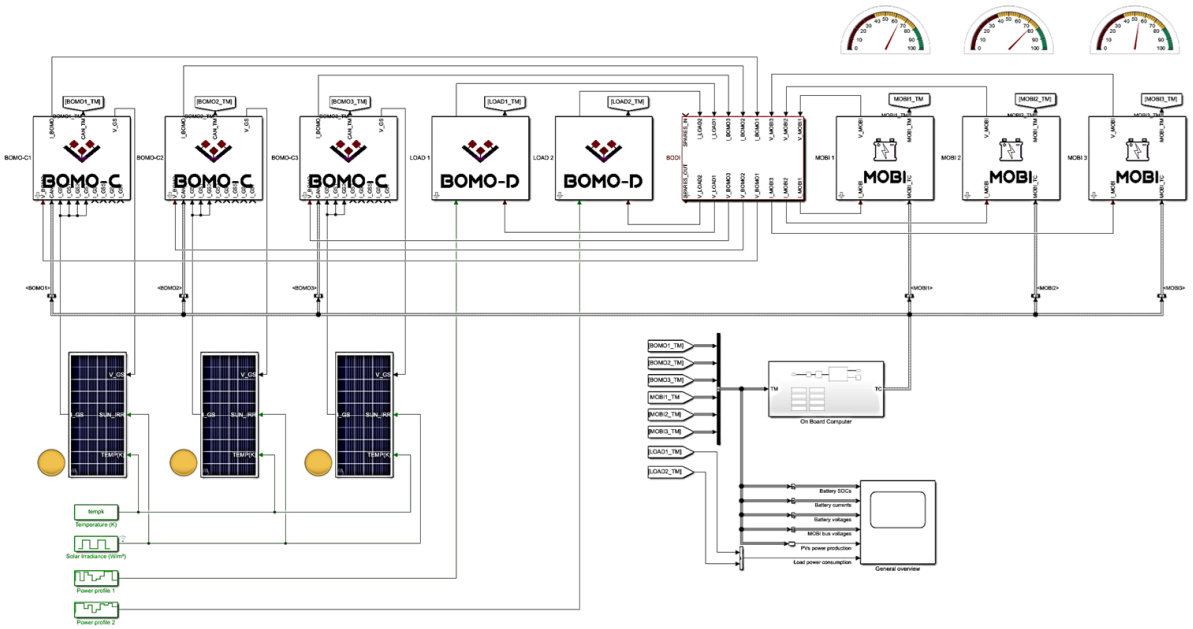

Figure 6.1 – MATLAB Simulink simulation model of the proposed modular electrical architecture applied to the use case system for secondary and tertiary control verification.

However, the experimental work carried out has highlighted the importance of certain phenomena, such as the impact of line resistances on the steady state of current sharing. These observations have enriched the simulation models used in this section, or at least guided the choices made in their simplification.

Indeed, in order to simulate scenarios over longer durations within an acceptable timeframe, the internal current and voltage regulation loops implemented at the primary control level have been approximated by first-order systems, with the exception of the simulations presented in paragraph 6. 2 , whose dynamics are intrinsically linked to those of these internal loops.

Thus, after defining the objectives and main parameters of secondary and tertiary controls in paragraph 6. 1 , paragraph 6. 2 focuses on two possible implementations to restore the bus voltage to nominal value, as mentioned in the conclusion of the previous chapter. Finally, in order to conclude the presentation of the work undertaken in the present thesis, paragraphs 6.3 to 6.5 detail the incremental implementation of the three proposed components to maintain the satellite's power supply capacity throughout the mission. It allows to obtain an overall simulation of the system, integrating all control components, from primary to tertiary control and conclude the study.

6. 1 Global strategy definition

In order to determine the overall strategy for secondary and tertiary controls, a summary of all system parameters is first proposed. Broadly speaking, they can be classified into 3 categories.

6. 1. 1 System’s inputs

System inputs are those parameters which cannot be influenced by the control in any way, and which define the system's electrical environment or physical limits. They include the following parameters:

1. Installed PV sections number;
2. The configuration of the distribution network and the characteristic resistance of each line;
3. The number of MOBI connected to the network;
4. The configuration of each battery and the resulting capacity;
5. End-of-charge voltage of each battery;
6. Optimal and maximum charging current for each battery;
7. Nominal bus reference voltage;
8. The maximum value of the equivalent droop coefficient.

Although the nominal bus voltage can also be regarded as a system control variable or measurement, it is considered here in the sense of the reference value, i.e. the assumption made when defining the system and, more specifically, when sizing the solar generators. Indeed, in the proposed electrical architecture, the polarization voltage of the generators is imposed by the bus voltage, so this reference signal becomes a system input once the section configuration is fixed.

It should be noted, however, that it is possible – and necessary – to distinguish this parameter from the reference variable actually sent to the various modules. The latter corresponds to a system control signal.

6. 1. 2 Control signals

Considering the primary controls implemented, particularly the droop control, the following control signals can be identified:

1. Reference voltages for local control;
2. Droop control coefficients for each battery module;
3. The number of sections to be connected to each solar panel.

This last parameter serves as a reminder that, although stability analyses have overlooked the role of solar panels and BOMO-Cs in the system by considering only the equivalent linearized impedance range that could characterize them in steady state, this aspect is an integral part of the system control to be implemented. Indeed, at system level, the DET management integrated into the BOMO-C corresponds strictly speaking to very basic primary control which requires to be supervised at secondary and tertiary levels.

Although the BOMO-Cs, as well as the BOMO-Ds, has not been integrated into the demonstrator, their role to interface with the MOBIs and perform the power production conditioning and distribution functions is essential since they also provide the observability needed to control the system properly.

6. 1. 3 Feedback variables

This observability is achieved by sharing the required measurements on the common CAN network, either periodically or on request. The main available measurements are listed below.

1. Batteries voltage;
2. Batteries current;
3. Batteries SOC estimation;
4. Bus-side current of each module – MOBI and BOMOs;
5. Bus voltage of each module.

In these variables, it's important to note the difference for all converter-equipped modules – the MOBIs in this case – between the module's current seen from the bus and that seen from the battery side. Indeed, while the bus voltage is more or less the same for all modules, the same is not necessarily true for the battery voltage when considering different SOCs or battery configurations. This highlights the importance, at this level of control, of unifying the quantities used by using the "Per unit system" or by dealing only with power and energy instead of current and capacity. This second, more intuitive approach will be used later.

A second point of attention concerns the notion of bus voltage. Considering the model developed in Chapters 3 and 4, based on the conductance matrix, as many bus voltages as there are control modules can be defined. In a realistic system, this number increases even further if it is considered that the various BOMOs – whatever their type – can provide a measurement of the bus voltage at their terminals. Thus, in the following, the method for constructing the generic bus voltage measurement, noted $V_{BUS_{MEAS}}$ will therefore be made explicit for each application case. Indeed, although all these voltages are relatively close to each other, consideration of one or the other allows some nuance to be brought to this measurement, allowing a degree of flexibility depending on the objective sought.

6. 1. 4 Secondary and tertiary control components

The objectives of the secondary and tertiary controls can be divided into three categories.

The first corresponds to the objectives intrinsically imposed by the primary raison d'être of the on-board electrical system and all that this implies.

This is particularly the case for objectives linked to controlling the production and injection of electrical power, and controlling battery recharging. These two major components of power system control are intimately linked to each other, since the output generated by the latter is the input required by the former, as shown in Figure 6.2, with the two components cascading from one to the other. This cascading is explained and made possible by the fact that their dynamics are very different.

Thus, the aim of battery charge control is to determine the power required at any given moment to recharge all the batteries, noted $P_{BAT_{REF}}$, in a taper voltage, taper current – constant current, constant voltage – cycle, based on the individual voltage of each battery – an image of its SOC. This charge control corresponds to management of the energy stored in the system, and its characteristic time is of the order of an hour, which justifies considering it as a tertiary system control function.

Solar generators power injection control is designed to ensure that, in the medium term, the right amount of power is injected by the solar generators to recharge the batteries, whatever the consumption of the

rest of the system. This control is carried out at $1Hz$, so the injected power can be rapidly adapted to load variations, and therefore corresponds to a secondary control.

The second category of objectives corresponds to those directly dictated by the standards that apply to the system. As mentioned in the conclusion to the previous chapter, this is the case of bus voltage restoration, which is necessary if the system is to be considered a regulated bus system as defined by the ECSS in [100]. As this is a control component linked to the quality of power distribution, it is integrated into secondary control in the same way as the power generation control, although in terms of dynamics, it is positioned between the latter and the internal regulations of primary control, with a period of the order of a millisecond.

The last component of the control strategy shown in Figure 6.2 falls into the last category of objectives, corresponding to the optimization of system operation. It has been demonstrated in Chapter 3 that when a very high ratio of droop coefficients is adopted, the system became less stable and its performance is affected. The same observation has been made in the previous chapter when considering a case where a module reaches its physical operating limits – the current limitation of a MOBI. Both of these configurations can be reached if, during charging, one module reaches full load before the others.

To avoid this situation, a SOC balancing method is implemented. This balancing, which is carried out continuously during the charging and discharging phases, also takes into account aspects that could disturb current sharing, as well as the specific characteristics of each module, such as battery size. By defining the value of the droop control coefficient for all the modules, it implements a kind of macro-BMS and allows only a single equivalent battery to be considered from the point of view of the components presented above, which greatly simplifies their implementation.

In the following sections, the implementation of each of these secondary and tertiary control components is detailed, proposing, where relevant, several possible implementations and discussing their respective benefits.

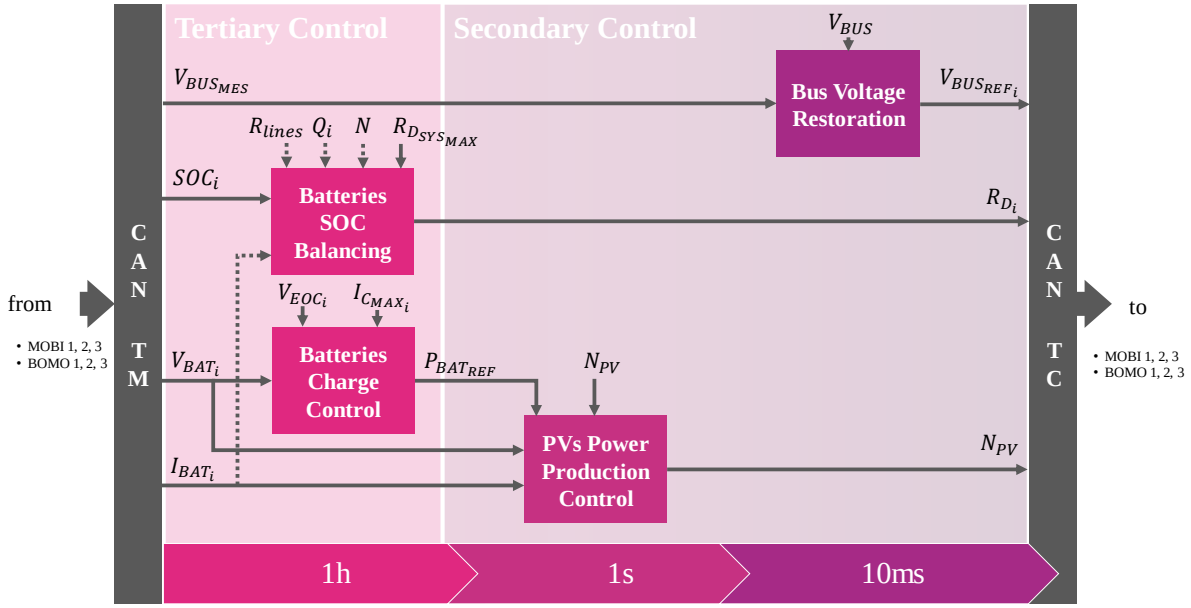

Figure 6.2 – Proposed Secondary and Tertiary control strategy diagram.

6. 2 Bus voltage restoration

In order to restore the bus voltage and to eliminate droop control-induced variations, a slower external voltage loop is added to the bus voltage. This bus voltage can be defined in different ways, depending on where it is measured on the system. This choice is mainly conditioned by the point of the network for which the need for precision is then strictest. In the proposed architecture, two points are of particular importance.

The first is the connection point of the solar panels. As their characteristics, and therefore the power they deliver, are fundamentally linked to the voltage at their terminal, it is desirable to control this with a high degree of accuracy. It is even possible, if a slight variation in voltage is accepted, to modulate it to reach a desired operating point - the MPP or any other point corresponding to the power required by the system.

But in a more standard context, the aim is generally to obtain good power quality for downstream loads, which in part means a fixed voltage at their terminal. Thus, by considering the bus voltage as the voltage across the loads, we ensure that they are supplied under the best possible conditions.

In the literature, this function is also often performed on the average voltage of all the modules [2]. However, this implies a greater number of communications, which is not justified by the gain it brings. This choice is generally made in view of the limited number of observables, which is not problematic in our case thanks to the multiple measurements available on the system. What's more, it doesn't take into account and compensate for losses in the harness, as is the case when regulating the voltage directly at the load input.

The second choice to be made when implementing this function relates to its location, i.e. whether it should be implemented locally or centrally. The key factor in making this compromise is the desired bandwidth. Indeed, depending on the choice of location, bandwidth limitations are not the same. Generally speaking, 3 limitations need to be taken into account:

1. The first is the time required to communicate the various signals required.
   For this aspect, reducing the number of signals required helps to limit the impact, which reinforces the importance of selecting a single control point.

2. The second is the maximum achievable refresh rate.

    a. In the case of a centralized implementation, this depends in part on the performance of the OBC. It processes a very large number of functions, and to limit the complexity of its programming, a single refresh rate is defined. This frequency can go up to a hundred hertz for specific units, but is generally 1Hz for EPS-related functions, which means that interesting dynamic performance cannot be envisaged for bus voltage restoration.

    b. In the case of a distributed implementation – in MOBIs, for example – the processing frequency is more flexible and often faster, so the limitation is again imposed by the performance of the communication network.

3. The last and probably most important limitation is the one induced by the communication channel's throughput, and is to be dissociated from the first. This limit is due to the bandwidth that can be allocated to a function, so as not to overload the bus.

Considering that the control bus is used – a single communication bus for all the platform's equipment – and that one frame is sufficient to communicate all the necessary information, frequencies of 8 to 32Hz are frequently used for RTU or AOCS equipment. This limitation, corresponding to a CAN bus utilization factor of around 0.5%, is deliberately set relatively low in view of the number of potential subscribers.
To reach higher values, a specific EPS CAN bus may be envisaged – thus requiring additional equipment to interface it with the command and control bus.

In the latter case, and considering that the system requires to be robust to communication errors, it is possible to calculate the maximum achievable utilization factor, as defined in [158]:

$$Utilization\ factor = \frac{Data\ frame\ size}{(2 \times Data\ frame\ size) + Error\ frame\ size} \qquad 6.1$$

Using the CAN bus extended frame format as defined in [159], this corresponds to a maximum utilization factor of around 46%. Taking into account an additional margin to allow the exchange of all telemetry, it seems that a $1kHz$ regulation is achievable - corresponding to a utilization factor of 12%.

In MATLAB Simulink, this is implemented by a "rate transition" block which allows to define a Zero-Order Hold (ZOH). The voltage restoration then merely corresponds to an additional external voltage loop – here implementing a digital PI controller – acting on the voltage reference sent to the different battery modules and used to perform the primary controls – droop control and local voltage regulations – as shown in the figure below.

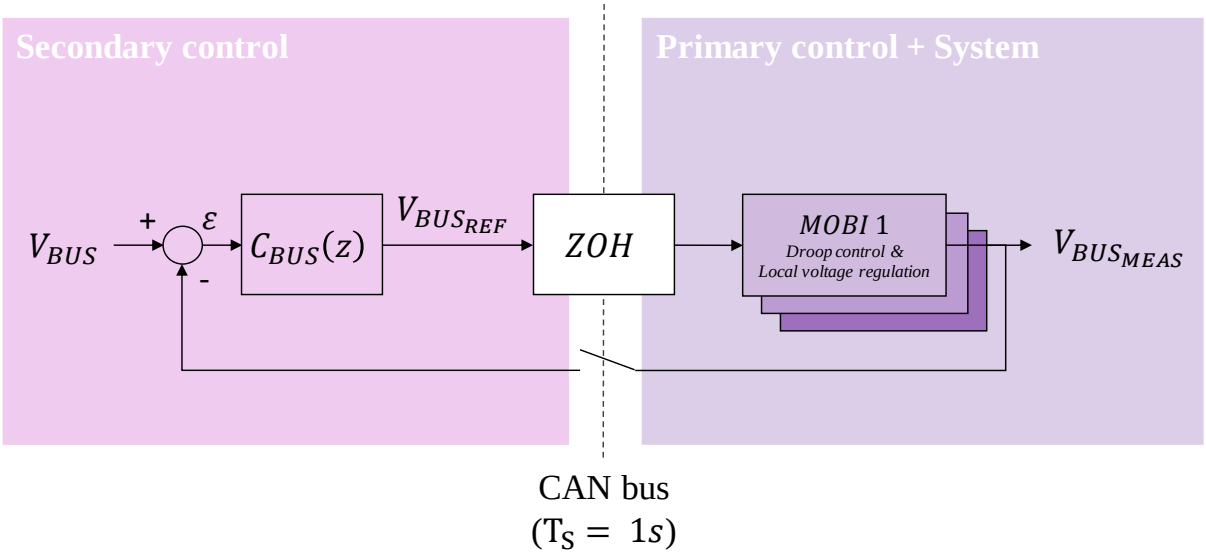

Figure 6.3 – Bus voltage restoration based on an external regulation loop updating the voltage reference provided to the droop controlled battery modules.

The same configuration and power profile than in the experimental case presented in the previous chapter are used. This allows to get the results presented in Figure 6.4.

The quantities measured on the actual system are also shown for ease of comparison.

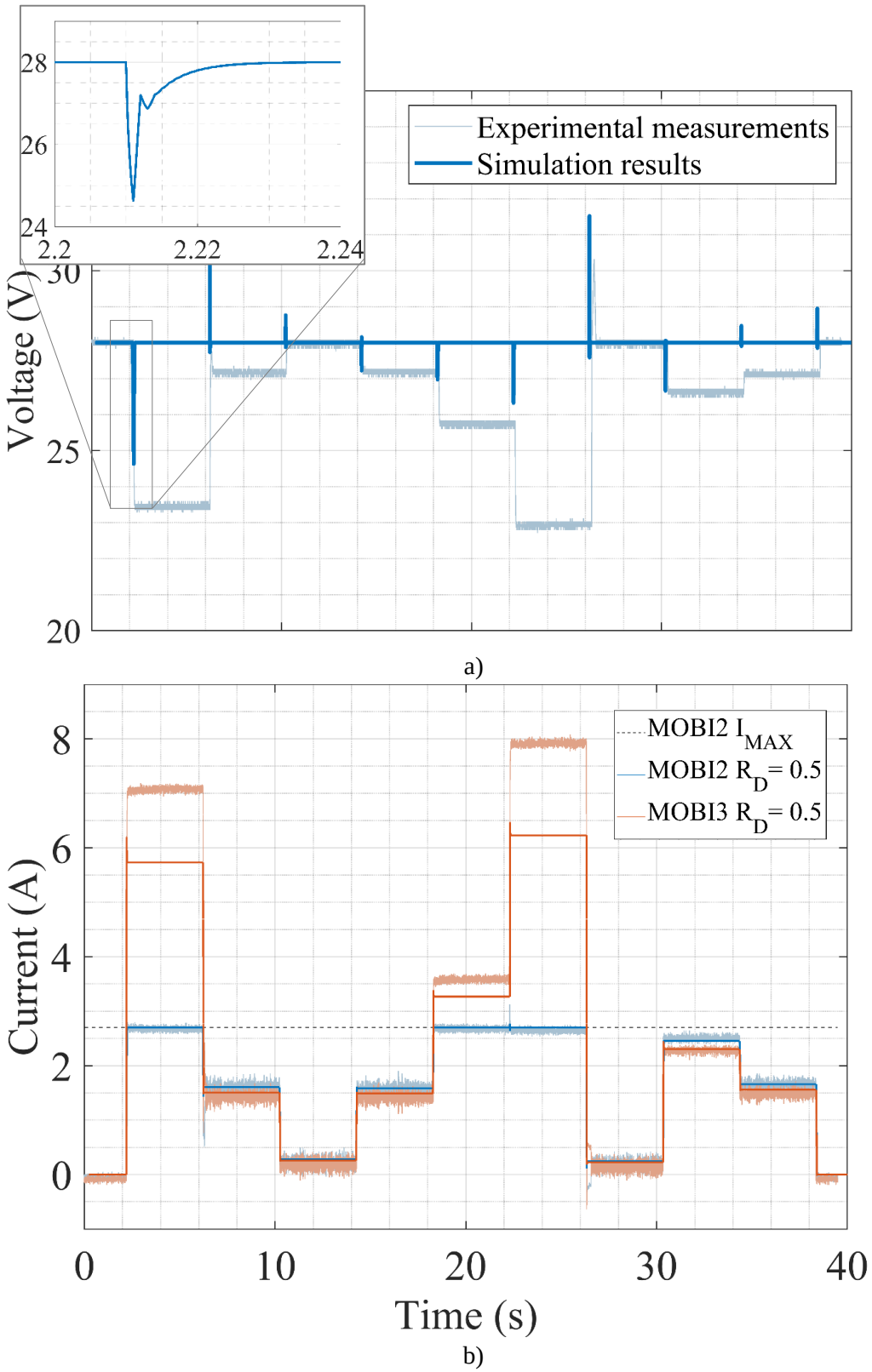

Figure 6.4 – Bus voltage (a) and currents (b) simulation results in comparison to experimental results with bus voltage restoration implemented.

Figure 6.4 a) shows the voltage restored by implementing a PI corrector. Transient variations are of the same order of magnitude as those obtained in experiment, albeit slightly reduced. This is due to the fact that the voltage variation dynamic is more or less the same as the implemented control dynamic.

On the other hand, at steady state, reached in around $20ms$, the bus voltage is well restored to $28V$. This does not affect current sharing, which remains identical to what was observed in practice, as can be seen in Figure 6.4 b).

However, a variation is noticeable at high currents, particularly when the MOBI 2 reaches saturation. The currents then reached by MOBI 3 are lower than those observed in experimentation. This is directly due to the increased voltage, which, at constant power, induces a lower current at modules level, thus moving away from the operating limits.

Despite this, it can still be observed that the transient with the highest amplitude occurs when one of the modules is in current saturation, demonstrating the need for consistent control of sharing.

6. 3 Battery SOC Balancing

In order to meet the objective of balancing the SOC of the various batteries composing the system, droop control coefficients are adapted. Indeed, balancing is directly linked to current sharing, with the SOC of each battery corresponding to the integral of its current.

Figure 6.5 a) and b) illustrate the divergence between SOCs in the case of three different batteries and considering unequal line resistances, respectively during charging and discharging at constant power, starting from identical SOCs.

It can be observed that over the laps of time considered, corresponding in terms of order of magnitude to charging or discharging phases at full power – as defined by the case study – the imbalance can reach 25%.

In the case of charging, this means that while the overall system charge level is around 90%, MOBI 1 exceeds its maximum SOC, which in a real-life situation could lead at the very least to severe degradation of battery performance, and at worst to thermal runaway, resulting in the destruction of the battery and all surrounding equipment.

The same applies to discharging: although a high discharge rate is unlikely to induce thermal runaway, emptying a li-ion battery completely generally leads to its loss.

Obviously, by carrying out successive charging and discharging cycles, even though some of the logic is reversed, part of the error is accumulated and accentuates the imbalance.

Balancing means compensating for all the disturbances impacting the current sharing precision identified in the previous chapters. However, another cause of SOC divergence for an equal current is the disparity between the capacities of each battery, expressed in energy.

However, by definition, the SOC imbalance between modules corresponds to the integral of the current-sharing error, so it is possible to directly determine the adaptation to be made to the SOC calculation, without having to implement regulation in the conventional sense of the term. Indeed, for an open-loop system to have a static error of zero, it is sufficient for the loop to have a pure integral component upstream of any disturbance injection, which is what the SOC estimation does for each battery by nature.

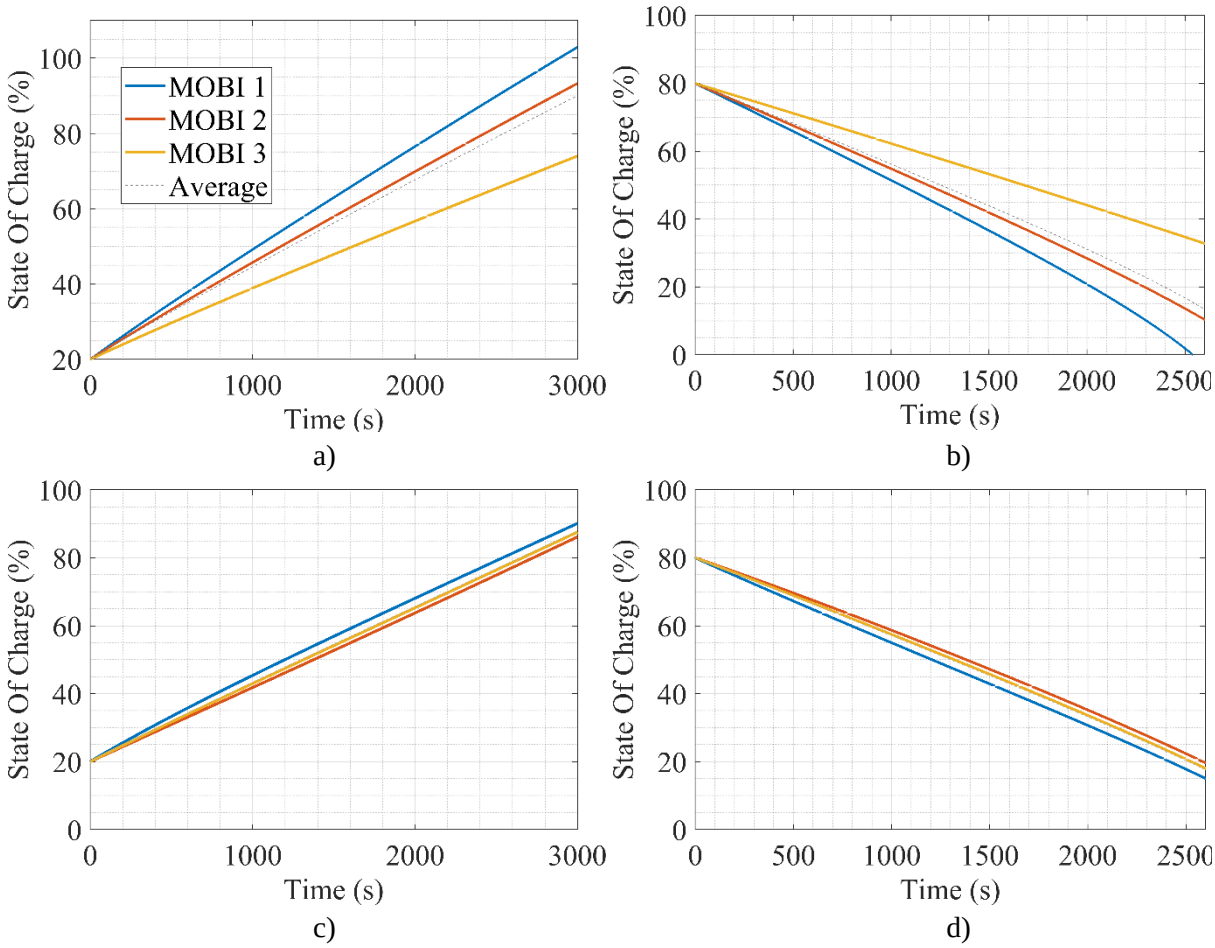

Figure 6.5 – SOC evolutions without any R_D adaptation – a) and b) – and with the method proposed in [87] – c) and d) – respectively during battery charge and discharge with identical initial SOC.

Based on this property, a large number of methods are proposed in the literature for adapting droop coefficients as a function of SOC, such as the one detailed in [87] and reproduced in Figure 6.5 c) and d).

This method is based on the principle which states that during charge a battery with a high SOC – closed to full charge – should absorb less current than a battery with a lower SOC, and thus, that a higher droop coefficient should be given to the first compared to the second, and reversely during discharge.

It can be seen that this does indeed limit the gap between SOC. This significant improvement is due to the fact that, in addition to the adaptation presented above, the differences in capacity between the different batteries making up the system are taken into account in the law for determining the droop parameters, as scaling factors.

However, in the application considered in [87], line resistances are neglected, which is not the case in this thesis.

As a result, the SOC difference between modules does not fall below 5% in either load or unload.

In order to improve accuracy and make adaptation more generic – notably without the need to consider parameters specific to each module – a new adaptation law is proposed.

Unlike the previous method, which takes as a reference value a SOC of 100% during charge and 0% during discharge, the average SOC is used as a reference value which enables to calculate a balancing error for each module. It is then possible to define an expression based on the same logic as above, which naturally tends towards zero error:

$$\begin{cases} R_{D\,charge_i} = R_{D_{SYS_{MAX}}} + \alpha \dfrac{SOC_i - SOC_{AVG}}{|SOC_i - SOC_{AVG}| + \beta} \\ R_{D\,dicharge_i} = R_{D_{SYS_{MAX}}} - \alpha \dfrac{SOC_i - SOC_{AVG}}{|SOC_i - SOC_{AVG}| + \beta} \end{cases} \quad 6.2$$

with α and β being tunable factors controlling the amplitude and steepness of transition of the adaptation law as shown in Figure 6.6 and $R_{D_{SYS_{MAX}}}$ determined accordingly to the criteria defined in Chapter 4.

The advantage of the above formula is twofold:

1. control the adaptation limit values by choosing the α coefficient, to ensure compliance with operating conditions;
2. achieve good balancing accuracy, by adopting the adaptation factor β such that its ratio with α is relatively large to obtain a high gain around zero error, and without introducing discontinuities as shown in the figure below.

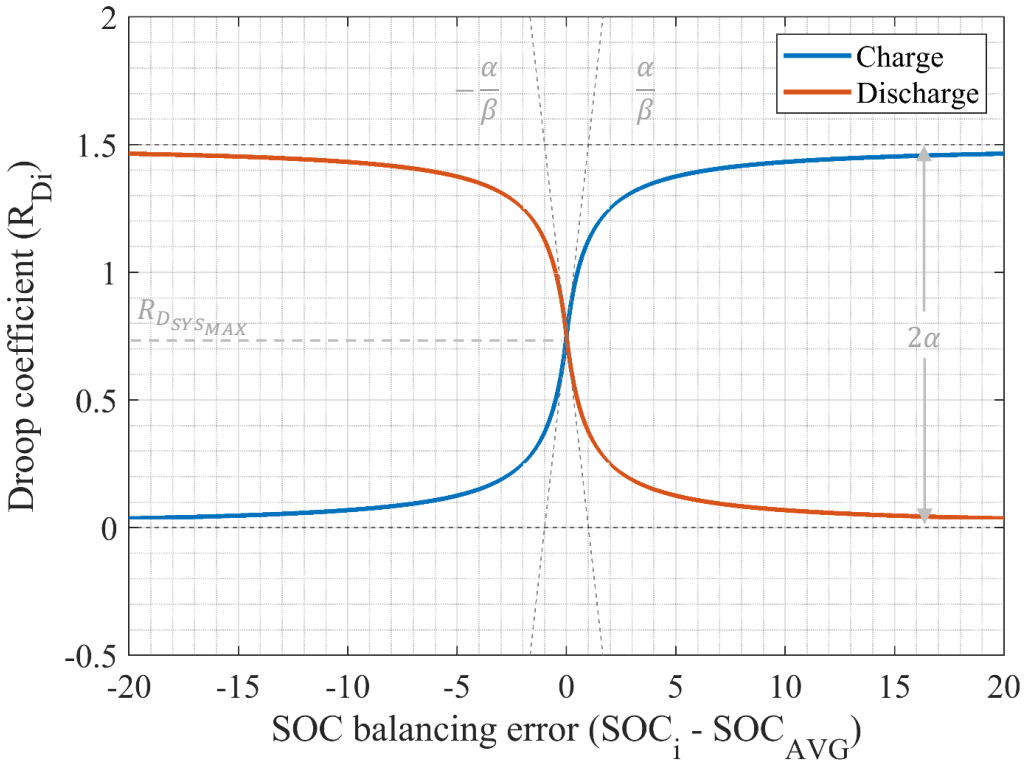

Figure 6.6 – R_D adaptation characteristics for charge and discharge in function of SOC balancing error.

Controlling the dispersion of droop coefficients also enables to establish a maximum ratio between the different units of a system. Indeed, although balancing is critical, there is no particular constraint on the speed of convergence, so there is no need to adopt extreme values.

All the more so as, during the convergence period, which corresponds to a phase in which the current sharing is not consistent with the respective capacities of each battery, if no limitation is taken, dangerous currents could be reached – for a module overcharged relatively to the others during the discharge phase and conversely for a module in relative undercharge during the recharge phase, for example.

The results obtained on the same system as above, with $\alpha = R_{D_{SYS_{MAX}}} = 0.75$ and $\beta = 1$ are presented in Figure 6.7.

It can thus be observed that the proposed adaptation law both maintains very good SOC balancing accuracy – less than 1% dispersion, which is lower than the accuracy of SOC estimators in general – and performs a relatively fast balance recovery in the event of initial imbalance – convergence in around 40 minutes for an initial SOC deviation of 30%.

As mentioned in section 6. 1. 4 , balancing the states of charge, and thus equalizing the charge and discharge profiles of each module, is not only of interest for maintaining system performance, but also for homogenizing the ageing of each battery, which has the effect of increasing the lifetime of the overall pack, and is therefore an additional advantage of this method.

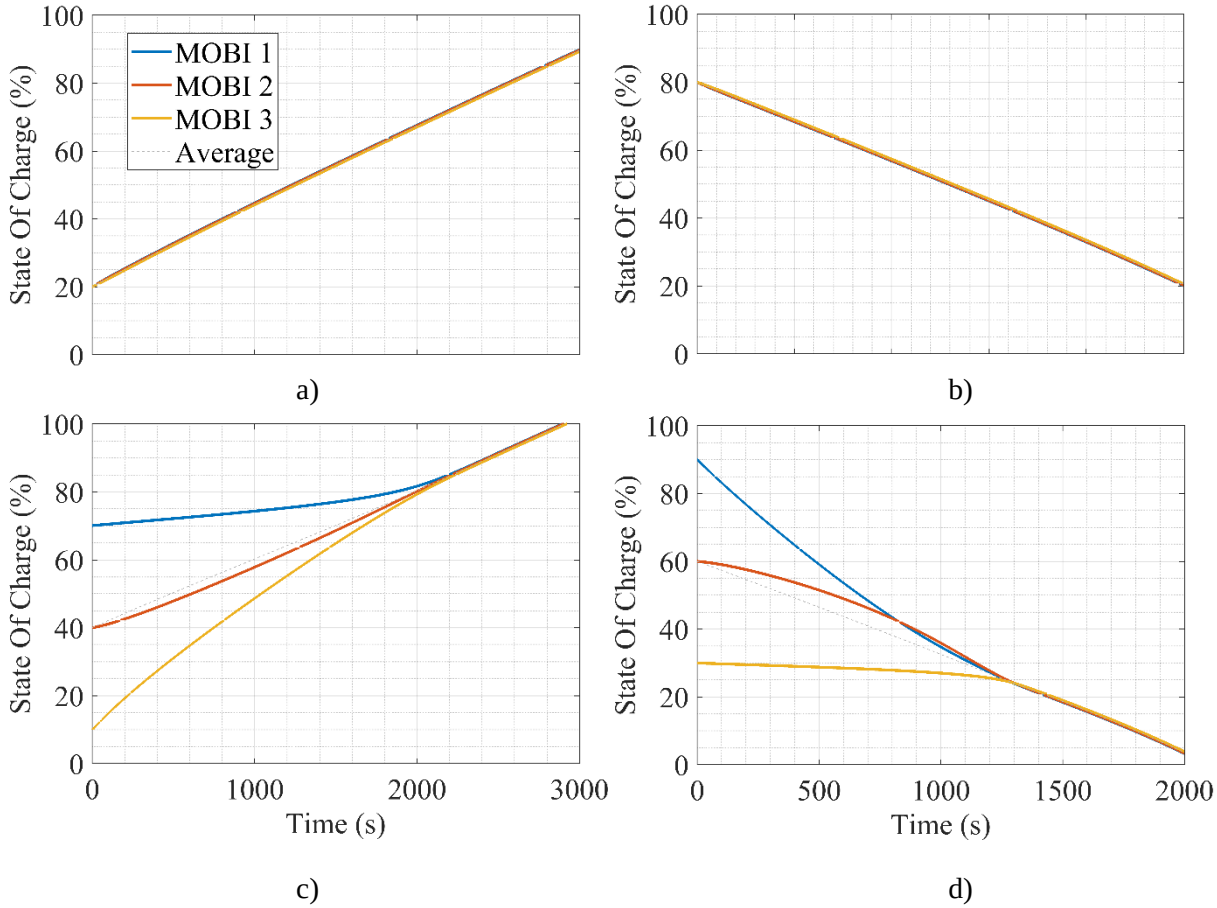

Figure 6.7 – SOC evolutions with the proposed R_D adaptation considering balanced initial SOCs – a) and b) – and unbalanced initial SOCs – c) and d) – respectively during charge and discharge.

From a control strategy point of view, this also has the advantage of greatly simplifying the implementation of charge management, since only one equivalent battery can be considered. In particular, this avoids multiplying the number of charge control loops with the number of modules present. However, to achieve constant current, constant voltage charging, it is necessary to control these two variables, either by summing them or by average. The following sections shows how this could be implemented.

6. 4 Power Production Management

First and foremost, the battery current needs to be regulated so that the charging phase can be carried out at constant current – taper voltage - around the C-rate required by each battery. In conventional unregulated bus architectures, the battery current is commonly regulated by controlling the power injected by the solar generators.

In the case of several modules with different conversion stages and therefore different reference voltage levels for each battery, the currents cannot be trivially added together to generate a single reference.

In order to be valid at all levels of the system, the power is used. Modulo the losses induced by the converter stages, which can be compensated by regulation, this has the advantage to be conservative even through power conversion stages.

The power injection of the PV is directly proportional to the number of PV section connected to the power bus thanks to the BOMO-C, when considering a constant voltage applied to them.

$$P_{SECTION} = I_{SECTION} \times V_{BUS} \tag{6.3}$$

$$\Leftrightarrow P_{BOMO} = P_{SECTION} \times N_{PV} \quad , \quad N_{PV} \in \mathbb{N} \tag{6.4}$$

with $I_{SECTION}$, the current production of a single section for a given voltage and N_{PV}, the number of connected section.

This relation shows that the number of section to connect can simply be determined from the total current to inject from the PV to supply the loads and recharge the batteries. Because the section current varies over time in function of sun irradiance, temperature and aging, in addition with the disturbances mentioned above, it is proposed to calculate the number of section to connect via a PI regulator as shown in Figure 6.8.

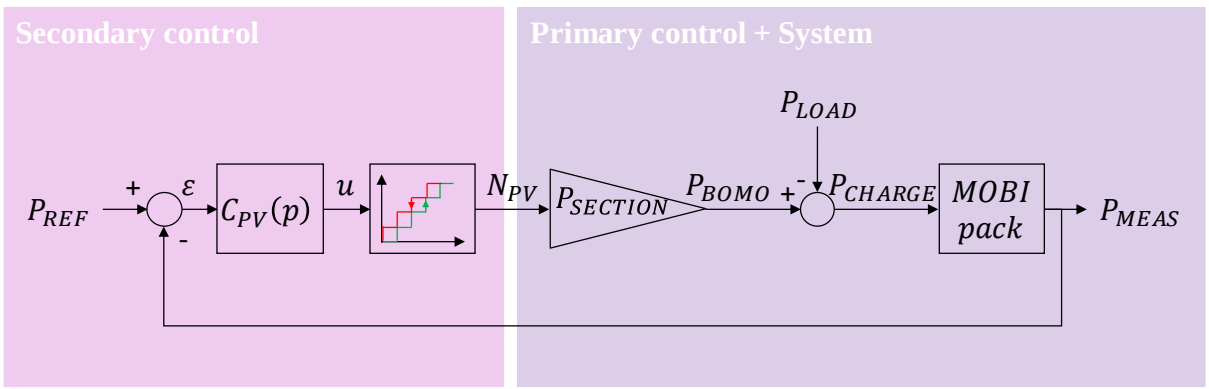

Figure 6.8 – Power production management block diagram.

It can be seen how important it is here to implement primary control as well as consistent current sharing. Indeed, although the latter is considered a tertiary control since its primary objective is to balance the energy storage levels in the system's various batteries, from a power management point of view, it also has the essential role of balancing the contributions of each module within its operating range.

These elements make it possible to consider all MOBIs as a single macro-module. While this makes it easier to control the power balance, it necessitates to choose a variable on which the regulation will be slaved, in the same way as the choice of reference voltage discussed earlier in this chapter.

Considering that this regulation is performed at a relatively slow frequency – $1Hz$ – the data bus utilization factor and processor load are no longer limiting factors. In order to regulate the power used to charge the battery of each MOBI as precisely as possible, the individual powers on the battery side are calculated and added together.

$$P_{MEAS} = \sum_{i=1}^{N} I_{BAT_i} V_{BAT_i} \tag{6.5}$$

This choice enables all losses associated with power conversion and distribution to be compensated through regulation.

In this way, the appropriate power is injected from the solar panels, so that the power received by each battery is as close as possible to the power required, within the limits of the power available, as shown in Figure 6.9.

Indeed, as the power consumed by the system's loads takes priority over battery recharging in order to fulfill the satellite's mission, it is possible that the latter may reach levels that do not allow the recharging power set-point to be reached. This is notably the case between 0 and $300s$, then between 1200 and $1500s$ in the curves below.

In this case, the control variable of the number of PV section to be connected reaches saturation and the batteries, being in bus voltage regulation mode, absorb only the residual power.

This observation highlights the interlocking nature of the proposed control strategy:

1. MOBIs first regulate the bus voltage, enabling loads and solar generators to operate nominally.

2. The solar generators and associated BOMO-Cs modulate the injected power to optimally charge the batteries.

Although this interdependence may at first sight appear to be a constraint, since the elements seem unable to function without each other, it is in fact the fruit of the combined approach of a hierarchical architecture and the application of the subsidiarity principle presented in Chapter 2: the most critical functions are carried out in a distributed manner, which increases their speed and reduces their sensitivity to failures, while the functions subject to weaker constraints – particularly from a dynamic point of view – are deported.

The result is an overall more robust system.

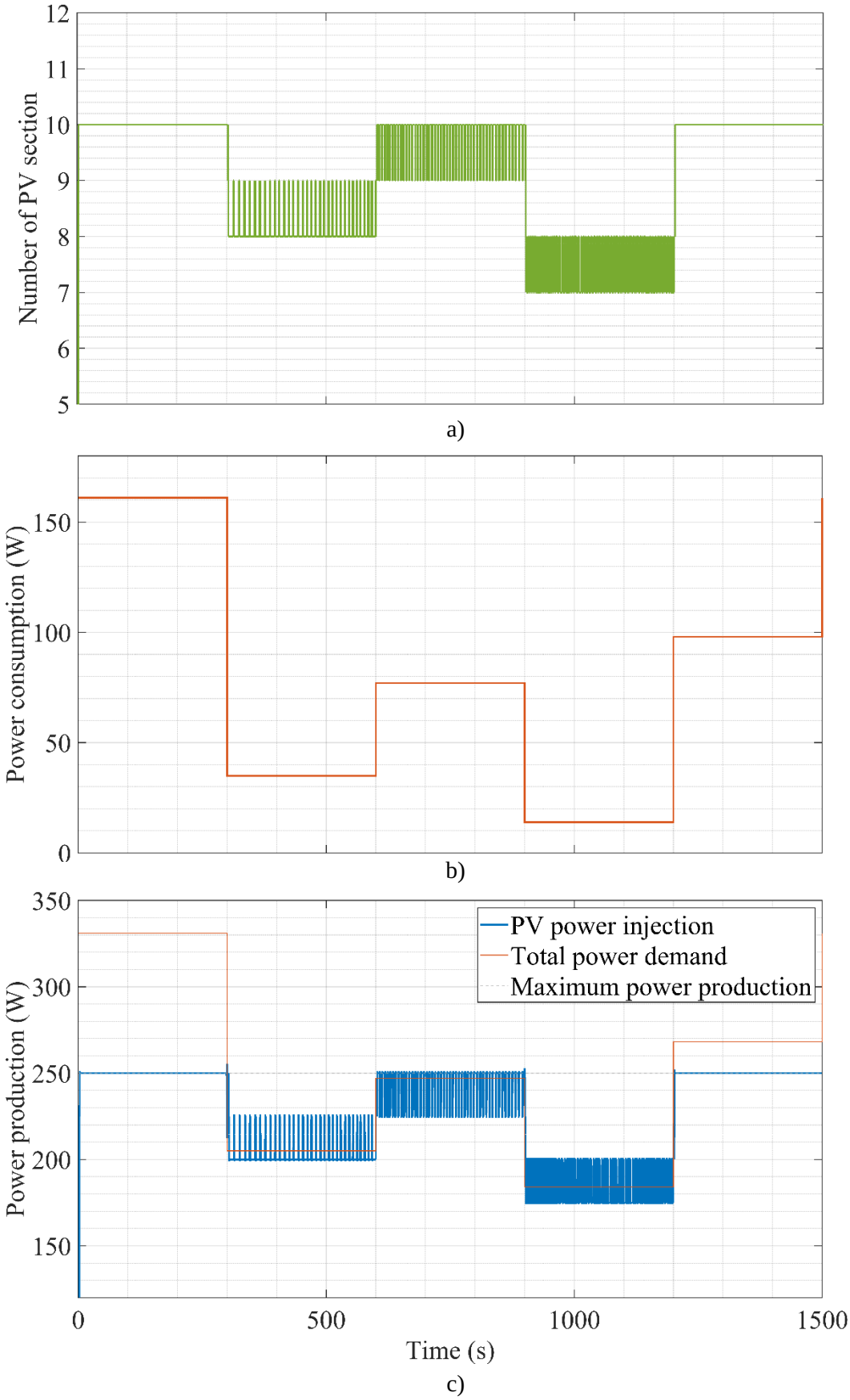

Figure 6.9 – Power production management simulation results.

Back to Figure 6.9, it can be remarked that in phases where the power demand – load power and battery charging power – is lower than the maximum power available, the system oscillates at a frequency of a few hertz. This is due to the nature of DET control, which corresponds to a discrete power control whose step is defined by the power of each section as defined above.

When the power required corresponds to a value between two section numbers, it is therefore normal to see the system oscillate between these two values. This oscillation, which can be seen in inset a) above, achieves the required power when considering the average values and, at these frequencies, poses no problem from a battery point of view.

Indeed, the C-rates indicated by manufacturers for the charging and discharging phases of battery cells correspond to the average values applied to them for controlled ageing, and are generally accompanied by absolute values not to be exceeded to protect cell integrity. These are also the values that are set as MOBI limitations, and thus enable the modules to absorb the peaks induced by DET control and which might be above the nominal value.

On the other hand, while these oscillations have no significant impact on the batteries, they do have one on the primary power bus, where droop control induces voltage variations, as can be seen in Figure 6.11. To limit this impact, the oscillation number should be reduced as far as possible.

In this goal, a hysteresis coupled to control quantization is implemented, in accordance with the graph shown in Figure 6.8 and visible on the block diagram presented above.

Implementing this function is a simple way of reducing the speed of oscillation: for a given period, the number of oscillations is divided by 4 - see the zoomed-in insert in Figure 6.11.

The reduction in oscillations thus achieved preserve the fact that the average value of the battery powers is equal to the set point without, even temporarily, higher values than without hysteresis being reached – no instability induced.

Thus, by adapting the power set point according to the nominal charging current I_{CHARGE} and the voltage of each battery as defined by the equation below, at each sampling period of the regulation loop, it is possible to control their individual current as represented in Figure 6.12.

$$P_{REF\,i} = I_{CHARGE_i} V_{BAT_i} \tag{6.6}$$

Hence

$$P_{REF} = \sum_{i=1}^{N} I_{CHARGE_i} V_{BAT_i} \tag{6.7}$$

It is worth noting that this regulation can be carried out on the current of a single module, the currents of the other modules can also be considered as disturbances, in the same way as the consumption of the loads – a battery in charge is in itself a load seen by others. In addition to showing the robustness of the control strategy, this property highlights the fact of being able to reduce the number of communications necessary to achieve regulation. This is all the more interesting at the level of higher regulation since it can in particular make it possible to carry out only one regulation loop instead of one per battery, which is particularly interesting when the number of modules becomes large in order to limit the calculation load on the processing modules.

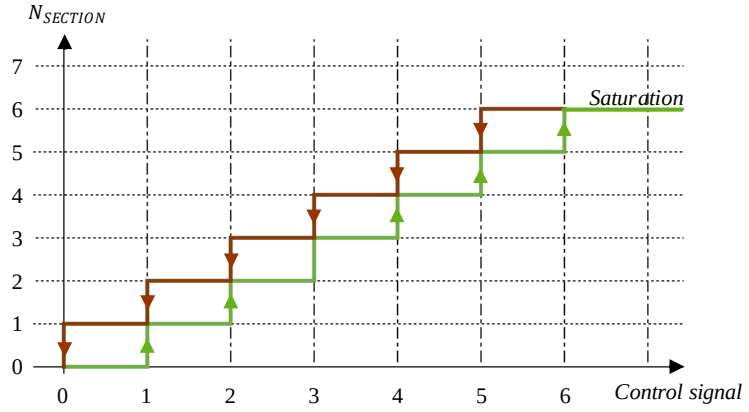

Figure 6.10 – Number of section allocation function considering a limitation to 6 sections.

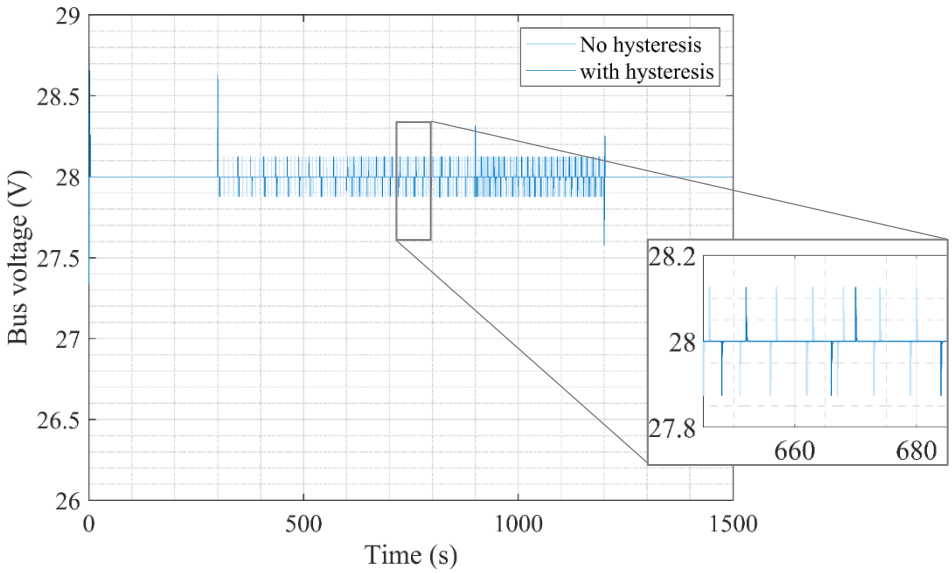

Figure 6.11 – Simulated bus voltage variations with and without the hysteresis on PV sections control signal.

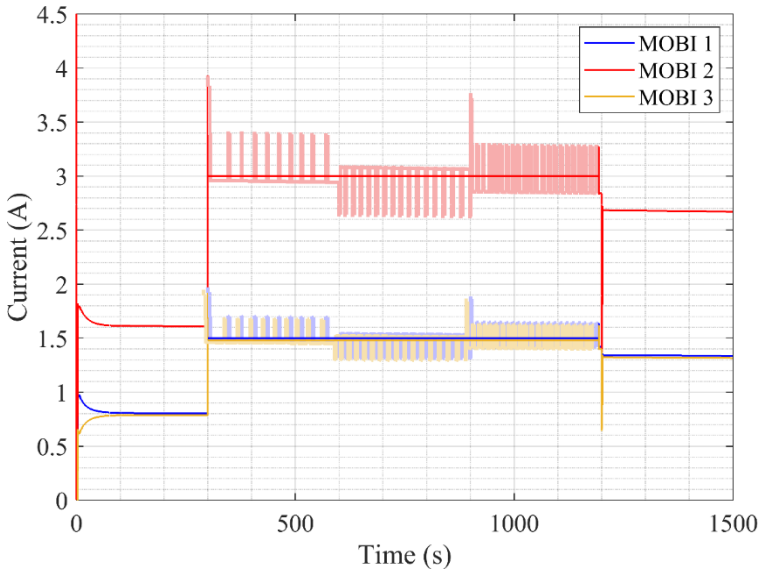

Figure 6.12 – Simulated batteries current real and average values during charge.

Indeed, this regulation alone does not make it possible to manage the complete charge of the battery, it only takes into account one of two typical phases. For end-of-charge management in particular, the control strategy requires a final component.

6. 5 Battery Charge Management

Supposing that the other components of the proposed control strategy are implemented, the battery charge management is the last control component to be implemented to complete the overall strategy. It generally has two objectives:

1) Determine the set point of the power production control loop

2) Define charging targets for each battery

In order to take into account all possible configurations at the battery level, the most complete solution is to set up a regulation loop per battery.

Like the management of power production, the time constraint of this regulation – which is even lower to the former – does not significantly limit the quantity of usable resource, both in terms of processing the calculations to be carried out, and in terms of bandwidth usage of the communication bus. This low resource requirement makes it possible to make this function implementable both centrally in the OBC and distributed in the MOBI. This second option has the advantage of accentuating the modularity of the control strategy.

Thus in each of the MOBI, the following control can be implemented:

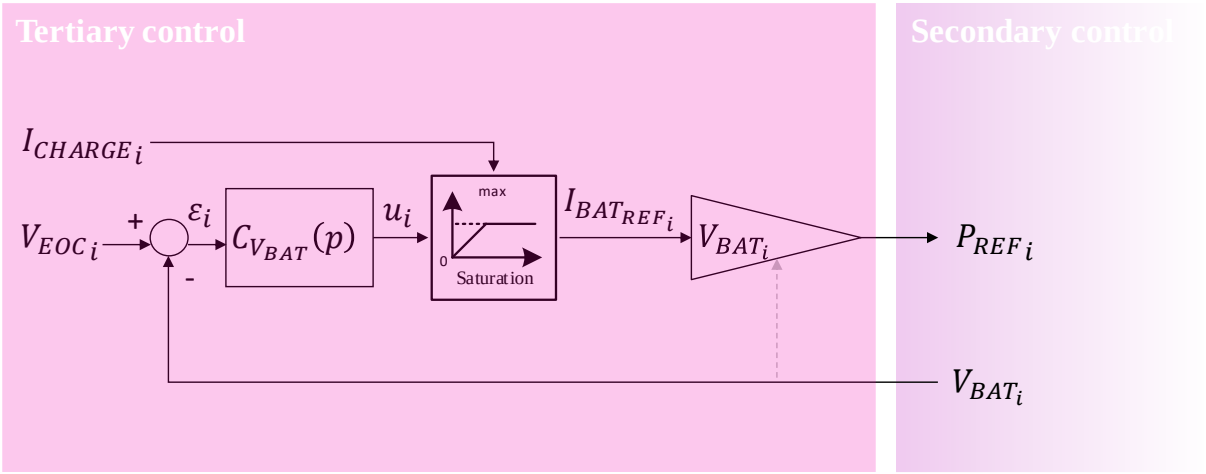

Figure 6.13 – Individual battery charge regulation loop on battery voltage.

The sum of the references thus generated makes it possible to determine the reference power at the system level to be supplied to the solar panel regulation seen in the previous section. Implemented on a system with three different batteries, the results presented in Figure 6.14 are thus obtained. For this example and to show the flexibility of the proposed control, the MOBI configurations are respectively defined in simulation as 8S1P, 4S2P and 12S1P.

During charging, the constant current phases followed by the constant voltage phases can clearly be observed, as soon as the SOCs are balanced, and this, while the characteristic charging currents of each battery and their end of charge voltage, respectively noted I_{CHARGE} and V_{EOC}, are not equal from one

module to another. It can also be observed in these figures that despite the differences between the values at the level of each battery, the transition between the constant current phase and the constant voltage phase is synchronized from one battery to another.

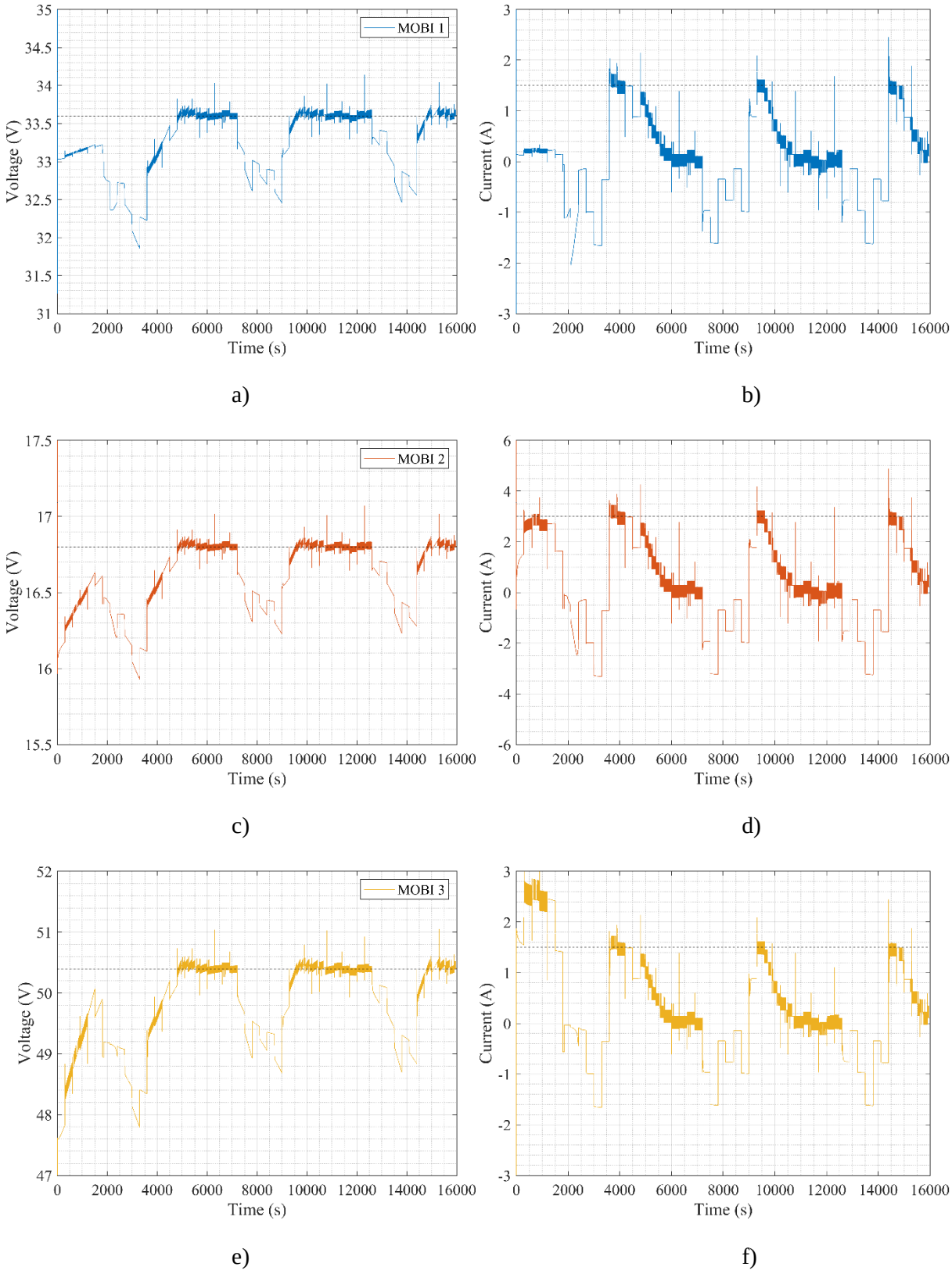

Figure 6.14 – Simulated batteries individual voltages and currents evolution over three Earth orbits.

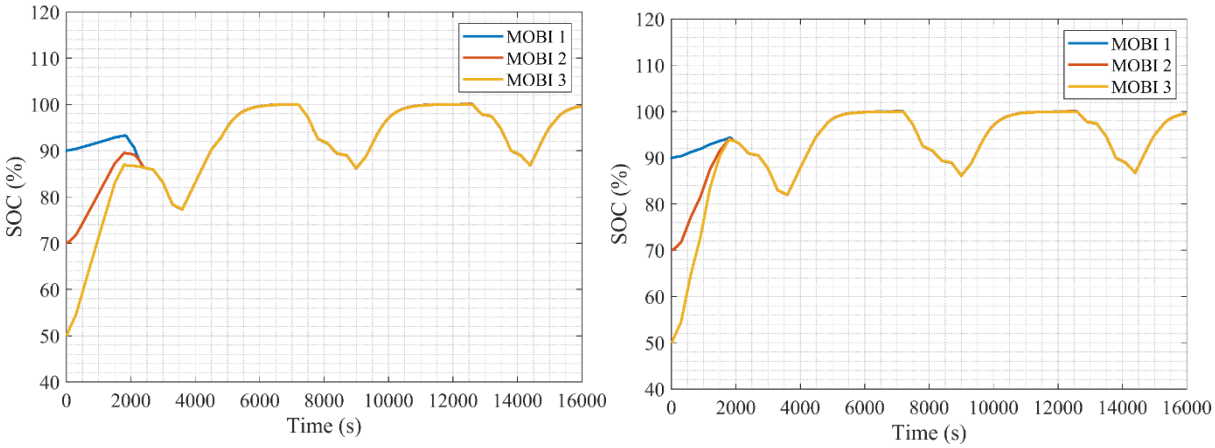

a) b)

Figure 6.15 – Simulated batteries SOC evolution over three Earth orbits with individual battery voltage regulation loops (a) and a single regulation loop (b).

b) This makes it possible to show that a single regulation loop, on a single battery, could be sufficient to control the charging of all the batteries, as was suggested at the conclusion of the previous section on the injected power regulation loop by the PV, provided that this last is also adapted to only take into account the power of this battery as feedback signal.

b)

Figure 6.15 allows to compare the performances for these two implementations and it shows that the results obtained are almost identical.

The only difference appears at during the initial balancing phase. The behavior during this period depends on the relative SOCs of each battery compared to the one which is regulated.

In the case presented in inset b), the unique regulation loop implemented is carried out on the battery of MOBI 1 which is also the most charged battery. By action of the integral component of the power regulation loop, the power control injected at the system level therefore increases as long as the MOBI 1 battery current does not reach its nominal value.

However, at the same time, the SOC balancing function determines that MOBI 1 must charge less than the other modules which have lower SOCs, by adapting the droop coefficients.

c) Thus, overall, this explains why a greater power is injected by the BOMO-Cs than in the case of N independent regulation loops where the power would be limited by the sum of all the nominal load powers. Consequently SOCs converge quicker in the case presented in inset b) of

b)

Figure 6.15 than in the case presented in inset a).

Although this tends to induce excessively high currents at the level of the other batteries making up the system, considering that each module has its own absolute current limitation, that the balancing phase is only momentary and that it is little realistic that such an imbalance occurs during the life of the

satellite, the risk of this inducing complications can be considered negligible compared to the benefit provided.

This property makes it possible to consider reconfiguring the regulation control in multiple ways – in the event of loss of communication for example – but also in the case of a system evolving over time.

The updating or operating mode change phases are critical steps when carried out in operation and it is always preferable to avoid them and this is precisely what this property allows us to avoid.

Indeed, it would be possible in a completely transparent manner, starting from a system comprising only one module, to add elements without the control needing to be structurally updated.

This last observation thus makes it possible to demonstrate that the overall control strategy, obtained in this section thanks to the implementation of its last component, has the same modularity as that sought at the level of the hardware architecture of the system, constraints at the heart of the present study.

6. 6 Conclusion

In this last chapter, after having defined a secondary and tertiary control strategy, the implementation and simulation results of its different components were presented.

This thus made it possible to give an example of what is possible to achieve based on the primary control detailed in the previous chapters and which was at the heart of the developments of this work.

Through this example, the adaptable nature that a global strategy could achieve and the possibility of controlling ever more complex systems from the point of view of the number of equipment, with simple laws were also demonstrated.

The perspectives that this first approach allows us to outline are numerous, which will constitute the subject of future developments to be carried out.

CHAPTER 7.

Conclusions

Summary

To conclude the present thesis, a brief summary of the achieved work is assembled in this ultimate chapter. Subsequently, potential limitations of the presented analysis and proposed solutions are discussed. For each of them, the main assumptions and pieces of resolution are detailed. Last, an overview of the further developments required to complete the work carried out during this PhD thesis is then drawn and the perspectives for their realization are provided.

7. 1 Summary

After having introduced the global context of the study and especially the specificities of the space electrical power systems, a detailed study of the state-of-the-art of those was performed focusing on systems modelling, control and stability analysis. This allowed to understand the main issues and challenges related to the development of distributed and modular power architectures. Especially it showed the importance of the implementation of an appropriate current sharing control when parallelizing voltage sources. In this field, a spotlight has been put on the interest of the droop control for the considered application. In addition, it demonstrated the complexity to adopt an appropriate formalism to study these systems, in particular in terms of stability. Two main obstacles were identified to tackle this challenge: the difficulty encountered to have a comprehensive coverage of the diversity of the systems under study and their nonlinear characteristics in most cases in the first hand, and the lack of methods to model and study the stability of multi-converter systems.

The third chapter has aimed to present the prerequisite for the developments detailed in the rest. Thus, the global guidelines followed to design the control strategy has been presented as well as the study case. In addition to this, individualized solutions to overcome the identified challenges have been proposed per type of systems. Thus, it has been proposed to consider a homogenized power converter model based on the hypothesis that state feedback linearization could be applied on the different converters composing the system. The loads have also been characterized and based on their large-signal characteristics, an analysis has been done to assess how their linearization could allow to simplify the modelling of the overall system for stability analysis purpose without reducing its representativeness. To this end, the key role of the distribution network modelling associated with the Kron reduction was demonstrated. The combination of these methods is one of the main contribution of the present thesis.

These preliminary developments have allowed to study the impact on the stability of the different parameters individually in chapter 4 and more particularly to the droop control parameters. The main interest of the proposed approach is to be able to assess the stability of the system for any possible configuration – and even beyond – by combining the proposed modeling approach with a pseudo Monte Carlo experiment to approximate the root area in the S-plane, thus extending the classical root locus analysis. It has resulted in the definition of some criteria and guidelines to be applied to guarantee the system proper operation.

The experimental demonstrator designed to verify these developments have then been the subject of the fifth chapter. The different modules composing it have thus been introduced with a specific focus on the MOBI which required an important co-design work. Indeed, this module and more particularly the control laws it implements are the real heart of the proposed strategy. Indeed, the MOBI was responsible to implement and execute the whole primary control functions which made of it the cornerstone of the developed demonstrator. The results obtained on this experimental setup, designed as a full scale implementation of the defined use case, have been presented. The observations performed on the different configuration studied have thus allowed to mainly validate the primary control implementation.

Based on this, chapter 6 have completed the definition of the overall control strategy by the proposition of secondary and tertiary control methods to handle the power and energy management of the system. These lasts have been implemented and tested in simulations. As a conclusion it allowed to simulate a completely modular system over a series of orbits. The same performances than the reference system introduced in chapter 3 have been demonstrated while the modularity and reconfigurability of the overall EPS have been significantly enhanced.

7. 2 Discussions

One might notice that in the study of the system's stability, the input voltage of each converter is considered as constant which is not the case when considering actual batteries. In spite of the fact that the proposed homogenized converter model implementing feedback linearization can tackle this fluctuation, the dynamical behavior of the battery side is not addressed by this method. The line serial equivalent inductance in particular plays a predominant role in the transient performances of actual power converters and limits the power steps they are able to handle. This shortcoming has however been considered as negligible in the present work since the power converters are located at the closest to the battery as possible in the propose electrical architecture, thus reducing at its minimum the battery side serial inductance.

In addition to what has been detailed in this manuscript, the work achieved in the present PhD thesis has brought to light many challenges which are still to tackle. Regarding the primary control implementation, and more precisely regarding the droop control, the results observed on the experimental setup have allowed to identify practical limitations to its adaptation, in terms of current sharing accuracy. Even if it allowed to validate the global operation of the method, the intrinsic inner loops performances of the COTS converters integrated to the MOBI did not allow to perform a precise assessment on the reachable performances. Since the phenomenon has been studied and the root cause identified, the implementation and test of the method within the same functional component of the voltage and current inner loops would contribute to enhance the precision thus fully validate the approach. This could be achieved in future developments.

7. 3 Future work

Regarding the secondary and tertiary control, the possibility to develop a MPPT directly by the adaptation of the common bus voltage reference at the MOBI levels, in the same manner than the voltage restoration proposed in Chapter 6, has been imagined during the thesis but, by lack of time, its development has not been undertaken. The interest of such an adaptation would be to be able to optimize the use of the solar panels at the price of small primary bus variations. This would allow to reduce the switching of the BOMO's DET to enhance the power quality, the reduction of the emission of some harmonics in case of strong EMC requirements being an important concern.

The study of complementary control laws by the resolution of optimization problem to better take into account system limitations and operating mode would be an interesting evolution of the tertiary control, enabling to make the system more flexible with regards to abnormal events and thus preventing excessive uses of the FDIR putting the system in safe mode. These methods could make the system more independent to ground supervision required to reconfigure the satellite following an alarm trigger. More generally, it could simply allow a better anticipation of parameter fluctuation such as the loss of solar panels Sun pointing at some phases of the mission. Indeed, the present strategy only focuses on

the nominal operating mode of the satellite and even if it is designed to operate properly for all phases, optimal operation could be reached thanks to these addings.

In addition, the validation of the proposed global control strategy by its implementation in the actual demonstrator would be relevant in order to compare it with more conventional approaches. The scalability it aims to offer could thus be evaluated. In addition, a practical procedure to connect an additional module during operation could be developed and tested. This functionality would be easily implemented with the proposed control architecture since it would mainly consist in an update of the secondary and tertiary control parameters. Moreover, implementing these functionalities would make it possible to use the system in a more representative environment.

The development of the Spaceship FR in the Centre Spatial de Toulouse could offer the opportunity to implement the proposed strategy at the scale of an extra-terrestrial base. This project, initiated by the CNES and the ESA, aims to develop and experiment in real conditions the technologies and competences required to settle on the Moon and explore it. In this frame, 10 major development priorities have been identified, among which the power unit.

In a more conventional approach and shorter term, the CNES initiated in 2023 a dual study with Airbus Defence and Space and Thales Alenia Space to prepare the spatialization of the MOBI following the qualification of the BOMO in the previous years. The interest of developing such modules in every space application such as LEO, GEO missions and even space orbital stations have thus been assessed in order to identify a potential first program to give the proposed distributed and modular electrical power architecture its first space flight.

Bibliography

[1] ESA Space Debris Office, 'ESA's Annual Space Environment Report', ESA, Germany, May 2021.
[2] OECD, *The Space Economy in Figures: How Space Contributes to the Global Economy*. OECD, 2019. doi: 10.1787/c5996201-en.
[3] *LOI n° 2008-518 du 3 juin 2008 relative aux opérations spatiales*. 2008.
[4] Mission Operations Directorate Space Flight Training Division, 'International Space Station Familiarization', National Aeronautics and Space Administration, Houston, Texas, USA, TD9702A, Jul. 1998.
[5] 'Why Space Radiation Matters - NASA'. Accessed: Nov. 11, 2023. [Online]. Available: https://www.nasa.gov/missions/analog-field-testing/why-space-radiation-matters/
[6] 'Radiation: satellites' unseen enemy'. Accessed: Nov. 11, 2023. [Online]. Available: https://www.esa.int/Enabling_Support/Space_Engineering_Technology/Radiation_satellites_unseen_enemy
[7] J. Windsor, M.-H. Deredempt, and R. De-Ferluc, 'Integrated modular avionics for spacecraft — User requirements, architecture and role definition', in *2011 IEEE/AIAA 30th Digital Avionics Systems Conference*, Oct. 2011, pp. 8A6-1-8A6-16. doi: 10.1109/DASC.2011.6096141.
[8] J. Windsor and K. Hjortnaes, 'Time and Space Partitioning in Spacecraft Avionics', in *2009 Third IEEE International Conference on Space Mission Challenges for Information Technology*, Jul. 2009, pp. 13–20. doi: 10.1109/SMC-IT.2009.11.
[9] 'Modularity', *Wikipedia*. Oct. 29, 2023. Accessed: Nov. 08, 2023. [Online]. Available: https://en.wikipedia.org/w/index.php?title=Modularity&oldid=1182500885
[10] V. Frigant and B. Jullien, 'Comment la production modulaire transforme l'industrie automobile', *Rev. Déconomie Ind.*, no. 145, pp. 11–44, 2014, doi: 10.4000/rei.5722.
[11] 'How satellites work', cnes. Accessed: Dec. 19, 2023. [Online]. Available: https://cnes.fr/en/how-satellites-work
[12] Y. K. Tan and S. K. Panda, *Review of Energy Harvesting Technologies for Sustainable WSN*. IntechOpen, 2010. doi: 10.5772/13062.
[13] 'Galileo lithium-ion battery'. Accessed: Dec. 19, 2023. [Online]. Available: https://www.esa.int/ESA_Multimedia/Images/2019/10/Galileo_lithium-ion_battery
[14] 'Sentinel-3 Spacecraft – Copernicus'. Accessed: Dec. 19, 2023. [Online]. Available: https://spaceflight101.com/copernicus/sentinel-3-spacecraft/
[15] Q. Hilpert, S. Caux, F. Bonnet, and M. Malagoli, 'Primary Control and Large-Signal Stability Criteria of an Enhanced Electrical Power System for Space Applications', in *2021 22nd IEEE International Conference on Industrial Technology (ICIT)*, Mar. 2021, pp. 470–475. doi: 10.1109/ICIT46573.2021.9453699.
[16] J. J. Rojas, Y. Takashi, and M. Cho, 'A Lean Satellite Electrical Power System with Direct Energy Transfer and Bus Voltage Regulation Based on a Bi-Directional Buck Converter', *Aerospace*, vol. 7, no. 7, p. 94, Jul. 2020, doi: 10.3390/aerospace7070094.
[17] S.-S. Jang, S.-H. Kim, S.-R. Lee, and J.-H. Choi, 'The Failure Analysis of Paralleled Solar Array Regulator for Satellite Power System in Low Earth Orbit', *J. Astron. Space Sci.*, vol. 28, no. 2, pp. 133–141, Jun. 2011, doi: 10.5140/JASS.2011.28.2.133.
[18] T. Lim, 'A MODULAR ELECTRICAL POWER SYSTEM ARCHITECTURE FOR SMALL SPACECRAFT', *Theses Diss.--Electr. Comput. Eng.*, Jan. 2016, doi: http://dx.doi.org/10.13023/ETD.2016.331.
[19] J. G.-L. Gonzalez-Llorente, A. Andrzej Lidtke, R. Hurtado, and K.-I. Okuyama, 'Single-Bus and Dual-Bus Architectures of Electrical Power Systems for Small Spacecraft', *J. Aerosp. Technol. Manag.*, Oct. 2019, doi: 10.5028/jatm.v11.1086.
[20] Francis Davies, 'Overview of International Space Station Electrical Power System', presented at the EnergyTech 2016, Johnson Space Center, 2016.

[21] K. Watanabe, M. Uesugi, and M. Komatsu, ‘Verification and analysis for small signal stability of Electric Power Systems for the international space station/JEM’, in *INTELEC 2009 - 31st International Telecommunications Energy Conference*, JAXA, Oct. 2009, pp. 1–6. doi: 10.1109/INTLEC.2009.5351765.
[22] E. B. Gietl, E. W. Gholdston, F. Cohen, B. A. Manners, and R. A. Delventhal, ‘The architecture of the electric power system of the International Space Station and its application as a platform for power technology development’, in *Collection of Technical Papers. 35th Intersociety Energy Conversion Engineering Conference and Exhibit (IECEC) (Cat. No.00CH37022)*, Jul. 2000, pp. 855–864 vol.2. doi: 10.1109/IECEC.2000.870884.
[23] E. B. Gietl, Edward W. Gholdston, Bruce A. Manners, and Rex A. Delventhal, ‘The Electric Power System of the International Space Station - A Platform for Power Technology Development’, *NASA*, p. 12, 2000.
[24] M. Nasir, H. A. Khan, A. Hussain, L. Mateen, and N. A. Zaffar, ‘Solar PV-Based Scalable DC Microgrid for Rural Electrification in Developing Regions’, *IEEE Trans. Sustain. Energy*, vol. 9, no. 1, pp. 390–399, Jan. 2018, doi: 10.1109/TSTE.2017.2736160.
[25] S. Konar and A. Ghosh, ‘Interconnection of islanded DC microgrids’, in *2015 IEEE PES Asia-Pacific Power and Energy Engineering Conference (APPEEC)*, Nov. 2015, pp. 1–5. doi: 10.1109/APPEEC.2015.7380986.
[26] S. Augustine, N. Lakshminarasamma, M. K. Mishra, and T. Sreekanth, ‘MPP tracking of PV based low voltage DC microgrid system with adaptive droop algorithm’, in *2015 IEEE 42nd Photovoltaic Specialist Conference (PVSC)*, Jun. 2015, pp. 1–4. doi: 10.1109/PVSC.2015.7356297.
[27] M. Lonkar and S. Ponnaluri, ‘An overview of DC microgrid operation and control’, in *IREC2015 The Sixth International Renewable Energy Congress*, Mar. 2015, pp. 1–6. doi: 10.1109/IREC.2015.7110892.
[28] D. Chen and L. Xu, ‘AC and DC Microgrid with Distributed Energy Resources’, in *Technologies and Applications for Smart Charging of Electric and Plug-in Hybrid Vehicles*, O. Veneri, Ed., Cham: Springer International Publishing, 2017, pp. 39–64. doi: 10.1007/978-3-319-43651-7_2.
[29] J.-M. Pierson *et al.*, ‘DATAZERO: Datacenter With Zero Emission and Robust Management Using Renewable Energy’, *IEEE Access*, vol. 7, pp. 103209–103230, 2019, doi: 10.1109/ACCESS.2019.2930368.
[30] D. Chen and L. Xu, ‘DC microgrid with variable generations and energy storage’, in *IET Conference on Renewable Power Generation (RPG 2011)*, Sep. 2011, pp. 1–6. doi: 10.1049/cp.2011.0167.
[31] E. Hossain, E. Kabalci, R. Bayindir, and R. Perez, ‘Microgrid testbeds around the world: State of art’, *Energy Convers. Manag.*, vol. 86, pp. 132–153, Oct. 2014, doi: 10.1016/j.enconman.2014.05.012.
[32] M. V. Satya Sai Chandra, B. D. B, L. V. Kumar, and S. Mohapatro, ‘Voltage Control and Energy Management of Solar PV fed Stand-alone Low Voltage DC Microgrid for Rural Electrification’, in *2020 21st National Power Systems Conference (NPSC)*, Dec. 2020, pp. 1–6. doi: 10.1109/NPSC49263.2020.9331911.
[33] T. D. Khoa, L. T. Dos Santos, M. Sechilariu, and F. Locment, ‘Load shedding and restoration real-time optimization for DC microgrid power balancing’, in *2016 IEEE International Energy Conference (ENERGYCON)*, Apr. 2016, pp. 1–6. doi: 10.1109/ENERGYCON.2016.7514092.
[34] Y. Krim, M. Sechilariu, F. Locment, and A. Alchami, ‘Global Cost and Carbon Impact Assessment Methodology for Electric Vehicles’ PV-Powered Charging Station’, *Appl. Sci.*, vol. 12, no. 9, Art. no. 9, Jan. 2022, doi: 10.3390/app12094115.
[35] S. Cheikh-Mohamad, M. Sechilariu, F. Locment, and Y. Krim, ‘PV-Powered Electric Vehicle Charging Stations: Preliminary Requirements and Feasibility Conditions’, *Appl. Sci.*, vol. 11, no. 4, Art. no. 4, Jan. 2021, doi: 10.3390/app11041770.
[36] Christian Elisabelar, Cécile Fiachetti, Thierry Jamin, and Laurence Melac, ‘TTVS - Module XIII. Architecture électrique’. CNES.
[37] A. Aho *et al.*, ‘High Efficiency Lattice-Matched 4J Space Solar Cells on GaAs’, in *2019 European Space Power Conference (ESPC)*, Sep. 2019, pp. 1–3. doi: 10.1109/ESPC.2019.8932092.
[38] M. G. Villalva, J. R. Gazoli, and E. R. Filho, ‘Comprehensive Approach to Modeling and Simulation of Photovoltaic Arrays’, *IEEE Trans. Power Electron.*, vol. 24, no. 5, pp. 1198–1208, May 2009, doi: 10.1109/TPEL.2009.2013862.

[39] S. Motahhir, A. E. Ghzizal, and A. Derouich, ‘Modélisation et commande d’un panneau photovoltaïque dans l’environnement PSIM’, Open Science Framework, preprint, Aug. 2019. doi: 10.31219/osf.io/wth8y.
[40] M. G. Villalva, J. R. Gazoli, and E. R. Filho, ‘Modeling and circuit-based simulation of photovoltaic arrays’, in *2009 Brazilian Power Electronics Conference*, Sep. 2009, pp. 1244–1254. doi: 10.1109/COBEP.2009.5347680.
[41] ‘A simple approach to determine the solar cell diode ideality factor under illumination’, *Sol. Energy*, vol. 85, no. 5, pp. 769–775, May 2011, doi: 10.1016/j.solener.2011.01.009.
[42] T. Eshappa, R. Ranjan, and N. D. Ghatpande, ‘Effect of solar cell capacitance and interface cable inductance on the shunt switch current transients in spacecraft power conditioning unit’, in *International Conference on Recent Advances and Innovations in Engineering (ICRAIE-2014)*, May 2014, pp. 1–5. doi: 10.1109/ICRAIE.2014.6909298.
[43] A. Garrigos, J. M. Blanes, J. A. Carrasco, and J. B. Ejea, ‘Influence of the Parasitic Solar Array Capacitance in the Sequential Switching Shunt Series Regulator’, in *MELECON 2006 - 2006 IEEE Mediterranean Electrotechnical Conference*, May 2006, pp. 1198–1201. doi: 10.1109/MELCON.2006.1653316.
[44] P. A. Cotfas, D. T. Cotfas, P. N. Borza, D. Sera, and R. Teodorescu, ‘Solar Cell Capacitance Determination Based on an RLC Resonant Circuit’, *Energies*, vol. 11, no. 3, p. 672, Mar. 2018, doi: 10.3390/en11030672.
[45] A. Jain, S. Sharma, and A. Kapoor, ‘Solar cell array parameters using Lambert W-function’, *Sol. Energy Mater. Sol. Cells*, vol. 90, no. 1, pp. 25–31, Jan. 2006, doi: 10.1016/j.solmat.2005.01.007.
[46] O. Tremblay, L. Dessaint, and A. Dekkiche, ‘A Generic Battery Model for the Dynamic Simulation of Hybrid Electric Vehicles’, in *2007 IEEE Vehicle Power and Propulsion Conference*, Sep. 2007, pp. 284–289. doi: 10.1109/VPPC.2007.4544139.
[47] Cheng Zhang, Walid Allafi, Quang Dinh, Pedro Ascencio, and James Marco, ‘Online estimation of battery equivalent circuit model parameters and state of charge using decoupled least squares technique’, *Energy*, vol. 142, pp. 678–688, Jan. 2018, doi: 10.1016/j.energy.2017.10.043.
[48] J. P. Rivera-Barrera, N. Muñoz-Galeano, and H. O. Sarmiento-Maldonado, ‘SoC Estimation for Lithium-ion Batteries: Review and Future Challenges’, *Electronics*, vol. 6, no. 4, Art. no. 4, Dec. 2017, doi: 10.3390/electronics6040102.
[49] P. Spagnol, S. Rossi, and S. M. Savaresi, ‘Kalman Filter SoC estimation for Li-Ion batteries’, in *2011 IEEE International Conference on Control Applications (CCA)*, Sep. 2011, pp. 587–592. doi: 10.1109/CCA.2011.6044480.
[50] Y. Preger *et al.*, ‘Degradation of Commercial Lithium-Ion Cells as a Function of Chemistry and Cycling Conditions’, *J. Electrochem. Soc.*, vol. 167, no. 12, p. 120532, Sep. 2020, doi: 10.1149/1945-7111/abae37.
[51] F. Leng, C. M. Tan, and M. Pecht, ‘Effect of Temperature on the Aging rate of Li Ion Battery Operating above Room Temperature’, *Sci. Rep.*, vol. 5, no. 1, p. 12967, Oct. 2015, doi: 10.1038/srep12967.
[52] M. Adaikkappan and N. Sathiyamoorthy, ‘Modeling, state of charge estimation, and charging of lithium-ion battery in electric vehicle: A review’, *Int. J. Energy Res.*, vol. 46, no. 3, pp. 2141–2165, 2022, doi: 10.1002/er.7339.
[53] M. S. Ramkumar *et al.*, ‘Review on Li-Ion Battery with Battery Management System in Electrical Vehicle’, *Adv. Mater. Sci. Eng.*, vol. 2022, p. e3379574, May 2022, doi: 10.1155/2022/3379574.
[54] M. S. Hossain Lipu *et al.*, ‘Intelligent algorithms and control strategies for battery management system in electric vehicles: Progress, challenges and future outlook’, *J. Clean. Prod.*, vol. 292, p. 126044, Apr. 2021, doi: 10.1016/j.jclepro.2021.126044.
[55] J. Ben Salah, C. Valentin, H. Jerbi, and C. Z. Xu, ‘Geometric synthesis of a hybrid limit cycle for the stabilizing control of a class of nonlinear switched dynamical systems’, *Syst. Control Lett.*, vol. 60, no. 12, pp. 967–976, Dec. 2011, doi: 10.1016/j.sysconle.2011.08.005.
[56] V. Choudhary, T. Hegarty, and D. Pace, ‘Under the hood of a noninverting buck-boost converter’, p. 25, 2016.
[57] Q. Ullah, X. Wu, and U. Saleem, ‘Current Controlled Robust Four-Switch Buck-Boost DC-DC Converter’, in *2021 International Conference on Computing, Electronic and Electrical Engineering (ICE Cube)*, Oct. 2021, pp. 1–6. doi: 10.1109/ICECube53880.2021.9628275.

[58] J.-K. Shiau and C.-W. Ma, 'Li-Ion Battery Charging with a Buck-Boost Power Converter for a Solar Powered Battery Management System', *Energies*, vol. 6, no. 3, Art. no. 3, Mar. 2013, doi: 10.3390/en6031669.
[59] K. P. Vijayaragavan, 'Feasibility of DC microgrids for rural electrification', European Solar Engineering School, 2017. Accessed: Mar. 29, 2019. [Online]. Available: http://urn.kb.se/resolve?urn=urn:nbn:se:du-25850
[60] L. Kunjumuhammed, S. Kuenzel, and B. Pal, *Simulation of power system with renewables*. London: Academic press, 2020.
[61] Yue Song, David J. Hill, and Tao Liu, 'The optimal admittance matrix problem in DC networks', *Electr. Power Syst. Res.*, vol. 189, p. 106754, Dec. 2020, doi: 10.1016/j.epsr.2020.106754.
[62] G. De Carne *et al.*, 'Which Deepness Class Is Suited for Modeling Power Electronics?: A Guide for Choosing the Right Model for Grid-Integration Studies', *IEEE Ind. Electron. Mag.*, vol. 13, no. 2, pp. 41–55, Jun. 2019, doi: 10.1109/MIE.2019.2909799.
[63] J. M. Guerrero, J. C. Vasquez, J. Matas, L. G. de Vicuna, and M. Castilla, 'Hierarchical Control of Droop-Controlled AC and DC Microgrids—A General Approach Toward Standardization', *IEEE Trans. Ind. Electron.*, vol. 58, no. 1, pp. 158–172, Jan. 2011, doi: 10.1109/TIE.2010.2066534.
[64] O. Palizban and K. Kauhaniemi, 'Hierarchical control structure in microgrids with distributed generation: Island and grid-connected mode', *Renew. Sustain. Energy Rev.*, vol. 44, pp. 797–813, Apr. 2015, doi: 10.1016/j.rser.2015.01.008.
[65] A.-C. Braitor, G. Konstantopoulos, and V. Kadirkamanathan, 'Stability analysis of DC micro-grids with CPLs under novel decentralized primary and distributed secondary control', *Automatica*, vol. 139, p. 110187, May 2022, doi: 10.1016/j.automatica.2022.110187.
[66] C. Ciurans, N. Bazmohammadi, J. C. Vasquez, C. G. Dussap, J. Guerrero, and F. Gòdia, 'Hierarchical Control of Space Closed Ecosystems – Expanding Microgrid Concepts to Bioastronautics', *E E E Ind. Electron. Mag.*, 2020, Accessed: Sep. 23, 2020. [Online]. Available: https://vbn.aau.dk/en/publications/hierarchical-control-of-space-closed-ecosystems-expanding-microgr
[67] D. Burmester, R. Rayudu, W. Seah, and D. Akinyele, 'A review of nanogrid topologies and technologies', *Renew. Sustain. Energy Rev.*, vol. 67, pp. 760–775, Jan. 2017, doi: 10.1016/j.rser.2016.09.073.
[68] Y. Gu, X. Xiang, W. Li, and X. He, 'Mode-Adaptive Decentralized Control for Renewable DC Microgrid With Enhanced Reliability and Flexibility', *IEEE Trans. Power Electron.*, vol. 29, no. 9, pp. 5072–5080, Sep. 2014, doi: 10.1109/TPEL.2013.2294204.
[69] R. O. de Magalhães and H. J. P. Moreira, 'Space Power Topology Selection and its System Level Modeling and Control', 2020.
[70] C. Ezio *et al.*, 'Electrical Power Subsystem for the Euclid Spacecraft', 2017.
[71] F. Gao, R. Kang, J. Cao, and T. Yang, 'Primary and secondary control in DC microgrids: a review', *J. Mod. Power Syst. Clean Energy*, vol. 7, no. 2, pp. 227–242, Mar. 2019, doi: 10.1007/s40565-018-0466-5.
[72] S. Bacha, I. Munteanu, and A. I. Bratcu, *Power Electronic Converters Modeling and Control: with Case Studies*. in Advanced Textbooks in Control and Signal Processing. London: Springer London, 2014.
[73] F. Otoofi, M. H. Asemani, and N. Vafamand, 'Polytopic-LPV Robust Control of Power Systems Connected to Renewable Energy Sourcess', in *2019 6th International Conference on Control, Instrumentation and Automation (ICCIA)*, Oct. 2019, pp. 1–6. doi: 10.1109/ICCIA49288.2019.9030956.
[74] M. R. Asadi and M. H. Kazemi, 'Robust State-Feedback Local Voltage Control for Islanded Uncertain DC Microgrids Using LPV Modeling', in *2023 9th International Conference on Control, Instrumentation and Automation (ICCIA)*, Dec. 2023, pp. 1–7. doi: 10.1109/ICCIA61416.2023.10506399.
[75] R. A. F. Ferreira, H. A. C. Braga, A. A. Ferreira, and P. G. Barbosa, 'Analysis of voltage droop control method for dc microgrids with Simulink: Modelling and simulation', in *2012 10th IEEE/IAS International Conference on Industry Applications*, Nov. 2012, pp. 1–6. doi: 10.1109/INDUSCON.2012.6452563.

[76] W. Chen, 'High Efficiency, High Density, PolyPhase Converters for High Current Applications'. Linear Technology, Sep. 1999.
[77] Y. Huang and C. K. Tse, 'Circuit Theoretic Classification of Parallel Connected DC–DC Converters', *IEEE Trans. Circuits Syst. Regul. Pap.*, vol. 54, no. 5, pp. 1099–1108, May 2007, doi: 10.1109/TCSI.2007.890631.
[78] and and, 'A novel droop method for converter parallel operation', *IEEE Trans. Power Electron.*, vol. 17, no. 1, pp. 25–32, Jan. 2002, doi: 10.1109/63.988666.
[79] Shiguo Luo, Zhihong Ye, Ray-Lee Lin, and F. C. Lee, 'A classification and evaluation of paralleling methods for power supply modules', in *30th Annual IEEE Power Electronics Specialists Conference. Record. (Cat. No.99CH36321)*, Jul. 1999, pp. 901–908 vol.2. doi: 10.1109/PESC.1999.785618.
[80] 'Current Sharing', sunpower-uk.com. Accessed: Nov. 26, 2019. [Online]. Available: https://www.sunpower-uk.com/glossary/what-is-current-sharing/
[81] P. Liu, P. Huang, W. Xiao, H. H. Zeineldin, and M. Elmoursi, 'Improved digital average current sharing control strategy for DC microgrids', in *IECON 2014 - 40th Annual Conference of the IEEE Industrial Electronics Society*, Oct. 2014, pp. 4300–4305. doi: 10.1109/IECON.2014.7049149.
[82] S. K. Mazumder, M. Tahir, and K. Acharya, 'Master–Slave Current-Sharing Control of a Parallel DC–DC Converter System Over an RF Communication Interface', *IEEE Trans. Ind. Electron.*, vol. 55, no. 1, pp. 59–66, Jan. 2008, doi: 10.1109/TIE.2007.896138.
[83] S. Baek, Y. Cho, and T. Koo, 'Average Current Sharing Control Strategy for Parallel Operation of UPS with Low Bandwidth Communication', in *2019 IEEE Applied Power Electronics Conference and Exposition (APEC)*, Mar. 2019, pp. 2445–2451. doi: 10.1109/APEC.2019.8721793.
[84] M. A. Bianchi, I. G. Zurbriggen, M. Ordonez, and M. Anun, 'Dynamic performance improvement of DC microgrids during Constant-Power Load transients', in *2016 IEEE 7th International Symposium on Power Electronics for Distributed Generation Systems (PEDG)*, Jun. 2016, pp. 1–6. doi: 10.1109/PEDG.2016.7527100.
[85] R. A. F. Ferreira, H. A. C. Braga, A. A. Ferreira, and P. G. Barbosa, 'Analysis of voltage droop control method for dc microgrids with Simulink: Modelling and simulation', in *2012 10th IEEE/IAS International Conference on Industry Applications*, Fortaleza, CE, Brazil: IEEE, Nov. 2012, pp. 1–6. doi: 10.1109/INDUSCON.2012.6452563.
[86] W. W. Weaver, R. D. Robinett, G. G. Parker, and D. G. Wilson, 'Energy storage requirements of dc microgrids with high penetration renewables under droop control', *Int. J. Electr. Power Energy Syst.*, vol. 68, pp. 203–209, Jun. 2015, doi: 10.1016/j.ijepes.2014.12.070.
[87] T. Dragičević, J. M. Guerrero, J. C. Vasquez, and D. Škrlec, 'Supervisory Control of an Adaptive-Droop Regulated DC Microgrid With Battery Management Capability', *IEEE Trans. Power Electron.*, vol. 29, no. 2, pp. 695–706, Feb. 2014, doi: 10.1109/TPEL.2013.2257857.
[88] X. Lu, J. M. Guerrero, K. Sun, and J. C. Vasquez, 'An Improved Droop Control Method for DC Microgrids Based on Low Bandwidth Communication With DC Bus Voltage Restoration and Enhanced Current Sharing Accuracy', *IEEE Trans. Power Electron.*, vol. 29, no. 4, pp. 1800–1812, Apr. 2014, doi: 10.1109/TPEL.2013.2266419.
[89] W. Jiang, J. Zhao, K. Qu, L. Mao, Y. Zhu, and H. Liu, 'An Enhanced Drop Control Method for DC Microgrids with Accurate Current Sharing and DC Bus Voltage Restoration', in *2019 4th International Conference on Intelligent Green Building and Smart Grid (IGBSG)*, Sep. 2019, pp. 727–731. doi: 10.1109/IGBSG.2019.8886270.
[90] M. Mosayebi, S. M. Sadeghzadeh, M. H. Khooban, and J. M. Guerrero, 'Decentralised non-linear I–V droop control to improve current sharing and voltage restoration in DCNG clusters', *IET Power Electron.*, vol. 13, no. 2, pp. 248–255, 2020, doi: 10.1049/iet-pel.2019.0263.
[91] A. D. Bintoudi, C. Timplalexis, G. Mendes, J. M. Guerrero, and C. Demoulias, 'Design of Space Microgrid for Manned Lunar Base: Spinning-in Terrestrial Technologies', in *Aalborg University's Research Portal*, IEEE Signal Processing Society, Sep. 2019, p. 8932024. doi: 10.1109/ESPC.2019.8932024.
[92] M. Cousineau and B. Cougo, 'Interleaved converter with massive parallelization of high frequency GaN switching-cells using decentralized modular analog controller', in *2015 IEEE Energy Conversion Congress and Exposition (ECCE)*, Sep. 2015, pp. 4343–4350. doi: 10.1109/ECCE.2015.7310274.

[93] J. Hu, J. Duan, H. Ma, and M. Chow, 'Distributed Adaptive Droop Control for Optimal Power Dispatch in DC Microgrid', *IEEE Trans. Ind. Electron.*, vol. 65, no. 1, pp. 778–789, Jan. 2018, doi: 10.1109/TIE.2017.2698425.
[94] G. Tian, Y. Zheng, G. Liu, and J. Zhang, 'SOC Balancing and Coordinated Control Based on Adaptive Droop Coefficient Algorithm for Energy Storage Units in DC Microgrid', *Energies*, vol. 15, no. 8, Art. no. 8, Jan. 2022, doi: 10.3390/en15082943.
[95] Z. Cheng *et al.*, 'A novel cascaded control to improve stability and inertia of parallel buck-boost converters in DC microgrid', *Int. J. Electr. Power Energy Syst.*, vol. 119, p. 105950, Jul. 2020, doi: 10.1016/j.ijepes.2020.105950.
[96] F. Chen, R. Burgos, D. Boroyevich, J. C. Vasquez, and J. M. Guerrero, 'Investigation of Nonlinear Droop Control in DC Power Distribution Systems: Load Sharing, Voltage Regulation, Efficiency, and Stability', *IEEE Trans. Power Electron.*, vol. 34, no. 10, pp. 9404–9421, Oct. 2019, doi: 10.1109/TPEL.2019.2893686.
[97] S. Whaite, B. Grainger, and A. Kwasinski, 'Power Quality in DC Power Distribution Systems and Microgrids', *Energies*, vol. 8, no. 5, Art. no. 5, May 2015, doi: 10.3390/en8054378.
[98] N. Khosravi, A. Abdolvand, A. Oubelaid, Y. A. Khan, M. Bajaj, and S. Govender, 'Improvement of power quality parameters using modulated-unified power quality conditioner and switched-inductor boost converter by the optimization techniques for a hybrid AC/DC microgrid', *Sci. Rep.*, vol. 12, no. 1, Art. no. 1, Dec. 2022, doi: 10.1038/s41598-022-26001-8.
[99] 'Passive Current Sharing Boosts Power and Reliability', Power Electronics. Accessed: Nov. 26, 2019. [Online]. Available: https://www.powerelectronics.com/content/passive-current-sharing-boosts-power-and-reliability
[100] ESA Requirements and Standards Section, 'ECSS-E-ST-20C Rev.2 – Electrical and electronic', ECSS, Noordwijk, The Netherlands, Apr. 2022.
[101] S. Anand, B. G. Fernandes, and J. Guerrero, 'Distributed Control to Ensure Proportional Load Sharing and Improve Voltage Regulation in Low-Voltage DC Microgrids', *IEEE Trans. Power Electron.*, vol. 28, no. 4, pp. 1900–1913, Apr. 2013, doi: 10.1109/TPEL.2012.2215055.
[102] P. Wang, X. Lu, X. Yang, W. Wang, and D. Xu, 'An Improved Distributed Secondary Control Method for DC Microgrids With Enhanced Dynamic Current Sharing Performance', *IEEE Trans. Power Electron.*, vol. 31, no. 9, pp. 6658–6673, Sep. 2016, doi: 10.1109/TPEL.2015.2499310.
[103] A. Bratcu, I. Munteanu, B. Seddik, and B. Raison, 'Maximum Power Point Tracking of Grid-connected Photovoltaic Arrays by sing Extremum Seeking Control', *J. Control Eng. Appl. Inform.*, vol. 10, pp. 3–12, Dec. 2008.
[104] J. Chai and Y. Peng, 'Coordinated Power Control for Islanded DC Microgrids Based on Bus-Signaling and Fuzzy Logic Control', in *2018 2nd IEEE Conference on Energy Internet and Energy System Integration (EI2)*, Oct. 2018, pp. 1–6. doi: 10.1109/EI2.2018.8581985.
[105] B. Bendib, H. Belmili, and F. Krim, 'A survey of the most used MPPT methods: Conventional and advanced algorithms applied for photovoltaic systems', *Renew. Sustain. Energy Rev.*, vol. 45, no. C, pp. 637–648, 2015.
[106] K. Hwang, K. Lee, and I. Kim, 'A High Speed Solar MPPT Controller Design', IEEE, Jun. 2019, pp. 1029–1034. doi: 10.1109/ISIE.2019.8781420.
[107] D. Ryu, Y. Kim, and H. Kim, 'Optimum MPPT Control Period for Actual Insolation Condition', in *2018 IEEE International Telecommunications Energy Conference (INTELEC)*, Oct. 2018, pp. 1–4. doi: 10.1109/INTLEC.2018.8612419.
[108] Z. Xuan, K. Qing, Y. Wentao, X. Jie, L. Feng, and Y. Xiangan, 'Power Assessment Indices of Solar Arrays under MPPT and DET methods for Spacecraft', in *2019 European Space Power Conference (ESPC)*, Sep. 2019, pp. 1–4. doi: 10.1109/ESPC.2019.8932076.
[109] M. K. K. Reddy and V. Sarkar, 'LPPT control of a photovoltaic system against sudden drop of irradiance', in *2017 6th International Conference on Computer Applications In Electrical Engineering-Recent Advances (CERA)*, Oct. 2017, pp. 562–567. doi: 10.1109/CERA.2017.8343391.
[110] P Bala Sai Kiran, 'Limited Power Control of a Grid Connected Photovoltaic System', masters, Indian Institute of Technology Hyderabad, 2015. Accessed: Aug. 26, 2020. [Online]. Available: http://raiith.iith.ac.in/1672/

[111] A.-C. Braitor, *Advanced Hierarchical Control and Stability Analysis of DC Microgrids*. in Springer Theses. Cham: Springer International Publishing, 2022. doi: 10.1007/978-3-030-95415-4.
[112] M. M. Hoque, M. A. Hannan, and A. Mohamed, 'Optimal CC-CV charging of lithium-ion battery for charge equalization controller', in *2016 International Conference on Advances in Electrical, Electronic and Systems Engineering (ICAEES)*, Nov. 2016, pp. 610–615. doi: 10.1109/ICAEES.2016.7888119.
[113] S. Sepasi, 'Adaptive state of charge estimation for battery packs', 2014. doi: 10.13140/RG.2.1.4737.5209.
[114] Michael. J. Lain and E. Kendrick, 'Understanding the limitations of lithium ion batteries at high rates', *J. Power Sources*, vol. 493, p. 229690, May 2021, doi: 10.1016/j.jpowsour.2021.229690.
[115] E. Wikner and T. Thiringer, 'Extending Battery Lifetime by Avoiding High SOC', *Appl. Sci.*, vol. 8, no. 10, Art. no. 10, Oct. 2018, doi: 10.3390/app8101825.
[116] Y. Chen, E. Macii, and M. Poncino, 'Workload-driven frequency-aware battery sizing', Jul. 2017. doi: 10.1109/ISLPED.2017.8009196.
[117] L. Gao, Y. Liu, H. Ren, and J. Guerrero, 'A DC Microgrid Coordinated Control Strategy Based on Integrator Current-Sharing', *Energies*, vol. 10, p. 1116, Aug. 2017, doi: 10.3390/en10081116.
[118] C. Yin, H. Wu, M. Sechilariu, and F. Locment, 'Power Management Strategy for an Autonomous DC Microgrid', *Appl. Sci.*, vol. 8, p. 2202, Nov. 2018, doi: 10.3390/app8112202.
[119] M. Sechilariu, B. C. Wang, F. Locment, and A. Jouglet, 'DC microgrid power flow optimization by multi-layer supervision control. Design and experimental validation', *Energy Convers. Manag.*, vol. 82, pp. 1–10, Jun. 2014, doi: 10.1016/j.enconman.2014.03.010.
[120] M. Sechilariu, B. Wang, and F. Locment, 'Power management and optimization for isolated DC microgrid', in *Automation and Motion 2014 International Symposium on Power Electronics, Electrical Drives*, Jun. 2014, pp. 1284–1289. doi: 10.1109/SPEEDAM.2014.6872087.
[121] B. Robyns, A. Davigny, and C. Saudemont, 'Methodologies for supervision of Hybrid Energy Sources based on Storage Systems – A survey', *Math. Comput. Simul.*, vol. 91, pp. 52–71, May 2013, doi: 10.1016/j.matcom.2012.06.014.
[122] S. Cheikh-Mohamad, M. Sechilariu, and F. Locment, 'Real-Time Power Management Including an Optimization Problem for PV-Powered Electric Vehicle Charging Stations', *Appl. Sci.*, vol. 12, no. 9, Art. no. 9, Jan. 2022, doi: 10.3390/app12094323.
[123] L. T. Dos Santos, M. Sechilariu, and F. Locment, 'Prediction-based optimization for islanded microgrid resources scheduling and management', in *2015 IEEE 24th International Symposium on Industrial Electronics (ISIE)*, Jun. 2015, pp. 760–765. doi: 10.1109/ISIE.2015.7281564.
[124] W. Bai, M. Sechilariu, and F. Locment, 'On-grid/off-grid DC microgrid optimization and demand response management', in *2020 22nd European Conference on Power Electronics and Applications (EPE'20 ECCE Europe)*, Sep. 2020, pp. 1–10. doi: 10.23919/EPE20ECCEEurope43536.2020.9215679.
[125] M. Sechilariu, 'Intelligent Energy Management of Electrical Power Systems', *Appl. Sci.*, vol. 10, no. 8, Art. no. 8, Jan. 2020, doi: 10.3390/app10082951.
[126] M. Sechilariu, F. Locment, and L. T. D. Santos, 'A conceptual framework for full optimal operation of a grid-connected DC microgrid', in *2018 IEEE International Conference on Industrial Electronics for Sustainable Energy Systems (IESES)*, Jan. 2018, pp. 296–301. doi: 10.1109/IESES.2018.8349892.
[127] L. Bakule, 'Decentralized control: An overview', *Annu. Rev. Control*, vol. 32, no. 1, pp. 87–98, Apr. 2008, doi: 10.1016/j.arcontrol.2008.03.004.
[128] N. Yang, 'Control and analysis of DC Microgrid with multiple distributed generators', phdthesis, Université de Technologie de Belfort-Montbeliard, 2015. Accessed: Mar. 29, 2019. [Online]. Available: https://tel.archives-ouvertes.fr/tel-01875402/document
[129] A.-C. Braitor, G. Konstantopoulos, and V. Kadirkamanathan, 'Admittance matrix computation and stability analysis of droop controlled DC micro-grids with CPL', Feb. 2020.
[130] L. Meng, T. Dragicevic, J. C. Vasquez, and J. M. Guerrero, 'Tertiary and Secondary Control Levels for Efficiency Optimization and System Damping in Droop Controlled DC–DC Converters', *IEEE Trans. Smart Grid*, vol. 6, no. 6, pp. 2615–2626, Nov. 2015, doi: 10.1109/TSG.2015.2435055.

[131] M. Car, M. Vasak, and V. Lesic, ‘Control of a buck-boost DC-DC power converter for microgrid energy storage’, in *2017 19th International Conference on Electrical Drives and Power Electronics (EDPE)*, Dubrovnik: IEEE, Oct. 2017, pp. 122–127. doi: 10.1109/EDPE.2017.8123267.
[132] H. Zhu and D. Zhang, ‘Design Considerations of Sequential Switching Shunt Regulator for High-Power Applications’, *IEEE Trans. Ind. Electron.*, vol. 67, no. 11, pp. 9358–9369, Nov. 2020, doi: 10.1109/TIE.2019.2956403.
[133] Suresh Singh, Aditya R. Gautam, and Deepak Fulwani, ‘Constant power loads and their effects in DC distributed power systems: A review’, *Renew. Sustain. Energy Rev.*, vol. 72, pp. 407–421, May 2017, doi: 10.1016/j.rser.2017.01.027.
[134] W. Du, J. Zhang, Y. Zhang, and Z. Qian, ‘Stability Criterion for Cascaded System With Constant Power Load’, *IEEE Trans. Power Electron.*, vol. 28, no. 4, pp. 1843–1851, Apr. 2013, doi: 10.1109/TPEL.2012.2211619.
[135] M. Charrada, H. Piquet, N. Roux, and E. Bru, ‘Stability analysis of DC networks: Coupling phenomenon between equipment connected to a single DC bus’, in *2013 IEEE 11th International Workshop of Electronics, Control, Measurement, Signals and their application to Mechatronics*, Jun. 2013, pp. 1–7. doi: 10.1109/ECMSM.2013.6648965.
[136] F. Gao, S. Bozhko, S. Yeoh, G. Asher, and P. Wheeler, ‘Stability of multi-source droop-controlled Electrical Power System for more-electric aircraft’, in *2014 IEEE International Conference on Intelligent Energy and Power Systems (IEPS)*, Jun. 2014, pp. 122–126. doi: 10.1109/IEPS.2014.6874163.
[137] M. S. Sadabadi, A. Karimi, and H. Karimi, ‘Fixed-order decentralized/distributed control of islanded inverter-interfaced microgrids’, *Control Eng. Pract.*, vol. 45, pp. 174–193, Dec. 2015, doi: 10.1016/j.conengprac.2015.09.003.
[138] Y. Li *et al.*, ‘Stability Analysis and Location Optimization Method for Multiconverter Power Systems Based on Nodal Admittance Matrix’, *IEEE J. Emerg. Sel. Top. Power Electron.*, vol. 9, no. 1, pp. 529–538, Feb. 2021, doi: 10.1109/JESTPE.2019.2954560.
[139] Universidad Tecnológica de Pereira and A. Garcés-Ruíz, ‘Small-signal stability analysis of DC microgrids considering electric vehicles’, *Rev. Fac. Ing. Univ. Antioquia*, no. 89, pp. 52–58, 2018, doi: 10.17533/udea.redin.n89a07.
[140] B. H. Cho, J. R. Lee, and F. C. Y. Lee, ‘Large-signal stability analysis of spacecraft power processing systems’, *IEEE Trans. Power Electron.*, vol. 5, no. 1, pp. 110–116, Jan. 1990, doi: 10.1109/63.46005.
[141] M. A. Bianchi, I. G. Zurbriggen, F. Paz, and M. Ordonez, ‘Improving DC Microgrid Dynamic Performance Using a Fast State-Plane-Based Source-End Controller’, *IEEE Trans. Power Electron.*, vol. 34, no. 8, pp. 8062–8078, Aug. 2019, doi: 10.1109/TPEL.2018.2878383.
[142] A. Tahim, D. Pagano, E. Lenz, and V. Stramosk, ‘Modeling and Stability Analysis of Islanded DC Microgrids Under Droop Control’, *Power Electron. IEEE Trans. On*, vol. 30, pp. 4597–4607, Aug. 2015, doi: 10.1109/TPEL.2014.2360171.
[143] J.-J. E. Slotine and W. Li, *Applied nonlinear control*. Englewood Cliffs, N.J: Prentice Hall, 1991.
[144] M. Cupelli, L. Zhu, and A. Monti, ‘Why Ideal Constant Power Loads Are Not the Worst Case Condition From a Control Standpoint’, *IEEE Trans. Smart Grid*, vol. 6, no. 6, pp. 2596–2606, Nov. 2015, doi: 10.1109/TSG.2014.2361630.
[145] F. A. Kassab, B. Celik, F. Locment, M. Sechilariu, and T. M. Hansen, ‘Combined Optimal Sizing and Energy Management of a DC Microgrid using MILP’, in *2023 IEEE Belgrade PowerTech*, Jun. 2023, pp. 1–6. doi: 10.1109/PowerTech55446.2023.10202939.
[146] M. Huguenin *et al.*, ‘Statistical Sizing of a Satellite Power Subsystem’, in *2023 13th European Space Power Conference (ESPC)*, Oct. 2023, pp. 1–6. doi: 10.1109/ESPC59009.2023.10298153.
[147] P. Landiech, ‘Overview on CNES Micro and Mini Satellites Missions : In Flight, Under Development and Next’, p. 8, Aug. 2008.
[148] Q. Hilpert, S. Caux, F. Bonnet, and M. Malagoli, ‘SPACE Grid: Smart and distributed Power Architecture and Control for Electrical Grid’, in *2019 European Space Power Conference (ESPC)*, Sep. 2019, pp. 1–6. doi: 10.1109/ESPC.2019.8932030.

[149] F. P. Priya and K. Latha, ‘Feedback Linearization Control of Boost Converter’, in *2019 2nd International Conference on Intelligent Computing, Instrumentation and Control Technologies (ICICICT)*, Jul. 2019, pp. 169–173. doi: 10.1109/ICICICT46008.2019.8993341.
[150] H. Zheng and D. Shuai, ‘Nonlinear control of Boost converter by state feedback exact linearization’, in *2012 24th Chinese Control and Decision Conference (CCDC)*, May 2012, pp. 3502–3506. doi: 10.1109/CCDC.2012.6244559.
[151] A. Trias and J. L. Marín, ‘The Holomorphic Embedding Loadflow Method for DC Power Systems and Nonlinear DC Circuits’, *IEEE Trans. Circuits Syst. Regul. Pap.*, vol. 63, no. 2, pp. 322–333, Feb. 2016, doi: 10.1109/TCSI.2015.2512723.
[152] G. Kron, ‘Tensor analysis of networks’, 1939. doi: 10.2307/3613666.
[153] F. Dorfler and F. Bullo, ‘Kron Reduction of Graphs With Applications to Electrical Networks’, *IEEE Trans. Circuits Syst. Regul. Pap.*, vol. 60, no. 1, pp. 150–163, Jan. 2013, doi: 10.1109/TCSI.2012.2215780.
[154] C. Sinibaldi, P. Spizzi, F. Bonnet, and B. Vella, ‘BOMO : Modular Boxes for a Modular Architecture’, *12th European Space Power Conference*, Juan-les-Pins, in press.
[155] Bruno Vella, François Bonnet, Lionel Perret, and Pierre Spizzi, ‘SPECIFICATION TECHNIQUE DU BESOIN BOitiers MOdulaires BOMO’. Aug. 10, 2018.
[156] C. Sinibaldi, B. Vella, F. Bonnet, and P. Spizzi, ‘Modular Boxes for a Modular Architecture’, in *Small Satellite Conference*, Logan, Utah, USA, Aug. 2019.
[157] F. BONNET, P. BOAN, and Q. HILPERT, ‘Smart Battery Modules for Distributed Electrical Power Systems’, in *2023 13th European Space Power Conference (ESPC)*, Oct. 2023, pp. 1–7. doi: 10.1109/ESPC59009.2023.10298144.
[158] ESA Requirements and Standards Section, ‘ECSS-E-ST-50-15’, ECSS, Noordwijk, The Netherlands, Mar. 2011.
[159] Robert Bosch GmbH, ‘CAN Specification Version 2.0’, Stuttgart, 1991.

Annexe

A 1. Use case definition

The definition of a consistent use case was essential in order to apply the developments done in the present thesis to it, without going into the practical details of their implementation, e.g. the parallel-serial configuration of the solar array or the different ageing phenomena.

A.1. 1 Mission orbit

The type of orbit of the mission is the original parameter since all the others depend on it. It is usually chosen according to the operational objective of the mission but in the present case the scenario of a LEO orbit mission is chosen. At an average altitude of 400 kilometers, it corresponds to the most common orbit for current and future missions. The environmental characteristics of the LEO orbit are listed in the table below.

Table 0.1 - Low Earth Orbit characteristics.

Variables	Values	Units
Altitude range	[370 ; 460]	km
Inclination	51.6	deg
Orbit period of which day of which eclipse	93 62 31	min
Solar flux average	1370	$W.m^{-2}$
External temperature range	[-170 ; 125]	°C

A.1. 2 Power consumption and bus voltage

The choice of payload is generally intrinsically linked to the choice of orbit, and therefore the main part of the satellite's power budget is derived from it.

Without placing ourselves in a consumption scenario corresponding precisely to a given type of mission – such as earth observation or telecommunication LEO satellites – it is possible to draw some broad characteristics on what is most often encountered at these orbits. Typical power consumption profiles are often composed of a constant component and a variable one. The constant component corresponds to the basic power consumption needed by the overall system to operate properly, payload and platform combined, and also corresponds to the safe mode power consumption. This permanent consumption is due to every electronic circuits which are constantly operating such as the AOCS, the CDH or the heaters of the thermal control. Even if the consumption of these lasts can slightly vary depending on the satellite’s exposure to the sun, they only induce a little ripple of the power consumption as thermal aspects are relatively slow compared to other – electrical – phenomena. The variable component of the power consumption is induced by the sub-systems whose mission requires them to respond to specific events, mostly related to the location of the spacecraft in its orbit.

These considerations, based on the study of actual systems telemetry, allow to determine the power consumption budget of the different equipment given in the table below.

Table 0.2 - Use-case power consumption profile.

Equipment	Power consumption (W)		Duration (min) (if applicable)	
Constant power consumption	P_{const}	60	-	-
Thermal control*	P_{th}	40 ±20% at a 5 min period	-	-
Imagery system shooting	P_{sh}	70	T_{sh}	20
Telemetry	P_{tm}	55	T_{tm}	5

It can then be calculated that the average power consumption of the study-case during a whole orbit P_{avg} is about 110 watts and that the maximum output power P_{max} reaches 230 watts which is equivalent to a Myriade platform These values are the main constraints to size the rest of the EPS, but nevertheless, have to be coupled with secondary constraints which are related to the chosen power terminals.

Thus, as described in Chapter 3, for a regulated bus voltage of 28V, the maximum specified power is 1500W, which is sufficient for the determined power budget and justifies the choice of this value for the present use case.

Of course, there is nothing to prevent the choice of a higher bus voltage, and this is increasingly the case since, in addition to reducing losses, it allows us to get closer to the operating voltages of certain equipment such as plasma propulsion units (PPU).

A.1. 3 Cycled energy and global battery capacity

Based on the power budget, it is possible to calculate the cycled energy i.e. the energy to be accumulated during the day to supply the satellite during eclipses, the PV being out of service during this period of time:

$$E_{cycled} = \int P_{night}.dt = P_{night} \cdot T_{night} \quad 0.1$$

In a first approximation, it can be considered that the power consumption during the night P_{night} equals the average power consumption P_{avg}determined earlier which induces a proportional relation between the power consumption and the duration of the eclipse. But the resulting value would not take into account the distribution of the power demand between the night and the day, which may be different from one orbit to another. In actual systems, a margin of about 10% is thus included to P_{avg} to cover the worst case of power consumptions.

$$E_{cycled} = P_{avg} \cdot T_{night} \cdot margin \quad 0.2$$

$$E_{cycled} \approx 65.5\ W.h \quad 0.3$$

Then, based on the considerations presented in the previous chapter regarding the maximal DOD of 20% to optimize battery ageing, the global required energy capacity of the battery pack E_{req} can be calculated:

$$E_{req} = \frac{E_{cycled}}{DOD} \approx 328\, W.h \qquad 0.4$$

In order to be consistent with both non-regulated and fully regulated bus architectures, the considered battery nominal voltage is equal to the bus voltage i.e. 28 volts – which typically corresponds to an 8S battery considering standard 18650 cells. It is then possible to determine the battery pack capacity:

$$C_{req} = \frac{E_{req}}{V_{nom}} \approx 12\, A.h \qquad 0.5$$

Nevertheless, when dealing with fully regulated architectures, in which the voltages could not be the same at every stages, it is more relevant to consider the battery capacity as an energy and it is notably considering the energy that the solar panels are sized.

A.1. 4 Power production and Solar array sizing

The total power generation capacity needs to overcome ~~to~~ the loads power consumption as well as the required power to charge the batteries with the aim of ensuring that all batteries are charged properly at the end of the illumination phase, in accordance to the DOD. As expressed by the following equation, this is equivalent to store the same amount of energy which is needed during the night.

$$P_{REQ} = P_{avg} + \frac{E_{cycled}}{T_{day}} \approx 205\, W \qquad 0.6$$

The minimum number of sections which is required can thus be calculated, based on the worst case power production of a single section. This last parameter is highly variable since the photovoltaic cells do not have the same level of standardization than the battery cells and that it is very dependent on the chosen technology.

Thus, in the same manner than for the battery, in order to be compatible with the main conditioning systems without any a priori, the PV sections are determined so the primary bus voltage is always below their maximum power point and so that they can be considered as current sources. Then, determining a typical configuration of 10 solar array sections, the minimal required section's short circuit current $I_{SC_{min}}$ can be approximated.

$$I_{SC_{min}} = \frac{P_{REQ}}{10 \cdot V_{OP}} \approx 0.73\, A \qquad 0.7$$

with $V_{OP} = V_{BUS}$ in case of the use of DET, which is considered for the present numerical application, and $V_{OP} = V_{MP}$ in case of the use of an MPPT.

In practical, since the ageing phenomena and the environmental conditions such as the temperature and the sun irradiance are very impacting the solar array performances, consequential margins are also applied. Thus, for the sake of simplification, these phenomena are neglected and sections of $I_{SC} = 1A$ and $V_{OC} = 35V$ are considered – approximatively corresponding to a maximum power of 25 watts.

The elements mentioned here only allow the calculation of the large signal behaviors of the system and elements as important as the input and output filters of each unit must be taken into account. The main difficulty is the great disparity of the types of interface but also the dependence of the sizing of these elements on the type of architecture used.

RÉPUBLIQUE FRANÇAISE
Liberté
Égalité
Fraternité

Université de Toulouse

Titre : Modélisation et détermination des stratégies de conditionnement de puissance pour des réseaux de puissance répartis pour des applications embarquées aéronautiques et spatiales.

Mots clés : électronique de puissance, conditionnement de puissance, aérospatial, Architecture électrique

Résumé : Le système d'alimentation électrique (EPS) est l'un des systèmes les plus critiques, sinon le plus critique, d'un vaisseau spatial si l'on considère qu'un vaisseau spatial n'est rien d'autre qu'un système électrique et que le but de l'EPS est de générer, conditionner, stocker et distribuer l'énergie électrique à l'ensemble du système. En d'autres termes, il est le premier maillon de la chaîne alimentaire et s'il cesse de fonctionner, c'est tout le système qui est perdu. Le besoin de robustesse et de fiabilité qui en découle, ainsi que l'environnement particulièrement isolé et hostile dans lequel il doit fonctionner, ont orienté les choix de conception du PSE et conduit à un système à très haut rendement, électriquement parlant, mais au prix d'un manque de flexibilité. Néanmoins, le contexte actuel et les développements récents donnent l'opportunité de repenser profondément la conception de l'EPS et c'est ce que le CNES et Airbus font depuis plusieurs années. L'architecture électrique modulaire et distribuée qui a émergé de ces développements offre un grand nombre de possibilités en termes de contrôle, mais aussi des défis en termes de stabilité et d'optimisation. La présente thèse a donc pour objectif de démontrer que des lois de commandes intégrés dans les modules de conditionnement permettent une régulation de la charge batterie et une stabilité du réseau de bord quelle que soit la topologie du bus de puissance et des profils de consommation. Pour ce faire, une modélisation paramétrique du système a été réalisé en s'inspirant des méthodes de modélisation utilisée dans les problématiques de microgrids terrestres. Les modèles des différents éléments du système ont ainsi été intégrés sous Matlab et Matlab Simulink afin de simuler un système typique inspiré de satellites développés par le CNES. Une étude bibliographique approfondie a été réalisée pour identifier des lois de pilotages utilisées dans des problématiques similaires et qui auraient un intérêt à être adaptées sur des applications spatiales. Ces lois de contrôle ont ainsi été testées en simulation, une attention particulières étant portée sur les aspects de stabilité du système, ce qui a permis d'en sélectionner les plus adaptées afin de les valider expérimentalement sur un démonstrateur mis en place sur le même modèle. Basée sur ces résultats, une stratégie globale est proposée.

Title: Modeling and determining of power conditioning strategies for distributed power networks for aeronautical and spaceborne applications.

Key words: power electronics, power conditionning, aerospace, Electrical architecture

Abstract: The electrical power system (EPS) is one of the most critical systems, if not the most critical, of a spacecraft considering that a spacecraft is nothing but an electrical system and the purpose of the EPS is to generate, condition, store and distribute electrical power to the entire system. In other words, it is the first link in the food chain and if it stops working, the whole system is lost. The resulting need for robustness and reliability, as well as the particularly isolated and hostile environment in which it must operate, have guided the design choices of the EPS and led to a system with very high efficiency, electrically speaking, but at the cost of a lack of flexibility. Nevertheless, the current context and recent developments give the opportunity to deeply rethink the design of the EPS and this is what CNES and Airbus have been doing for several years. The modular and distributed electrical architecture that has emerged from these developments offers many possibilities in terms of control, but also challenges in terms of stability and optimization. The objective of this thesis is thus to demonstrate that control laws integrated in the conditioning modules allow a regulation of the battery charge and a stability of the onboard network whatever the topology of the power bus and the consumption profiles. To do this, a parametric modeling of the system was carried out by being inspired by the modeling methods used in the problems of terrestrial microgrids. The models of the various elements of the system were thus integrated under Matlab and Matlab Simulink in order to simulate a typical system inspired by satellites developed by the CNES. A thorough bibliographical study was carried out to identify control laws used in similar problems and which would be of interest to be adapted to space applications. These control laws have been tested in simulation, with particular attention to the stability constraints, which allowed to select the most suitable ones in order to validate them experimentally on a demonstrator set up on the same model. Based on these results, a global strategy is proposed.